Universidade do Minho
Escola de Engenharia

Sílvia Cristina Gomes Pereira

Genetically engineered new spider silk chimeras for bone regeneration

Janeiro de 2011

Genetically engineered new spider silk chimeras for bone regeneration
Silvia Cristina Gomes Pereira
UMinho | 2011

Universidade do Minho
Escola de Engenharia

Sílvia Cristina Gomes Pereira

Genetically engineered new spider silk chimeras for bone regeneration

Tese de Doutoramento
Programa Doutoral em Engenharia de Tecidos,
Medicina Regenerativa e Células Estaminais

Trabalho efectuado sob a orientação do
Professor Rui L. Reis
e do
Professor João F. Mano

Janeiro de 2011

DECLARAÇÃO

Nome: Sílvia Cristina Gomes Pereira

Endereço electrónico: silvia.gomes@dep.uminho.pt

Telefone: 966322742

Número do cartão do cidadão: 11474010

Título tese: Gnetically engineered new spidet silk chimeras for bone regeneration

Orientador(es): Professor Rui Reis e Professor João Mano

Ano de conclusão: 2011

Ramo de Conhecimento do Doutoramento: Programa Doutoral em Engenharia de Tecidos, Medicina Regenerativa e Células Estaminais

É AUTORIZADA A REPRODUÇÃO PARCIAL DESTA TESE/TRABALHO (indicar, caso tal seja necessário, nº máximo de páginas, ilustrações, gráficos, etc.), APENAS PARA EFEITOS DE INVESTIGAÇÃO, MEDIANTE DECLARAÇÃO ESCRITA DO INTERESSADO, QUE A TAL SE COMPROMETE;

Universidade do Minho, ___/___/_____

Assinatura: _____

To my family

Acknowledgments

After all the research work and writing the moment as come to express my sincere appreciation to all the people that in one way or another contributed for this thesis. For sure without them the accomplishment of this work would not be possible.

First, I would like to thank my supervisor Professor Rui Reis for giving the opportunity of being a PhD student at the 3B's research group where I had all the support and freedom to pursuit my research interest. I am also grateful for the chance to participate in the writing and managing of several research projects, for sure these skills and knowledge will be extremely important for my future professional life. To Professor João Mano, I am grateful for his intelligent critics and guidance that without a question contributed in a decisive way for the accomplishment of this thesis. To Isabel Leonor (commonly known as Belinha), my sincere and enormous gratitude for her encouragement, friendship, thoughtful advice and supervision during my good and bad moments. Thank you for being always there.

To Professor David Kaplan, for its crucial and decisive contribution to this thesis I will be always grateful. Without your support and guidance this thesis would never be possible. Also, by opening the doors of your group you gave me the chance to learn and grow as a researcher and to contact with amazing and friendly people that were always there for me. I am very grateful to all the people from Tufts, Aneta, Monica, Nicolle, Dean, Heather, Guokui, Sreevidhya and Carmen for your friendship, encouragement and support to this work. To Olena, Keiji and Jabier I will be always grateful for your enormous help and patience during the work we developed together, for your friendship and for all the happy and funny moments spent together. To Milva, Rossella and Cleyton, I will never forget all the interesting conversations and the funny moments we spent. Also from Boston, thank you to my roommates Iffet, Jerome, Tanya, Zuzana and Maayke for the conversations, support in bad moments, cinema sessions and happy experiences.

Since this thesis would never be possible without a scholarship I thank Fundação para a Ciência e Tecnologia (FCT) for providing my PhD grant (SFRH/BD/28603/2006), which supported the costs with human resources and part of this work.

During these past years at the 3B's group I had the chance to contact and work with different personalities, which was a golden opportunity to open my mind and improve my social and human skills and at the same time a lesson for life. To the ones more close to me - Paula Lopez, Vitor Júnior and Helena Lima - I have no words to describe how you made this load easier to carry. Thank you for the crazy, deep and nonsensical talks and for the support during the bad moments and the laughs during the good ones. Thank you to Iva and Ricardo Pires for your friendship and of course for being my faithful "roadmates" during these long trips between Taipas and Braga. Thank you to Ricardo Silva for your help during my first stapes into the amazing world of chitosan and for the interesting and intelligent discussions. Also I would like to thank to Helena Azevedo, Márcia Rodrigues, Marta Silva, Ana Rita, Simone Silva, Bruno Ferreira, Alexandra Marques, Albino Martins, Paulo Bessa, Tiago Silva, Tírcia Santos, Liliana Gomes, Virgínia Araújo and Wojciech Szymczyk for your friendship and support during my research at the 3B's group.

Estou eternamente grata à minha mãe e a Golçalves pela compreensão, apoio incondicional, carinho e amor, mesmo durante os momentos mais difíceis, que me permitiram chegar onde me encontro hoje. Sem vocês esta tese não seria possível.

Ao meu amor e companheiro de "viagem", Duarte, obrigada pelo amor, compreensão, PACIÊNCIA (e muita), carinho e força durante os maus momentos em que as dúvidas se avolumaram no horizonte e por estar sempre presente durante os bons momentos.

POPH
PROGRAMA OPERACIONAL POTENCIAL HUMANO

FCT Fundação para a Ciência e a Tecnologia
MINISTÉRIO DA CIÊNCIA, TECNOLOGIA E ENSINO SUPERIOR

TERC TISSUE ENGINEERING RESOURCE CENTER
Tufts University | National Institutes of Health | Columbia University
National Institute of Biomedical Imaging and Bioengineering

QREN QUADRO DE REFERÊNCIA ESTRATÉGICO NACIONAL
PORTUGAL 2007.2013

UNIÃO EUROPEIA
Fundo Social Europeu

Genetically engineered new spider silk chimeras for bone regeneration

Abstract

Tissue engineering and regenerative medicine are emerging fields focused on the development of tissues and organs that can be used in transplantation surgeries for the replacement or repair of damaged tissues or organs. This accomplishment would discard the need to use autologous and allogenic grafts, overcoming problems such as donor rejection, disease transmission or organ scarcity. The materials science field contributes directly for the achievement of this goal through the functionalization of natural or synthetic polymers or with the development of new biopolymers with diverse mechanical and biological characteristics. More recently, many research studies show the potential of using biotechnology approaches to generate new bioactive multifunctional materials engineered at the molecular level. An advantage of using genetically bioengineered biopolymers is the possibility of generating new genetic variants carrying different functional domains.

The main goal of this thesis is to develop new multifunctional proteins that can be used in the fabrication of a new generation of biomaterials with improved features such as infection control, enhanced cell functions and better mechanical performance. As a result, the main objectives of this thesis are:

I. Design of new functionalized spider silk fusion proteins through the combination of six repeats of the consensus unit for the native sequence of the major ampullate dragline silk I from *Nephila clavipes* (6mer) with two different types of proteins: bone sialoprotein (BSP) and the human antimicrobial peptides, namely human neutrophil defensin 2 (HNP-2), human neutrophil defensins 4 (HNP-4) and hepcidin. The four protein domains were fused with spider silk through recombinant DNA technology and the new chimeric proteins and silk alone were expressed in *Escherichia coli* RY-3041 strain. 6mer, 6mer+BSP, 6mer+HNP-2, 6mer+HNP-4 and 6mer+hepcidin were purified with affinity chromatography and their identity was confirmed.

II. Study the *in vitro* activity of the new chimeric proteins to verify if protein domains maintained their activity. Attenuated total reflection Fourier transform infrared (ATR-FTIR) results show that the spider silk domain, 6mer, maintained its ability to self-organize into a β-sheet conformation, an important feature related with its mechanical properties. Additionally, *in vitro* mineralization studies demonstrated that 6mer+BSP

fusion protein with BSP retained the ability to induce the deposition of CaP. Finally, radial diffusion tests showed that the antimicrobial domains present in 6mer+HNP-2, 6mer+HNP-4 and 6mer+Hepcidin proteins maintained bactericidal activity.

III. Assess the mechanical properties and roughness of 6mer+BSP protein films and its behaviour in the presence of calcium ions. Since 6mer+BSP was synthesized for bone regeneration applications the study of these parameters is important. In this way, atomic force microscopy (AFM) was used for imaging and for force spectroscopy. The results obtained show that 6mer+BSP had a higher stiffness than 6mer protein. For both proteins the roughness values were similar. In the presence of Ca ions, the AFM imaging showed the ability of 6mer+BSP chimeric protein to form supramolecular networks through ionic crosslinking.

IV. Address the *in vitro* activity of the new chimeric proteins. Cell culture studies with human mesenchymal stem cells (hMSC) indicated that 6mer+BSP protein sustained hMSC proliferation and differentiation into the osteogenic lineage. In the case of 6mer+HNP-2, 6mer+HNP-4 and 6mer+hepcidin proteins *in vitro* cell studies demonstrated that these new proteins were capable of sustaining the proliferation of mammalian osteosarcoma cell line (SaOs-2).

V. Finally, based on the results obtained with the *in vitro*, 6mer+BSP and 6mer+hepcidin were selected for *in vivo* studies and the results showed no major differences between the inflammatory responses to the 6mer+BSP and 6mer+Hepcidin films and the responses observed for the controls 6mer, poly-lactic-glycolic-acid (PLGA) and empty implants.

The results obtained in this thesis demonstrated that 6mer+BSP, 6mer+HNP-2, 6mer+HNP-4 and 6mer+hepcidin bioengineered proteins represent promising protein-based biomaterial for future biomedical applications. Additionally, the results reported here also highlight the potential of using new genetically engineered proteins to develop new hybrid multifunctional biomaterials for tissue engineering and regenerative medicine applications. This new generation of multifunctional proteins can combine different functionalities such as enhanced cell adhesion, mineral nucleation and infection control, and therefore exclude the need for additional chemical modification which has considerable disadvantages.

Novas quimeras de seda de aranha geneticamente modificadas para aplicação em regeneração de osso

Resumo

Engenharia de tecidos e medicina regenerativa têm como principal objectivo o desenvolvimento de estruturas para substituição de tecidos e órgãos danificados. Este feito excluiria a necessidade de utilizar implantes autólogos ou alogénicos, ultrapassando os problemas de rejeição e escassez de órgãos e de transmissão de doenças associados a este tipo de intervenções. A área de ciências dos materiais contribui directamente para o alcance deste objectivo através da funcionalização de polímeros naturais ou sintéticos e do desenvolvimento de novos polímeros. Estudos recentes mostram as vantagens do uso da biotecnologia na síntese de novos materiais bioactivos e multifuncionais. Os estudos descritos nesta tese centram-se no uso da engenharia genética para o desenvolvimento de novas proteínas multifuncionais para aplicação no desenvolvimento de uma nova geração de materiais dotados de diversas características vantajosas tais como a capacidade de controlar infecções e de induzir melhores respostas a nível celular e propriedades mecânicas superiores. Desta forma, os principais objectivos desta tese são:

I. Desenvolvimento de novas proteínas quiméricas através da fusão de seis unidades-consenso da sequencia nativa da proteína "*major ampullate dragline silk I*", da espécie *Nephila clavipes* (6mer), com dois tipos diferentes de proteínas: sialoproteína do osso (BSP) e péptidos com propriedades antimicrobianas, "*human neutrophil defensin 2*" (HNP-2), "*human neutrophil defensins 4*"(HNP-4) and "*hepcidin*". Utilizando a tecnologia de ADN recombinante, estes domínios proteicos foram fundidos com a sequência da seda e as novas proteínas foram expressas na estirpe de *Escherichia coli* RY-3041. As proteínas 6mer, 6mer+BSP, 6mer+HNP-2, 6mer+HNP-4 e 6mer+hepcidin foram purificadas por cromatografia de afinidade e a sua identidade foi confirmada.

II. Estudar, através de estudos *in vitro*, a actividade dos domínios proteicos das novas proteínas. As análises de infravermelho por transformada de Fourier com reflexão total atenuada (ATR-FTIR) demonstram que o domínio da seda de aranha, 6mer, manteve a sua capacidade de auto-organização em estruturas "*β-sheet*", imprescindível para as propriedades mecânicas desta proteína. Os testes de mineralização *in vitro* com a proteína 6mer+BSP mostram que o domínio BSP manteve

a sua capacidade para induzir a deposição de fosfatos de cálcio. Os testes de difusão radial com 6mer+HNP-2, 6mer+HNP-4 e 6mer+hepcidin mostram que estas mantiveram a sua actividade anti-bacteriana.

III. Caracterização das propriedades mecânicas e da rugosidade das membranas de proteína 6mer+BSP, e do seu comportamento na presença dos iões de cálcio. Este estudo é importante na medida em que a proteína 6mer+BSP foi concebida para aplicações em osso. O microscópio de força atómica (AFM) foi utilizado para a colheita de imagens e para espectroscopia de força. Os resultados mostram que as membranas de 6mer+BSP são mais rígidas que as de 6mer. Os valores de rugosidade são semelhantes para ambos os tipos de membranas. Na presença de iões Ca^{2+} as imagens de AFM mostram que a proteína 6mer+BSP é capaz de formar complexos supra-moleculares através de reticulação iónica.

IV. Caracterização *in vitro* da resposta celular às novas proteínas. O estudo com células estaminais mesenquimais humanas (hMSC) indicaram que a proteína 6mer+BSP é capaz sustentar a sua proliferação e diferenciação osteogénica. Os testes com 6mer+HNP-2, 6mer+HNP-4 e 6mer+hepcidin mostram que estas proteínas sustentaram a proliferação de uma linha celular derivada de osteosarcoma de mamífero (SaOs-2).

V. Com base nos resultados obtidos as proteínas 6mer+BSP e 6mer+hepcidin foram seleccionadas para estudos *in vivo*. A comparação das respostas inflamatórias entre os implantes de 6mer+BSP e de 6mer+hepcidin e entre os controlos de 6mer, ácido poli-láctico-glicólico (PLGA) e sem implante não mostrou diferenças significativas.

Os resultados descritos nesta tese mostram que as proteínas 6mer+BSP, 6mer+HNP-2, 6mer+HNP-4 e 6mer+hepcidin, desenvolvidas através de engenharia genética, constituem promissores biomateriais proteicos para futuras aplicações na área biomédica. Estes resultados também destacam o potencial da engenharia genética no desenvolvimento de novas proteínas para o fabrico de novos materiais híbridos e multifuncionais para aplicação em engenharia de tecidos e medicina regenerativa. Estas proteínas combinam várias funcionalidades como melhor adesão celular, deposição de minerais e controlo de infecções, excluindo a necessidade de modificações químicas adicionais.

Table of Contents

List of abbreviations

A
ALP - Alkaline phosphatase
AFM - Atomic force microscopy
ACS - Accelerating calcification solution
APC - Allophycocyanine
ATCC - American-Type Culture Collection
ATR-FTIR - Attenuated Total Reflection Fourier Transform Infrared

B
bFGF - Basic fibroblast growth factor
BMP - Bone morphogenetic proteins
B. mori - *Bombyx mori*
BSA - Bovine serum albumin
BSP - Bone sialoprotein

C
Ca - calcium
CaP - Calcium phosphates
CD - Circular dichroism
CDI - Carbonyl diimidazole
cDNA – Complementary DNA
COL1A1 - Collagen type I alpha 1
COL2A1 - Collagen type II alpha 2
CPI - Alkaline Phosphatase, Calf Intestinal enzyme

D
d - Cantilever deflection
DCC - Dicyclohexyl-carboiimide
DLS - Dynamic light scattering
DMEM - Dulbecco's modified Eagle's medium
DNA - Deoxyribonucleic acid

E
E - Elastic modulus
E. coli - *Escherichia coli*
EDC - 1-ethyl-3-(3-dimethylaminopropyl)-carbodiimide
EDS - Energy dispersive spectrometer
EDTA - Ethylenediaminetetraacetic acid
EGD - Epidermal growth factor

F
FACS - Florescence activated cell sorting
FBS - Fetal bovine serum
FDA - Food and Drug Administration
FITC - Fluorescein isothiocyanate

G
GAPDH - Glyceraldehyde 3-phosphate dehydrogenase
GPa – Gigapascal

H
HEPES - 4-(2-hydroxyethyl)-1-piperazineethanesulfonic acid
H&E - Hematoxylin and eosin
HGF - Hepatocyte growth factor
HMSC - Human mesenchymal stem cells
HNP-1 - Human neutrophil defensin 1
HNP-2 - Human neutrophil defensin 2
HNP-4 - Human neutrophil defensin 4
HD-5 - Human defensins 5
HD-6 - Human defensins 6

I
IBSP - Integrin bone sialoprotein
IGF – Insulin-like growth factor
IL-2R - Interleukin-2 receptor
IPTG - Isopropyl β-D-thiogalactoside

L
LB - Luria-Bertani
LDS - Lithium dodecyl sulphate
LPS - Lipopolysaccharide

M
MAPs - Mussel adhesive proteins
MaSpI - Major ampullate spidroin protein 1
MaSp2 - Major ampullate spidroin protein 2
MALDI-TOF - Matrix assisted laser desorption time-of-flight
Mg – Magnesium
MQ – Milli-Q
mM - Milimolar
mRNA – Messenger ribonucleic acid
M - Molar

N
Na – Sodium
nm - Nanometer
N. clavipes - *Nephila clavipes*
NHS - N-hydroxysuccinimide
Ni-NTA – Niquel-nitrilotriacetic acid

O
OD – Optical density

P
PBS - Phosphate buffer
PCL – Poly-caprolactone
PDGF - Platelet-derived growth factor
PE - Phycoerythrin
PLA – Poly-lactic-acid
PLGA - Poly-lactic-glycolic-acid
PLL – Poly-L-lactide
poly-A - Poly-alanine

P - Phosphorous

R
R_a - average height
Real time qRT-PCR - Real time quantitative reverse transcription-polymerase chain reaction
RMS - Root mean square

S
SaOs-2 - Human osteosarcoma cell line
SDS-PAGE - Sodium dodecyl sulfate polyacrylamide gel electrophoresis
SDF - Stromal cell-derived factor 1
SEM - Scanning electron microscopy
S. aureus - *Staphylococcus aureus*

T
TBS - Tris Buffered Saline
TBSTT - TBS with tween 20
TCP – Tissue culture plate
TGF - Transforming growth factor

U
UV - Ultraviolet light
µm - Microgram
µm - Micrometer

V
VEGF - Vascular endothelial growth factor
v/v - Volume per volume
w/v - Weight per volume

Z
z - Cantilever vertical position

θ - Ellipticity

The following table refers to a list of abbreviations for the amino acids.

Amino acid nomenclature

Amino acid full name	Abbreviations
Arginine	Arg / R
Glutamine	Gln / Q
Phenylalanine	Phe / F
Tyrosine	Tyr / Y
Tryptophan	Trp / W
Lysine	Lys / K
Glycine	Gly / G
Alanine	Ala / A
Histidine	His / H
Serine	Ser / S
Proline	Pro / P
Glutamic acid	Glu / E
Aspartic acid	Asp / D
Threonine	Thr / T
Cysteine	Cys / C
Methionine	Met / M
Leucine	Leu / L
Asparagine	Asn / N
Isoleucine	Ile / I
Valine	Val / V

List of figures **Page**

Chapter I – General introduction - Genetically Engineered Proteins for Tissue Engineering

Chapter II – Materials and Methods

Chapter III – Spider silk-bone sialoprotein fusion proteins for bone tissue engineering

Chapter IV – AFM study of morphology and mechanical properties of a chimeric spider silk and bone sialoprotein protein for bone regeneration

Chapter V – Antimicrobial functionalized genetically engineered spider silk

Chapter VI – *In vivo* biological responses to chimeric proteins: silk proteins functionalized with bone sialoprotein

Chapter VII – Biological responses to spider silk-antibiotic fusion protein

List of tables **Page**

Short c*urriculum vitae*

Sílvia Gomes is graduated in Biology, by the Faculty of Sciences, University of Porto and has an MSc in Genetic Resources and Biodiversity, by the Faculty of Sciences, University of Porto, Portugal. During the past six years she has been a researcher at the 3B's Research Group – Biomaterials, Biodegradables and Biomimetics, Department of Polymer Engineering, University of Minho, where she developed her PhD research work under the supervision of Professor Rui Reis, Professor João Mano and Doctor Isabel Leonor. This research work is the result of a strong collaboration with Professor David L. Kaplan, a Professor & Chair at the Department of Biomedical Engineering, Tufts University, where Sílvia Gomes worked for two years for her PhD project.

As a researcher of the 3B's group Sílvia Gomes was also involved in the preparation of several grant proposals submitted at the Portuguese Foundation for Science and Technology – FCT – and at the European Union. One of the proposals submitted to FCT was and at the moment she is providing scientifically support and coordination to the R&D project CHIMERA (PTDC/EBB-EBI/109093/2008) "Development of new chimeric proteins to be used in the fabrication of a novel biomaterial for bone regeneration application".

List of publications

This thesis is based on the following publications:

1. **Gomes S**, Leonor IB, Mano JF, Reis RL and Kaplan DL, 2011, Spider silk-bone sialoprotein fusion proteins for bone tissue engineering, Soft Matter, *submitted*.

2. **Gomes S**, Numata K, Leonor IB, Mano JF, Reis RL and Kaplan DL, 2011, AFM study of morphology and mechanical properties of a chimeric spider silk and bone sialoprotein protein for bone regeneration, Biomacromolecules, *submitted*.

3. **Gomes S**, Leonor IB, Mano JF, Reis RL and Kaplan DL, 2011, Antimicrobial functionalized genetically engineered spider silk, Biomaterials, *submitted*.

4. **Gomes S**, Gallego- Llamas J, Leonor IB, Mano JF, Reis RL and Kaplan DL, 2011, In vivo biological responses to chimeric proteins: silk proteins functionalized with bone sialoprotein, Adv Funct Mater., *submitted*.

5. **Gomes S**, Gallego- Llamas J, Leonor IB, Mano JF, Reis RL and Kaplan DL, 2011, Biological responses to spider silk-antibiotic fusion protein, J Tissue Eng Regen Med., *submitted*.

6. **Gomes S**, Leonor IB, Mano JF, Reis RL and Kaplan DL, 2011, Genetically engineered proteins for tissue engineering, Prog Polym Sci. , *submitted*.

Other publications:

1. **Gomes S**, Boulon ME, Oliveira AL, Leonor IB, Mano JF and Reis RL, 2008, Mineralization of Chitosan Membrane Using a Double Diffusion System for Bone Related Applications , Advanced Materials Forum , **IV** : 77

2. **Gomes S**, Rodrigues MT, Leonor IB, Gomes ME, Mano JF and Reis RL, 2008, Conversion of corallina officinalis into calcium phosphates by using hydrothermal treatment and their potential for bone tissue engineering application, Tissue Engineering Part A, **14 (5)** : 831-831

3. Lopes A, Lopes-Lima M, Bobos I, Ferreira J, **Gomes S**, Reis RL**,** Mano JF and Machado J, 2010, The effects of *Anodonta cygnea* biological fluids on biomineralization of chitosan membranes, J Memb Sci., 364 (1-2): 82-89.

<u>Book chapters</u>

1. Leonor IB, **Gomes S**, Bessa PC, Casal M, Mano JF and Reis RL, 2008, New biomineralization strategies on natural-based polymeric materials for bone tissue engineering approaches, In Natural-based Polymers for Biomedical Applications, eds.

Reis R.L., Neves N.M.,Mano J.F., Gomes M.E., Marques A.P., Azevedo H.S., Woodhead Publishing Limited, Cambridge, 193-230.

Communications in conferences

1. Bessa PC, **Gomes S**, Leonor IB, Klosch B, Redl H, Reis RL and Casal M, Osteoinduction of human fat derived stem cells and murine C2C12 cell line by recombinant human bone morphogenetic protein-2, Congresso Nacional Microbiotec'07, Lisboa, Portugal, December 2007.

2. Silva TH, Alves A, Ferreira BM, **Gomes S**, Sousa RA, Mano JF, Neves NM and Reis RL, Methodologies for the isolation of several marine origin polymers and ceramics with high potential for valorisation, PROTEUS Project Public Meeting, Vigo, Spain, December 2007.

3. Bessa PC, **Gomes S**, Leonor IB, Klosch B, Redl H, Casal M and Reis RL, Natural origin biomimetic scaffolds for the delivery of human bone morphogenetic protein-2 produced by recombinant technology, InVents 4th Marie Curie Cutting Edge Conference (Biocompatibility evaluation and biological behaviour of polymeric biomaterials), Algarve, Portugal, October 2007.

4. **Gomes S** , Boulon ME, Leonor IB, Mano JF and Reis RL, Mineralization of Chitosan Membrane Using a Double Diffusion System for Bone Related Applications, XIII Conference of Sociedade Portuguesa de Materiais, Porto, Portugal, April 2007.

5. **Gomes S** , Rodrigues MT, Oliveira JM, Gomes ME, Leonor IB, Mano JF and Reis RL, Hydrothermal Conversion Of *Corallina officinalis* Algae Into Calcium Phosphate Scaffolds For Bone Tissue Engineering Strategies, 3rd Marie Curie Cutting-Edge Conference "Biomineralisation of polymeric materials, bioactive biomaterials and biomimetic methodologies" , Funchal, Portugal, June 2008.

6. **Gomes S**, Leonor IB, Mano JF, Reis RL and Kaplan DL, Functionalized Silk Biomaterials for Bone Formation and Infection Control, Gordon conference – Proteins -, Holderness, NH, USA, June 2009.

Abstract

To overcome the limitations of the traditionally used autografts, allografts and, to a less extent, synthetic materials there is the need o develop a new generation of scaffolds comprising different features such as adequate mechanical and structural support, able to control cell attachment, migration, proliferation and differentiation and being bio-resorbable, allowing for the body to heal itself at the same rate as the implant degradation. Genetic engineering offers the possibility to express biological components already present in nature and to generate new peptides and protein sequences by establishing new artificial self-assembling peptides or by fusing together different bioactive domains or protein motifs. In this way, with genetic engineering is possible to generate alternative sequences with tunable properties that can be used as promising biomaterials for medical applications.

In this review we address some of the most frequently used proteins for tissue engineering and biomedical applications and describe the techniques most commonly used to functionalize protein-based biomaterials by combining them with bioactive molecules in order to enhance their biological performance. Finally we highlight the use of novel design approaches, namely genetic engineering, for protein heterologous expression and the synthesis of new protein-based biopolymers, focusing the advantages of these functionalized biopolymers when compared with their counterparts extracted directly from nature and modified by techniques such as physical adsorption or chemical modification.

1. Introduction

Treatment of injured tissues or organs focuses on the use of autologous and allogenic grafts [1]. However, this practice has significant limitations for the patient and health systems worldwide. Autologous grafts cause donor site morbidity and consequent loss of organ functionality. Allografts are associated with risk of disease transmission and require the use of immunosuppressants with associated side effects [2, 3]. In the field of orthopaedic implants, autologous and allogenic grafts account for 90% of the grafts currently used, with synthetic materials (metals, polymers, ceramics and composite systems) used in 10% of surgery cases. In the three types of grafts there are numerous cases of implant failure as a consequence of undesirable local tissue responses

resulting in implant loosening, insufficient osseointegration, osteolysis, inflammation and infection [4, 5]. These complications account for a failure rate of 13 to 30% in the case of autografts and 20 to 40% for allografts [6] .Besides autologous and allogenic grafts, synthetic materials have also been used for controlled drug delivery systems, scaffolds design and orthopaedic fixation as screws, pins or rods [7, 8]. Nevertheless, synthetic polymers are too hydrophobic and need additional bulk or surface modifications to render the material more biocompatible and suitable for implantation [9]. Therefore, there is a need for alternatives to these practices. Tissue engineering and regenerative medicine offer an approach to circumvent the present therapies with new methods of health care treatment with the purpose of improving the quality of life [6, 10]. This improvement can come in the form of new cytocompatible and non-toxic biomaterials for the manufacture of a new generation of scaffolds comprising adequate mechanical and structural support and able to control cell attachment, migration, proliferation and differentiation [4, 11]. Furthermore, this future generation of scaffolds should not behave as a permanent prosthesis but instead should perform as bio-resorbable temporary implants, allowing for the body to heal itself at the same rate as the implant degradation [11, 12].

In recent years a small number of synthetic biodegradable polymers, mainly polyesters containing glycolic (PLG) or lactic (PLL) acids and caprolactone (PCL) were approved by the Food and Drug Administration (FDA) for use in sutures [12]. Epicel™ (autologous keratinocyte skin graft to treat severe burn victims from Genzyme Biosurgery, Cambridge, MA), Carticel® (autologous chondrocyte transplantation to treat cartilage injury from Genzyme Biosurgery, Cambridge, MA) [13], MACI™ for matrix-induced autologous chondrocyte implantation (Genzyme Biosurgery, Cambridge, MA) where chondrocytes are supplied seeded onto a type I/III collagen scaffold secured to the skin injury with fibrin glue [14], and Aplifraf (bovine collagen I matrix seeded with keratinocytes for wound care from Organogenesis, Canton, MA)[15], are products for cell therapy also available in the market. Other examples of products already commercially available are Atrigel® (Atrix Laboratories, Fort Collins, Co, USA) a system of biodegradable polymers for drug delivery [16] and the calcium phosphate based products Collagraft (Zimmer, Warsaw, IN; and Collagen Corporation, Palo Alto, CA) and ProOsteon (Interpore international, Irvine, CA) for bone applications [6]. However,

since giving a detailed description of these and other products available in the market is not the purpose of this review we advise the reader to address other reports for more information [6, 12-16].

Despite the enormous research effort during the last few decades materials scientist have not fully developed a new generation of biocompatible biomaterials [12]. This limitation of tissue engineering to move forward from the laboratory into the clinic is the result of many issues, including legal, the need to develop functional blood vessel networks to nourish the new tissues mainly inside scaffolds, inability of the biomaterials to promote the formation of functional tissues, and many related issues [12]. For these reasons it is critical to develop the next generation of biomaterials that will address the limitations above. New approaches in the fields of bionanotechnology, protein engineering and bionano-fabrication will play a role in the development of these next generation biomaterials [17].

In this review we address some biopolymers already being used or with potential applications in regenerative medicine and tissue engineering, giving special focus to proteins and protein-based biomaterials. Additionally, we will also focus on the different approaches used for functionalization of these biomaterials in order to improve performance, mechanical efficiency, biocompatibility and degradability, usually with a goal towards control of these processes. This overview will be followed by a description of the novel design approaches, namely genetic engineering, enabling the synthesis of new protein-based biopolymers inspired in nature but without many of the drawbacks of their native counterparts when extracted directly from natural sources. Additional information can be found in recent related reviews addressing the use of biomimetic materials in tissue engineering [18], the application of protein templates for tissue engineering [4], the synthetic modification of proteins and peptides [19] and the use of bioengineering for biomaterials design [20, 21] just to name some examples.

2. Natural proteins for biomedical applications

The similarity between natural polymers and macromolecules forming extracellular matrices suggest an innate ability for some of these polymers to interact with cells and

biomolecules present in host tissues, offering mild immunological reactions when compared with synthetic materials [11, 22, 23]. Natural polymers such as fibrin, fibronectin, collagen, elastin, silk, keratin, chitosan, alginate, amylose/amylopectin and hyaluronic acid are widely used in tissue engineering [22, 24]. Within the myriad of biopolymers present in nature, proteins are the most sophisticated group in terms of chemistry [25]. Therefore some proteins with potential use in the biomedical field will be addressed in the next paragraphs. Table I.1 addresses some of the basic features of the animal proteins described in this section.

Collagen is synthesized by fibroblasts and is the most abundant protein in the mammalian body, accounting for 20-30% of the total protein [26]. Its primary functions in tissues are to provide mechanical support [27] and to control cell adhesion, cell migration and tissue repair [28]. Collagens form a large family of triple helical molecules with about 28 different types described [29]. All collagens share the same triple-helical structure where three parallel polypeptides, α-chains, coil around each other forming a right handed triple helix chain. In animals these collagen triple helices are known as tropocollagen and its hierarchical organization into more complex structures generates the fibers and networks in tissues such as bone, skin tendons, basement membranes and cartilage [30, 31]. Collagen is easy to modify and process and its abundance, nonantigenicity, biodegradability, biocompatibility and plasticity make collagen a promising biopolymer for applications in the medical and pharmaceutical fields and tissue engineering purposes [27]. Reconstituted gels of Type I collagen are widely used for biomedical applications and its main sources are animal tissues such as skin and tendons [24, 32]. Collagen scaffolds have been extensively used for soft tissue repair [33], vascular [34] and dermal tissue engineering [35, 36], bone repair [37] and as a carrier for the delivery of drugs [38] and biologically active molecules [39]. Additionally, collagens can also be used to fabricate microspheres for cell encapsulation and drug loading for controlled release.

However, despite the wide range of applications collagens matrices lack the mechanical properties required for hard tissue during initial implantation. For this reason collagen is often blended with other materials, either synthetic [40] or natural [41], to overcome mechanical limitations [4].

Fibronectin is also a component of the extracellular matrix with important functions such as structural support and signalling for cell survival, migration, contractility, differentiation and growth factor signalling [42]. Fibronectin is synthesized by different cell types, such as fibroblasts and is secreted as a dimer with disulfide bonds formed between the 230-270KDa subunits. These subunits are formed by three types of repeating modules named type I, II and III [43]. Fibronectin is a multi-domain glycoprotein with a remarkable number of biological functions, many of which are mediated through interactions with integrins, such as via the RGD sequences present in fibronectin. Besides binding to cell integrins, fibronectin binds to other biologically important molecules such as heparin, collagen/gelatin and fibrin [44]. Since fibronectin is biocompatible and easily recognized by cell integrins, the use of fibronectin or domains of the protein to functionalize scaffolds for tissue engineering is often considered [45]. Polymeric scaffolds of chitosan [46, 47], collagen [48] and hyaluronic acid [49] have been modified with fibronectin to improve cell adhesion and proliferation.

Additionally, fibronectin-mimetic peptide-amphiphiles were used in the fabrication of nanofibers and gels with excellent cell adhesion properties [45]. Another strategy was to prepare fibronectin-terminated multilayer films of poly-lysine and dextran sulphate for the study of the spreading behaviour of human umbilical vein endothelial cells. The cells spread to a greater extent and in a more symmetric manner on the films coated with fibronectin, suggesting that such fibronectin coated films may represent a promising strategy to control cell interactions with the materials in tissue engineering [62].

Together with collagen and fibronectin, **elastin** is also part of the core architecture supporting cell adhesion and growth [50]. Elastin fibers are mainly present in connective and vascular tissues, the lungs and skin. Elastin is a polymer of tropoelastin monomeric precursor and elastin fibers are an important component of the extracellular matrix to impart elasticity to organs and tissues. Hydrophobic domains present in the elastin sequence are responsible for these elastic properties [63, 64]. Elastin also has chemotactic activity, inducing cell proliferation and regulating cell differentiation, with the specific binding of integrin $\alpha_v\beta_3$ to the C-terminus in tropoelastin [65]. Due to its characteristics elastin is of interest for drug delivery and

tissue engineering and has been used in the fabrication of hybrid materials in combinations with collagen [66], gelatin [67], polycaprolactone (PCL) [68] and silk [69] for the production of vascular grafts [70], hydrogels [71], bone repair [72] and for drug delivery [73]. However, the crosslinking occurs between the water-soluble tropoelastin monomers to form the insoluble and stable elastin fibers limits the use of elastin from animal origin [50]. Therefore artificial proteins incorporating elastin-like peptides have been of interest for the development of new protein-based biomaterials [74, 75] with properties similar to native elastin [76].

Fibrin is another example of a specialized extracellular matrix protein with potential application for tissue engineering. However, unlike collagen, elastin and fibronectin, fibrin networks form mostly during blood clotting. Fibrin is the result of fibrinogen polymerization in the presence of thrombin [77]. Fibrinogen is a 340 kDa protein present in plasma formed by pairs of three different polypeptides, Aα, Bβ and γ, held together by disulfide bridges [78]. Fibrin and fibrinogen are two important components in blood clotting, fibrinolysis, cellular and matrix interactions, inflammation, wound healing and neoplasia [54]. In the particular case of clot formation, thrombin cleavage both Aα and Bβ chains at their N-termini, leading to the exposure of polymerization sites in both chains [79]. Subsequently the combination of these polymerization sites leads to the formation of double-strand twisted fibrils. These fibrin protofibrils undergo lateral aggregation and form branches, producing a three dimensional network [80]. Blood clots are further stabilized by covalent bonds formed by the plasma transglutaminase, factor XIII, making the clot more mechanically stable and less susceptible to enzymatic digestion [81]. Fibrin is a viscoelastic polymer and is used clinically as a medical adhesive; fibrin sealants are FDA approved. Furthermore, fibrin is also used for skin repair, replacing sutures and staples in fixation of skin grafts promoting a better wound healing [82], and in the transplantation of keratinocytes in burned patients [32]. Fibrin is also a promising biopolymer for applications in tissue engineering, in the repair of damaged tissues [83, 84], and drug delivery, as a carrier for growth factors [85].

Additionally, two proteinaceous components of the extracellular matrix, laminins and vitronectin, are mainly used to coat synthetic and natural polymer-based materials to improve cellular response. **Laminins** are cell adhesion glycoproteins

localized in the extracellular matrix of the basement membrane and are able to bind to other matrix proteins [55]. Recently, lamimin-derived peptides have been used as coatings to induce the adhesion of different cell types such as hepatocytes [86] and human dermal fibroblasts [87]. Also, these peptides are being studied for drug delivery in the development of targeting drug-loaded systems for cancer treatments [88]. **Vitronectin** is a multifunctional glycoprotein present in the extracellular matrix where it binds to glycosaminoglycans, collagen, plasminogen and urokinase-receptor and its RGD allows it to mediate the adhesion and spreading of cells [56]. This multipartner binding makes vitronectin an attractive biopolymer for tissue engineering and to induce cell attachment when used as a surface coating [89, 90].

The proteins described above are extracellular matrix proteins and have been more commonly used for tissue engineering and regenerative medicine applications. However, in the past few years other proteins have also emerged as potential biopolymers for the fabrication of new biomaterials, such as **Keratin** [91]. Moreover, since it is a protein shared by all mammals with a highly conserved amino acid sequence it is expected to offer good cell and tissue responses [57]. keratin fibers are hierarchically structured proteins present in hard and filamentous structures, such as hairs, horns and nails [91]. The presence of a LDV cell binding domain in keratin amino acid sequence [91] suggests utility for the fabrication of scaffolds for tissue engineering. Keratin based biomaterials have been used to support adhesion, spread and growth of L929 fibroblast cells [92], and the growth and differentiation of osteoblasts (MC3T3-E1) [93]. Keratin films have an inhibitory effect on the IgE receptor-stimulated histamine release from mast cells, making it suitable for use in antiallergenic materials [94].

As collagen and keratin, **silk** is another example of a hierarchically structured fibrous protein. Silk is characterized by its outstanding mechanical properties out-competing high performance man made fibers such as Kevlar, nylon and high-tensile steel, and by its self-assembly leading to fibers with a complex hierarchical arrangement [25]. Silk-protein-based fibers are produced by insects [95] and spiders [60] which use it for different ends such as cocoon and nest construction.

Table I.1. Basic features of some of the proteins with potential applications in the biomedical field.

Protein	Main functions	Basic structure	Relevant properties
Collagen [28, 31]	Structural protein in tissues such as connective tissue, tendon, skin, bone and cartilage	Three parallel polypeptide chains formed by GXY (G - glycine, X - usually proline, Y - usually 4-hydroxyproline) repeats and arranged in triple helix	Biodegradability, low antigenecity and biocompatibility
Fibronectin [42, 44]	Structural support and cell signalling	Dimer of two non-identical polypetide chains bonded at the carboxyl end by disulfide bonds	Multi-domain protein with cell (RGD motif), collagen and fibrin binding motifs
Elastin [50-52]	Structural protein found predominantly in connective tissue of arteries, ligaments, skin and lung	Cross-linked units of tropoelastin formed by hydrophobic (often 3 to 6 repeats of GVGVP, GGVP and GVGVAP) and hydrophilic lysine domains	Temperature dependent self-assembly and phase separation behaviour
Fibrin [53, 54]	Blood clotting, fibrinolysis, cellular and matrix interactions, inflammation and wound healing	Resultant from the polymerization and cross-linking of fibrinogen units after thrombin cleavage	Growth factor binding and interaction with cells such as platelets, leucocytes, fibroblasts and endothelial cells
Laminins [55]	Major components of basement membranes underlying epithelial and endothelial cells and embedding Schwann, muscle and fat cells	Heterotrimers of one β, one α and one γ chain, which represent different gene products	Self-assembly and binding to several matrix proteins and integrins
Vitronectin [56]	Regulates clot formation and immune response, provides biological cues for cell adhesion, migration and proliferation and extracellular anchoring	In human blood is found as a single chain or as a dimer while in the extracellular matrix exists as a disulfide-linked vitronectin multimer	Multi-domain protein with an RGD motif to mediate the attachment and spreading of cells and binding motifs for collagen, heparin, plasminogen, glycosaminoglycan and fibrin binding motifs
Keratin [57, 58]	Structural protein in the cytoskeletons of vertebrate epithelial cells and epidermis appendages such as hair, nails and wool	Formed by α-helical coiled-coil dimers assembled into 10 nm wide filaments	Biocompatibility, good cell attachment and growth
Silk [59, 60]	Building element of many arthropod nests, cocoons and prey traps	Highly repetitive core domain of alternating poly-A hydrophobic and G rich hydrophilic motifs	Self-assembly and remarkable mechanical properties
MAPs [61]	Substrate adhesion	Repetitive sequence, with molecular weights ranging between 5 and 120 kDa and high presence of 3,4-dihydroxyphenyl-L-alanine (DOPA)	Function over a wide range of temperatures, humidity and salinity and form permanent bonds to a wide variety of surfaces

However, despite the multitude of functions and different protein structures, many silk-based fibers have similar amino acid compositions and high levels of crystallinity. Silkworm silk produced by the silkworm species *Bombyx mori* is the most well studied silk protein [95]. The silk fiber is formed by two microfilaments embedded in glue-like glycoproteins named sericin which works as a coating. Each microfilament results from the assembly of a hydrophobic ~370 kDa heavy-chain fibroin protein, a relatively hydrophilic ~25 kDa light-chain fibroin and a 30 kDa P25 protein [96]. Spider dragline silk has a slightly different structure with a core filament formed by two spidroin molecules, major ampullate spidroin protein 1 (MaSp1) and 2 (MaSp2), coated by glycoproteins and lipids [97]. The remarkable mechanical features of the different types of silk are in part due to the presence of α-helix and β-turns, responsible for its elastic properties, alternating with β-sheets which confer toughness to silk fibers. The strong molecular cohesion occurring with amide-amide interactions in the β-sheet crystalline regions is thought to be responsible for the remarkable stiffness of silk fibers [98]. In *B. mori* silk, the hexapeptide repeat GAGAGS is involved in the formation of the β-sheets. In spider silk besides GA sequences there are also poly-Ala blocks and both motifs contribute for the formation of anti-parallel β-sheets [98]. These poly-A and GA motifs are embedded in amorphous regions formed by either GGX (X can be Tyr, Leu or Gln) or GPGXX motifs believed to be responsible for the elastic features [99]. The outstanding mechanic features and biocompatibility are reasons why silk has been used through the millennia in such diverse applications as hunting, fabrication of paper, wound dressing, textiles and sutures [59]. With new technologies in the fields of polymer synthesis and processing, silk continues to be an important topic of research for biomaterial and biomedical research. In the case of *B. mori* silk, sericulture provides the product used by the textile industry and in medical sutures [60]. Additionally, this silk is being studied for tissue engineering in the form of scaffolds for a range of tissue needs, such as corneal regeneration [100, 101], cartilage repair [102, 103], vascular grafts [104, 105], bone regeneration [106, 107] and drug delivery [108, 109]. As mentioned above *B. mori* silk is available in large supplies from sericulture, and is therefore most commonly used for the above studes. In the case of spiders, it is difficult to breed spider species due to their cannibalistic behaviour. With the advance of biotechnology tools it is now possible to bioengineer spider silk genes

to produce spider silk-like proteins [110], such as for tissue engineering [111], cell culture [112], nerve regeneration [113, 114] and wound dressings [115].

Mussel adhesive proteins (MAPs) are produced by marine mussels and used in the formation of the byssal threads which allow the animal to anchor to substrates. A common feature to all the adhesives produced by mussels is the presence of the amino acid 3,4-dihydroxyphenyl-L-alanine (DOPA). DOPA residues are key elements for the chemisorption to substrates underwater and the crosslinking process within the adhesive molecules [116]. These natural adhesives display outstanding properties in terms of function under harsh marine environments with wide temperature, salinity and humidity fluctuations and the mechanical effects of tides, waves and currents [117]. These remarkable properties make MAPs attractive biomaterials as bioadhesives. MAPs have been used as bioadhesives for cells [118] and tissues [119], and as self-adhesive micro-encapsulated drug carriers for biotechnological, tissue engineering and biomedical applications [120]. MAP derivatives were also used in the fabrication of adhesive-coated meshes as wound sealants, replacing tradition sutures, staples and tacks [61].

The proteins addressed above are widely used for tissue engineering and biomedical applications and can be obtained from animal sources. Moreover, the majority of proteins used in the development of new scaffolds for tissue engineering are extracted from natural sources. However, this strategy can have side effects since in the case of proteins extracted from animal tissues, such as collagen and fibrin; there are risks of disease transmission and allergic reactions. Biotechnology can be a powerful approach and tool kit to address this problem, since many of these proteins can be expressed in heterologous systems such as *Escherichia coli*, thereby overcoming the disadvantages inherent to native sources.

3. Techniques for the functionalization of protein-based biomaterials

The properties of protein-based biomaterials can be improved by combining them with bioactive molecules to enhance *in vitro* and/or *in vivo* functions. This chapter refers to approaches used for functionalization of these biomaterials. The surface of protein-derived scaffolds can be modified by physical adsorption, physical entrapment (encapsulation) or by chemical modification. These techniques are

commonly used to functionalize protein-based biomaterials with different biologically active molecules, such as growth factors and antibiotics, improving cell and tissue responses.

Physical adsorption is a simple immobilization procedure and is frequently used to attach bioactive molecules such as extracellular matrix proteins or growth factors to the surface of scaffolds by dip coating [121]. Adsorption efficiency is dependent on the physical and chemical properties of the material, including wettability, surface topography, functional groups, pH and electrical charge, among other factors [122]. Many biomaterials are hydrophobic, therefore, methods are needed to enhance wettability to make them more hydrophilic. Physical methods such as bombardment with ions, UV light and plasma modification are used to disrupt chemical bonds between carbon and non-carbon atoms generating unsaturated bonds and radicals which react with oxygen, increasing hydrophilicity and enhancing reactivity towards biological molecules [122]. Natural polymers have the advantage of being rich in reactive chemical groups (hydroxyl, carboxyl, amide) which make them more hydrophilic and capable of interacting with bioactive molecules. Collagen and silk are examples of protein-based materials that have been functionalized through adsorption of bioactive molecules, including bone morphogenetic proteins (BMPs) [123, 124], basic fibroblast growth factor (bFGF) [125], vascular endothelial growth factor (VEGF) [126] and therapeutic compounds such as antibiotics [127] and heparin [128] as it is summarized in Table I.2. In most of these studies the protein-based scaffolds were soaked in a solution containing the bioactive component. In other cases the proteins were blended with the bioactive molecule in solution and then cast to form scaffolds [129].

Since adsorption is based on relatively weak or moderate electrostatic, van der Waals , hydrogen and hydrophobic interactions the binding stability of the adsorbed molecules can vary depending on environmental conditions. In this way, changes in pH, ionic strength and adsorbed species concentration of the surrounding medium can result in an uncontrolled release of the immobilized species [121]. For example, bone morphogenetic proteins (BMPs) tend to diffuse away from the fracture area and high doses are required to induce the desired osteogenic response. The release profile of BMP-2 from collagen sponges shows an initial burst during the first 10 minutes, where

the carrier loses around 30% of the BMP-2, followed by slow release during the next 3 to 5 days. This initial burst release can cause clinical complications, such as ectopic bone formation, soft tissue hematomas and bone resorption [130, 131].

To overcome these issues, **covalent immobilization** has been widely used since it has the advantage of providing stable attachment of bioactive agents to polymeric scaffolds. With proper design, covalent conjugation has proven to be a very effective strategy to control the release profile of the immobilized agent since these molecules are retained for longer time periods at the delivery site, when compared with adsorption [11]. Carbodiimide coupling is broadly used in protein chemistry to react activated surface carboxylic acid groups from protein-based scaffolds with the amines present on the peptide or protein to be immobilized [132, 133]. Carboxylic groups are activated by using 1-ethyl-3-(3-dimethylaminopropyl)-carbodiimide (EDC) mixed with either N-hydroxysuccinimide (NHS), dicyclohexyl-carboiimide (DCC) or carbonyl diimidazole (CDI) [132, 133]. This basic protein chemistry has been extensively used to immobilize molecules as it is shown in Table I.2, including BMPs and RGD peptides onto silk and collagen scaffolds. A drawback of this coupling method is the difficulty in characterizing the new peptide-protein scaffolds, due to the background noise from the protein scaffold itself, making it difficult to measure the signal coming from the small amount of peptide immobilized on the scaffold surface in order to quantify how much peptide was immobilized [133]. Another drawback can be the presence of reactive amine groups aside from the N-terminal amine. These reactive side groups need to e protected, followed by deprotection after the coupling chemistry is carried out, although the use of harsh conditions can affect the biological activity of the immobilized molecules [132].

Glutaraldehyde, polyethylene glycol diacrylate and hexamethylene diisocyanate can be used to bridge the amine groups present in the peptide or protein to be immobilized and in the protein based scaffolds [133, 134]. Glutaraldehyde has been used to couple insulin [135] and lipase [136] onto silk scaffolds and to crosslink blends of collagen and silk [137]. However, the potential release of toxic residual molecules formed during the crosslinking process is a concern if these biomaterials are to be used for biomedical applications [134].

Encapsulation of bioactive molecules within protein matrices has also been explored as a method to control the release of bioactive agents. In many cases chemical modifications are required in order to have better control over the release profile of the encapsulated molecules. Crosslinked gelatin microspheres later impregnated with basic fibroblast growth fact (bFGF) and loaded into collagen sponges were used in order to have controlled release of bFGF at a defect site [138] (Table I.2). Furthermore, crosslinked collagen microspheres loaded with bovine serum albumin (BSA) and nerve growth factor were prepared and release profiles assessed [139]. In both studies collagen microspheres had to be crosslinked in order to reduce the initial burst and attain better control of protein release. EDC and NHS were also used as coupling reagents to covalently bind 2,3-dihydroxybenzoic to gelatin microspheres, which were incorporated into a reconstituted collagen scaffold for a wound dressing [140]. Silk microspheres were used for the encapsulation of bioactive proteins and other molecules, exploiting the self-assembly properties of silk to control the release profile [141].

Many formulations and delivery strategies have been explored in order to achieve functionalization and sustained release of different molecules. However, in the particular case of bioactive proteins loaded into protein-based scaffolds, protein structure and topology must be considered in order to prevent protein denaturation, as a consequence of the adsorption or immobilization processes, and protein aggregation during the release period which can result in the loss of bioactivity [11, 179]. Proteins in denatured forms are often antigenic and can induce immunogenic reactions with negative clinical consequences [179].

Most of the methods being used for functionalization of polymeric structures and drug release have some disadvantages and new strategies are clearly needed. Advances in the fields of self-assembly and biotechnology, mainly via recombinant DNA approaches, can offer some important options to address the deficiencies noted above, to help in the development of the next generation of biomaterials.

Table I.2. Summary of protein based scaffolds functionalized with different bioactive molecules.

Protein matrices	Modification process	Modifying molecule	Application	References
Collagen	EDC/NHS covalent immobilization	VEGF	Vascularisation/angiogenesis	[142, 143]
		FGF/VEGF	Vascularisation/angiogenesis	[144]
		Heparin	BMP/FGF/PDGF delivery system	[145-147]
	Traut's Reagent and Sulfo-SMCC covalent immobilization	poly-Histidine antibody	BMP delivery system	[148]
		VEGF	Vascularisation/angiogenesis	[149]
	Adsorption	BMP-2	BMP delivery system	[150]
		FGF	Cartilage regeneration/Growth factor delivery	[151, 152]
	Microsphere encapsulation	BMP-7	BMP delivery system	[153]
		VEGF	Vascularisation/angiogenesis	[154]
Gelatin	EDC covalent immobilization	TGF-beta	Cartilage regeneration	[155]
	Adsorption	TGF-beta/IGF	Cartilage regeneration	[156]
		FGF	Growth factor delivery	[151]
		Fibronectin	Cartilage regeneration	[157]
	Microsphere encapsulation	TGF-beta	Chondrogenesis/cartilage regeneration	[158, 159]
		BMP-2/VEGF	Angiogenesis and osteogenesis	[160]
		BMP-2	Growth factor delivery	[161]
Fibrin	Microsphere encapsulation	FGF	Angiogenesis	[162]
		BMP-2	Bone regeneration	[163, 164]
	Patterning immobilization	FGF-2	Tissue engineering	[165]
Heparin	Michael type addition	BMP-2	Bone/ligament regeneration	[166]
		HGF	Hepatocyte differentiation	[167]
Silk	Cyanuric chloride immobilization	Lactose	Hepatocyte attachment	[168]
	Cross-linking	Gelatin	Tendon tissue engineering	[169]
	Adsorption	FGF	Growth factor delivery	[170]
		Gelatin	Drug/Growth factor delivery	[171]
		Collagen/chodroitin-6-sulfate/hyaluronan	Tendon tissue engineering	[172]

		Collagen	tendon tissue engineering	[173, 174]
		BMP-2	Bone regeneration	[175]
	Microsphere encapsulation	IGF	Drug/Growth factor delivery	[176]
	Blend	Gelatin	Tissue engineering	[177]
Silk/collagen	Adsorption	SDF-1	tendon tissue engineering	[178]

4. Recombinant proteins for tissue engineering

Since mammalian tissues are the main source of materials as collagen, gelatin, fibrin and elastin there are concerns with disease transmission and immunogenic responses in *in vivo* studies, as well as batch-to-batch variability [20, 180]. To overcome these limitations, peptide synthesis and recombinant DNA protein methodologies have been explored. Chemical synthesis can be a quick and efficient method to fabricate short peptides in relatively small quantities [181]. However, the synthesis of peptide sequences with more than 35-40 amino acids is not feasible due to a drop in yield and efficiency paralleled by an exponential increase in cost [182]. Recombinant DNA technology provides well established protocols for cloning, mutation and gene fusion in different host cells for the expression of peptides and proteins with a broad range of sizes [183]. Furthermore, the increased efficiency in making synthetic oligonucleotides and the use of standardized kits and protocols for cloning and protein expression make the transgenic production approach more cost-effective for large scale protein production [183]. Besides engineering biological components already present in nature as shown in Table I.3, the field of synthetic biology is also focused on the design of new peptides and protein sequences. This can be achieved by establishing new artificial self-assembling peptides or by fusing together different bioactive domains or protein motifs that are not otherwise found together in nature. Table I.4 gives an overview of the studies published during the past few years using this approach [183]. Since genetic engineering offers the possibility of altering the amino acid sequence of the expressed protein by adding or substituting codons, it is possible to generate alternative sequences with tunable properties that can be used as promising biomaterials for medical applications.

Below we will address some of the proteins that have been effectively cloned and expressed in different recombinant systems. The potential of genetic engineering to be used as a tool for the functionalization of biopolymers with different bioactive peptides through the synthesis of new fusion proteins will also be discussed.

Collagen has been cloned and expressed in recombinant systems (Table I.3). The use of recombinant collagen has benefits since it can be a safe product with useful self-assembly features [183] and the possibility of being functionalized with bio-instructive domains [20] such as cell adhesion ligands [180]. Over the past 20 years

recombinant systems for the large scale-production of recombinant collagen have been developed and optimized. Recombinant collagen has been expressed in mammalian cells, insect cells, *Escherichia coli* (*E. coli*), transgenic tobacco, mice and silkworm [184]. From these recombinant hosts only the mammalian cells expressed collagen with 4-hydroxyproline content identical to native collagen. However, since the level of protein production was low (0.6-20 mg/ml) this system was not commercially viable [185]. Since the production cost in yeast and *E. coli* is much lower than in mammalian cell culture, a multigene expression technology was adopted in order to overcome the absence of the enzyme prolyl 4-hydroxylase, an essential element in the synthesis of fully hydroxylated collagens [185]. The absence of this enzyme leads to non-triple-helical and non-functional collagen molecules, which are unstable below physiological temperatures and thus unsuitable for medical applications. Hence, the multigene expression approach based on the co-expression of procollagen polypeptide chains and α- and β-subunits of proyl 4-hydroxylase using the yeast, *Pichia pastoris,* was developed [186]. Collagen types I, II and III were expressed with a 4-hydroxyproline content identical to the native human proteins and expression levels of 0.2 to 0.6 g/ml in 2 L bioreactors were achieved [186]. The use of recombinant collagen as a gel has been reported for chondrocytes [187], as a microcarrier [188], as corneal substitutes [189] and for bone regeneration applications [190]. Furthermore, customized collagen-like peptides formed with tandem repeats of the D4 domain of human collagen type II, a critical sequence for supporting the migration of chondrocytes, were also reported [140]. Chondrocytes seeded on polyglycolic acid scaffolds coated with this collagen-like protein formed cartilaginous constructs with superior properties to the scaffolds coated with native type II collagen [191]. These advances highlight the importance of recombinant DNA technology in the synthesis of proteins with applications that until now have only been available from animal sources.

Recombinant DNA technology was particularly advantageous in the expression of large and repetitive proteins such as silk. As in the case of collagen, different expression hosts have been explored for the biosynthesis of spider silk (Table I.3). Major ampullate silk was successfully expressed by bovine mammary epithelial cells, hamster kidney cells, insect cells and in the milk of transgenic goats, generally with low

yields [241]. However, bacteria can be grown at large scales and have the advantage of being easier to handle and more cost-effective. Therefore, *E. coli* has been actively pursued as an expression host for spider silks. Since bacterial hosts have distinct codon usages, silk sequences from different spider species were reverse transcribed into cDNA, using the *E. coli* codon preferences, and double stranded oligonucleotides coding for different domains of silk proteins were prepared [242]. These double strand oligonucleotides were then assembled into synthetic genes coding for silk proteins [241]. This cloning strategy was employed with successes for the expression of *Nephila clavipes* consensus sequence for major ampullate silk protein 1 (MaSp1) and MaSp2 [243] and the flagelliform silk protein [235] from the same species. Cloning and expression in *E. coli*, of both major ampullate silks ADF-3 and ADF-4 from the species *Araneus diadematus* was also reported (Table I.3) with yields between 140 and 360 mg/ml [234]. Besides *E. coli*, other hosts for the cloning and expression of spider silks have also been explored. The yeast *Pichia pastoris* is considered an attractive host for the expression of recombinant proteins since this expression system is well developed for industrial fermentation, reaching high cell densities using low-cost media. For these reasons it was successfully used for the expression of spider silk dragline using genes of up to 3,000 codons with no evidence of truncated synthesis, a common occurrence in *E. coli* host [233]. Plants such as tobacco and *Arabidopsis thaliana* are also being explored as transgenic host systems for silk proteins, with yields of 2% in tobacco leaves, 8.5% in *A. thaliana* leaf apoplasts and 18% in the endoplasmic reticulum of seeds [241]. Similar approaches as above for collagens and silks have been applied to the fabrication of recombinant elastin-like proteins that mimic native elastin (Table I.3) [50]. These new protein polymers have a modular structure formed with repeats of the pentapeptide $(VP\text{-}Xaa\text{-}Yaa\text{-}G)_n$ where Xaa is either G or A and Yaa can be any residue but P. These recombinant elastin-like proteins are capable of reversible temperature-dependant self assembly in aqueous medium [74].

Additionally there is the possibility of amino acid substitutions in the pentapeptide repeats and previous studies have shown that the replacement of G by A leads to mechanical changes in the protein from elastic to plastic [244]. Synthetic amphiphilic block copolymers with distinct block polarity composed of hydrophilic and hydrophobic segments can also be generated [74].

Table I.3. Biopolymers expressed in recombinant systems and their potential uses.

Protein	Expression system	Advantages/Applications	References
Collagen I	Transgenic corn	Food and pharmaceutical industries	[192]
	Yeast *Pichia pastoris*	Identical 4-hydroxyproline content to human collagen; medical applications such as corneal replacement	[186, 189, 193]
	Yeast *Saccharomyces cerevisiae*	Study of collagen expression and maturation	[194, 195]
	Mammalian HT1080 cells	Optimization of recombinant collagen expression and isolation methodology	[196, 197]
	Insect cells	Optimization of recombinant collagen expression and isolation methodology; Structural studies	[198, 199]
	Mammalian, mouse milk	Optimization of recombinant collagen expression	[200, 201]
	E. coli JM109 strain	Large quantities production / Therapeutic, biomaterial, or bioengineering applications,	[202]
	E. col	Bone tissue engineering	[190]
Collagen II	Yeast *Pichia pastoris*	Identical 4-hydroxyproline content to human collagen	[186]
	Insect cells	Optimizing recombinant collagen expression systems	[203]
Collagen III	Yeast *Pichia pastoris*	Higher production level; Identical 4-hydroxyproline content to human collagen; Scientific and medical applications such as corneal replacement	[186, 189, 204]
	Yeast *Saccharomyces cerevisiae*	Optimizing recombinant collagen expression systems	[205]
	Insect cells	4-hydroxyproline content similar to human collagen; Study of collagen chain association and folding	[206, 207]
	Silkworm	Viable expression system for bulk protein expression	[208]
Collagen V	Mammalian cells	Structural studies	[209]
Collagen VI	Mammalian cells	Collagen and heparin binding studies	[210]
Collagen VII	Mammalian cells	Study of dystrophic epidermolysis genetic disorder	[211]
Collagen X	Mammalian HEK293 cells	Optimizing recombinant collagen expression systems	[212]
Collagen XI	*E. coli* BL21	Study the regulation of collagen fibrillogenesis	[213]

Collagen-like protein	Mammalian HT1080 cells	Biomedical applications	[191, 214]
Gelatin-like proteins	Yeast *Pichia pastoris*	Biomedical applications	[215]
Elastin-like peptides	Yeast *Pichia pastoris*	Optimizing cloning and expression process	[216]
	E. coli strain BL21-Gold	Vascular replacement; Tissue engineering, controlled drug release and cell encapsulation; Biomedical applications	[217-224]
	E. coli BLR strain	Biomedical applications	[225]
Spider silk major ampullate from *Nephila clavipes*	*E. coli* RY-3041	Structural studies/Biomedical applications	[226, 227]
	E. coli SG 13009pREP4	Structural studies/Biomedical applications	[228]
	E. coli BL21	Structural studies/Biomedical applications	[229-231]
	E. coli M109 strain	Structural studies/Biomedical applications	[232]
	Yeast *Pichia pastoris*	Structural studies/Biomedical applications	[233]
Spider silk major dragline proteins ADF-3 and ADF-4 from *Araneus diadematus*	*E. coli* BLR strain	Structural studies/Biomedical applications	[234]
Spider silk flagelliform from *Nephila clavipes*	*E. coli* BL21 strain	Structural studies/Biomedical applications	[235]
Spider silk like proteins - NcDS, (SpI)7 and [(SpI)4/(SpII)1]4	*E. coli* BL21 strain	Structural studies/Biomedical applications	[236]
Fibrinogen	Mammalian cells	Fibrin sealant	[237]
	Yeast *Pichia pastoris*	Fibrin sealant	[238]
Fibronectin	*E. coli*	Cell adhesion	[239, 240]

These block copolymers exhibit tunable mechanical and amphiphilic properties dependent on the amino acid substitution. The flexibility of these block copolymer designs extends the range of applications from micelles formed by self-assembly of amphiphilic sequences for drug delivery, to temperature responsive hydrogels for cell encapsulation and coatings of medical devices to improve host responses [245-247]. Genetic engineering also offers the possibility of enriching the sequences of proteins to improve their biological activity by fusing them with other protein motifs with specific bioactivities (Table I.4). Initial elastin matrices for cell adhesion showed that cells did not adhere to these biomaterials [248]. RGD and REV cell adhesion peptide sequences were inserted into the elastins leading to a dramatic increase in cell attachment [246, 247]. Silk-based block copolymers were also engineered to carry an RGD cell binding domain for intracellular gene delivery and by confocal laser scanning microscopy was possible to observe the presence of labelled DNA inside cells demonstrating the potential of these silk bioengineered block copolymers as highly tailored gene delivery systems [249]. The addition of a recognition site for an enzyme with proteolytic activity can also be incorporated into the sequences, favouring biomaterials degradation [250]. The fusion of the *N. clavipes* consensus sequence for MaSp1 with proteins such as dentin matrix protein and bone sialoprotein, involved in calcium phosphate deposition in teeth and bone [251, 252], respectively, also had positive results from a biomaterials perspective [253, 254]. In both fusion proteins the silk domain retained its self assembly properties and the dentin matrix protein and bone sialoprotein domains maintained their ability to induce the deposition of calcium phosphates. These results demonstrated the potential of chimeric proteins for applications in tissue engineering and regenerative medicine for the design of new protein-based scaffolds for bone regeneration [253, 254].

Furthermore, promising results were also obtained when the *N. clavipes* consensus sequence for MaSp1 was fused with antimicrobial peptides, namely neutrophil defensins 2 and 4 and hepcidin, using a step-by-step cloning methodology [255]. The cloning and expression of these new fusion proteins expanded these chimera or fusion approaches to include antimicrobial-functionalized protein-based biomaterials [255] offering a path forward in reducing the use of antibiotics to prevent

infection in implants and in the design of a new generation of protein-based materials bioengineered to prevent the onset of infections.

Other proteins have also been expressed as fusion proteins with biological activity, such as FGF2-FNIII9-10 formed by a fibronectin fragment FNIII9-10 connected to the carboxy terminus of fibroblast growth factor 2 (FGF-2). Previous studies reported the synergistic effect of fibronectin and FGF-2 on osteoblast adhesion. The FGF2-FNIII9-10 fusion protein showed a significant increase in cell adhesion and proliferation when compared with FNIII9-10 alone [262]. The cell-binding domain of human fibronectin was also fused with epidermal growth factor (EGF), important in tissue regeneration to accelerate wound healing and enhance cell proliferation. The new construct, designated as C-EGF, had both cell-adhesive and EGF activity and the recombinant construct may be an effective drug delivery system for EGF in therapeutic situations [276]. EGF polypeptide was fused with collagen type III and the new construct retained the triple helix of collagen and the mitogenic activity of EGF, suggesting that this protein could be used as a biocompatible, biodegradable and adhesive fibrous mitogen for tissue regeneration [263].

The examples outlined above highlight the potential of synthetic biology in the synthesis of biopolymers for tissue engineering and regenerative medicine (Figure I.1.).

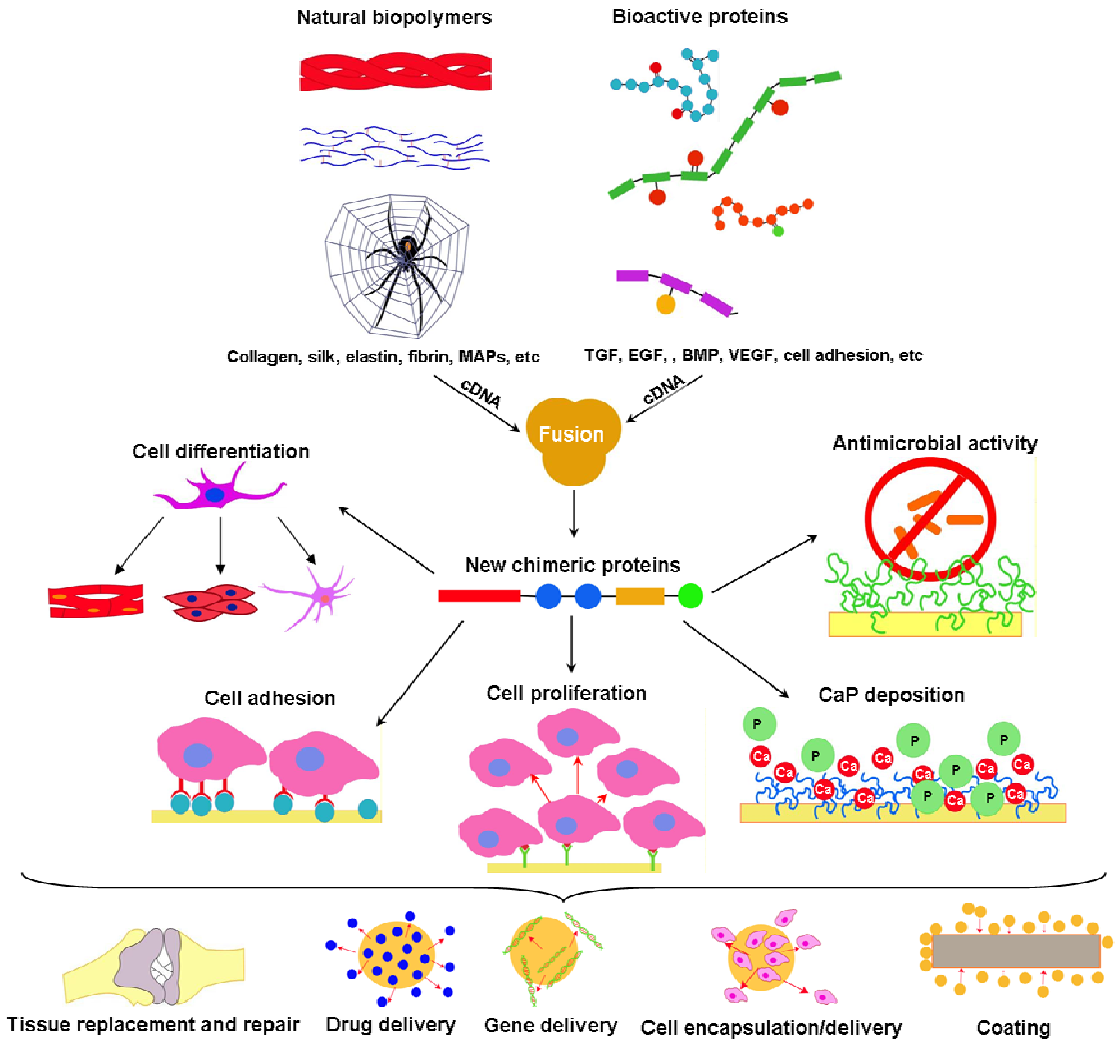

Figure I.1. Scheme highlighting some of the features and applications of chimeric protein-based biomaterials synthesized through recombinant DNA technology.

Table I.4. New chimeric proteins with potential application in the biomedical field.

Fusion protein	Expression system	Applications	References
R136K (FGF-1 mutant) + collagen biding domain	*E. coli* BL21 (pLysS) strain	Selective binding to collagen and potent angiogenic, mitogenic and chemotactic activity for endothelial cells	[256, 257]
VEGF + collagen biding domain	*E. coli* BL21 strain	Improve diabetic wound healing	[258]
FGF + fibronectin cell-binding domain	*E. coli* JM109 strain	Stimulates angiogenesis, biomedical applications/tissue engineering	[259]
FGF + collagen-binding domain	*E. coli* BL21strain	Delivery systems/Biomedical applications/Tissue engineering	[260]
FGF + glutathione S-transferase (GST-bFGF)	*E. coli*	Stimulate the growth of human umbilical vein endothelial cells	[261]
FGF2 + Fibronectin (FGF2-FNIII9-10)	*E. coli* TOP10 strain	Delivery of bioactive molecules	[262]
EGF + collagen-binding domain	*E. coli* BL21(DE3) strain	Delivery systems/Biomedical applications/Tissue engineering	[260]
EGF-collagen	Insect cells	Tissue engineering applications	[263]
EGF + immunoglobulin G (IgG) Fc region (EGF-Fc)	*E. coli* BL21 strain	Cell adhesion	[264]
Silk + elastin (SELP-47 K)	*E. coli*	Promote cell attachment and growth/Tissue Engineering	[265]
Spider silk + dentin matrix protein	*E. coli* RY-3041 strain	Biomedical applications/Tissue engineering	[254]
Spider silk + bone sialoprotein	*E. coli* RY-3041 strain	Biomedical applications/Tissue engineering	[253]
Spider silk + antimicrobial domain (HNP-2, HNP-4 and hepcidin)	*E. coli* RY-3041 strain	Biomedical applications/Tissue engineering	[255]
Bombyx mori silk + RGD + elastin (FES8)	*E. coli* BL21 strain	Biomedical applications	[266]
RGDS + silk fibroin (RGDSx2 fibroin)	Silkworm	Facilitate chondrogenesis	[267]
Collagen + GYIPEAPRDGQAYVRKDGEWVLLSTFL	*E. coli* BL21 strain	Stabilize the triple helix formed in the proteins/Biomedical applications	[268]
BMP-2 + collagen-biding domain	*E. coli* BL21strain	Bone repair	[269-271]
TGF-B1-F1 and TGF-B1-F2 + collagen-binding domain	*E. coli*	Biomedical applications/Tissue engineering	[272]
hbFGF-F1 and hbFGF-F2 + collagen-binding domain	*E. coli*	Biomedical applications/Tissue engineering	[273]
PDGF + collagen-binding domain	*E. coli* BL21 strain	Tissue regeneration and wound repair	[274]
Fibrinectin III7–10 + cadherin 11 EC 1–2	*E. coli* Rosetta-gami strain	Orthopaedic regeneration	[275]

Fibronectin cell-binding domain-EGF (C-EGF)	*E. coli* HBIOI strain	Drug delivery	[276]
Fibronectin cell-binding domain-EGF (FNCBD-EGF)	*E. coli*	Skin wounds, catheter-injured arteries, and hind limb muscles	[277]
RGD/EGF/hydrophobic sequence E12 (ERE–EGF)	*E. coli*	Controlling cell functions	[278]
NGF-β + collagen-binding domain	*E. coli* BL21strain	Delivery system for neuronal development and regeneration	[279]

5. Conclusions

Genetic engineering makes it possible to develop new biopolymers with a complexity and functionality resembling natural polymers formed in nature. By using synthetic DNA it is possible to combine different functional domains for a fusion protein, merging cell adhesion and migration, mechanical properties and antimicrobial factors, towards multifunctional biomaterial systems. This approach obviates the need for several chemical methodologies, such as covalent binding of bioactive motifs and crosslinking, which can have drawbacks of protein denaturation and residuals with toxicity. Although there has been a significant progress in exploiting genetic engineering for tissue engineering and regenerative medicine purposes during recent years, there remains a lot to be explored in order to take full advantage of the outstanding potential of genetic engineering to be used as a tool in the development of the next generation of custom-design biomaterials.

Acknowledgements

Sílvia Gomes thanks the Portuguese Foundation for Science and Technology (FCT) for providing her a PhD grant (SFRH/BD/28603/2006). This work was carried out under the scope of the FIND & BIND project funded by the agency EU-EC (FP7 program), the FCT R&D project ProteoLight (PTDC/FIS/68517/2006) funded by the FCT agency, the Chimera project (PTDC/EBB-EBI/109093/2008) funded by the FCT agency, the NIH (P41 EB002520) Tissue Engineering Resource Center and the NIH (EB003210 and DE017207).

References

1. Tsubouchi M, Matsui S, Banno Y, Kurokawa K, Kawakami K. Overview of the clinical application of regenerative medicine products in Japan. Health Policy 2008;88:62-72.

2. Masuko T, Iwasaki N, Yamane S, Funakoshi T, Majima T, Minami A, et al. Chitosan–RGDSGGC conjugate as a scaffold material for musculoskeletal tissue engineering. Biomaterials 2005;26:5339-5347.

3. Weir MD, Xu HHK. Osteoblastic induction on calcium phosphate cement-chitosan constructs for bone tissue engineering. J Biomed Mater Res A 2010;94A(1):223-233.

4. George A, Ravindran S. Protein templates in hard tissue engineering. Nano Today 2010;5:254-266.

5. Zhang L, Rodriguez J, Raez J, Myles AJ, Fenniri H, Webster T. Biologically inspired rosette nanotubes and nanocrystalline hydroxyapatite hydrogel nanocomposites as improved bone substitutes. Nanotechnology 2009;20:175101-175113.

6. Laurencin CT, Ambrosio AMA, Borden MD, Cooper JA. Tissue engineering: orthopedic applications. Annu Rev Biomed Eng 1999;1:19-46.

7. Gunatillake PA, Adhikari R. Biodegradable synthetic polymers for tissue engineering. Eur Cell Mater 2003;5:1-16.

8. Sokolsky-Papkov M, Agashi K, A.Olaye, Shakesheff K, Domb AJ. Polymer carriers for drug delivery in tissue engineering. Adv Drug Deliv Rev 2007;59(4-5):187-206.

9. Mark Kvd, Park J, Bauer S, Schmuki P. Nanoscale engineering of biomimetic surfaces: cues from the extracellular matrix. Cell Tissue Res 2010;339(1):131-153.

10. Williams DJ, Sebastine IM. Tissue engineering and regenerative medicine: manufacturing challenges. IEE Proc-Nanobiotechnol 2005;152(6):207-210.

11. Biondi M, Ungaro F, Quaglia F, Netti PA. Controlled drug delivery in tissue engineering. Adv Drug Deliv Rev 2008;60:229-242.

12. Kohn J, Welsh WJ, Knight D. A new approach to the rationale discovery of polymeric biomaterials. Biomaterials 2007;28:4171-4177.

13. Bie CD. Genzyme: 15 years of cell and gene therapy research. Regen Med 2007;2(1):95-97.

14. Basad E, Ishaque B, Bachmann G, Stürz H, Steinmeyer J. Matrix-induced autologous chondrocyte implantation versus microfracture in the treatment of cartilage defects of the knee: a 2-year randomised study. Knee Surg Sports Traumatol Arthrosc 2010;18:519-527.

15. Zaulyanov L, Kirsner RS. A review of a bi-layered living cell treatment (Apligraf) in the treatment of venous leg ulcers and diabetic foot ulcers. Clin Interv Aging 2007;2(1):93-98.

16. Degim IT, Çelebi N. Controlled delivery of peptides and proteins. Curr Pharm Des 2007;13:99-117.

17. Taylor PM, Cass AEG, Yacoub MH. Extracellular matrix scaffolds for tissue engineering heart valves. Prog Pediatr Cardiol 2006;21:219-225.

18. Patterson J, Martino MM, Hubbell JA. Biomimetic materials in tissue engineering. . Materials Today 2010;13(1-2):14-22.

19. Krishna OD, Kiick KL. Protein- and peptide-modified synthetic polymeric biomaterials. Biopolymers 2010;94(1):32-48.

20. Romano NH, Sengupta D, Chung C, Heilshorn SC. Protein-engineered biomaterials: nanoscale mimics of the extracellular matrix Biochim Biophys Acta 2010;doi:10.1016/j.bbagen.2010.07.005.

21. Zelzer M, RV RVU. Next-generation peptide nanomaterials: molecular networks, interfaces and supramolecular functionality. Chem Soc Rev 2010;39(9):3351-3357.

22. Mano JF, Silva GA, Azevedo HS, Malafaya PB, Sousa RA, Silva SS, et al. Natural origin biodegradable systems in tissue engineering and regenerative medicine: present status and some moving trends. J R Soc Interface 2007;4(17):999-1030.

23. Silva SS, Mano JF, Reis RL. Potential applications of natural origin polymer-based systems in soft tissue regeneration. Crit Rev Biotechnol 2010;30(3):200-221.

24. Chung HJ, Park TG. Surface engineered and drug releasing pre-fabricated scaffolds for tissue engineering. Adv Drug Deliv Rev 2007;59:249-262.

25. Heim M, Römer L, Scheibel T. Hierarchical structures made of proteins. The complex architecture of spider webs and their constituent silk proteins. Chem Soc Rev 2010;39(1):156-164.

26. Harkness RD. Biological functions of collagen. Biol Rev 1961;36:399-463.

27. Lee CH, Singla A, Lee Y. Biomedical applications of collagen. Int J Pharm 2001;221:1-22.

28. Kadler KE, Baldock C, Bella J, Boot-Handford RP. Collagens at a glance. J Cell Sci 2007;120(12):1955-1958.

29. Veit G, Kobbe B, Keene DR, Paulsson M, Koch M, Wagener R. Collagen XXVIII, a novel von Willebrand factor A domain containing protein with many imperfections in the collagenous domain. J Biol Chem 2006;81(6):3494-3504.

30. Heino J, Huhtala M, Käpylä J, Johnson MS. Evolution of collagen-based adhesion systems. Int J Biochem Cell Biol 2009;41:341-348.

31. Shoulders MD, Raines RT. Collagen structure and stability. Annu Rev Biochem 2009;78:929-958.

32. Hubbell JA. Materials as morphogenetic guides in tissue engineering. Curr Opin Biotechnol 2003;14(5):551-558.

33. Pabbruwe MB, Kafienah W, Tarlton JF, Mistry S, Fox DJ, Hollander AP. Repair next term of meniscal previous termcartilagenext term white zone tears using a stem cell/previous termcollagennext term-scaffold implant Biomaterials 2010;31(9):2583-2591.

34. Park IS, Kim SH, Kim YH, Kim IH, Kim SH. A collagen/smooth muscle cell-incorporated elastic scaffold for tissue-engineered vascular grafts. J Biomater Sci Polym Ed 2009;20(11):1645-1660.

35. Helary C, Bataille I, Abed A, Illoul C, Anglo A, Louedec L, et al. Concentrated collagen hydrogels as dermal substitutes. Biomaterials 2010;31(3):481-490.

36. Wehrhan F, Nkenke E, Melnychenko I, Amann K, Schlegel KA, Goerlach C, et al. Skin repair using a porcine collagen I/III membrane--vascularization and epithelization properties. Dermatol Surg 2010;36(6):919-930.

37. Lyons FG, Al-Munajjed AA, Kieran SM, Toner ME, Murphy CM, Duffy GP, et al. The healing of bony defects by cell-free collagen-based scaffolds compared to stem cell-seeded tissue engineered constructs. Biomaterials 2010;31(35):9232-9243.

38. Kleinmann G, Larson S, Hunter B, Stevens S, Mamalis N, Olson RJ. Collagen shields as a drug delivery system for the fourth-generation fluoroquinolones. Ophthalmologica 2007;221(1):51-56.

39. Maeda M, Keiichi Kadota MK, Akihiko Sano and Keiji Fujioka. Sustained release of human growth hormone (hGH) from collagen film and evaluation of effect on wound healing in db/db mice. J Control Release 2001;77(3):261-272.

40. Jeong SI, Kim SY, Cho SK, Chong MS, Kim KS, Kim H, et al. Tissue-engineered vascular grafts composed of marine collagen and PLGA fibers using pulsatile perfusion bioreactors. Biomaterials 2007;28(6):1115-1122.

41. Tierney CM, Haugh MG, Liedl J, Mulcahy F, Hayes B, O'Brien FJ. The effects of collagen concentration and crosslink density on the biological, structural and mechanical properties of collagen-GAG scaffolds for bone tissue engineering J Mech Behav Biomed Mater 2009;2(2):202-209.

42. Faralli JA, Schwinn MK, Gonzalez JM, Filla MS, Peters DM. Functional properties of fibronectin in the trabecular meshwork. Exp Eye Res 2009;88(4):689-693.

43. Mao Y, Schwarzbauer JE. Fibronectin fibrillogenesis, a cell-mediated matrix assembly process Matrix Biology 2005;24(6):389-399.

44. Pankov R, Yamada KM. Fibronectin at a glance. J Cell Sci 2002;115:3861-3863.

45. Rexeisen EL, Fan W, Pangburn TO, Taribagil RR, Bates FS, Lodge TP, et al. Self-Assembly of fibronectin mimetic peptide-amphiphile nanofibers. Langmuir 2009;26(3):1953-1959.

46. Amaral IF, Unger RE, Fuchs S, Mendonça AM, Sousa SR, Barbosa MA, et al. Fibronectin-mediated endothelialisation of chitosan porous matrices. Biomaterials 2009;30:5465-5475.

47. Custódio CA, Alves CM, Reis RL, Mano JF. Immobilization of fibronectin in chitosan substrates improves cell adhesion and proliferation. J Tissue Eng Regen Med 2010;4:316-323.

48. Bush KA, Pins GD. Carbodiimide conjugation of fibronectin on collagen basal lamina analogs enhances cellular binding domains and epithelialization. Tissue Eng Part A 2010;16(3):829-838.

49. Barbucci R, Magnani A, Chiumiento A, Pasqui D, Cangioli I, Lamponi S. Fibroblast cell behavior on bound and adsorbed fibronectin onto hyaluronan and sulfated hyaluronan substrates. Biomacromolecules 2005;6(2):638-645.

50. Almine JF, Bax DV, Mithieux SM, Nivison-Smith L, Rnjak J, Waterhouse A, et al. Elastin-based materials. Chem Soc Rev 2010;39:3371-3379.

51. Nettles DL, Chilkoti A, Setton LA. Applications of elastin-like polypeptides in tissue engineering. Adv Drug Deliv Rev 2010;62(15):1479-1485.

52. Vrhovski B, Weiss AS. Biochemistry of tropoelastin. Eur J Biochem 1998;258(1):1-18.

53. Janmey PA, Winer JP, Weisel JW. Fibrin gels and their clinical and bioengineering applications. J R Soc Interface 2009;6(30):1-10.

54. Mosesson MW, Siebenlist KR, Meh DA. The structure and biological features of fibrinogen and fibrin. Ann N Y Acad Sci 2001;936:11-30.

55. Durbeej M. Laminins. Cell Tissue Res 2010;339:259-268.

56. Schvartz I, Seger D, Shaltiel S. Vitronectin. Int J Biochem Cell Biol 1999;31(5):539-544.

57. Hill P, Brantley H, Dyke MV. Some properties of keratin biomaterials: kerateines Biomaterials 2010;31(4):585-593.

58. Lane EB, McLean WHI. Keratins and skin disorders. J Pathol 2004;204(4):355-366.

59. Hardy JG, Scheibel TR. Silk-inspired polymers and proteins. Biochem Soc Trans 2009;37:677-681.

60. Omenetto FG, Kaplan DL. New opportunities for an ancient material. Science 2010;329(5991):528-531.

61. Murphy JL, Vollenweider L, Xu F, Lee BP. Adhesive performance of biomimetic adhesive-coated biologic scaffolds. Biomacromolecules 2010;DOI: 10.1021/bm1007794.

62. Wittmer CR, Phelps JA, Saltzman WM, Tassel PRV. Fibronectin terminated multilayer films: protein adsorption and cell attachment studies. Biomaterials 2007;28:851-860.

63. Debelle L, Tamburro AM. Elastin: molecular description and function. Int J Biochem Cell Biol 1999;31(2):261-272.

64. Muiznieks LD, Weiss AS, Keeley FW. Structural disorder and dynamics of elastin. Biochem Cell Biol 2010;88(2):239-250.

65. Rodgers UR, S.Weiss A. Integrin αvβ3 binds a unique non-RGD site near the C-terminus of human tropoelastin. Biochimie 2004;86:173-178.

66. Sionkowska A, Skopinska-Wisniewska J, Gawron M, J. Kozlowska AP. Chemical and thermal cross-linking of collagen and elastin hydrolysates. Int J Biol Macromol 2010;47:570-577.

67. Lamprou D, Zhdan P, Labeed F, Lekakou C. Gelatine and gelatine/elastin nanocomposites for vascular grafts: processing and characterization. J Biomater Appl 2010;doi: 10.1177/0885328210364429.

68. McClure MJ, Sell SA, Simpson DG, Walpoth BH, Bowlin GL. A three-layered electrospun matrix to mimic native arterial architecture using polycaprolactone, elastin, and collagen: a preliminary study Acta Biomater 2010;6(7):2422-2433.

69. Hu X, Wang X, Rnjak J, Weiss AS, Kaplan DL. Biomaterials derived from silk-tropoelastin protein systems. Biomaterials 2010;31(32):8121-8131.

70. Wise SG, Byrom MJ, Waterhouse A, Bannon PG, Ng MKC, Weiss AS. A multilayered synthetic human elastin/polycaprolactone hybrid vascular graft with tailored mechanical properties. Acta Biomater 2010;7(1):295-303.

71. Dinerman AA, Cappello J, El-Sayed M, Hoag SW, Ghandehari H. Influence of Solute Charge and Hydrophobicity on Partitioning and Diffusion in a Genetically Engineered Silk-Elastin-Like Protein Polymer Hydrogel. Macromol Biosci 2010;10(10):1235-1247.

72. Rocha LB, Adam RL, Leite NJ, Metze K, Rossi MA. Biomineralization of polyanionic collagen–elastin matrices during cavarial bone repair. J Biomed Mater Res A 2006;79A(2):237-245.

73. Bessa PC, Machado R, Nürnberger S, Dopler D, Banerjee A, Cunha AM, et al. Thermoresponsive self-assembled elastin-based nanoparticles for delivery of BMPs J Control Release 2010;142(3):312-318.

74. Kim W, Chaikof EL. Recombinant elastin-mimetic biomaterials: emerging applications in medicine. Adv Drug Deliv Rev 2010;doi:10.1016/j.addr.2010.04.007.

75. Laura Martín MA, Alessandra Girotti, F. Javier Arias and J. Carlos Rodríguez-Cabello. Synthesis and characterization of macroporous thermosensitive hydrogels from recombinant elastin-like polymers. Biomacromolecules 2009;10(11):3015-3022.

76. Maskarinec SA, Tirrell DA. Protein engineering approaches to biomaterials design. Curr Opin Biotechnol 2005;16(4):422-426.

77. Smith GF. Fibrinogen–fibrin conversion. The mechanism of fibrin-polymer formation in solution. Biochem J 1980;185(1):1-11.

78. Blomäck B, Hessel B, Hogg D. Disulfide bridges in NH2-terminal part of human fibrinogen Thromb Res 1976;8:639-658.

79. Siebenlist KR, Diorio JP, Budzynski AZ, Mosesson MW. The polymerization and thrombin-binding properties of des-(Bβ1-42) fibrin. J Biol Chem 1990;265(30):18650-18655.

80. Ferry JD, Morrison PR. Preparation and properties of serum and plasma proteins. VIII. The conversion of human fibrinogen to fibrin under various conditions. J Am Chem Soc 1947;69(2):388-400.

81. Lorand L, Graham RM. Transglutaminases: crosslinking enzymes with pleiotropic functions. Nat Rev Mol Cell Biol 2003;4:140-156.

82. Spotnitz WD. Fibrin sealant: past, present, and future: a brief review. World J Surg 2010;34:632-634.

83. Ahmann KA, Weinbaum JS, Johnson SL, Tranquillo RT. Fibrin degradation enhances vascular smooth muscle cell proliferation and matrix deposition in fibrin-based tissue constructs fabricated in vitro. Tissue Eng Part A 2010;16(10):3261-3270.

84. Lee Y-B, Polio S, Lee W, Dai G, Menon L, Carroll RS, et al. Bio-printing of collagen and VEGF-releasing fibrin gel scaffolds for neural stem cell culture. Exp Neurol 2010;223(2):645-652.

85. Kang S-W, Kim i-S, Park K-S, Cha B-H, Shim J-H, Kim JY, et al. Surface modification with fibrin/hyaluronic acid hydrogel on solid-free form-based scaffolds followed by BMP-2 loading to enhance bone regeneration. Bone 2010;doi:10.1016/j.bone.2010.09.029.

86. Kikkawa Y, Takahashi N, Matsuda Y, Miwa T, Akizuki T, Kataoka A, et al. The influence of synthetic peptides derived from the laminin α1 chain on hepatocyte adhesion and gene expression Biomaterials 2009;30(36):6888-6895

87. Hozumi K, Akizuki T, Yamada Y, Hara T, Urushibata S, Katagiri F, et al. Cell adhesive peptide screening of the mouse laminin α1 chain G domain. Arch Biochem Biophys 2010;503(2):213-222.

88. Sarfati G, Dvir T, Elkabets M, Apte RN, Cohen S. Targeting of polymeric nanoparticles to lung metastases by surface-attachment of YIGSR peptide from laminin Biomaterials 2010;doi:10.1016/j.biomaterials.2010.09.014.

89. Schleicher I, Parker A, Leavesley D, Crawford R, Upton Z, Xiao Y. Surface modification by complexes of vitronectin and growth factors for serum-free culture of human osteoblasts. Tissue Eng 2005;11(11-12):1688-1698.

90. Steele JG, Johnson G, Underwood PA. Role of serum vitronectin and fibronectin in adhesion of fibroblasts following seeding onto tissue culture polystyrene. J Biomed Mater Res A 1992;26(7):861-884.

91. Reichl S. Films based on human hair keratin as substrates for cell culture and tissue engineering. Biomaterials 2009;30(36):6854-6866.

92. Yamauchi K, Maniwa M, Takeshi Mori. Cultivation of fibroblast cells on keratin-coated substrata. J Biomater Sci Polym Ed 1998;9(3):259-270.

93. Tachibana A, Kaneko S, Tanabe T, Yamauchi K. Rapid fabrication of keratin–hydroxyapatite hybrid sponges toward osteoblast cultivation and differentiation. Biomaterials 2005;26:297-302.

94. Fujii T, Murai S, Ohkawa K, Hirai T. Effects of human hair and nail proteins and their films on rat mast cells. J Mater Sci: Mater Med 2008;19:2335-2342.

95. Sutherland TD, Young JH, Weisman S, Hayashi CY, Merritt DJ. Insect silk: one name, many materials. Annu Rev Entomol 2010;55:171-188.

96. Sehnal F, Žurovec M. Construction of silk fiber core in Lepidoptera. Biomacromolecules 2004;5:666-674.

97. Mahoney DV, Vezie DL, Eby RK, Adams WW, Kaplan D. Aspects of the morphology of dragline silk of *Nephila clavipes*. In: Kaplan D, Adams WW, Farmer B, Viney C, editors. Silk Polymers: American Chemical Society, 1997. p. 196-210.

98. Sponner A, Vater W, Monajembashi S, Unger E, Grosse F, Weisshart K. Composition and hierarchical organisation of a spider silk. PLoS ONE 2007;2(10):e998.

99. Beek JDv, Hess S, Vollrath F, Meier BH. The molecular structure of spider dragline silk: folding and orientation of the protein backbone. Proc Natl Acad Sci USA 2002;99(16):10266-10271.

100. Gil ES, Mandal BB, Park S-H, Marchant JK, Omenetto FG, Kaplan DL. Helicoidal multi-lamellar features of RGD-functionalized silk biomaterials for corneal tissue engineering. Biomaterials 2010;31(34):8953-8963.

101. Lawrence BD, Marchant JK, Pindrus MA, Omenetto FG, Kaplan DL. Silk film biomaterials for cornea tissue engineering. Biomaterials 2009;30(7):1299-1308.

102. Chao P-HG, Yodmuang S, Wang X, Sun L, Kaplan DL, Vunjak-Novakovic G. Silk hydrogel for cartilage tissue engineering. J Biomed Mater Res B Appl Biomater 2010;95B(1):84-90.

103. Wang Y, Bella E, Lee CSD, Migliaresi C, Pelcastre L, Schwartz Z, et al. The synergistic effects of 3-D porous silk fibroin matrix scaffold properties and hydrodynamic environment in cartilage tissue regeneration. Biomaterials 2010;31(17):4672-4681.

104. Soffer L, Wang X, Zhang X, Kluge J, Dorfmann L, Kaplan DL, et al. Silk-based electrospun tubular scaffolds for tissue-engineered vascular grafts. J Biomater Sci Polym Ed 2008;19(15):653-664.

105. Zhou J, Cao C, Xilan Ma JL. Electrospinning of silk fibroin and collagen for vascular tissue engineering. Int J Biol Macromol 2010;47:514-519.

106. Kim HJ, Kim U-J, Kim HS, Li C, Wada M, Leisk GG, et al. Bone tissue engineering with premineralized silk scaffolds. Bone 2008;42(6):1226-1234.

107. Sofia S, McCarthy MB, Gronowicz G, Kaplan DL. Functionalized silk-based biomaterials for bone formation. J Biomed Mater Res 2001;54(1):139-148.

108. Lammel AS, Hu X, Park S-H, Kaplan DL, Scheibel TR. Controlling silk fibroin particle features for drug delivery. Biomaterials 2010;31(16):4583-4591.

109. Uebersax L, Merkle HP, Meinel L. Insulin-like growth factor I releasing silk fibroin scaffolds induce chondrogenic differentiation of human mesenchymal stem cells J Control Release 2008;127(1):12-21.

110. Spiess K, Lammel A, Scheibel T. Recombinant spider silk proteins for applications in biomaterial. Macromol Biosci 2010;10(9):998-1007.

111. Kluge JA, Rabotyagova O, Leisk GG, Kaplan DL. Spider silks and their applications. Trends Biotechnol 2008;26(5):244-251.

112. Widhe M, Bysell H, Nystedt S, Schenning I, Malmsten M, Johansson J, et al. Recombinant spider silk as matrices for cell culture. Biomaterials 2010;doi:10.1016/j.biomaterials.2010.08.061.

113. Allmeling C, Jokuszies A, K KR, Kall S, Vogt PM. Use of spider silk fibres as an innovative material in a biocompatible artificial nerve conduit. J Cell Mol Med 2006;10(3):770-777.

114. Allmeling C, Jokuszies A, Reimers K, Kall S, Choi CY, Brandes G, et al. Spider silk fibres in artificial nerve constructs promote peripheral nerve regeneration. Cell Prolif 2008;41(3):408-420.

115. Baoyong L, Jian Z, Denglong C, Min L. Evaluation of a new type of wound dressing made from recombinant spider silk protein using rat models Burns 2010;36(6):891-896.

116. Waite JH. The DOPA ephemera: a recurrent motif in invertebrates. Biol Bull 1992;183(1):178-184.

117. Deming TJ. Mussel byssus and biomolecular materials. Curr Opin Chem Biol 1999;3(1):100-105.

118. Hwang DS, Sim SB, Cha HJ. Cell adhesion biomaterial based on mussel adhesive protein fused with RGD peptide Biomaterials 2007;28(28):4039-4046.

119. Brubaker CE, Kissler H, Wang L-J, Kaufman DB, Messersmith PB. Biological performance of mussel-inspired adhesive in extrahepatic islet transplantation. Biomaterials 2010;31(3):420-427.

120. Lim S, Choi YS, Kang DG, Song YH, Cha HJ. The adhesive properties of coacervated recombinant hybrid mussel adhesive proteins Biomaterials 2010;31(13):3715-3722.

121. Beutner R, Michael J, Schwenzer B, Scharnweber D. Biological nano-functionalization of titanium-based biomaterial surfaces: a flexible toolbox. J R Soc Interface 2010;7(1):S93-S105.

122. Bačáková L, Filová E, Rypáček F, Švorčík V, Starý V. Cell adhesion on artificial materials for tissue engineering. . Physiol Res 2004;53(1):S35-S45.

123. Friess W, Uludag H, Foskett S, Biron R, Sargeant C. Characterization of absorbable collagen sponges as recombinant human bone morphogenetic protein-2 carriers International Journal of Pharmaceutics 1999;185(1):51-60.

124. Karageorgiou V, Tomkins M, Fajardo R, Meinel L, Snyder B, Wade K, et al. Porous silk fibroin 3-D scaffolds for delivery of bone morphogenetic protein-2 in vitro and in vivo. Journal of Biomedical Materials Research Part A 2006;78A(2):324-334.

125. Wongpanit P, Ueda H, Tabata Y, Rujiravanit R. In vitro and in vivo release of basic fibroblast growth factor using a silk fibroin scaffold as delivery carrier. J Biomater Sci Polym Ed 2010;21(11):1403-1419.

126. Kleinheinz J, Jung S, Wermker K, Fischer C, Joos U. Release kinetics of VEGF165 from a collagen matrix and structural matrix changes in a circulation model. Head & Face Medicine 2010;6:17.

127. Kilian O, Hossain H, Flesch I, Sommer U, Nolting H, Chakraborty T, et al. Elution kinetics, antimicrobial efficacy, and degradation and microvasculature of a new gentamicin-loaded collagen fleece. J Biomed Mater Res B Appl Biomater 2008;90B(1):210-222.

128. Wang X, Zhang X, Castellot J, Herman I, Iafrati M, Kaplan DL. Controlled release from multilayer silk biomaterial coatings to modulate vascular cell responses. Biomaterials 2008;29(7):894-903.

129. Zhao J, Shinkai M, Takezawa T, Ohba S, Chung U-i, Nagamune T. Bone regeneration using collagen type I vitrigel with bone morphogenetic protein-2 Journal of Bioscience and Bioengineering 2009;107(3):318-323.

130. Han D, Liu W, Ao Q, Wang G. Optimal delivery systems for bone morphogenetic proteins in orthopedic applications should model initial tissue repair structures by using a heparin-incorporated fibrin–fibronectin matrix Med Hypotheses 2008;71(3):374-378.

131. Shields LBE, Raque GH, D.Glassman S, Campbell M, Vitaz T, Harpring J, et al. Adverse effects associated with high-dose recombinant human bone morphogenetic protein-2 use in anterior cervical spine fusion. Spine 2006;31(5):542-547.

132. Hersel U, Dahmen C, Kessler H. RGD modified polymers: biomaterials for stimulated cell adhesion and beyond Biomaterials 2003;24(24):4385-4415.

133. Murphy AR, Kaplan DL. Biomedical applications of chemically-modified silk fibroin. J Mater Chem 2009;19(36):6443-6450.

134. Rafat M, Li F, Fagerholm P, Lagali NS, Watsky MA, Munger R, et al. PEG-stabilized carbodiimide crosslinked collagen–chitosan hydrogels for corneal tissue engineering. Biomaterials 2008;29(29):3960-3972.

135. Zhang Y-Q, Ma Y, Xia Y-Y, Shen W-D, Mao J-P, Zha X-M, et al. Synthesis of silk fibroin-insulin bioconjugates and their characterization and activities *in vivo*. J Biomed Mater Res B Appl Biomater 2006;79B(2):275-283.

136. Chatterjee S, Barbora L, Cameotra SS, Mahanta P, Goswami P. Silk-fiber immobilized lipase-catalyzed hydrolysis of emulsified sunflower oil. Appl Biochem Biotechnol 2009;157(3):593-600.

137. Yeo S, Oh J-E, Jeong L, Lee TS, Lee SJ, Park WH, et al. Collagen-based biomimetic nanofibrous scaffolds: preparation and characterization of collagen/silk fibroin bicomponent nanofibrous structures. Biomacromolecules 2008;9(4):1106-1116.

138. Kimura Y, Tsuji W, Yamashiro H, Toi M, Inamoto T, Tabata Y. In situ adipogenesis in fat tissue augmented by collagen scaffold with gelatin microspheres containing basic fibroblast growth factor. J Tissue Eng Regen Med 2010;4(1):55-61.

139. Chan OCM, So K-F, Chan BP. Fabrication of nano-fibrous collagen microspheres for protein delivery and effects of photochemical crosslinking on release kinetics. J Control Release 2008;129(2):135-143.

140. Adhirajan N, Shanmugasundaram N, Shanmuganathan S, Babu M. Functionally modified gelatin microspheres impregnated collagen scaffold as novel wound dressing to attenuate the proteases and bacterial growth Eur J Pharm Sci 2009;36(2-3):235-245.

141. Wang X, Wenk E, Matsumoto A, Meinel L, Li C, Kaplan DL. Silk microspheres for encapsulation and controlled release J Control Release 2007;117(3):360-370.

142. Miyagi Y, Chiu LLY, Cimini M, Weisel RD, Radisic M, Li R-K. Biodegradable collagen patch with covalently immobilized VEGF for myocardial repair Biomaterials 2011;32(5):1280-1290

143. Shen YH, Shoichet MS, Radisi M. Vascular endothelial growth factor immobilized in collagen scaffold promotes penetration and proliferation of endothelial cells Acta Biomater 2008;4(3):477-489.

144. Nillesen STM, Geutjes PJ, Wismans R, Schalkwijk J, Daamen WF, Kuppevelt THv. Increased angiogenesis and blood vessel maturation in acellular collagen–heparin scaffolds containing both FGF2 and VEGF. Biomaterials 2007;28(6):1123-1131.

145. Sun B, Chen B, Zhao Y, Sun W, Chen K, Zhang J, et al. Crosslinking heparin to collagen scaffolds for the delivery of human platelet-derived growth factor. J Biomed Mater Res B Appl Biomater 2009;91(1):366-372.

146. Teixeira S, Yang L, Dijkstra PJ, Ferraz MP, Monteiro FJ. Heparinized hydroxyapatite/collagen three-dimensional scaffolds for tissue engineering. J Mater Sci Mater Med 2010;21(8):2385-2392.

147. Wu JM, Xu YY, Li ZH, Yuan XY, Wang PF, Zhang XZ, et al. Heparin-functionalized collagen matrices with controlled release of basic fibroblast growth factor J Mater Sci Mater Med 2011;DOI: 10.1007/s10856-010-4176-4.

148. Zhao Y, Zhang J, Wang X, Chen B, Xiao Z, Shi C, et al. The osteogenic effect of bone morphogenetic protein-2 on the collagen scaffold conjugated with antibodies. J Control Release 2010;141(1):30-37.

149. He Q, Zhao Y, Chen B, Xiao Z, Zhang J, Chen L, et al. Improved cellularization and angiogenesis using collagen scaffolds chemically conjugated with vascular endothelial growth factor. Acta Biomater 2010;doi:10.1016/j.actbio.2010.10.022.

150. Takeda Y, Tsujigiwa H, Nagatsuka H, Nagai N, Yoshinobu J, Okano M, et al. Regeneration of rat auditory ossicles using recombinant human BMP-2/collagen composites. J Biomed Mater Res A 2005;73A(2):133-141.

151. Côté M-F, Laroche G, Gagnon E, Chevallier P, Doillon CJ. Denatured collagen as support for a FGF-2 delivery system: physicochemical characterizations and in vitro release kinetics and bioactivity. Biomaterials 2004;25(17):3761-3772.

152. Maehara H, Sotome S, Yoshii T, Torigoe I, Kawasaki Y, Sugata Y, et al. Repair of large osteochondral defects in rabbits using porous hydroxyapatite/collagen (HAp/Col) and fibroblast growth factor-2 (FGF-2). J Orthop Res 2010;28(5):677-686.

153. Gavénis K, Klee D, Pereira-Paz RM, Walter Mv, Mollenhauer J, Schneider U, et al. BMP-7 loaded microspheres as a new delivery system for the cultivation of human chondrocytes in a collagen type-I gel. J Biomed Mater Res B Appl Biomater 2007;82B(2):275-283.

154. Borselli C, Ungaro F, Oliviero O, d'Angelo I, Quaglia F, Rotonda MIL, et al. Bioactivation of collagen matrices through sustained VEGF release from PLGA microspheres. J Biomed Mater Res A 2010;92A(1):94-102.

155. Chou C-H, Cheng WTK, Lin C-C, Chang C-H, Tsai C-C, Lin F-H. TGF-beta1 immobilized tri-co-polymer for articular cartilage tissue engineering. J Biomed Mater Res B Appl Biomater 2006;77B(2):338-348.

156. Srouji S, Rachmiel A, Blumenfeld I, Livne E. Mandibular defect repair by TGF-beta and IGF-1 released from a biodegradable osteoconductive hydrogel. J Craniomaxillofac Surg 2005;33(2):79-84.

157. Kuo Y-C, Ku I-N. Effects of gel concentration, human fibronectin, and cation supplement on the tissue-engineered cartilage. Biotechnol Prog 2007;23(1):238-245.

158. Fan H, Hu Y, Li X, Wu H, Lv R, Bai J, et al. Ectopic cartilage formation induced by mesenchymal stem cells on porous gelatin-chondroitin-hyaluronate scaffold containing microspheres loaded with TGF-beta1. Int J Artif Organs 2006;29(6):602-611.

159. Ogawa T, Akazawa T, Tabata Y. In vitro proliferation and chondrogenic differentiation of rat bone marrow stem cells cultured with gelatin hydrogel microspheres for TGF-beta1 release. J Biomater Sci Polym Ed 2010;21(5):609-621

160. Kempen DHR, Lu L, Heijink A, Hefferan TE, Creemers LB, Maran A, et al. Effect of local sequential VEGF and BMP-2 delivery on ectopic and orthotopic bone regeneration. Biomaterials 2009;30(14):2816-2825.

161. Kempen DHR, Lu L, Hefferan TE, Creemers LB, Maran A, Classic KL, et al. Retention of in vitro and in vivo BMP-2 bioactivities in sustained delivery vehicles for bone tissue engineering Biomaterials 2008;29(22):3245-3252.

162. Royce SM, Askari M, Marra KG. Incorporation of polymer microspheres within fibrin scaffolds for the controlled delivery of FGF-1. J Biomater Sci Polym Ed 2004;15(10):1327-1336.

163. Chung Y-I, Ahn K-M, Jeon S-H, Lee S-Y, Lee J-H, Tae G. Enhanced bone regeneration with BMP-2 loaded functional nanoparticle-hydrogel complex. J Control Release 2007;121(1-2):91-99.

164. Park K-H, Kim H, Na SMaK. Bone morphogenic protein-2 (BMP-2) loaded nanoparticles mixed with human mesenchymal stem cell in fibrin hydrogel for bone tissue engineering. J Biosci Bioeng 2009;108(6):530-537.

165. Campbell PG, Miller ED, Fisher GW, Walker LM, Weiss LE. Engineered spatial patterns of FGF-2 immobilized on fibrin direct cell organization. Biomaterials 2005;26(33):6762-6770.

166. Lee J, Choi WI, Tae G, Kim YH, Kang SS, Kim SE, et al. Enhanced regeneration of the ligament-bone interface using a poly(L-lactide-co-ε-caprolactone) scaffold with local delivery of cells/BMP-2 using a heparin-based hydrogel. Acta Biomater 2011;7(1):244-257.

167. Kim M, Lee JY, Jones CN, Revzin A, Tae G. Heparin-based hydrogel as a matrix for encapsulation and cultivation of primary hepatocytes. Biomaterials 2010;31(13):3596-3603.

168. Gotoh Y, Niimi S, Hayakawa T, Miyashita T. Preparation of lactose–silk fibroin conjugates and their application as a scaffold for hepatocyte attachment. J Mater Chem 2004;25(6):1131-1140.

169. Fan H, Liu H, Wang Y, Toh SL, Goh JC. Development of a silk cable-reinforced gelatin/silk fibroin hybrid scaffold for ligament tissue engineering. Cell Transplant 2008;17(12):1389-1401.

170. Wongpanit P, Ueda H, Tabata Y, Rujiravanit R. In vitro and in vivo release of basic fibroblast growth factor using a silk fibroin scaffold as delivery carrier. J Biomater Sci Polym Ed 2010;21(11):1403-1419.

171. Qiang Lu, Xiaohui Zhang, Xiao Hu, Kaplan DL. Green process to prepare silk fibroin/gelatin biomaterial scaffolds. Macromol Biosci 2010;10(3):289-298.

172. Seo Y-K, Yoon H-H, Song K-Y, Kwon S-Y, Lee H-S, Park Y-S, et al. Increase in cell migration and angiogenesis in a composite silk scaffold for tissue-engineered ligaments. J Orthop Res 2009;27(4):495-503.

173. Chen X, Qia Y-Y, Wang L-L, Yin Z, Yin G-L, Zou X-H, et al. Ligament regeneration using a knitted silk scaffold combined with collagen matrix. Biomaterials
2008;29(27):3683-3692

174. Takezawa T, Ozaki K, Takabayashi C. Reconstruction of a hard connective tissue utilizing a pressed silk sheet and type-I collagen as the scaffold for fibroblasts. Tissue Eng 2007;13(6):1357-1366.

175. Kirker-Head C, Karageorgiou V, Hofmann S, Fajardo R, Betz O, Merkle HP, et al. BMP-silk composite matrices heal critically sized femoral defects. Bone 2007;41(2):247-455.

176. Wenk E, Meinel AJ, Wildy S, Merkle HP, Meinel L. Microporous silk fibroin scaffolds embedding PLGA microparticles for controlled growth factor delivery in tissue engineering. Biomaterials 2009;30(13):2571-2581.

177. Gil ES, Frankowski DJ, Bowman MK, Gozen AO, Hudson SM, Spontak RJ. Mixed protein blends composed of gelatin and Bombyx mori silk fibroin: effects of solvent-induced crystallization and composition. Biomacromolecules 2006;7(3):728-735.

178. Shen W, Chen X, Chen J, Yin Z, Heng BC, Chen W, et al. The effect of incorporation of exogenous stromal cell-derived factor-1 alpha within a knitted silk-collagen sponge scaffold on tendon regeneration. Biomaterials 2010;31(28):7239-7249.

179. Wu F, Jin T. Polymer-based sustained-release dosage forms for protein drugs, challenges, and recent advances AAPS PharmSciTech 2009;9(4):1218-1229.

180. Langer R, Tirrell DA. Designing materials for biology and medicine. Nature 2004;428:487-492.

181. Sato AK, Viswanathan M, Kent RB, Wood CR. Therapeutic peptides: technological advances driving peptides into development Curr Opin Biotechnol 2006;17(6):638-642.

182. Kastin AJ. Handbook of biologivally avtive peptides. Burlington: Elsevier, 2006.

183. Kyle S, Aggeli A, Ingham E, McPherson MJ. Production of self-assembling biomaterials for tissue engineering. Trends Biotechnol 2009;27(7):423-433

184. Báez J, Olsen D, Polarek JW. Recombinant microbial systems for the production of human collagen and gelatin. Appl Microbiol Biotechnol 2005;69(3):245-252.

185. Olsen D, Yang C, Bodo M, Chang R, Leigh S, Baez J, et al. Recombinant collagen and gelatin for drug delivery Adv Drug Deliv Rev 2003;55(12):1547-1567.

186. Myllyharju J, Nokelainen M, Vuorela A, Kivirikko KI. Expression of recombinant human type I-III collagens in the yeast pichia pastoris. Biochem Soc Trans 2000;28(4):353-357.

187. Pulkkinen HJ, Tiitu V, Valonen P, Jurvelin JS, Lammi MJ, Kiviranta I. Engineering of cartilage in recombinant human type II collagen gel in nude mouse model in vivo. Osteoarthritis and Cartilage 2010;18(8):1077-1087.

188. Dame MK, Varani J. Recombinant collagen for animal product-free dextran microcarriers In Vitro Cell Dev Biol Anim 2008;44(10):407-414.

189. Liu W, Merrett K, Griffith M, Fagerholm P, Dravida S, Heyne B, et al. Recombinant human collagen for tissue engineered corneal substitutes. Biomaterials 2008;29(9):1147-1158.

190. Wang Y, Cui FZ, Hu K, Zhu XD, Fan DD. Bone regeneration by using scaffold based on mineralized recombinant collagen. J Biomed Mater Res B Appl Biomater 2008;86(1):29-35.

191. Ito H, Steplewski A, Alabyeva T, Fertala A. Testing the utility of rationally engineered recombinant collagen-like proteins for applications in tissue engineering. J Biomed Mater Res A 2006;76A(3):551-560.

192. Zhang C, Baez J, Pappu KM, Glatz CE. Purification and characterization of a transgenic corn grain-derived recombinant collagen type I alpha 1. Biotechnol Prog 2009;25(6):1660-1668.

193. Nokelainen M, Tu H, Vuorela A, Notbohm H, Kivirikko KI, Myllyharju J. High-level production of human type I collagen in the yeast *Pichia pastoris*. Yeast 2001;18(9):797-806.

194. Olsen DR, Leigh SD, Chang R, McMullin H, Ong W, Tai E, et al. Production of human type I collagen in yeast reveals unexpected new insights into the molecular assembly of collagen trimers. J Biol Chem 2001;276(26):24038-24043.

195. Toman PD, Chisholm G, McMullin H, Giere LM, Olsen DR, Kovach RJ, et al. Production of recombinant human type I procollagen trimers using a four-gene expression system in the yeast *Saccharomyces cerevisiae*. J Biol Chem 2000;275(30):23303-23309.

196. Fertala A, Sieron AL, Ganguly A, Li SW, Ala-Kokko L, Anumula KR, et al. Synthesis of recombinant human procollagen II in a stably transfected tumour cell line (HT1080). Biochem J 1994;298(1):31-37.

197. Geddis AE, Prockop DJ. Expression of human COL1A1 gene in stably transfected HT1080 cells: the production of a thermostable homotrimer of type I collagen in a recombinant system. Matrix 1993;13(5):399-405.

198. Myllyharju J, Lamberg A, Notbohm H, Fietzek PP, Pihlajaniemi T, Kivirikko KI. Expression of wild-type and modified proα chains of human type I procollagen in insect cells leads to the formation of stable [α1(I)]2α2(I) collagen heterotrimers and [α1(I)]3 homotrimers but not [α2(I)]3 homotrimers. J Biol Chem 1997;272:21824-21830.

199. Tomita M, Kitajima T, Yoshizato K. Formation of recombinant human procollagen I heterotrimers in a baculovirus expression system. J Biochem 1997;121(6):1061-1069.

200. John DCA, Watson R, Kind AJ, Scott AR, Kadler KE, Bulleid NJ. Expression of an engineered form of recombinant procollagen in mouse milk. Nat Biotechnol 1999;17(4):385-389.

201. Toman PD, Pieper F, Sakai N, Karatzas C, Platenburg E, Wit Id, et al. Production of recombinant human type I procollagen homotrimer in the mammary gland of transgenic mice. Transgenic Res 1999;8(6):415-427.

202. Buechter DD, Paolella DN, Leslie BS, Brown MS, Mehos KA, Gruskin EA. Co-translational Incorporation of trans-4-hydroxyproline into recombinant proteins in bacteria. J Biol Chem 2003;278(1):645-650.

203. Nokelainen M, Helaakoski T, Myllyharju J, Notbohm H, Pihlajaniemi T, Fietzek PP, et al. Expression and characterization of recombinant human type II collagens with low and high contents of hydroxylysine and its glycosylated forms. Matrix Biol 1998;16(6):329-338.

204. Vuorela A, Myllyharju J, Nissi R, Pihlajaniemi T, Kivirikko KI. Assembly of human prolyl 4-hydroxylase and type III collagen in the yeast Pichia pastoris: formation of a stable enzyme tetramer requires coexpression with collagen and assembly of a stable collagen requires coexpression with prolyl 4-hydroxylase. EMBO J 1997;16(22):6702-6712.

205. Vaughan PR, Galanis M, Richards KM, Tebb TA, Ramshaw JAM, Werkmaister JA. Production of recombinant hydroxylated human type III collagen fragment in *Saccharomyces cerevisiae*. DNA Cell Biol 1998;17(6):511-518.

206. Lamberg A, Helaakoski T, Myllyharju J, Peltonen S, Notbohm H, Pihlajaniemi T, et al. Characterization of human type III collagen expressed in a baculovirus system. Production of a protein with a stable triple helix requires coexpression with the two types of recombinant prolyl 4-hydroxylase subunit. J Biol Chem 1996;271(20):11988-11995.

207. Tomita M, Ohkura N, Ito M, Kato T, Royce PM, Kitajima T. Biosynthesis of recombinant human pro-alpha 1(III) chains in a baculovirus expression system: production of disulphide-bonded and non-disulphide-bonded species containing full-length triple helices. Biochem J 1995;312(3):847-853.

208. Tomita M, Munetsuna H, Sato T, Adachi T, Hino R, Hayashi M, et al. Transgenic silkworms produce recombinant human type III procollagen in cocoons. Nat Biotechnol 2003;21:52-56.

209. Fichard A, Tillet E, Delacoux F, Garrone R, Ruggiero F. Human recombinant α1(V) collagen chain. J Biol Chem 1997;272:30083-30087.

210. Tillet E, Wiedemann H, Golbik R, Pan T-C, Zhang R-Z, Mann K, et al. Recombinant expression and structural and binding properties of α1 (VI) and α2(VI) chains of human collagen type VI. Eur J Biochem 1994;221(1):177-187.

211. Chen M, Costa FK, Lindvay CR, Han Y-P, Woodley DT. The Recombinant Expression of Full-length Type VII Collagen and Characterization of Molecular Mechanisms Underlying Dystrophic Epidermolysis Bullosa. J Biol Chem 2002;277(3):2118-2124.

212. Frischholz S, Beier F, Girkontaite I, Wagner K, Pöschl E, Turnay J, et al. Characterization of human type X procollagen and its NC-1 domain expressed as recombinant proteins in HEK293 cells. J Biol Chem 1998;273(8):4547-4555.

213. Warner LR, Blasick CM, Brown RJ, Oxford JT. Expression, purification, and refolding of recombinant collagen alpha1(XI) amino terminal domain splice variants. Protein Expr Purif 2007;52(2):403-409

214. Steplewski A, Majsterek I, McAdams E, Rucker E, Brittingham RJ, Ito H, et al. Thermostability gradient in the collagen triple helix reveals its multi-domain structure. J Mol Biol 2004;338(5):989-998.

215. Werten MWT, Teles H, Moers APHA, Wolbert EJH, Sprakel J, Eggink G, et al. Precision gels from collagen-inspired triblock copolymers. Biomacromolecules 2009;10(5):1106-1113.

216. Sallach RE, Conticello VP, Chaikof EL. Expression of a recombinant elastin-like protein in *Pichia pastoris*. Biotechnol Prog 2009;25(6):1810-1818.

217. Jordan SW, Haller CA, Sallach RE, Apkarian RP, Hanson SR, Chaikof EL. The effect of a recombinant elastin-mimetic coating of an ePTFE prosthesis on acute thrombogenicity in a baboon arteriovenous shunt. Biomaterials28 2007;6(1191-1197).

218. Nagapudi K, Brinkman WT, Leisen J, Thomas BS, Wright ER, Haller C, et al. Protein-based thermoplastic elastomers. Macromolecules 2005;38(2):345-354.

219. Panitch A, Yamaoka T, Fournier MJ, Mason TL, Tirrell DA. Design and biosynthesis of elastin-like artificial extracellular matrix proteins containing periodically spacedfibronectin CS5 domains. Macromolecules 1999;32(5):1701-1703.

220. Sallacha RE, Cui W, Balderrama F, Martinez AW, Wen J, Haller CA, et al. Long-term biostability of self-assembling protein polymers in the absence of covalent crosslinking. Biomaterials 2010;31(4):779-791.

221. Woodhouse KA, Klement P, Chen V, Gorbet MB, Keeley FW, Stahl R, et al. Investigation of recombinant human elastin polypeptides as non-thrombogenic coatings. Biomaterials 2004;25(19):4543-4553.

222. Wright ER, McMillan RA, Cooper A, Apkarian RP, Conticello VP. Thermoplastic elastomer hydrogels via self-assembly of an elastin-mimetic triblock polypeptide. Adv Funct Mater 2002;12(2):149-154.

223. Wu X, Sallach R, Haller CA, Caves JA, Nagapudi K, Conticello VP, et al. Alterations in physical cross-linking modulate mechanical properties of two-phase protein polymer networks. Biomacromolecules 2005;6(6):3037-3044.

224. Yamaoka T, Tamura T, Seto Y, Tada T, Kunugi S, Tirrell DA. Mechanism for the phase transition of a genetically engineered elastin model peptide (VPGIG)40 in aqueous solution. Biomacromolecules 2003;4(6):1680-1685.

225. Nagapudi K, Brinkman WT, Leisen JE, Huang L, McMillan RA, Apkarian RP, et al. Photomediated solid-state cross-linking of an elastin−mimetic recombinant protein polymer. Macromolecules 2002;35(5):1730-1737.

226. Rabotyagova O, Cebe P, Kaplan DL. Self-assembly of genetically engineered spider silk block copolymers. Biomacromolecules 2009;10:229–236.

227. Rabotyagova OS, Cebe P, Kaplan DL. Role of polyalanine domains in β-sheet formation in spider silk block copolymers. Macromol Biosci 2010;10:49-59.

228. Prince JT, McGrath KP, DiGirolamo CM, Kaplan DL. Construction, cloning, and expression of synthetic genes encoding spider dragline silk. Biochemistry 1995;34(34):10879-10885.

229. Arcidiacono S, Mello C, Kaplan DL, Cheley S, Bayley H. Purification and characterization of recombinant spider silk expressed in Escherichia coli. . Appl Microbiol Biotechnol 1998;49(1):31-38.

230. Fahnestock SR, Irwin SL. Synthetic spider dragline silk proteins and their production in Escherichia coli. Appl Microbiol Biotechnol 1997;47(1):23-32.

231. Lewis RV, Hinman M, Kothakota S, Fournier MJ. Expression and purification of a spider silk protein: a new strategy for producing repetitive proteins. Protein Expr Purif 1996;7(4):400-406.

232. Fukushima Y. Genetically engineered syntheses of tandem repetitive polypeptides consisting of glycine-rich sequence of spider dragline silk. Biopolymers 1998;45(4):269-279.

233. Fahnestock SR, Bedzyk LA. Production of synthetic spider dragline silk protein in *Pichia pastoris.* Appl Microbiol Biotechnol 1997;47(1):33-39.

234. Huemmerich D, Helsen CW, Quedzuweit S, Oschmann J, Rudolph R, Scheibel T. Primary structure elements of spider dragline silks and their contribution to protein solubility. Biochemistry 2004;43(42):13604-13612.

235. Zhou Y, Wu S, Conticello VP. Genetically directed synthesis and spectroscopic analysis of a protein polymer derived from a flagelliform silk sequence. Biomacromolecules 2001;2(1):111-125.

236. Mello CM, Soares JW, Arcidiacono S, Butle MM. Acid extraction and purification of recombinant spider silk proteins. Biomacromolecules 2004;5(5):1849-1852.

237. Butler SP, O'Sickey TK, Lord ST, Lubon H, Gwazdauskas FC, Velande WH. Secretion of recombinant human fibrinogen by the murine mammary gland. Transgenic Res 2004;13(5):437-450.

238. Tojo N, Miyagia I, Miuraa M, Ohi H. Recombinant human fibrinogen expressed in the yeast Pichia pastoris was assembled and biologically active. Protein Expr Purif 2008;59(2):289-296.

239. Cutler SM, Garca AJ. Engineering cell adhesive surfaces that direct integrin α5β1 binding using a recombinant fragment of fibronectin. Biomaterials 2003;24(10):1759-1770.

240. Rico P, González-García C, Petrie TA, García AJ, Salmerón-Sánchez M. Molecular assembly and biological activity of a recombinant fragment of fibronectin (FNIII(7-10)) on poly(ethyl acrylate). Colloids Surf B Biointerfaces 2010;78(2):310-316.

241. Vendrely C, Scheibel T. Biotechnological production of spider-silk proteins enables new applications. Macromol Biosci 2007;7(4):401-409.

242. Scheibel T. Spider silks: recombinant synthesis, assembly, spinning, and engineering of synthetic proteins. Microb Cell Fact 2004;3(1):14.

243. Prince JT, McGrath KP, DiGirolamo CM, Kaplan DL. Construction, cloning, and expression of synthetic genes encoding spider dragline silk. Biochemistry 1995;34(34):10879-10885.

244. Urry DW, Luan CH, Parker TM, Gowda DC, Prasad KU, Reid MC, et al. Temperature of polypeptide inverse temperature transition depends on mean residue hydrophobicity. J Am Chem Soc 1991;113(11):4346-4348.

245. Barbosa JS, Ribeiro A, Testera AM, Alonso M, Arias FJ, Rodríguez-Cabello JC, et al. Development of biomimetic chitosan-based hydrogels using an elastin-like polymer. Adv Eng Mater 2010;12(1-2):B37-B44.

246. Costa RR, Custódio CA, Testera AM, Arias FJ, Rodríguez-Cabello JC, Alves NM, et al. Stimuli-responsive thin coatings using elastin-like polymers for biomedical applications. Adv Funct Mater 2009;19(20):3210-3218.

247. Nicol A, Gowda DC, Parker TM, Urry DW. Cell adhesive properties of bioelastic materials containing cell attachment sequences. In: Gebelein C, Carraher C, editors. Biotechnology and bioactive polymers. New York: Plenum Press, 1994.

248. Urry DW, Nicol A, Gowda DC, Hoban LD, McKee A, Williams T, et al. Medical applications of bioelastic materials. In: Gebelein CG, editor. Biotechnological polymers: medical, pharmaceutical and industrial applications. Atlanta, Georgia: Technomic Publishing Co. Inc., 1993. p. 82-103.

249. Numata K, J JH, Subramanian B, Kaplan DL. Gene delivery mediated by recombinant silk proteins containing cationic and cell binding motifs. J Control Release 2010;146(1):136-143.

250. Arias FJ, Reboto V, Martín S, López I, Rodríguez-Cabello JC. Tailored recombinant elastin-like polymers for advanced biomedical and nano(bio)technological applications Biotechnol Lett 2006;28(10):687-695.

251. Benesch J, Mano JF, Reis. RL. Proteins and their peptide motifs in acellular apatite mineralization of scaffolds for tissue engineering. Tissue Eng Part B 2008;14(4):433-445.

252. Ganss B, Kim RH, Sodek J. Bone sialoprotein. Crit Rev Oral Biol Med 1999;10(1):79-98.

253. Gomes S, Leonor IB, Mano JF, Reis RL, Kaplan DL. Spider silk-bone sialoprotein as a novel fusion protein for bone tissue engineering. Soft Matter 2010;*Submitted*.

254. Huang J, Wong C, George A, Kaplan DL. The effect of genetically engineered spider silk-dentin matrix protein 1 chimeric protein on hydroxyapatite nucleation. Biomaterials 2007;28:2358–2367.

255. Gomes S, Leonor IB, Mano JF, Reis RL, Kaplan DL. Antimicrobial functionalized genetically engineered spider silk. Biomaterials 2010;*Submitted*.

256. Brewster LP, Washington C, Brey EM, Gassman A, Subramanian A, Calceterra J, et al. Construction and characterization of a thrombin-resistant designer FGF-based collagen binding domain angiogen. Biomaterials 2008;29(3):327-336.

257. Pang Y, Wang X, Ucuzian AA, Brey EM, Burgess WH, Jones KJ, et al. Local delivery of a collagen-binding FGF-1 chimera to smooth muscle cells in collagen scaffolds for vascular tissue engineering. Biomaterials 2010;31(5):878-885.

258. Yan X, Chen B, Lin Y, Li Y, Xiao Z, Hou X, et al. Acceleration of diabetic wound healing by collagen-binding vascular endothelial growth factor in diabetic rat model. Diabetes Res Clin Pract 2010;90(1):66-72.

259. Hashi H, Hatai M, Kimizuka F, Kato I, Yaoi Y. Angiogenic activity of a fusion protein of the cell-binding domain of fibronectin and basic fibroblast growth factor. Cell Struct Funct 1994;19(1):37-47.

260. Nishi N, Matsushita O, Yuube K, Miyanaka H, Okabe A, Wada F. Collagen-binding growth factors: production and characterization of functional fusion proteins having a collagen-binding domain. Proc Natl Acad Sci USA 1998;95(12):7018-7023.

261. Sheng Z, Chang S-B, Chirico WJ. Expression and purification of a biologically active basic fibroblast growth factor fusion protein. Protein Expr Purif 2003;27(2):267-271.

262. Jang J-H, Chung C-P. Engineering and expression of a recombinant fusion protein possessing fibroblast growth factor-2 and fibronectin fragment Biotechnol Lett 2004;26(24):1837-1840.

263. Hayashi M, Tomita M, Yoshizato K. Production of EGF–collagen chimeric protein which shows the mitogenic activity Biochim Biophys Acta 2001;1528(2-3):187-195.

264. Ogiwara K, Nagaoka M, Cho C-S, Akaike T. Construction of a novel extracellular matrix using a new genetically engineered epidermal growth factor fused to IgG-Fc. Biotechnol Lett 2005;27(20):1633-1637.

265. Qiu W, Huang Y, Teng W, Cohn CM, Cappello J, Wu X. Complete recombinant silk-elastinlike protein-based tissue scaffold. Biomacromolecules 2010;11(12):3219-3227.

266. Yang M, Tanaka C, Yamauchi K, Ohgo K, Kurokawa M, Asakura T. Silk-like materials constructed from sequences of Bombyx mori silk fibroin, fibronectin, and elastin. J Biomed Mater Res A 2008;84(2):353-363.

267. Kambe Y, Yamamoto K, Kojima K, Tamada Y, Tomita N. Effects of RGDS sequence genetically interfused in the silk fibroin light chain protein on chondrocyte adhesion and cartilage synthesis. Biomaterials 2010;31(29):7503-7511

268. Du C, Wang M, Liu J, Pan M, Cai Y, Yao J. Improvement of thermostability of recombinant collagen-like protein by incorporating a foldon sequence. Appl Microbiol Biotechnol 2008;79(2):195-202.

269. Chen B, Lin H, Wang J, Zhao Y, Wang B, Zhao W, et al. Homogeneous osteogenesis and bone regeneration by demineralized bone matrix loading with collagen-targeting bone morphogenetic protein-2. Biomaterials 2007;28(6):1027-1035

270. Chen B, Lin H, Zhao Y, Wang B, Zhao Y, Liu Y, et al. Activation of demineralized bone matrix by genetically engineered human bone morphogenetic protein-2 with a collagen binding domain derived from von Willebrand factor propolypeptide. J Biomed Mater Res A 2007;80(2):428-434.

271. Zhao Y, Chen B, Lin H, Sun W, Zhao W, Zhang J, et al. The bone-derived collagen containing mineralized matrix for the loading of collagen-binding bone morphogenetic protein-2. J Biomed Mater Res A 2009;88(3):725-734.

272. Tuan TL, Cheung DT, Wu LT, Yee A, Gabriel S, Han B, et al. Engineering, expression and renaturation of targeted TGF-beta fusion proteins. Connect Tissue Res 1996;34(1):1-9.

273. Andrades JA, Wu LT, Hall FL, Nimni ME, Becerra J. Engineering, expression, and renaturation of a collagen-targeted human bFGF fusion protein. Growth Factors 2001;18(4):261-275.

274. Lin H, Chen B, Sun W, Zhao W, Zhao Y, Dai J. The effect of collagen-targeting platelet-derived growth factor on cellularization and vascularization of collagen scaffolds. Biomaterials 2006;27(33):5708-5714.

275. Zhang Y, Xiang Q, Dong S, Li C, Zhou Y. Fabrication and characterization of a recombinant fibronectin/cadherin bio-inspired ceramic surface and its influence on adhesion and ossification in vitro. Acta Biomater 2010;6(3):776-785

276. Kawase Y, Ohdate Y, Shimojo T, Taguchi Y, Kimizuka F, Kato I. Construction and characterization of a fusion protein with epidermal growth factor and the cell-binding domain of fibronectin FEBS Lett 1992;298(2-3):126-128.

277. Ishikawa T, Terai H, Yamamoto T, Harada K, Kitajima T. Delivery of a growth factor fusion protein having collagen-binding activity to wound tissues. Artif Organs 2003;27(2):147-154.

278. Elloumi I, Kobayashi R, Funabashi H, Mie M, Kobatake E. Construction of epidermal growth factor fusion protein with cell adhesive activity. Biomaterials 2006;27(18):3451-3458.

279. Sun W, Lin H, Chen B, Zhao W, Zhao Y, Dai J. Promotion of peripheral nerve growth by collagen scaffolds loaded with collagen-targeting human nerve growth factor-beta. J Biomed Mater Res A 2007;84(4):1054-1061.

This thesis focuses in the development and characterization of new silk based chimeric proteins for future application in tissue engineering. So, the main goals of this work are:

1. Design of new protein sequences combining spider silk (6mer) and bone sialoprotein (BSP) and spider silk and the antimicrobial peptides human neutrophil defensins 2 and 4 (HNP-2 and HNP-4) and hepcidin. The new proteins were named 6mer+BSP, 6mer+HNP-2, 6mer+HNP-4 and 6mer+hepcidin;
2. Test the activity of the new proteins;
3. Evaluate the *in vitro* biocompatibility of the developed proteins;
4. Assess the mechanical properties of 6mer+BSP and its behaviour in the presence of Ca^{2+} ions;
5. Evaluate the *in vivo* behaviour of some of these proteins (6mer+BSP and 6mer+hepcidin).

The intent of this chapter is to a give a general overview of the different methodologies used in the different experiment studies performed during the course of this thesis with the purpose of testing the following hypothesis:

1. Different protein domains can be combined without disturbing silk self-assembly properties and the respective biological activity of the new protein domains added;
2. The new silk based proteins can be processed into protein films capable of sustaining cell proliferation and/or differentiation;
3. 6mer+BSP has similar mechanical properties to silk alone;
4. The new proteins are biocompatible and have no cytotoxic effects;
5. The new chimeric proteins induce mild inflammatory responses during *in vivo* tests

In this thesis two different types of chimeric proteins were developed. Chapter III describes the cloning and expression of 6mer+BSP chimeric protein, which combines the mechanical properties of spider silk with the biological properties of BSP such as: ability to induce the deposition of calcium phosphate (CaP) and to stimulate cell

adhesion. Also, in this chapter we have the results for the ability of 6mer+BSP to support osteogenic differentiation. Additionally, since 6mer+BSP is to be used for bone regeneration applications, in chapter IV the mechanical properties, mainly the elasticity, of 6mer+BSP and 6mer films are assessed by using atomic force microscopy (AFM). Also, the roughness of these films was measured and the capacity of 6mer+BSP and 6mer proteins to form supramolecular networks in the presence of Ca^{2+} ions was also evaluated. In chapter V is described the design of a new set of chimeric proteins with antimicrobial properties, 6mer+HNP-2, 6mer+HNP-4 and 6mer+hepcidin, and its antimicrobial activity and biocompatibility were also assessed through proper activity tests. The two final chapters describe *in vivo* inflammatory responses to 6mer+BSP and 6mer+hepcidin. The overall experimental approach described in this thesis aims to develop and test new chimeric proteins for biomedical applications. The present chapter describes with more detail the different methodologies and instruments used to develop and characterized, from material and biological perspectives, the different proteins. This set of methodologies is summarized in Table 1 and can be divided as follows:

1. Gene design and cloning of 6mer, 6mer+BSP, 6mer+HNP-2, 6mer+HNP-4 and 6mer+hepcidin;
2. Proteins expression, purification and identification;
3. Secondary structure characterization to confirm the ability of 6mer silk domain to form β-sheet when combined with other protein domains and to assess the overall secondary conformation of the new chimeric proteins;
4. *In vitro* activity tests to evaluate the biological activity of BSP, HNP-2, HNP-4 and hepcidin domains when combined with silk;
5. AFM analyses to assess the mechanical properties and roughness of 6mer+BSP and 6mer films and the behaviour of these proteins in the presence of Ca^{2+};
6. Biological tests to assess the *in vitro* and *in vivo* performance of the new proteins.

Table II.1. Brief overview of the methodologies described in this chapter.

Proteins	*In vitro* activity tests	Structure analyses	Mechanical tests	Biological tests	
				in vitro	*in vivo*
6mer+BSP	Mineralization	Fourier Transform Infrared (FTIR) Atomic Force Microscopy (AFM) Circular Dichroism (CD)	AFM spectroscopy	Human mesenchymal stem cells (HMSC)	Subcutaneous implant (mice)
6mer+HNP-2	Antimicrobial activity (*Escherichia coli* and *Staphylococcus aureus*)	FTIR / CD	–	Osteosarcoma cell line (SaOs-2)	–
6mer+HNP-4			–		–
6mer+hepcidin			–		Subcutaneous implant (mice)

1. Materials

In this thesis different chimeric proteins were developed. The coding sequence for BSP was purchased from the Harvard clone collection "The ORFeome Collaboration", Dana-Farber/Harvard Cancer Center, Boston MA, (Clone Identification: HsCD00082642). The oligonucleotide coding sequences for HNP-2, HNP-4 and Hepcidin were purchased from Invitrogen, CA, USA. For the other reagents, details will be given when used for the first time during this chapter. All reagents were used and stored according with the instructions and safety protocols provided by the supplier.

2. Gene design and cloning

This section intents to give a more detailed overview of the methodologies used in the construction of the cloning vector, the gene design and the cloning of the new chimeric proteins (Figure II.1).

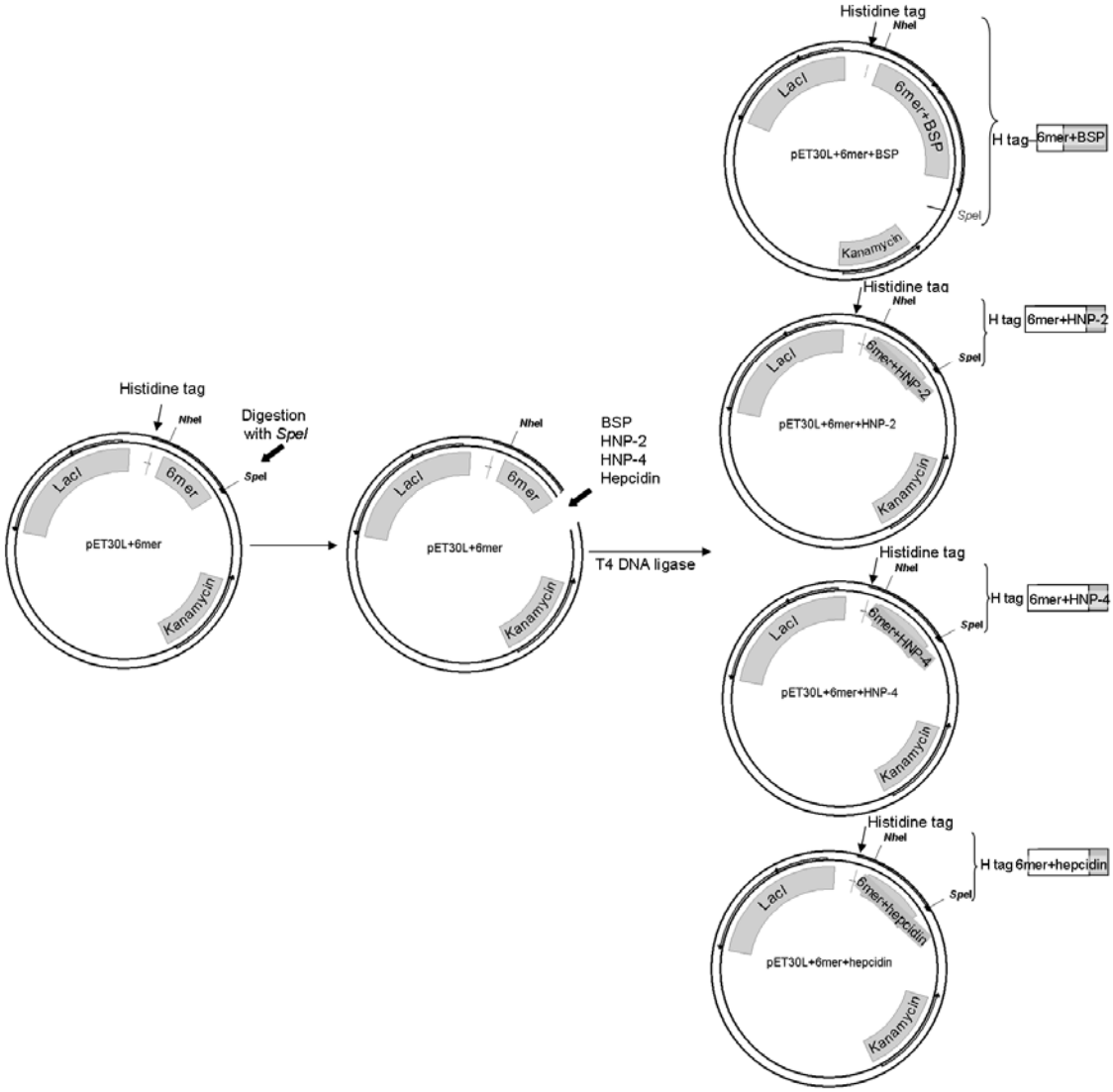

Figure II.1. Overview of the cloning process for the different chimeric proteins.

2.1. pET30L bacterial vector

A cloning cassette linker with *Nco*I and *Xho*I restriction sites was generated through the annealing of two complementary synthetic nucleotide sequences, 30aNHistop and 30aNHibottom as it is shown in the Figure II.2. Annealing reaction of a 20 pmol/µl oligonucleotide mixture solution (30aNHistop and 30aNHibottom) took place by decreasing the temperature from 95 to 20ºC at a gradient of 0.1ºC/s. The resultant double strand oligonucleotide linker was inserted in vector pET30a(+) (Novagen, San Diego) after the digestion with *Nco*I and *Xho*I, restriction enzymes. Both restriction sites were preserved after digestion. The new cloning vector was designated pET30L [1].

For purification purposes, pET30L carries a N-terminal tag of six histidines. The presence of this histidine tag is very important since it allows the use of affinity chromatography for protein purification. This process will be discussed in more detail in section 3 of this chapter.

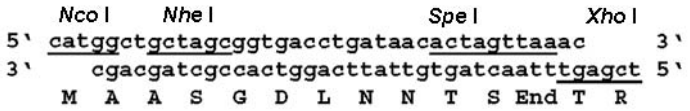

Figure II.2. Oligonucleotide sequence for pET30L linker. Adapted from Rabotyagova [1].

2.2. Cloning of 6mer coding sequence

The spider sequence unit used in this PhD project was selected based on a consensus motif derived from the back translation of *Nephila clavipes* MaSpI (Accession P19837) protein into complementary deoxyribonucleic acid (cDNA), considering a bacterial codon usage. Silk coding units (Figure II.3) were prepared as oligonucleotides sequences that were annealed in a reaction with a decreasing temperature from 95 to 20ºC at a gradient of 0.1ºC/s. A 20 pmol/µl oligonucleotide mixture solution was used for annealing. Later, double strand spider silk block motifs were digested with *Nhe*I and *Spe*I restriction enzymes and inserted into pET30L. T4 DNA ligase was used for ligation of silk inserts and the reaction was held at 16ºC. A total of six silk blocks were inserted using step-by-step cloning approach. The resultant silk block copolymer sequence was named 6mer.

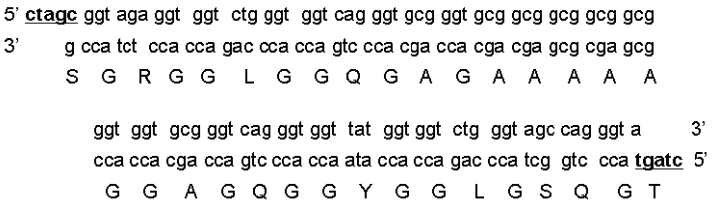

Figure II.3. Nucleotide and amino acid sequence for silk coding block. Restriction sites are underlined.

2.3. Cloning of BSP coding sequence

Human bone sialoprotein (BSP) cDNA sequence was obtained from a clone containing the bacterial plasmid pENTR223.1. pENTR223.1 vector is a 4311 bps plasmid with two genes, ccdB and CmR, located in the region flanked two restriction sites for

*Sfi*I enzyme. The ccdB gene (DNA gyrase inhibitor) provides a strong negative selection against the vector molecules retaining this gene, whereas CmR (chloramphenicol resistance gene) provides a positive selection for propagating the vector. During cloning, both genes are replaced by the inserted DNA, in this case BSP coding sequence, as it is shown in the.

pENTR223.1 was inoculated into Luria Bertani (LB) medium and grown overnight at 37ºC with shaking (200 rpm/min). Afterwards, the pENTR223.1 plasmid was extracted using Qiagen miniprep kit (28704) and digested with *SfiI* enzyme (New England Biolabs, R0123S), which cuts in the regions flanking the BSP cDNA sequence (Table 2). The digestion product was run in a 0.8% agarose gel. The band for the BSP cDNA sequence (951bp) was purified using a QIAquick gel extraction kit (Qiagen, 28706). For ligation of the BSP cDNA sequence to the 6mer spider silk clone, a linker was design. This linker contains in its central region a restriction site for *Sfi*I for the insertion of BSP cDNA sequence, and also restriction sites for *Spe*I (New England Biolabs, R0133S) and *Nhe*I (New England Biolabs, R0131S) related to the spider silk clone. For insertion of the linker in the expression vector pET30L, the vector was digested with *Spe*I, dephosphorylated with Alkaline Phosphatase, Calf Intestinal (CIP) enzyme (New England Biolabs, M0290S) and run on 0.8% agarose gel. The linearized vector was purified using the QIAquick gel extraction kit.

The linker was double digested with *Spe*I and *Nhe*I restriction enzymes generating compatible ends with those generated by *Spe*I with the expression vector pET30L. The linker was run on 0.8% agarose gel and purified using the QIAquick gel extraction kit. After, the linker was inserted in the linearized vector pET30L. The ligation reaction was carried out with T4 DNA ligase enzyme (New England Biolabs, M0202S).

For combining BSP and 6mer spider silk cDNA sequences, both vectors, pET30L carrying the linker (vector pET30L + linker), and pENTR223.1 alone, were digested with *Sfi*I. In the case of the linearized vector pET30L + linker, the ends generated by the digestion with *Sfi*I were dephosphorylated with CIP. After running the digestion products of both vectors in a 0.8% agarose gel, the bands corresponding to the BSP cDNA sequence and to the linearized vector pET30L + linker were purified using the QIAquick gel extraction kit. The ligation reaction between the vector pET30L + linker

and the BSP cDNA sequence was carried out with T4 DNA ligase. The new coding sequence was designated by 6mer+BSP (Table 2).

2.4. Cloning of HNP-2, HNP-4 and hepcidin coding sequences

The HNP-2, HPN-4 and hepcidin cDNA sequences were prepared through the annealing of synthetic single strand oligonucleotide sequences (Invitrogen, CA, USA): HNP-2 top and HNP-2 bottom, HNP-4 top and HNP-4 bottom and hepcidin top and hepcidin bottom (Table 2). The annealing reactions of a 20 pmol/µl oligonucleotide solution were carried out by decreasing the temperature from 95ºC to 20ºC with a gradient of 0.1ºC/s. The presence of the annealed products was verified using electrophoresis in 5% agarose gels. At the edges of each cDNA sequence, restriction sites are present for *Spe*I and for *Nhe*I for the insertion of the cDNA sequences into the vector pET30L. This vector already carried the DNA encoding of the silk block copolymer. For the insertion of the cDNA sequences into pET30L, the vector was digested with *Spe*I (New England Biolabs, MA, USA, R0133S), dephosphorylated with calf intestinal phosphatase (CIP) (New England Biolabs, M0290S) and run on 0.8% agarose gels. The linearized vector was purified using the QIAquick gel extraction kit (Qiagen, CA, USA, 28706).

The cDNA sequences were double digested with *Spe*I and *Nhe*I and the digestion products run in a 0.8% gel and the bands for the cDNA sequences were purified using a QIAquick gel extraction kit. HNP-2, HPN-4 and hepcidin cDNA were ligated individually to the silk 6mer present in the expression vector pET30L using T4 DNA ligase enzyme (New England Biolabs, M0202S). The new coding sequences were designated by 6mer+HNP-2, 6mer+HNP-4 and 6mer+hepcidin (Table 2).

2.5. Transformation of DH5α and RY-3041 *E. coli* strains

DH5α *E. coli* strain was used for plasmid cloning and RY-3041 strain was used for protein expression.

DH5α cells (Invitrogen, 18258-012) are suitable for the construction of gene banks or for the generation of cDNA libraries using plasmid-derived vectors and are also capable of being transformed efficiently with big plasmids. For transformation DH5α competent cells were thawed on ice and 100 µl of these cells were gently mixed

with 10µl of the ligation product (vector pET30L carrying 6mer, 6mer+BSP, 6mer+HNP-2, 6mer+HNP-4 and 6mer+hepcidin cDNAs). The reaction mixture was incubated on ice for 30 minutes. After, the cells were heat-shock for 45 seconds in a 42 ºC water bath and placed on ice for two minutes. 900 µl of Super Optimal broth with Catabolite repression medium (SOC) was added to the reaction mixture followed by one hour incubation at 37 ºC. Afterwards, 100 µl of the mixture was spread onto agar plates with 25 µg/ml kanamycin. Plates were incubated overnight at 37 ºC. In the following day plates were searched for positive clones.

Transformation of RY-3041 *E. coli* strain was done using a methodology very similar to DH5α cells. RY-3041 cells were thawed on ice and 20 µl of this cell suspension was mixed with 2 µl of the ligation product. Later, the cells were heat-shock for 90 seconds in a 42 ºC water bath and placed on ice for two minutes. 80 µl of SOC medium was added to reaction mixture followed by incubation for one hour at 37 ºC. Following incubation, the cell suspension was platted on an agar plate with 25 µg/ml kanamycin and left to incubate overnight for selection of positive clones.

Table II.2. Proteins nucleotide and amino acid sequences and the systems used for cloning and expression.

Protein	cDNA coding sequence and protein amino acid sequence	Cloning	Expression
6mer	agc ggt aga ggt ggt ctg ggt ggt cag ggt gcg ggt gcg gcg gcg gcg gcg ggt ggt gcg ggt S G R G G L G G Q G A G A A A A A G G A G cag ggt ggt tat ggt ggt ctg ggt agc cag ggt act agc ggt aga ggt ggt ctg ggt ggt cag ggt Q G G Y G G L G S Q G T S G R G G L G G Q G gcg ggt gcg gcg gcg gcg gcg ggt ggt gcg ggt cag ggt ggt tat ggt ggt ctg ggt agc cag ggt A G A A A A A G G A G Q G G Y G G L G S Q G act agc ggt aga ggt ggt ctg ggt ggt cag ggt gcg ggt gcg gcg gcg gcg gcg ggt ggt gcg ggt T S G R G G L G G Q G A G A A A A A G G A G cag ggt ggt tat ggt ggt ctg ggt agc cag ggt act agc ggt aga ggt ggt ctg ggt ggt cag ggt Q G G Y G G L G S Q G T S G R G G L G G Q G gcg ggt gcg gcg gcg gcg gcg ggt ggt gcg ggt cag ggt ggt tat ggt ggt ctg ggt agc cag ggt A G A A A A A G G A G Q G G Y G G L G S Q G act agc ggt aga ggt ggt ctg ggt ggt cag ggt gcg ggt gcg gcg gcg gcg gcg ggt ggt gcg ggt T S G R G G L G G Q G A G A A A A A G G A G cag ggt ggt tat ggt ggt ctg ggt agc cag ggt act agc ggt aga ggt ggt ctg ggt ggt cag ggt Q G G Y G G L G S Q G T S G R G G L G G Q G gcg ggt gcg gcg gcg gcg gcg ggt ggt gcg ggt cag ggt ggt tat ggt ggt ctg ggt agc cag ggt A G A A A A A G G A G Q G G Y G G L G S Q G **act agc** **T S**	DH5α *E. coli*	RY-3041 *E. coli*

6mer+BSP	**6mer** + tgg ccg tca agg ccg + W P S R P atg aag act gct tta att ttg ctc agc att ttg gga atg gcc tgt gct ttc tca atg aaa aat ttg cat cga aga M K T A L I L L S I L G M A C A F S M K N L H R R gtc aaa ata gag gat tct gaa gaa aat ggg gtc ttt aag tac agg cca cga tat tat ctt tac aag cat gcc V K I E D S E E N G V F K Y R P R Y Y L Y K H A tac ttt tat cct cat tta aaa cga ttt cca gtt cag ggc agt agt gac tca tcc gaa gaa aat gga gat gac Y F Y P H L K R F P V Q G S S D S S E E N G D D agt tca gaa gag gag gag gaa gaa gag gag act tca aat gaa gga gaa aac aat gaa gaa tcg aat S S E E E E E E E E T S N E G E N N E E S N gaa gat gaa gac tct gag gct gag aat acc aca ctt tct gct aca aca ctg ggc tat gga gag gac gcc E D E D S E A E N T T L S A T T L G Y G E D A acg cct ggc aca ggg tat aca ggg tta gct gca atc cag ctt ccc aag aag gct ggg gat ata aca aat T P G T G Y T G L A A I Q L P K K A G D I T N aaa gct aca aaa gag aag gaa agt gat gaa gaa gaa gag gag gaa gag gaa gga aat gaa aac K A T K E K E S D E E E E E E E E G N E N gaa gaa agc gaa gca gaa gtg gat gaa aac gaa caa ggc ata aac ggc acc agt acc aac agc E E S E A E V D E N E Q G I N G T S T N S aca gag gca gaa aac ggc aac ggc agc agc gga gga gac aat gga gaa gaa ggg gaa gaa gaa T E A E N G N G S S G G D N G E E G E E E agt gtc act gga gcc aat gca gaa gac acc aca gag acc gga agg cag ggc aag ggc acc tcg aag S V T G A N A E D T T E T G R Q G K G T S K aca aca acc tct cca aat ggt ggg ttt gaa cct aca acc cca cca caa gtc tat aga acc act tcc cca T T T S P N G G F E P T T P P Q V Y R T T S P cct ttt ggg aaa acc acc acc gtt gaa tac gag ggg gag tac gaa tac acg ggc gcc aat gaa tac gac P F G K T T T V E Y E G E Y E Y T G A N E Y D aat gga tat gaa atc tat gaa agt gag aac ggg gaa cct cgt ggg gac aat tac cga gcc tat gaa gat N G Y E I Y E S E N G E P R G D N Y R A Y E D gag tac agc tac ttt aaa gga caa ggc tac gat ggc tat gat ggt cag aat tac tac cac cac cag E Y S Y F K G Q G Y D G Y D G Q N Y Y H H Q ggc ctc atg ggc cac 3’ G L M G H	DH5α *E. coli*	RY-3041 *E. coli*
6mer+HNP-2	**6mer** + **act agc** tgt tat tgc cgt ata cct gct tgt att gca gga gaa cga cgt tat ggt act **T S** C Y C R I P A C I A G E R R Y G T tgt ata tat caa gga cgt tta tgg gct ttc tgt tgc 3’ C I Y Q G R L W A F C C	DH5α *E. coli*	RY-3041 *E. coli*
6mer+HNP-4	**6mer** + **act agc** gta tgt agt tgc cgt tta gtt ttc tgt cgt cga act gaa tta cgt gta gga **T S** V C S C R L V F C R R T E L R V G aat tgt tta ata ggt gga gtt agt ttc aca tat tgt tgc act cga gta 3’ N C L I G G V S F T Y C C T R V	DH5α *E. coli*	RY-3041 *E. coli*
6mer+hepcidin	**6mer** + **act agc** gat act cat ttc cct ata tgt att ttt tgc tgt gga tgt tgc cat cgt agt **T S** D T H F P I C I F C C G C C H R S aaa tgt ggt atg tgt tgc aaa act 3’ K C G M C C K T	DH5α *E. coli*	RY-3041 *E. coli*

2.6. Confirmation of DNA coding sequence by DNA sequencing

For confirming the inserts presence, after transformation, positive clones were selected and grown overnight. In the next day the plasmids were extracted with QIAprep spin miniprep kit (Qiagen 27106) according with the protocol provided by the supplier. The presence of the 6mer+BSP, 6mer+HNP-4, 6mer+HNP-2 and 6mer+hepcidin inserts was confirmed by DNA sequencing [2] with a ABI 3130XL DNA sequencer (Applied Biosystems, USA), at Tufts core facilities, using T7 and T7 term primers in pET30L vector.

3. Protein expression, purification and identification

After confirming the insertion of the coding sequence for 6mer, 6mer+BSP, 6mer+HNP-2, 6mer+HNP-4 and 6mer+hepcidin into pET30L vectors, these were used

for protein expression in *E. coli* RY-3041 bacterial strain. This section describes in more detail the expression and purification of the chimeric proteins and addresses the different methodologies and instruments used to confirm protein identity.

3.1. *E. coli* RY-3041 bacterial strain for protein expression

E. coli RY-3041 bacterial strain is a mutant strain of *E. coli* BLR(DE3) SlyD$^-$ defective in the expression of SlyD protein [3]. SlyD protein is a member of FK506-binding protein family and is one of the gene products initially identified as a suppressor of phage lysis [4]. This protein, SlyD, was reported in previous studies as co-eluting together with silk proteins during purification by Ni-NTA affinity chromatography. This happens due to the high content of histidine, an amino acid with known affinity for Ni-NTA columns. In *E. coli* RY-3041 strain the C-terminus, with high content of histidine amino acids, of SlyD protein was deleted to avoid its co-elution with the expressed protein. Pure silk extracts were obtained when silk was expressed in *E. coli* RY-3041 [5]. This is the reason why *E. coli* RY-3041 bacterial strain, kindly provided by Professor Ry Young (Texas A&M University, College station, TX, USA) was selected for the expression of the proteins described in this study.

3.2. Protein expression and purification

6mer, 6mer+BSP, 6mer+HNP-4, 6mer+HNP-2 and 6mer+hepcidin proteins were expressed in *E. coli* RY-3041 strain. Cells were cultivated at 37 ºC in Luria-Bertani (LB) medium or Hyper Broth^{TM} (Athens Enzyme Systems 0107-S) supplemented with 25 µg/ml kanamycin until an OD_{600} between 0.9 and 1 was reached. At this point, the protein expression was induced by adding isopropyl β-D-thiogalactoside (IPTG, Invitrogen, 15529019) to reach a final concentration of 0.5 mM. After 2 hours, cells were harvested by centrifugation at 6500 rpm. The cells pellet was resuspended in a denaturating buffer of 100 mM NaH_2PO_4, 10 mM Tris HCl and 8 M urea at pH 8.0 and left overnight with stirring for a complete cell lysis. Insoluble cell fragments and soluble proteins present in the cell lysate were separated by centrifugation at 11000 rpm.

The supernatant was mixed with Ni-NTA resin (Qiagen, 30250) and left for 2 hours with stirring. The supernatant/Ni-NTA resin mixture was loaded onto a glass Econo-column (Biorad) and washed several times with denaturating buffer at pH 8.0 and at pH 6.0.

The protein 6mer+BSP was eluted using denaturating buffer at pH 4.5 as it is shown in the Figure II.4. The purified proteins were first dialysed, for one day, against a 20 mM sodium acetate buffer, to keep a steady pH and avoid protein precipitation. After, an extensive dialysis, against water was done to remove all the salts. For dialysis the protein solutions were poured into cellulose ester snake skin membranes with a 100-500 Da molecular weight cutting off (Spectra/Por Biotech, 131054). Finally, the dialyzed proteins were lyophilized and kept at room temperature.

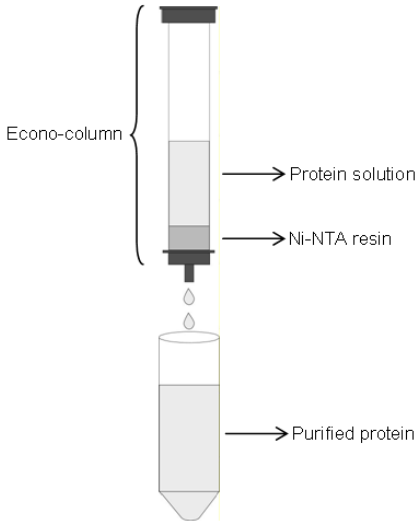

Figure II.4. Protein purification using Econo-column column.

3.3. Protein identification

Different methods and instruments were used to better characterize and identify the new chimeric proteins. These methodologies and instruments are described in the next sections.

3.3.1. Sodium dodecyl sulphate polyacrylamide gel electrophoresis - SDS-PAGE

SDS-PAGE was used as qualitative method to assess expression levels and molecular weight of 6mer, 6mer+BSP, 6mer+HNP-4, 6mer+HNP-2 and 6mer+hepcidin proteins. Protein solutions were mixed with NuPAGE LDS sample buffer (Invitrogen, NP0007) and heated at 80 ºC for 10 minutes. The samples were separated using a Bis-tris 4-12% gel (Invitrogen, NP0321BOX) at 200 V for 20 minutes. Afterwards, gels were stained with a colloidal blue kit (Invitrogen, LC6025) for detection of protein bands.

3.3.2. Western-blot

For the western blot, the His-Tag AP western kit was used according with the protocol provided by the supplier (70972, Novagen, EMD Biosciences, NJ, USA). Briefly, the bands were electro-transferred onto a nitrocellulose membrane at 30 V for 16 hours. Membranes were blocked for one hour with 3% bovine serum albumin (BSA) in tris buffered saline (TBS) buffer (blocking solution). After washing with TBS buffer, the membrane was incubated for 1 hour with mouse anti-histidine monoclonal antibody (Novagen) diluted 1:1000 in blocking solution. After a proper washing with TBSTT buffer (TBS with Tween 20), the membrane was incubated for 1 hour with goat anti-mouse IgG AP conjugated antibody diluted 1:5000 in blocking solution. Colorimetric detection was performed with a solution of 5-bromo-4-chloro-3-indolylphosphate (BCIP) and nitrobluetetrazolium (NBT).

3.3.3. Amino acid analysis

Amino acid analysis is a technique used for protein identification through the quantification of its amino acid composition. The protein or peptide is first hydrolyzed into its amino acids, which are then separated and analysed through chromatography.

In this study, amino acid analysis was carried out at Yale University, W. M. Keck Foundation Biotechnology Resource Laboratory (New Haven, CT USA). After an overnight *in vacuo* acid hydrolysis at 115 ºC the samples were loaded into a Hitachi L-8900 amino acid analyzer. The analyzer uses an ion-exchange column with a pH and temperature gradient to separate the amino acids. EZChrome Elite for Hitachi software was used to run the instrument and collect and analyze the data.

3.3.4. Matrix-assisted laser desorption/ionization-time of flight (MALDI-TOF)

MALDI is a type of mass spectroscopy that can provide valuable information on the structural organization of biomolecules such as: sequence, molecular weight, branching and linkage. MALDI was first developed for the analysis of molecules with large molecular weights. To obtain a signal, the sample is mixed with a solvent and after evaporation is subjected to a pulse from a laser. Due to the pulse nature of the laser source and its ability to ionize large molecules MALDI was coupled to a time-of-flight (TOF) analyser. MALDI-TOF is widely used, mainly due to its large mass range.

and higher sensitivity. This equipment produces protein fingerprints, which are later used to compare to a database of reference for protein identification [6]. In this thesis, MALDI-TOF (Tufts Core Facility, Voyager-DE Pro, Applied Biosystems, CA USA) was used to confirm the protein identity. For MALDI-TOF, the samples were dissolved in water in a concentration of 2 mg/ml.

3.3.5. Protein sequencing

Protein sequencing at Tufts Core Facility (ABI 494, Applied Biosystems, CA USA) was used to confirm the N-terminal amino acid sequence for the five proteins, 6mer, 6mer+BSP, 6mer+HNP-4, 6mer+HNP-2 and 6mer+hepcidin.

Sequence analysis was done with samples extracted from the protein bands observed in SDS-PAGE gels after electrophoresis and colloidal with blue staining. In-gel digestion of the samples it was done with trypsin or a mixture of trypsin and chymotrypsin, to get a better coverage of protein sequence. After proteolysis, the high complex protein mixtures were analysed by liquid chromatography (LC) coupled with tandem mass spectroscopy (MS) (LC/MS/MS). The search of LC/MS/MS data was done using the NCBI non-redundant protein database.

LC/MS/MS has the advantage of combining the ability of LC to separated different components of a mixture with MS ability to identify these components due to the fact that the mass spectra of several compounds are sufficiently specific to allow their identification with a high degree of confidence [7]. For instance, in many biological samples the compounds of interest are present in a mixture, LC/MS/MS can be very useful in solving the composition of these complex analytes.

4. Preparation of the protein films

Protein films were selected to be used for activity and biological studies. Films are easy to process and can be prepared with small quantities of protein, which is an advantage since it is difficult to express the large amounts of protein necessary to produce more complex structures such as porous matrices.

Based on published literature, different solvents, such as hexafluoroisopropanol (HFIP), were tested to dissolve the lyophilized proteins. Better results were obtained with water, which was selected as a solvent for dissolving

recombinant 6mer, 6mer+BSP, 6mer+HNP-4, 6mer+HNP-2 and 6mer+hepcidin proteins.

Proteins were dissolved in Milli-Q (MQ) water to a final concentration of 2% (w/v), for *in vitro* studies, and 4% (w/v) for *in vivo* studies.

60 µl of each protein solution was cast into a plastic non-adherent polystyrene surface or into the wells of tissue culture plates and left to dry at room temperature. The films were treated with a 70% methanol solution for 2 hours or 99% methanol for 30 minutes to induce the transition of secondary structure from random coil to β-sheet present in the 6mer. This transition is very important for silk mechanical properties which are in part a consequence of the amino acid chemistry where the hydrophilic GGX motif (G stands for glycine, X is mostly glutamine) alternates with poly-alanine (poly-A) motifs. The hydrophilic GGX motifs are responsible for the less crystalline regions and the poly-A motifs form the crystalline regions. The hydrophobic poly-A motifs are responsible for the formation of rigid and highly packed anti-parallel β-sheets [12] due to hydrogen bonding (Figure II.5), and generate the physical cross-links that stabilize silk structures in these crystalline regions. The GGX motif adopts a helical conformation forming an amorphous region that connects the poly-A motifs providing elasticity to the silk fibers [10]. The combination of glycine-rich domains with the poly-A regions and the formation of β-sheet cross-links between blocks give rise to the impressive mechanical properties of major ampullate silk fibers [13]. The treatment with organic solvents increases the number of hydrogen bonds between silk chain segments by removing water molecules, which disrupt inter- and intra-molecular hydrogen bonding in the silk matrix [9]. In this way, methanol treatment allows the formation of rigid and highly packed anti-parallel β-sheets due to hydrogen bonding, generating the physical cross-links that stabilize silk structures in the hydrophobic poly-alanine crystalline regions [10, 11]. The treatment with methanol produces films with improved mechanical properties and more resistant to the dissolution in water or other aqueous environments such as culture media.

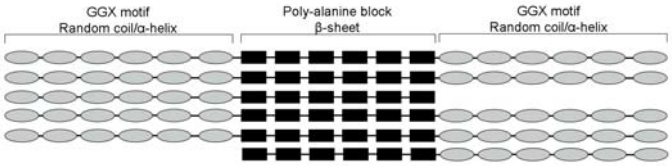

Figure II.5. Model for the crystalline assembly of silk.

For cell culture studies, the films were treated with 70% (w/w) ethanol solution for sterilization purposes. For *in vivo* studies besides treatment with 70% ethanol solution, the films were also exposed to UV light during 15 minutes on each side in order to assure that the films were sterilised.

As a control in the *in vivo* it was used PLGA films. In this way, PLGA was dissolved in dichloromethane in a 1:15 ratio (w/v) and 60 µl of this solution was casted into a polystyrene surface and left to dry at least for two days. Afterwards, the films were treated with 70% (v/v) ethanol solution and irradiated with UV for 15 minutes for sterilization reasons.

Also for *in vivo* studies, immediately before implantation, the films were hydrated with sterile phosphate buffered saline (PBS).

4.1. Secondary structure characterization

As in the case of other silk proteins, major ampullate silk protein presents a molecular structure formed by poly-A motifs involved in the formation of β-sheets in crystalline regions that alternate with less organized GGX motifs regions. In Figure II.6 it can be seen the amino acid sequences for 6mer hydrophobic and hydrophilic blocks. β-sheet and α-helix are responsible for protein secondary structure conformation. In this thesis attenuated total reflection Fourier transform infrared (ATR-FTIR) and circular dichroism (CD) analyses were used to assess the secondary structure of 6mer, 6mer+BSP, 6mer+HNP-2, 6mer+HNP-4 and 6mer+hepcidin. Although these techniques are not able to provide the same level of structural detail as for example nuclear magnetic resonance (NMR), they can be applied readily for a qualitative and quantitative analysis of protein secondary structure.

Hydrophobic Block:
GAGAAAAAGGAG

Hydrophilic Block:
QGGYGGLGSQGTSGRGGLGGQ

Figure II.6. Amino acid sequences for 6mer hydrophobic and hydrophilic blocks.

4.1.1. Attenuated total reflection Fourier transform infrared characterization

FTIR analysis works by shining an infrared light into a sample and detecting the wavelengths in the infrared region, which are emitted by the sample. Different compounds have characteristic bands in the infrared spectrum and in this study, amine I and II, are the most prominent vibrational bands of protein back-bone. The most sensitive spectral region for protein secondary structure analysis is amide I region (1700-1600 cm^{-1}) that results almost entirely from C=O stretch vibrations. Amide II region (1600-1450 cm^{-1}) derives mainly from N-H binding. Together C=O and N-H ligations contribute for the formation of hydrogen binding and thus for protein secondary conformation [14].

ATR-FTIR was performed on a model FT/IR-6200 (Jasco Inc., MD, USA) equipment. The characterization was performed before and after methanol treatment of 2% (m/v) films in order to investigate the secondary structure. Spectra were collected in the absorption mode at 8 cm^{-1} resolution and the region between 4000 and 400 cm^{-1} was scanned. The quantification of the secondary structure was based on the analysis of the amide I and amide II regions (1700 to 1450 cm^{-1}). The average percentage for the secondary structures, mainly β–sheet content in 6mer (control sample), 6mer+BSP, 6mer+HNP-2, 6mer+HNP-4 and 6mer+hepcidin proteins, was calculated through the integration of the area of each deconvoluted curve followed by the normalization of the obtained value to the total area of the amide I and amide II regions. Spectra were curve integrated in the amide regions using Burker Opus software.

4.1.2. Circular dichroism (CD) characterization

The CD concept is based on the fact that polarized light can be viewed as being made up of two circularly polarized components of equal magnitude: one rotating counter-clockwise (left handed, L) and the other rotating clockwise (right handed, R). If

after passage through the sample the R and L components are not absorbed or are absorbed at the same extent, the recombination of these two components would generate radiation polarized in the same plan. However, if R and L components are absorbed in different extents the resulting light will possess elliptical polarization (Figure II.7A) [15]. CD refers to the differential absorption of these two components by the sample. CD signals only appear when radiation absorption occurs due to the presence of optically active cromophores. In proteins, these cromophores can be peptide bonds (absorption below 240 nm), aromatic acid side chains (absorbing between 260 and 320 nm) and disulphide bonds (absorption around 260 nm) [15]. Through the analysis of peptide bonds is possible to assess β-sheet and α-helix composition of a protein/peptide molecule (Figure II.7B). Thus, CD has become increasingly recognized as a valuable structural analysis for addressing protein secondary conformation in solution [15].

CD spectroscopy was performed on an Aviv, Model 410 instrument (Biomedical, Inc. NJ USA). The spectra were collected between 260 and 180 nm with a step size of 1 nm in an averaging time of 1 s and five scans were collected for each sample. A baseline spectrum was subtracted from the samples. Sample cells with a 0.1 cm path length were used and the measurements were performed with 1 mg/ml protein solutions in a phosphate buffer (pH 7.4).

Furthermore, CD analysis was also used to assess changes in protein secondary conformation induced by the presence of divalent ions, mainly calcium and magnesium. In this case were used 1 mg/ml protein solutions in 0.1 mM HEPES buffer (pH 7.4) and in 0.1 mM HEPES containing Ca^{2+} or Mg^{2+} ions in a molar ratio of 1:1000 (protein:Ca).

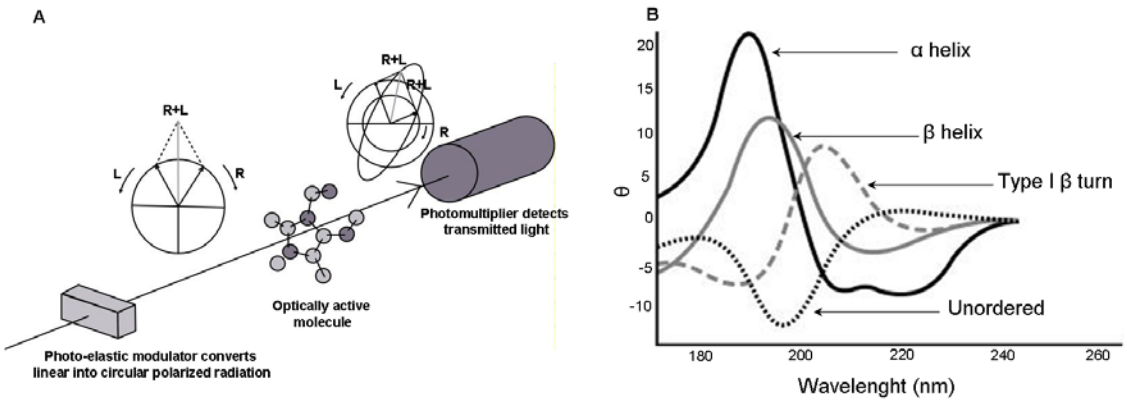

Figure II.7. A) CD effect. B) CD spectra associated with different types of secondary conformations. L, left polarized light and R, right polarized light.

5. *In vitro* experiments to assess the activity of the new chimeric proteins

In this section will be addressed the different activity testes used to determine if the fusion of 6mer silk with BSP, HNP-2, HNP-4 and Hepcidin interfered with the activity of these last four domains. Two different types of activity tests will be described: antimicrobial and mineralization tests. Antimicrobial tests were performed to determine if HNP-2, HNP-4 and hepcidin kept their activity after fusion with 6mer domain. Mineralization tests aim to test the ability of BSP to induce deposition CaP after fusion with the 6mer.

5.1. Evaluating the capacity of proteins films to induce mineralization

6mer+BSP and 6mer films were incubated during 1 and 6 hours at 37 ºC, with an accelerating calcification solution (ACS) with the following composition: 150 mM Na^+, 20 mM of HEPES, 3.75 mM Ca^{2+} and 2.32 mM PO_4^{3-}, at pH 7.4 [18]. This solution was adapted from the ACS solution used by Li and colleagues [18] and produced faster mineralization results when compared with simulated body fluid (SBF) solution.

After incubation the films were washed with MQ water and dried at room temperature. Field-emission scanning electron microscopy (FE-SEM) and energy dispersive spectroscopy (EDS) analyses were used to address possible mineral deposition during incubation with ACS.

5.2. Antimicrobial activity

Radial diffusion assay was selected to assess the antimicrobial activities of 6mer+HNP-2, 6mer+HNP-4 and 6mer+hepcidin. This methodology was adapted from Kirby-Bauer original method for testing the bacterial resistance to antibiotic drugs [16]. The main reasons why this method was selected were: its high sensitiveness, easy to use and has good reproducibility.

The purified recombinant proteins were tested for antimicrobial activity against Gram- *E. coli* (American-Type Culture Collection ATCC 25922, VA, USA,) and Gram+ *Staphylococcus aureus* (ATCC 25923), purchased from American-Type Culture Collection. The fact that both species do not demand for special growth conditions is one of the main reasons why they were selected for this study. Moreover, *E. coli* and *S. aureus* were previous used by other authors for antimicrobial tests, which makes it easier to compare the results obtained in this thesis with the results obtained by previous studies. The radial diffusion assay [16] was used to test three concentrations of the purified proteins dissolved in phosphate buffer (pH 7.4): 10, 50 and 100 μg/ml. The 6mer protein was used as a negative control in order to exclude the effect from silk itself and from possible contaminants derived from the expression and purification processes.

E. coli and *S. aureus* lawns were plated on LB-agar plates, using liquid *E. coli* and *S. aureus* cultures grown overnight at 37 ºC. A biopsy punch 8 mm in diameter was use to cut circles from filter paper (Whatman, 09-845B) that were used as blank susceptibility disks. For sterilization, the disks were immersed in a 70% (v/v) ethanol solution for 1 hour and left to dry for two hours in a hood. After drying, the discs were immersed in the different protein solutions, placed on the bacterial lawns and incubated overnight at 37ºC. The zones of growth inhibition formed around the susceptibility disks were measured by using *Image J* software to determine the number of pixels forming each zone of inhibition. Experiments were carried out in triplicate.

5.2.1. Dynamic light scattering (DLS)

DLS is a technique used to measure the fluctuations in the intensity of the light scattered by particles in a solution. This analysis is widely used to determine the diffusion coefficients and the sizes of particles in solution [17].

In the scope of this thesis, DLS analysis was selected to assess the possibility of protein aggregation that could interfere with the antimicrobial activity of 6mer+HNP-2, 6mer+HNP-4 and 6mer+hepcidin. As described in more detail in chapter V and in contrast to what was observed in previous reports for HNP-2, +HNP-4 and hepcidin proteins, the antimicrobial activity of the new chimeric proteins was not always concentration dependent. Since silk proteins are known to aggregate in solution with increased concentration the 6mer silk domain was pointed as the probable reason for this observation. In this way, DLS was used to address the probable relationship between protein concentration and the size of the aggregates resulting in a decrease of protein activity with increase concentration. A Zetasizer NanoZS instrument (ZEN3600, MALVERN Instruments, Worcestershire, UK) was used for DLS measurements. DLS was performed on solutions at the same concentrations used for the antibacterial assay described in section 5.1., mainly 10, 50 and 100 µg/ml. Samples were prepared in phosphate buffer (pH 7.4). The scattering light was collected at a 173º scattering angle.

6. Atomic force microscopy (AFM) characterization

Since its invention in 1986 AFM [19] as proven to be a useful and powerful instrument in the imaging of biological molecules such as proteins and DNA and also in the visualization of more complex systems as cells. Besides imaging, AFM can also be used to measure the local mechanical properties of soft samples.

A commercial AFM (Veeco Dimension V 3100 Scanning Probe Microscope, NY, USA) with a scanning range of 90 μm^2 and a z range of 7-8 µm was used for imaging and force-curve measurements. AFM cantilevers (Veeco, FESP) made of silicon with a spring constant of 3.152 N/m were used. AFM imaging and force-curve measurements were performed in the dry mode. Force curves were collected using contact mode AFM. Samples were imaged with tapping mode AFM. The tapping mode operation allows visualizing weakly adsorbed samples by eliminating the lateral forces between the probe tip and the sample. In this thesis, AFM force curve measurements were used to assess local mechanical properties of 6mer+BSP and 6mer films. By using AFM imaging was possible to acquire surface images from the protein films for roughness measurements and to evaluate the formation of protein networks in the presence of

calcium ion. Section analysis using Nanoscope image analysis software was used to determine the height of the imaged structures.

6.1. Mechanical characterization

For measuring the local mechanical properties of soft samples the AFM tip is used to indent the sample. This indentation results in a force curve used later to analyse the elastic response of the sample to the small loading force applied by the AFM tip. Also, the force curve values can be integrated into the Hertz model for elastic indentations and used to calculate the Young's modulus (*E*).

In a force curve, the cantilever deflection (d) is registered as a function of its vertical position (*z*), see equation 1 (Eq. 1). The slope of the force curve gives a qualitative idea of the sample elastic properties. For a stiff sample the force curve is characterized by a flat area when the tip is approaching the sample and by a slope region where the cantilever deflection is identical to the *z* movement, **d = *z***. However, in the case of a soft sample this slope region becomes shallower as a result of the decrease in the deflection value due to elastic indentation (δ),

$$d = z - \delta \quad \text{(Eq. 1)}$$

The Hooke law relates the deflection with the applied force through the force constant of the cantilever (k)

$$F = kd = k\,(z - \delta) \quad \text{(Eq. 2)}$$

The Hertz model allows us to relate the indentation δ with the loading force *F* and by using the Sneddon modification we have

$$F = \frac{2}{\pi} \cdot \frac{E}{1 - \nu^2} \cdot \delta^2 \cdot \tan(\alpha) \quad \text{(Eq. 3)}$$

where *E* is the elastic or Young's modulus, v is the Poisson ration of the sample, assumed to be 0.5 for incompressible materials, and α is the opening angle of the AFM tip. By combining equations 2 and 3 we have

$$kd = \frac{2}{\pi} \cdot \frac{E}{1 - \nu^2} \cdot \delta^2 \cdot \tan(\alpha) \quad \text{(Eq. 4)}$$

Whit the rearrangement of equation 3 we have an expression for indentation δ

$$\delta = \sqrt{\frac{kd}{(2/\pi)\,[E/(1-\nu^2)]\tan(\alpha)}} \quad \text{(Eq. 5)}$$

Since δ can not be detected directly by AFM it can be replaced by combining equations 1 and 5

$$z = d + \sqrt{\frac{kd}{(2/\pi)\,[E/(1-\nu^2)]\tan(\alpha)}} \quad \text{(Eq. 6)}$$

For data treatment we will use the more general form

$$|z - z_0| = d - d_0 + \sqrt{\frac{k\,(d - d_0)}{(2/\pi)\,[E/(1-\nu^2)]\tan(\alpha)}} \quad \text{(Eq. 7)}$$

d_0 and z_0 are the initial values of deflection and height, respectively.

Equation 7 was used to fit the date from the recorded force curves and to calculate the value of the elastic modulus, *E*, for each of the local measurements done in 6mer+BSP and 6mer films. A total of 100 force curves were recorded for both 6mer+BSP and 6mer films using the software NanoScope V (Veeco). *E* values were calculated by averaging over all points where the force curves were collected. Films were casted on mica, which was also used as a control. Force curves were collected using contact mode AFM.

6.2. Measuring films roughness

Roughness measurements were performed with the NanoScope V (Veeco). Two values were measured: the root mean square (RMS) and the arithmetic average height (R_a). RMS represents the standard deviation of the height values within a given area and it allows us to describe the surface roughness by statistical methods. R_a is the most frequently used roughness parameter and is defined as the average deviation of the roughness irregularities from the mean line over one sampling length. Because roughness values change with the scan size the measurements were performed using

three different scan windows: 20 x 20 μm^2, 10 x 10 μm^2 and 2 x 2 μm^2. Roughness measurements were performed on 2% protein films casted on mica. Mica was used as a control.

6.3. Assessing the formation of protein networks

In this thesis, AFM tapping mode imaging was used in a preliminary study to address the behaviour of 6mer+BSP molecules in the presence of divalent ion Ca^{2+}. Since 6mer+BSP is to be used for future bone regeneration applications its ability to bind Ca^{2+} ions is a very important feature for two reasons: first the deposition of CaP induced by BSP is believed to be related with the interaction between poly-E domains presence in this protein sequence; second, BSP, as many other proteins, as proven to be able to form calcium mediated networks, which could be an important feature for the osteointegration process, promoting the binding between the host tissue proteins and the implant.

For studying the formation of protein networks, 6mer+BSP and 6mer proteins were dissolved in three different solutions: (i) HEPES 0.1mM buffer, (ii) HEPES 0.1mM buffer containing magnesium (Mg) ions in a molar ratio of 1:1000 (protein:Mg) and (iii) HEPES 0.1mM buffer containing calcium (Ca) ions in a molar ratio of 1:1000 (protein:Ca)[20]. The final protein concentration was 0.01mg/ml. Protein solutions were deposited into a freshly cleaved mica surface and left to dry at room temperature.

7. Biological behaviour of the protein films

As mentioned previously in this chapter the biological behaviour of the new chimeric proteins was evaluated through *in vitro* and *in vivo* tests. *In vitro* cell tests were used to assess the biocompatibility of all the new chimeric proteins while the ability to sustain osteogenic differentiation was only assessed for 6mer+BSP and 6mer (control). 6mer+BSP and 6mer+hepcidin proteins were selected for *in vivo* studies. The selection of these proteins for *in vivo* studies was based in the promising results obtained during the *in vitro* studies. 6mer+hepcidin protein showed antimicrobial activity and was able to sustain the proliferation of mammalian cells and 6mer+BSP was able to induce the deposition of calcium phosphates and to sustain cell

proliferation and differentiation into the osteogenic lineage. The following sections address the methodologies used for *in vitro* and *in vivo* characterization.

7.1. *In vitro* cell tests

In this thesis, two different cell types were used to assess cell responses to the four recombinant proteins produced, osteosarcoma cell line (SaOs-2) and human Mesenchymal Stem Cells (hMSC).

In the case of 6mer+HNP-2, 6mer+HNP-4 and 6mer+hepcidin SaOs-2 cells were used to assess the possible cytotoxic effect of these protein films. In the case of 6mer+BSP films besides cytotoxicity there was also the need to study osteogenic differentiation of cells seeded onto these protein films, leading to the selection of hMSC for cell studies. The differentiation of hMSCs into osteoblasts was evaluated through real time quantitative reverse transcription-polymerase chain reaction (real time qRT-PCR). FE-SEM and EDS analyses were used to address cell morphology and possible mineral deposition during cell culture.

Alamar Blue was used to measure cell viability and cytotoxicity in both cell studies and 6mer films and Tissue culture plate (TCP) were used as controls in both studies.

7.1.1. Cell culture

SaOs-2 is an immortalized human osteosarcoma cell line (ATCC HTB-85), which was selected for these *in vitro* studies due to its osteoblastic features, such as elevated alkaline phosphatase activity and production of mineralized matrix [21]. Thus, this cell line offers a good study model for biopolymers such as 6mer+HNP-2, 6mer+HNP-4 and 6mer+hepcidin, primarily developed for future bone applications [21]. Cells were cultivated using basal medium consisting in Dulbecco's modified Eagle's medium (DMEM) supplemented with 10% (v/v) fetal bovine serum (FBS), 1% penicillin-streptomycin (v/v), at 37 ºC with 5% CO_2 in a humidified environment. After reaching confluence, cells were harvested with trypsin/EDTA and after counting cells were seeded at $3.0x10^3$ cells/cm^2 in a 96 well plate coated with the four different types of protein films (6mer+HNP-2, 6mer+HNP-4, 6mer+hepcidin, 6mer, control) and cultured for 3 days.

HMSC have been shown in previous studies to have capacity to differentiate into osteoblast when supplemented with certain growth factors. In this thesis, the hMSC were aspirated from bone marrow originated from a young healthy donor obtained from Lonza (Walkersville, MD). These cells were used to evaluate *in vitro* cell responses to 6mer+BSP films. Frozen passage 3, hMSC stocks were thawed and seeded at $3.0x10^3$ cells/cm^2 in a 96 wells plate, containing 6mer and 6mer+BSP films, using basal medium. The basal medium was DMEM supplemented with 10% (v/v) fetal bovine serum (FBS), 1% penicillin-streptomycin (v/v) and 10 ng of basic fibroblast growth factor (bFGF). Cells were cultivated at 37 ºC with 5% CO_2 in a humidified environment. After cells reach 80-90% confluence, the culture medium was changed from basal medium to osteogenic medium consisting in DMEM supplemented with 10% (v/v) FBS, 1% antibiotic/antimycotic, 100 nM dexamethasone, 10 mM β-glycerol phosphate and 0.05 mM ascorbic acid. Samples were collected after 3, 7 and 14 days of culture. 6mer+BSP and 6mer films cultured with osteogenic medium, without cells, were used as controls to test for the possible influence of cells on mineral deposition.

7.1.2. Cell viability tests

The Alamar blue (Invitrogen, DAL1025) assay was used to determine cell viability/proliferation after 3 days of culture for 6mer+HNP-2, 6mer+HNP-4, 6mer+hepcidin and after 3, 7 and 14 of cell culture for 6mer+BSP. In both studies, Alamar Blue reagent was added to the growth media in a 1:10 dilution ratio and data was collected using fluorescence at 530-560 nm excitation and 590 nm emission [23]. The Alamar Blue system incorporates an oxidation-reduction indicator (redox indicator) that fluoresces and changes colour as a result of chemical reduction of growth media due to cell metabolic activity. This redox indicator was demonstrated to be minimally toxic to cells. In these tests 6mer and TCP were used as controls.

7.1.3. Real time quantitative reverse transcription-polymerase chain reaction detection of osteogenic markers

Real time qRT-PCR enables reliable detection and measurement of products generated during each PCR cycle. This measurement is possible due to a dual-labeled

fluorogenic probe named TaqMan probe and provides very accurate and reproducible quantification of gene copies [22].

Real time qRT-PCR was used to assess the expression of osteogenic markers after three, seven and fourteen days of culture of hMSCs on 6mer+BSP films. So, for real time quantitative RT-PCR, the mRNA of cells was extracted using RNeasy mini kits (Qiagen, 74106) and cDNA synthesis was performed using High Capacity cDNA Reverse Transcription Kit (Applied Biosystems, 4368814), following the suppliers protocols. For the PCR reaction the TaqMan Universal PCR Master Mix (Applied Biosystems, 4304437) was used, following the procedure provided by the supplier, and the Taqman Gene Expression Assay was used to access the expression of the following genes: COL1A1 (collagen type I alpha 1, Hs00164004_m1), IBSP (integrin bone sialoprotein, Hs00173720_m1), ALP (alkaline phosphatase, Hs00758162_m1), GAPDH (Glyceraldehyde 3-phosphate dehydrogenase, Hs99999905_m1) and COL2A1 (collagen type II alpha 2, Hs01064869_m1). Results were normalized to GAPDH expression used has a housekeeping marker. 6mer and TCP were used as controls in this test.

7.2. *In vivo* tests

In this thesis *in vivo* studies were used to characterize the inflammatory response elicited by two of the four new chimeric proteins generated: 6mer+BSP and 6mer+hepcidin. In both *in vivo* studies the results obtained for 6mer+BSP and 6mer+hepcidin were compared with the outcomes observed for 6mer and poly-lactic-glycolic-acid (PLGA), a Food and Drug Administration - FDA - approved polymer, films and with a control exposed to the same treatments but with no implanted material. The inflammatory responses were evaluated after 2 and 6 weeks of grafting by histology and flow cytometry analysis.

7.2.1. Mouse subcutaneous implant

All procedures were conducted under animal care protocols approved by Tufts Institutional Animal Care and Use Committee.

All animals used in this study were five to seven weeks old balb/c female mice (Charles River breeding labs). Animals were maintained under general anesthesia with an isoflurane and oxygen delivery mask. Mice were positioned in ventral recumbency

and their backs were aseptically prepared for surgery. Under anesthesia, a part of the dorsal back was shaved with an electric razor and disinfected with ethanol 70% (v/v). After, a 1cm length incision was performed with fine scissors and the hydrated sample was implanted into a void space created in the subcutaneous area between skin and muscle layer. After insertion this skin incision was closed with a surgical suture line and again disinfected with a betadin solution (Figure II.8). The healing process at the incision region was monitored during the all study period and no deaths were registered during the experiment.

The mice were randomly assign to each of the four experimental groups and only one sample was implanted in each mouse in a total of five mice per tested group, 6mer, 6mer+BSP and PLGA. Also, five mice were used as a control group, subjected to the same surgical procedures as the implanted groups but with no sample implanted. A total of 40 mice were used in the experiment, distributed by four experimental groups each with two time points, 2 and 6 weeks.

In order to check for acute and chronic inflammatory responses, mice were euthanized by cervical dislocation after 2 and 6 weeks post-implantation and samples explanted along with the overlying skin for histological examination and flow cytometry analysis.

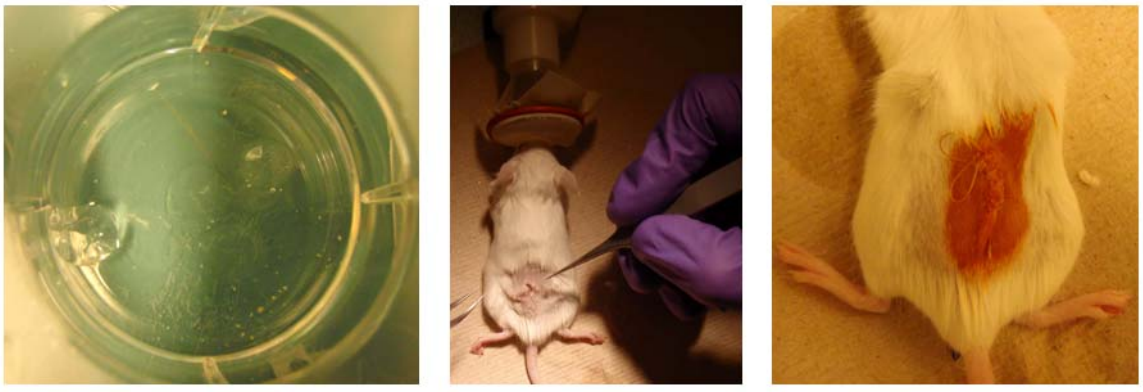

Figure II.8. Overview of the surgical procedure for films implantation.

7.2.2. Flow cytometry analysis

Flow cytometry analysis was used to assess the type and number of cells present in the host tissue around the implanted material. In this way, the tissue surrounding the graft and overlying skin was used for cell extraction. When present,

subcutaneous fat and muscle tissues were removed by scraping. The cleaned skin was minced with the help of fine scissors and digested for two hours, at 37ºC, in 5 ml mixture solution of 2 mg/ml collagenase IV (Invitrogen, 17104019) and 1.2 units/ml dispase (Invitrogen, 17105041) in PBS. After digestion the mixture was centrifuged at 1500rpm for 5 minutes at 4ºC and the pellet was resuspended at a density of 10^6 cells/ml in PBS supplemented with 0.5% BSA, flow cytometry buffer. The suspension solution was filtered with a cell strainer with 100 µm pore to eliminate non digested tissues and cell suspension was collected in a 50 ml falcon flask and centrifuged at 1500 rpm for 5 minutes at 4ºC. For the removing of red blood cells the pellet was resuspended in lysis buffer (NaCl 137 mM, Na_2HPO_4 8 mM, KH_2PO_4 1.46 mM, KCl 2.68 mM, in distilled water, pH 7.0) and incubated at room temperature for four to five minutes with occasional shaking. Lysis reaction was stopped by diluting the lysis buffer with 20 to 30 ml of PBS. Cells were spin down at 1500 rpm for five minutes at 4ºC followed by two washes with flow cytometry buffer. For antibody staining, cells pellet was resuspended in PBS, incubated for 15 minutes on ice in the presence of rat anti-mouse FcRII/III (clone 2.4G2, BD Pharmingen, 553141) antibody, to block non-antigen-specific binding of immunoglobulins to Fc receptors. After washing and centrifugation the pellet was again resuspended on PBS. Finally, for cell surface marker antigen analysis approximately 50µl of cell suspension were incubated for 30 minutes on ice antibody with one of the secondary antibodies described in Table 3.

Table II.3. Secondary antibodies used for cell labelling.

Secondary antibody	Target cells
Fluorescein isothiocyanate (FITC) conjugated rat anti-mouse monoclonal antibody CD3 (BD Pharmingen, 555274)	Thymocytes and mature T lymphocytes [32, 33]
Allophycocyanine (APC) rat anti-mouse polyclonal antibody CD25 (BD Pharmingen, 558643)	T and B lymphocytes [34, 35]
Alexa-conjugated rat anti-mouse monoclonal antibody CD4 (BD Pharmingen, 557667)	T helper (T_H) cells, immunosuppressive regulatory T cells and natural killer T (NK-T) cells [36, 37]
Alexa-conjugated rat anti-mouse monoclonal antibody CD8 (BD Pharmingen, 557668)	T suppressor/cytotoxfic cells [37, 38]
Phycoerythrin (PE) conjugated rat anti-mouse monoclonal antibody CD14 (BD Pharmingen, 557740)	Cells expressing CD14, a receptor for the complex formed by lipopolysaccharide (LPS) and a LPS binding protein present in plasma [39]

After incubation, samples were centrifuged at 1500 rpm for 5 minutes at 4ºC, washed twice with flow cytometry buffer and suspended in 200 to 300 µl of flow cytometry buffer with ethylenediaminetetraacetic acid (EDTA, Sigma, 431788) 5 mM to protect cells until flow cytometry analysis. For live/dead discrimination 5 µl of 7-amino-actinomycin D (7-AAD, BD Pharmingen, 559925) was added to each sample.

Cells were analyzed by a four-color FACSCalibur instrument equipped with a 488nm argon-ion laser and a 635nm red diode laser (Becton Dickinson, NJ, USA) and data was processed using FlowJo analysis software (Tree Star, Inc., OR, USA).

7.2.3. Histology

Retrieved samples together with the overlaying tissues were processed for histological examination to determine the extent of films degradation and to search for inflammation responses to the implanted materials. After collection, samples were immediately immersed in a buffered 4% formalin solution in PBS and sent for processing at Tufts Animal Pathology Core where samples were embedded in paraffin, cut into 10µm sections and stained with hematoxylin and eosin (H&E). H&E is widely used in histology for the recognition of various tissues as it can be seen in Figure II.9. Hematoxylin has blue purple colour and stains nucleic acids. Eosin is pink and colours proteins in an unspecific way. In *in vivo* studies with 6mer+BSP proteins the histology analysis was complemented with Alizarin and Von Kossa dyes for calcium deposits. Alizarin red is used to identify calcium deposits in tissue sections and acts by forming chelate complexes with calcium yielding a birefringent red salt. Alizarin can also react with other with other divalent ions like magnesium, manganese, barium and iron. However since the concentration of these ions in tissues is very low they should not interfering with the staining process [24]. Von Kossa is a stain that identifies anionic salts such as phosphate and carbonate salts which in most cases are bonded to calcium ions. So, this dye is an indirect way to detect calcium deposits since it does not bind directly to calcium [25].

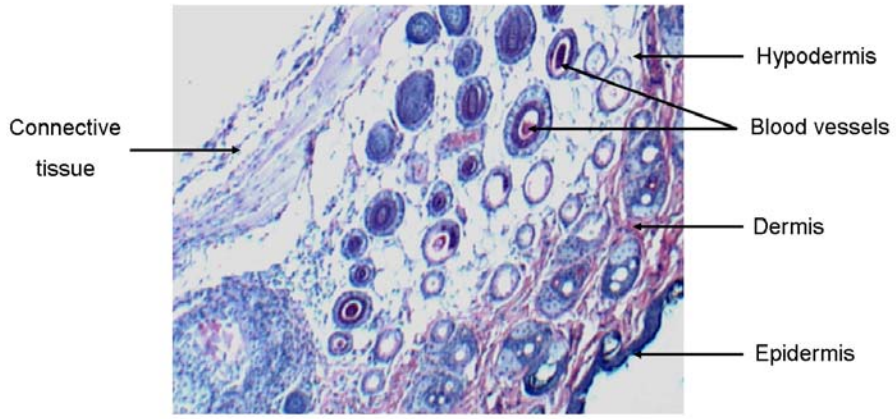

Figure II.9. Mouse skin section stained with hematoxylin and eosin.

8. Morphological and elemental analyses

For morphological and elemental characterization were used FE-SEM and EDS, respectively. SEM microscope is one of the most versatile instruments available for the examination and analysis of the microstructural characteristics of solid objects. Two of the most important features of SEM are its ability to take high-resolution images of bulk objects and its large depth of field, responsible, in part, for the three-dimensional appearance of the specimen image. For conceiving an image, SEM first generates high-energy electrons and focuses them into an electron beam used to scan the sample surface. These electrons are either absorbed or scattered by the sample and this energy exchange can be detected by SEM detectors and used to generate images from the sample surface [26].

EDS is an analytical technique used to evaluate the elemental composition of a certain material. EDS systems are excellent choices for a rapid qualitative and quantitative analysis of the elements forming a sample. This is accomplished through the emission of X-rays by the sample when bombarded by an electron beam, which leads to the ejection of electrons from the specimen surface. X-rays are emitted when electrons from a higher shell fill the vacant space left by the ejected electrons. EDS X-ray detector measures the number and the energy of the rays emitted. Element analysis is possible because the energy value of an emitted X-ray is specific for each element. EDS analysis attached to SEM microscopy allows us for an elemental analysis on microscopic sections of the materials [26].

8.1. Field-emission scanning electron microscopy (FE-SEM) characterization

In this thesis, FE-SEM (NanoSEM, FEI Nova 200) was used to assess mineral deposition on 6mer+BSP and 6mer films before and after incubation in ACS for different periods of time, as described in the section 5.1. In the biological tests (section 7.1.), the SEM analysis was also used to evaluate the morphology of cells seeded on the 6mer+BSP and 6mer films before and after 3, 7 and 14 days of cell culture in osteogenic medium. Samples were fixed with a 2.5% glutaraldehide solution in phosphate buffer (PBS) (w/w) and dehydrated in a series of ethanol-water solutions with increasing ethanol concentration (v/v): 25%, 30%, 50%, 70%, 80%, 90% and 100%. For FE-SEM analysis, samples were sputter coated with gold-palladium.

8.2. Energy dispersive spectroscopy analysis of mineral deposition

EDS analysis (EDAX- Pegasus X4M) was used to evaluate the elemental composition of the mineral deposited on the surface of 6mer+BSP and 6mer protein films. So, EDS analysis was used to characterize the surface of 6mer+BSP and 6mer films before and after incubation in ACS and to access mineral deposition onto 6mer+BSP and 6mer films after 3, 7 and 14 days of cell culture in osteogenic medium (please see the sections 5.1. and 7.1.). EDS analysis was done without coating.

9. Statistical analysis

SPSS 17.0 software was used to perform all statistical analysis described in this thesis. The Shapiro-Wilk test was use to test for the normality of the data. For data with no normal distribution, the nonparametric Mann-Whitney and Kruskal-Wallis tests were used to test for significant differences between two and more than two sets of data, respectively. For data with normal distribution was used one-way ANOVA with a Dunet's T3 or Bonferroni post hoc comparison for comparing more than two datasets and the parametric test t was used for comparing only two data sets. Statistical significance was defined as $p<0.05$.

References

1. Rabotyagova O, Cebe P, Kaplan DL. Self-assembly of genetically engineered spider silk block copolymers. Biomacromolecules 2009;10:229–236.

2. Sanger F, Nicklen S, Coulson AR. DNA sequencing with chain-terminating inhibitors. Proc Natl Acad Sci U S A 1977;74(12):5463-5467.

3. Yan S-Z, Beeler JA, Chen Y, Shelton RK, Tang W-J. The regulation of type 7 adenylyl cyclase by its C1b region and *Escherichia coli* peptidylprolyl isomerase, SlyD. J Biol Chem 2001;276(11):8500-8506.

4. Hottenrott S, Schumann T, Plückthun A, Fischer G, Rahfeld J-U. The *Escherichia coli* SlyD is a metal ion-regulated peptidyl-prolyl cis/trans-Isomerase. J Biol Chem 1997;272(25):15697-15701.

5. Huang J, Valluzzi R, Bini E, Vernaglia B, Kaplan DL. Cloning, expression, and assembly of sericin-like protein. J Biol Chem 2003;278(46):46117-46123.

6. Harvey DJ. Matrix-assisted laser desorption/ionization mass spectrometry of carbohydrates and glycoconjugates. Int J Mass Spectrom 1999;226(1):1-35.

7. Audrey RE. Liquid chromatography-mass-spectroscopy. West Sussex: John Wiley & Sons, Ltd, 2003.

8. Foo CWP, E.Bini, Huang J, Lee SY, Kaplan DL. Solution behavior of synthetic silk peptides and modified recombinant silk proteins. Appl Phys Mater Sci Process 2006;82:193–203.

9. Pérez-Rigueiro J, Viney C, Llorca J, Elices M. Mechanical properties of silkworm silk in liquid media. Polymer 2000;41:8433–8439.

10. Beek JDv, Hess S, Vollrath F, Meier BH. The molecular structure of spider dragline silk: folding and orientation of the protein backbone. Proc Natl Acad Sci USA 2002;99:10266-10271.

11. Hayashi CY, Shipley NH, Lewis RV. Hypotheses that correlate the sequence, structure, and mechanical properties of spider silk proteins. Int J Biol Macromol 1999;24(2-3):271-275.

12. Hayashi CY, Shipley NH, Lewis RV. Hypotheses that correlate the sequence, structure, and mechanical properties of spider silk proteins. Int J Biol Macromol 1999;24(271–275).

13. Bini E, Foo CWP, Huang J, Karageorgiou V, Kitchel B, Kaplan DL. RGD-functionalized bioengineered spider dragline silk biomaterial. Biomacromolecules 2006;7:3139-3145.

14. Krimm S, Bandekar J. Vibrational spectroscopy and conformation of peptides, polypeptides, and proteins. Adv Protein Chem 1986;38:181-364.

15. Kelly S, Jess T, Price N. How to study proteins by circular dichroism. Biochim Biophys Acta - Proteins & Proteomics 2005;1751(2):119-139.

16. Bauer AW, Kirby WM, Sherris JC, Turck M. Antibiotic susceptibility testing by a standardized single disk method. Am J Clin Pathol 1966;45(4):493-496.

17. Li S, Xing D, Li J. Dynamic light scattering application to study protein interactions in electrolyte solutions J Biol Phys 2004;30(4):313-324.

18. Liu Q, Weng J, Wijn JGCd, Blitterswijk TRv. A novel in vitro model to study the calcification ability of biomaterials. Fifht World Biomaterials Congress; 1996 May 2nd; Toronto, Canada; 1996. p. 29.

19. Binnig G, Quate CF, Gerber C. Atomic force microscope. Phys Rev Lett 1986;56(9):930-933

20. He G, Dahl T, Veis A, George A. Dentin matrix protein 1 initiates hydroxyapatite formation *in vitro*. Connect Tissue Res 2003;44(1):240-245.

21. Sevgi B. Rodan, Yasuo Imai, Mark A. Thiede, Gregg Wesolowski, David Thompson, Zvi Bar-Shavit, et al. Characterization of a human osteosarcoma cell line (Saos-2) with osteoblastic properties. Cancer Res 1987;47(15):4961-4966.

22. Heid CA, Stevens J, Livak KJ, Williams PM. Real time quantitative PCR. Genome Res 1996;6(2):986-994.

23. Lancaster MV, Fields RD, inventors. Antibiotic and cytotoxic drug susceptibility assays using resazurin and poising agents. USA Patent No. 5501959, 1996.

24. Churukian Cj. Pigments and minerals. In: Gamble M, Bancroft JD, editors. Theory and practice of histological techniques. Sixth edition ed: Elsevier 2008.

25. Braun-Falco O, Wolff HH, Plewig G, Burgdorf WHC. Dermathology. Second Edition ed. New York: Springer, 1996.

26. Goldstein J, Newbury DE, Joy DC, Lyman CE, Echlin P, Lifshin E, et al. Scanning Electron Microscopy and X-ray Microanalysis. Third Edition ed: Springer Science + Business Media, Inc., 2003.

Abstract

The remarkable mechanical characteristics of spider major ampullate spidroin protein suggest this polymer as a promising biomaterial to consider for the fabrication of scaffolds for bone regeneration. Herein, a new functionalized spider silk-bone sialoprotein fusion protein was designed, cloned, expressed, purified and the osteogenic activity studied. Bone sialoprotein (BSP) is a multi-domain protein with the ability to induce cell attachment and differentiation and the deposition of calcium phosphates (CaP). Attenuated Total Reflection Fourier Transform Infrared (ATR-FTIR) was used to assess the secondary structure of the fusion protein. *In vitro* mineralization studies demonstrated that this new fusion protein with BSP retained the ability to induce the deposition of CaP. Studies *in vitro* indicated that human mesenchymal stem cells had significant improvement towards osteogenic outcomes when cultivated in the presence of the new fusion protein *vs*. silk alone. The present work demonstrates the potential of this new fusion protein for future applications in bone regeneration.

1. Introduction

The increasing demand for organs and tissues represents a major health challenge worldwide. Bone grafting is the second most frequent transplant procedure after blood transfusion. Transplantation of bone tissue from autogeneic and allogeneic sources has been a major strategy in tissue repair. However, major challenges regarding transplantation remain, including the limited availability of suitable and safe tissues and organs, frequent adverse immune responses and disease transmission, loss of biological and mechanical properties after processing, high costs and worldwide scarcity [1]. As an option, tissue engineering has been explored for bone regeneration with the objective of generating bone functional equivalents to overcome the limitations of the currently used methodologies mentioned above [2]. For this purpose different polymers with diverse mechanical and biological characteristics have been studied with respect to support for regeneration of damaged bone tissue.

A particularly relevant polymer for consideration as biomaterial scaffolds in bone regeneration are silk proteins, derived from spiders and silkworms. Silks harbour remarkable mechanical properties, while also offering slow biodegradation in vivo and

appropriate biological compatibility [3]. While silkworm silk has been extensively studied with regard to bone tissue formation in vitro and vivo, spider silks have been less studied in this context.

Spiders produce different types of silk for different functions. Among these different silk types, the major ampullate silk, or dragline silk, secreted by the major ampullate gland presents tensile strength comparable to Kevlar ($4x10^9$ N/m^2) and extensibility around 35%, compared to 5% for Kevlar [4]. Major ampullate silk protein presents a molecular structure formed by beta sheet forming crystalline regions that alternate with less organize regions protein chains. These two regions correspond to two chemically distinct blocks in the protein polymer chains, where the hydrophilic GGX motifs (G stands for glycine and X is mostly glutamine) are responsible for the less crystalline regions and the poly-alanine (poly-A) motifs form the crystalline regions. The hydrophobic poly-A motifs are responsible for the formation of rigid and highly packed anti-parallel β-sheets [5] due to hydrogen bonding, and generating the physical crosslinks that stabilize silk structures in these crystalline regions. The GGX motif adopts a helical conformation forming an amorphous region that connects the poly-A motifs providing elasticity to the silk fibers [6]. The combination of glycine-rich domains with the polyalanine regions and the formation of β-sheet cross-links between blocks give rise to the impressive mechanical properties of major ampullate silk fibers [7].

The silk from the silkworm *Bombyx mori*, supplied in large scale by sericulture, however, no equivalent production process is currently available for spider silks. For this reason the production of spider silk is carried out in heterologous expression systems, such as *Escherichia coli*, as used by ours and other research groups to provide sufficient spider silk for study [7, 8]. Furthermore, the use of recombinant DNA technology in the synthesis of these protein based biopolymers has significant advantages over conventional production systems, allowing precise control of the protein primary sequence and thus chemistry, along the length and for control block distribution [8]. The major ampullate spidroin protein (MaSpI), produced by the spider species *Nephila clavipes*, is one of the spider silks most extensively studied using recombinant DNA technology [4]. The high strength, toughness, light weight and

expression in heterologous systems make MaSpI a suitable choice for the fabrication of high performance biomaterials for bone regeneration applications.

An advantage of using genetically bioengineered fibrous proteins such as spider silks is the possibility of generating new genetic variants carrying different functional domains. Therefore the synthesis of new chimeric proteins with enhanced features when compared with the native isolated counterparts, can offer multifunctional features that otherwise are difficult to obtain, require extensive chemical modifications or are challenging to control during preparation. Thus, MaSpI can be expressed together with other proteins resulting in a new chimeric proteins, retaining the self-assembly and outstanding mechanical performance of the native silk materials, but adding new functional features to improve or control biocompatibility and osseointegration. We have previously demonstrated this approach with both silica [9] and hydroxyapatite [10] nucleation domains fused to spider silk.

Different studies demonstrate the ability of bone sialoprotein (BSP) in inducing the attachment and migration of endothelial cells [11], together with adhesion and differentiation of osteoblasts [12] related to bone remodelling [13]. The ability to induce cell adhesion is related with the presence of a C-terminal RGD sequence in BSP that binds to integrins [14-18]. Additionally, *in vivo* studies indicate that previous incorporation of BSP into collagen [19, 20] or titanium [21] implants promoted osteoblast differentiation and proliferation and enhanced osteoinductive effects. Furthermore, BSP is also responsible for the deposition of calcium phosphate in bone tissues, specially after association with collagen type I [22]. There is some evidence that in the first stages of mineralization hydroxyapatite crystals nucleate and grow inside the 68 nm gaps (hole zones) present between the triple-helical collagen fibrils. As the crystals continue to grow they compress the collagen fibril molecules, eventually fusing to form plate shaped crystals [23, 24]. The labelling of BSP allowed the detection of this protein in these hole zones between the collagen fibrils suggesting that this protein may regulate the onset of calcification at these gap zones [25]. The flexible BSP structure is one reason for the ability of the protein to interact with different binding partners [26] including collagen [22], hydroxyapatite [27], matrix metalloproteinase, factor H [28], and integrin $\alpha_v\beta_3$ present in cell membranes [16, 17].

The objective of the present study was the generation of a new silk fusion protein through the combination of BSP and MaSp1 consensus sequences (Figure III.1A). The silk block carries six repeats of the consensus repeat unit for the native sequence of the major ampullate dragline silk I from *N. clavipes*. Each silk repeat is formed by a hydrophilic GGX motif and a hydrophobic poli-A motif (Figure III.1B).

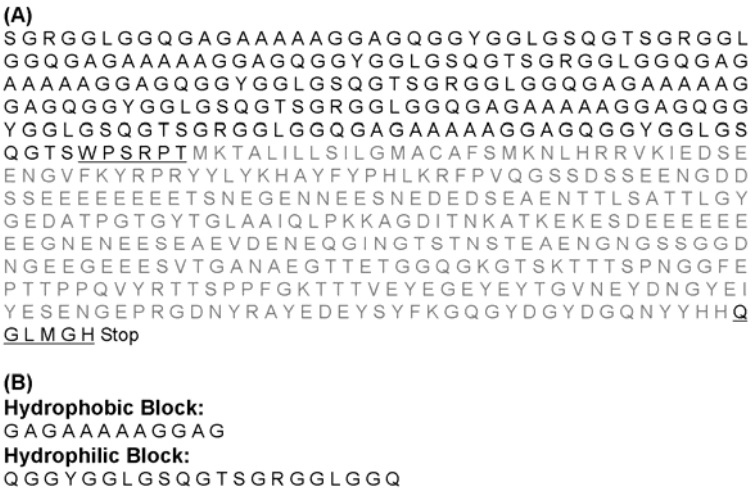

Figure III.1. (A) Amino acid sequence for the chimeric protein carrying the consensus repeats for MaSp1 and the BSP sequence. The linkers for the BSP sequence are underlined. The 6mer is in black and the BSP sequence in gray. (B) Amino acid sequences for the hydrophobic and hydrophilic blocks present in each of the six units forming the silk block copolymer (6mer).

The present work describes for the first time the assembly of a novel molecular-level biomaterial combining a spider silk consensus sequence with the complete sequence for BSP. When compared with previous silk chimeras [9, 10] this new fusion protein as the advantage of combining the remarkable mechanical performance and self-assembly capability of silk with the multi-domain BSP sequence. This multi-domain nature of BSP is advantageous in a way that will allows us to control at the same time different processes such as the deposition of calcium phosphates (CaP), cell adhesion, cell migration and the differentiation of different types of cells.

2. Materials and methods

2.1. Cloning of BSP into pET30L vector containing the silk modules

The vector pET30a+ (Novagen, San Diego Ca) was used for the construction of the vector pET30L carrying the silk block copolymer and its assembly was described in

our prior studies[8]. The spider silk block copolymer was cloned together with six histidine residues to facilitate purification[8]. The clone containing the bacterial plasmid pENTR223.1 carrying the human BSP cDNA sequence (Clone Identification: HsCD00082642) was purchased from the Harvard clone collection "The ORFeome Collaboration" (Dana-Farber/Harvard Cancer Center, Boston MA). The clones with pENTR223.1 plasmid carrying the BSP cDNA sequence were inoculated in Luria Bertani (LB) medium and grown overnight at 37ºC with shaking (200 rpm/min). The pENTR223.1 plasmid was extracted using Qiagen miniprep kit (28704) for plasmid isolation and digested with *SfiI* enzyme (New England Biolabs, R0123S) which cuts in the regions flanking the BSP cDNA sequence. The digestion product was run in a 0.8% agarose gel and the band for the BSP cDNA sequence (951bp) was purified using a QIAquick gel extraction kit (Qiagen, 28706). For ligation of the BSP cDNA sequence to the 6mer spider silk clone, a linker was designed containing in its central region a restriction site for *Sfi*I for insertion of the BSP clone, and also restriction sites for *Spe*I (New England Biolabs, R0133S) and *Nhe*I (New England Biolabs, R0131S) related to the spider silk clone. For insertion of the linker in the expression vector pET30L, the vector was digested with *Spe*I, dephosphorylated with Alkaline Phosphatase, Calf Intestinal (CIP) enzyme (New England Biolabs, M0290S) and run on 0.8% agarose gel. The linearized vector was purified using the QIAquick gel extraction kit. The linker was double digested with *Spe*I and *Nhe*I restriction enzymes generating compatible ends with those generated by *Spe*I with the expression vector pET30L. The linker was run on 0.8% agarose gel and purified using the QIAquick gel extraction kit. The linker was then inserted in the linearized vector pET30L. The ligation reaction was carried out with T4 DNA ligase enzyme (New England Biolabs, M0202S).

Escherichia coli DH5α cells (Invitrogen, 18258-012) were transformed with the ligation product and transformants were identified by incubation on agar plates containing 25 μg/ml kanamycin. The presence of the linker in the pET30L vector was confirmed by DNA sequencing. For the insertion of the BSP cDNA sequence both vector pET30L carrying the linker (vector pET30L + linker) and vector pENTR223.1 alone were digested with *Sfi*I. In the case of the linearized vector pET30L + linker the ends generated by the digestion with *Sfi*I were dephosphorylated with CIP. After running both digestion products in a 0.8% agarose gel the bands corresponding to the BSP

cDNA sequence and to the linearized vector pET30L + linker were purified using the QIAquick gel extraction kit. The ligation reaction between the vector pET30L + linker and the BSP cDNA sequence was carried out with T4 DNA ligase. *E. coli* DH5α cells transformed with the ligation product were identified by incubation in agar plates containing 25μg/ml kanamycin. The presence of the BSP insert was confirmed by DNA sequencing and the new constructs were named 6mer+BSP.

2.2. Protein expression, purification and identification

Both 6mer and 6mer+BSP proteins were expressed in *E. coli* RY-3041 strain, a mutant strain of *E. coli* BLR(DE3) defective in the expression of SlyD protein [29, 30]. Cells were cultivated at 37ºC in Luria-Bertani (LB) medium, with 25 μg/ml kanamycin until an OD_{600} between 0.9 and 1 was reached. At this point expression was induced by adding isopropyl β-D-thiogalactoside (IPTG, Invitrogen, 15529019) to a final concentration of 0.5 mM. After 2 hours cells were harvested by centrifugation at 6,500 rpm. The cells pellet was resuspended in a denaturating buffer (100 mM NaH_2PO_4, 10 mM Tris HCl, 8 M urea, pH 8.0) and left overnight with stirring for complete cell lysis. Insoluble cell fragments and soluble proteins present in the cell lysate were separated by centrifugation at 11,000rpm. The supernatant was mixed with Ni-NTA resin (Qiagen, 30250) and left for 2 hours with stirring. The supernatant/Ni-NTA resin mixture was loaded onto a glass Econo-column (Biorad) and washed several times with denaturating buffer at pH 8 and at pH 6.0. The protein 6mer+BSP was eluted using denaturating buffer at pH 4.5. The purified protein was dialysed first against a 20mM sodium acetate buffer followed by extensive dialysis against water using cellulose ester snake skin membranes with a 100-500Da molecular weight cutting off (Spectra/Por Biotech, 131054). Finally, the dialyzed proteins were lyophilized.

Protein sequencing (Tufts Core Facility, Boston, MA) and SDS-PAGE were used to confirm protein identity. For SDS-PAGE, proteins were mixed with NuPAGE LDS sample buffer (Invitrogen, NP0007) and heated at 80ºC during 10 minutes. Afterwards, the samples were separated using a bis-tris 4-12% gel (Invitrogen, NP0321BOX). For band detection was used the colloidal blue staining kit (Invitrogen, LC6025).

2.3. Film formation and secondary structure analysis

Both recombinant 6mer+BSP and 6mer proteins were dissolved in MQ water to a final concentration of 2% (w/v). Then 60µl of each protein solution was cast into a plastic non adherent polystyrene surface and left to dry at room temperature. The films were treated with a 70% methanol solution for 2 hours to induce the transition of secondary structure from random coil to β-sheet. For cell and mineralization studies the films were treated with 70% (w/w) ethanol solution for sterilization purposes.

The transition of the silk secondary structure was confirmed by Attenuated-Total Reflectance Fourier Transform Infrared Spectroscopy (ATR-FTIR) (Jasco model FT/IR-6200 type A). Spectra were collected in absorption mode at $8cm^{-1}$ resolution using 64 scans in the spectral range 4000 to $400cm^{-1}$. The quantification of secondary structure was based in the analysis of the amide I region (1700 to $1600cm^{-1}$). The average percentage for the secondary structures, mainly β–sheet content, for the 6mer (control) and 6mer+BSP proteins were calculated through the integration of the area of each deconvoluted curve followed by the normalization of the obtained value to the total area of the amide I region.

2.4. *In Vitro* Mineralization

To investigate the mineralization potential of the new chimeric protein 6mer+BSP, a protein solution was prepared as described previously and 60 µl of this solution was used to prepare films. The films were treated with methanol as described above, and a similar procedure was carried out for the control 6mer protein. Both protein films were incubated during 1 and 6 hours at 37ºC, with an accelerating calcification solution (ACS) of 150mM Na^+, 20mM of HEPES, 3.75mM Ca^{2+} and 2.32mM PO_4^{3-}, pH 7.4 [31] . At the end of the incubation periods of 1 and 6 hours the films were washed with MQ water and dried at room temperature.

2.5. *In Vitro* hMSCs responses to 6mer and 6mer+BSP films

Human mesenchymal stem cells (hMSC) were aspirated from bone marrow originated from a young healthy donor obtained from Lonza (Walkersville, MD). Frozen passage 3 hMSC stocks were thawed and seeded at $3.0x10^3$ cells/cm^2 in a 96 wells plate, containing 6mer and 6mer+BSP films, using basal medium consisting of

Dulbecco's modified Eagle's medium (DMEM) supplemented with 10% (v/v) fetal bovine serum (FBS), 1% penicillin-streptomycin (v/v) and 10ng of basic fibroblast growth factor (bFGF) at 37ºC with 5% CO_2 in a humidified environment. After cells reach 80-90% confluence culture medium was changed from basal medium to osteogenic medium consisting in DMEM supplemented with 10% (v/v) FBS, 1% antibiotic/antimycotic, 100nM dexamethasone, 10mM β-glycerol phosphate and 0.05mM ascorbic acid. Samples were collected after 3, 7 and 14 days of culture.

2.6. Analytical methods

Cell morphology was accessed through field-emission scanning electron microscopy (SEM) (NanoSEM, FEI Nova 200). Samples were fixed with a 2.5% glutaraldehide solution in phosphate buffer (PBS) (w/w) and dehydrated in a series of ethanol-water solutions with increasing ethanol concentration (w/w): 25%, 30%, 50%, 70%, 80%, 90% and 100%. For SEM observation the samples were sputter coated with gold-palladium.

Alamar Blue (Invitrogen, DAL1025) assay was used to determine cell viability/proliferation after 3, 7 and 14 days of culture. The Alamar Blue system incorporates an oxidation-reduction indicator (redox indicator) that fluoresces and changes colour as a result of chemical reduction of growth media due to cell metabolic activity. This redox indicator was demonstrated to be minimally toxic to cells. Alamar Blue reagent was added to the growth media in a 1:10 dilution ratio and data was collected using fluorescence at a 530-560nm excitation wavelength and 590nm emission wavelength[32].

For real time quantitative reverse transcription-polymerase chain reaction (real time qRT-PCR). the mRNA of cells was extracted using RNeasy mini kits (Qiagen, 74106) and cDNA synthesis was performed using High Capacity cDNA Reverse Transcription Kit (Applied Biosystems, 4368814). For the PCR reaction the TaqMan Universal PCR Master Mix (Applied Biosystems, 4304437) was used, following the procedure provided by the supplier, and the Taqman Gene Expression Assay was used to access the expression of the following genes: COL1A1 (collagen type I alpha 1, Hs00164004_m1), IBSP (integrin bone sialoprotein, Hs00173720_m1), ALP (alkaline phosphatase, Hs00758162_m1), GAPDH (Glyceraldehyde 3-phosphate dehydrogenase,

Hs99999905_m1) and COL2A1 (collagen type II alpha 2, Hs01064869_m1). Results were normalized to GAPDH expression used has a housekeeping marker.

2.7. 6mer and 6mer + BSP film characterization

Surface morphology of 6mer+BSP and 6mer films before and after incubation in ACS for different periods of time was characterized using field-emission scanning electron microscopy (SEM) (NanoSEM, FEI Nova 200). Samples were sputter coated with gold-palladium for SEM observation. Elemental composition of the mineral deposited on the surface of the protein films was characterized by energy dispersive spectrometer (EDS) (EDAX- Pegasus X4M) and no coating was used for this analysis. SEM and EDS characterization were also used to characterize 6mer+BSP and 6mer films after 3, 7 and 14 days of cell culture in osteogenic medium to access mineral deposition. 6mer+BSP and 6mer films cultured only with osteogenic medium, with no cells, were used as controls to test for the possible influence of cells on mineral deposition. For SEM, samples were sputter coated with gold-palladium and as mentioned before no coating was used for EDS analysis.

2.8. Statistical Analysis

SPSS 17.0 was used to perform statistical analysis. The Shapiro-Wilk test was used to test for the normality of the data. To compare between two sets of data mainly 6mer+BSP *vs* 6mer films (control) two statistical tests were used: two-tailed nonparametric Mann-Whitney test for non-normal distributed data and student t-test to analyse data with normal distributions. To test for significant differences between three experimental groups (3, 7 and 14 days) one-way ANOVA with a Bonferroni post hoc comparison was applied to the data with normal distribution and nonparametric Kruskal-Wallis test was used for the data with non-normal distribution. Statistical significance was defined as $p<0.05$.

3. Results

3.1. Cloning and expression of BSP silk chimera

The presence of the BSP insert in the cloning vector containing the silk modules was confirmed through DNA sequencing. SDS-PAGE indicates that both expression and

purification of the 6mer+BSP and the silk control, only 6mer, were successful and protein sequencing confirmed the N-terminal amino acid sequence. For 6mer+BSP protein the theoretical molecular weight is approximately 52kDa and with SDS-PAGE it is possible to observe a strong band at around 49kDa. In the case of the 6mer the estimated molecular weight is approximately 21.8kDa and the SDS-PAGE shows a band at 28 kDa (Figure III.2). After purification, dialysis and lyophilisation the yield of 6mer+BSP and 6mer was approximately 17mg/L and 25 mg/L, respectively.

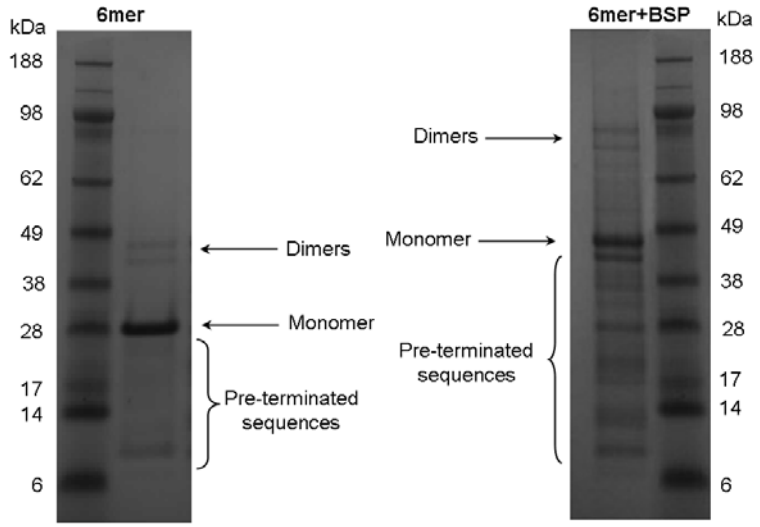

Figure III.2. SDS-PAGE gels for 6mer and 6mer+BSP proteins, stained with colloidal blue.

3.2. Film formation and secondary structure

The ATR-FTIR spectra of 6mer and 6mer+BSP films after 2 hours treatment with 70% methanol solution exhibited strong amide I (1700-1600 cm^{-1}) and amide II (1600-1500 cm^{-1}) regions (Figure III.3A). ATR-FTIR spectra for both protein films, 6mer+BSP and 6mer, exhibited vibrational modes in the range of 1650-1647 cm^{-1} amide I region, indicative of helix/random coil conformations and in the range of 1626-1628 cm^{-1}, amide I region, and at 1533 cm^{-1}, amide II region, both peaks indicative of antiparallel β-sheet structures [8, 33, 34]. After spectral deconvolution the percentage of helix/random coil and antiparallel β-sheet structures was determined (Figure III.3B). For both protein films the percentage of secondary structures was similar and statistical analysis indicated no significant ($p>0.05$) differences between the 6mer+BSP and 6mer control films. For helix/random coil conformations the percentages were

35% for the 6mer films and 32% for the 6mer+BSP films. For β-sheet structures the percentages were 33% and 32% for the 6mer and 6mer+BSP films, respectively.

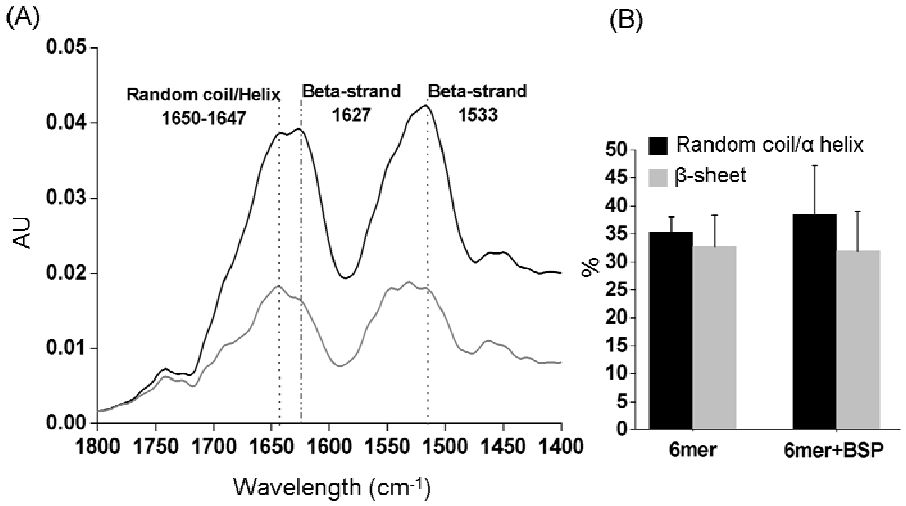

Figure III.3. (A) ATR-FTIR spectra of the 6mer and 6mer+BSP films after 2 hours of treatment with 70% methanol. (B) Percentage of β-sheet and random coil/helix conformations after ATR-FTIR spectra deconvolution of the 6mer and 6mer+BSP films.

3.3. Analysis of *in vitro* mineralization

After 1 hour in ACS at 37ºC SEM analysis did not generate evidence for the formation of minerals on either film, 6mer or 6mer+BSP (Figure III.4A). However, EDS analysis indicated the presence of calcium (Ca) and phosphorous (P) in the 6mer+BSP films but not in the 6mer films (Figure III.4B). The Ca/P ratios in 6mer+BSP films varied between 1.72 and 1.86. After 6 hours of incubation it was possible to observe by SEM the formation of mineral aggregates on the surface of the 6mer+BSP films, with diameters around 8-10µm (Figure III.4A). EDS analysis indicated a composition for Ca and P with Ca/P ratios between 1.82 and 2.03 (Figure III.4B). For the 6mer films, the formation of mineral was not observed even after at 6 hrs (Figure III.4A). These results are in agreement with the EDS analysis, where no mineral was detected on the 6mer control films surface after 6 hours of immersion in ACS (Figure III.4B).

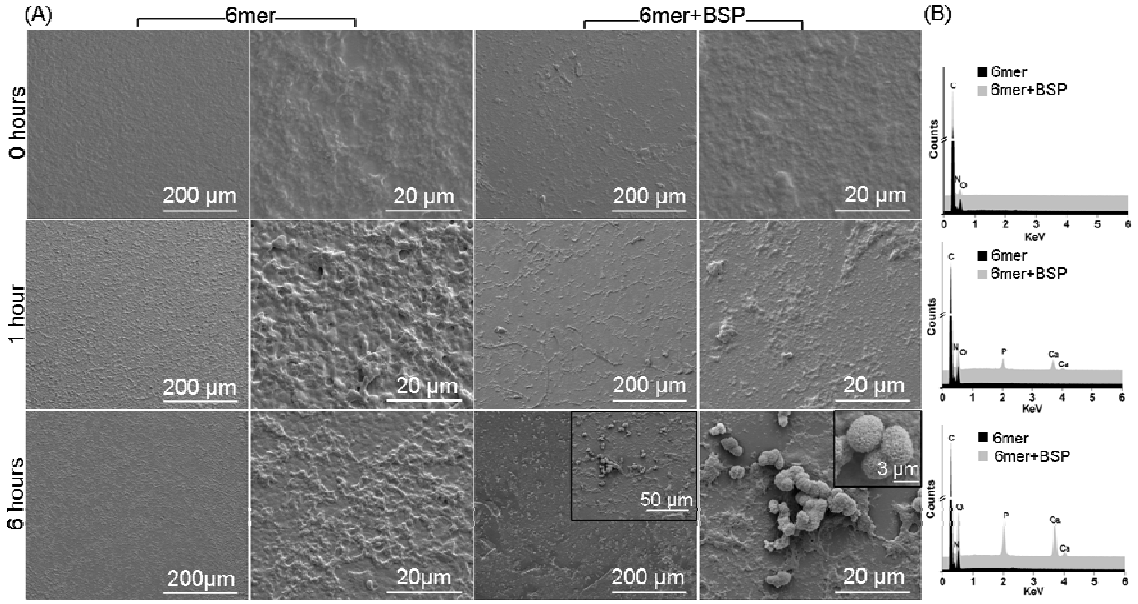

Figure III.4. (A) Surface morphologies and (B) EDS characterization of the 6mer and 6mer+BSP films before and after soaking in ACS solution for 1 and 6 hours.

3.4. *In vitro* hMSC responses to films

3.4.1. SEM-EDS analysis

After 3 days in osteogenic culture media no mineral formation was observed on the surface of the 6mer+BSP films (Figure III.5), although EDS characterization confirmed the presence of Ca on the surface (Figure III.6). At day 7 in osteogenic medium the Ca/P ratio varied between 0.90 and 1.19 (Figure III.6). As time in osteogenic medium increased the Ca/P ratio increased significantly up to 1.53 and 1.72 (Figure III.6). For the control 6mer+BSP films incubated in osteogenic medium without cells, mineral formation was observed by SEM after 14 days (Figures III.5). EDS characterization also detected the presence of Ca and P in the control films (Figure III.6), however there were differences between the films that were incubated in the presence of cells and the controls without cells. In the case of the controls a small amount of Ca and P was detected after 3 and 7 days of incubation (Figures III.6), while after 14 days the intensity of Ca and P signals increased significantly, reaching values for Ca/P ratios between 1.26 and 2.07 (Figure III.6).

For the 6mer films no mineral was observed after 3 days of culture (Figure III.5) and EDS analyses indicated considerably lower Ca/P ratios after 7 and 14 days of cell culture (Figure III.6) when compared with the 6mer+BSP (Figure III.6).

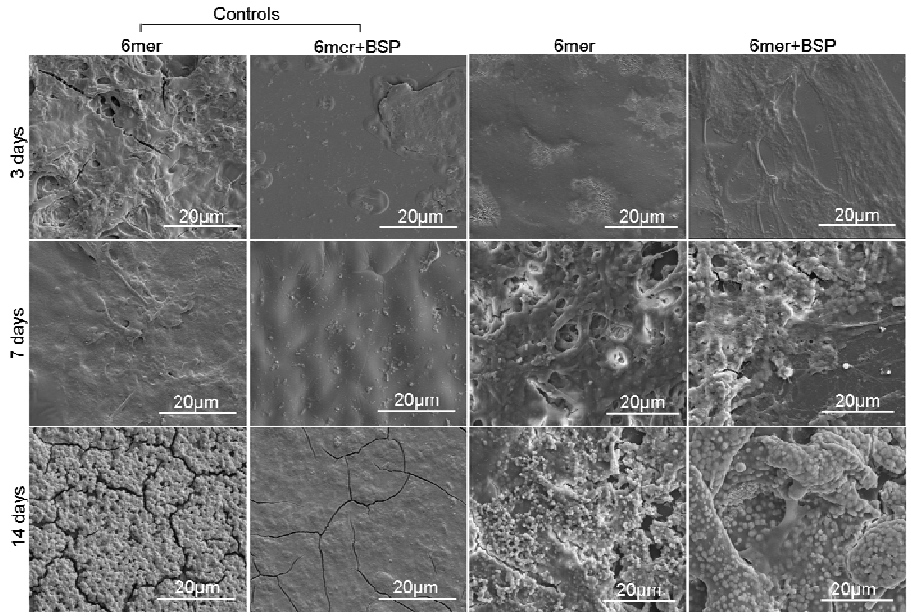

Figure III.5. Morphology of the 6mer and 6mer+BSP films seeded with hMSCs and cultured for 3, 7 and 14 days. In all assays, the 6mer and 6mer+BSP films without cells were used as controls.

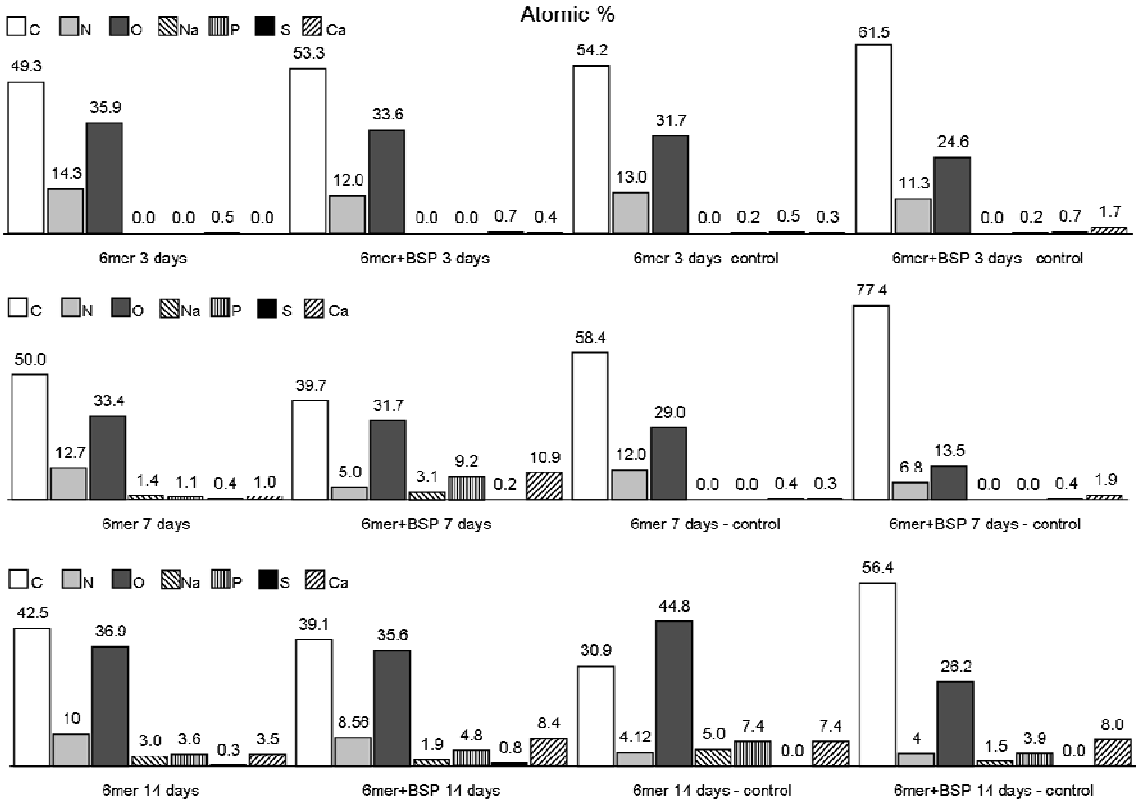

Figure III.6. EDS characterization of the 6mer and 6mer+BSP films seeded with hMSCs and cultured for 3, 7 and 14 days. In all assays, the 6mer and 6mer+BSP without cells were used as controls.

For 6mer films Ca and P were only detected after 7 days of culture with Ca/P ratios of 0.58-0.90. After 14 days this ratio had values of 0.64-0.97. For 6mer+BSP films only Ca was present after 3 days of cell culture and after 7 and 14 days the Ca/P ratios reached values of 0.90-1.19 and 1.53-1.72, respectively (Figure III.6).

SEM revealed differences regarding mineral morphology between the 6mer+BSP and 6mer films after 7 and 14 days (Figure III.5). SEM characterization also found that the cells cultured on 6mer+BSP films during the 3, 7 and 14 days of culture had osteoblastic-like morphology, based on their flattened and polygonal morphology with multiple filopodia or very thin extensions[35] (Figure III.5).

3.4.2. Cell viability

Cell viability/proliferation was measured after 3, 7 and 14 days of culture in osteogenic medium using the Alamar Blue assay and indicated that hMSCs cultured on 6mer+BSP films supported higher cell viability/proliferation ($p<0.05$) than cells cultured on 6mer films (Figure III.7).

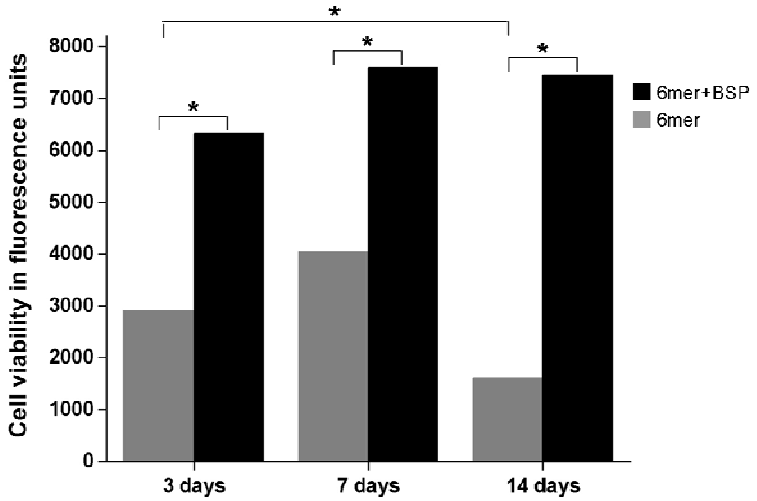

Figure III.7. Viability of cells seeded on the 6mer and 6mer+BSP films for 3, 7 and 14 days of culture and determined by Alamar Blue. Cell viability is expressed in relative fluorescence units. Asterisks indicate statistically significant differences ($p<0.05$).

3.4.3. Osteoblastic gene expression

The expression of genes COL1A1, ALP and IBSP after 3, 7 and 14 days of culture in osteogenic medium was up-regulated in cells cultured on the 6mer+BSP films (Figure

III.8). In the case of 6mer films there was significantly higher expression of COL1A1 after 3 and 7 days ($p<0.05$) of culture, however this expression level had a significant decrease ($p<0.05$) during time in culture. For the 6mer+BSP films after 14 days of culture the expression of COL1A1 was higher than the 6mer controls ($p<0.05$) (Figure III.8). For ALP expression, there was no significant difference ($p>0.05$) between the 6mer+BSP and 6mer films at 3 and 7 days of cell culture (Figure III.8). However, after 14 days in the 6mer+BSP films ALP expression reached levels significantly higher than those for the 6mer films ($p<0.05$). Furthermore, for the 6mer+BSP films there was a significant increase in ALP transcript level between 3 and 7 days of culture ($p<0.05$). For the 6mer films there was a progressive decrease ALP expression during time of culture however, this decrease was only significant between 7 and 14 days of culture ($p<0.05$). For BSP, expression levels were significantly higher for the 6mer+BSP films after 3 and 7 ($p< 0.0001$) days of culture when compared with control 6mer films. No significant difference was registered for this transcript after 14 days ($p>0.05$) between the 6mer+BSP and 6mer films (Figure III.8). During the time in culture a progressive increase for IBSP transcript was detected in the case of 6mer+BSP films, reaching significant values ($p<0.05$) between 3 and 7 days of culture. No expression of COL2A1, a chondrogenic gene, was detected under any of the conditions (data not shown).

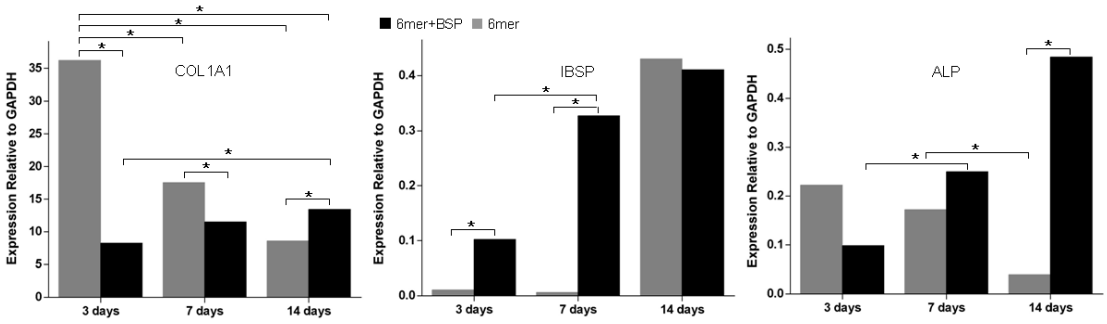

Figure III.8. Transcript levels from hMSCs cultured on the 6mer and 6mer+BSP films after 3, 7 and 14 days for genes COL1A1, ALP and IBSP. Asterisks indicate statistically significant differences ($p<0.05$).

4. Discussion

The design and characterization of a new chimeric protein resulting from the combination of six monomers of the consensus repeat for the spider silk protein

MaSp1 (6mer) with the human protein bone sialoprotein is reported. The DNA and protein sequences confirmed the successful cloning and expression of this new fusion. FTIR analysis demonstrated that the introduction of the BSP domain with the spider silk did not affect disrupt the self assembly capacity of the silk sequence, manifested through the formation of β-sheet after treatment with methanol (Figure III.3). Furthermore, this new protein retained the function of BSP to induce the nucleation of calcium phosphate (CaP), confirmed by EDS and SEM. EDS characterization showed that the incubation of 6mer+BSP films in ACS at 37ºC and pH 7.4 for one hour induced the deposition of CaP with a Ca/P ratio varying between 1.72 and 1.86, values close to those for hydroxyapatite (1.67) [36] (Figure III.4). In the case of the 6mer control films, no deposition of CaP was detected even after 6 hours of incubation in ACS (Figure III.4). This result indicates the predisposition of the 6mer+BSP sequence to induce the nucleation of CaP, due to the presence of the BSP domain, a sequence know to be involved in the mineralization process in bone tissue [25, 27].

EDS characterization of 6mer+BSP samples after 7 and 14 days of cell culture in osteogenic culture medium indicated an increase in Ca/P ratios from 0.90-1.19 at day 7 to values between 1.53-1.72 at day 14 (Figure III.6). These last values are very close to those found for tricalcium phosphate (1.50) and hydroxyapatite (1.67), respectively [36]. For 6mer samples there was also a slight increase in Ca/P ratio, however much lower that that obtained for 6mer+BSP.

For 6mer films after 3 days of cell culture the Ca/P ratio was 0 as no Ca or P was present, and this changed to 0.58-0.90 after 7 days. reaching values around 0.64-0.93 after 14 days in cell culture (Figure III.6). EDS analyses for the controls, 6mer+BSP and 6mer films incubated in osteogenic medium without cells indicated the precipitation of CaP in both types of films after 14 days of culture. However the rates for Ca and P deposition were significantly different from those registered for these samples when incubated in the presence of cells for the three periods of time. This fact is particularly obvious for the 6mer+BSP films without cells that register very small amounts of Ca and P deposition after 3 and 7 days in osteogenic medium. After 14 days of culture, Ca/P ratios reached values between 1.26 and 2.07 for 6mer+BSP without cells, versus those obtained for 6mer+BSP films with cells, 1.53-1.72 (Figure III.6).

SEM characterization provided an assessment of the morphology of the CaP formed on the films after cell culture. The morphologies of the minerals were different, mainly in the case of the 6mer+BSP films after cell culture *vs* 6mer+BSP films incubated with no cells (control) (Figure III.5). At day 14 the CaP films formed on 6mer+BSP films presented a globular cauliflower-like morphology while for the control samples, 6mer+BSP films without cells, a flat layer of CaP was observed (Figure III.5). Both the SEM and EDS results suggest that these differences in mineral morphology and in Ca/P deposition may be the result from the presence of cells that might play a role in the deposition and posterior modulation of calcium phosphates, inducing a more controlled mineralization process.

HMSC cultivated in osteogenic differentiation medium provided generated an osteoblast-like morphology during 3, 7 and 14 days of culture (Figure III.5) and Alamar Blue results (Figure III.7) indicated good cell viability/proliferation on the 6mer+BSP samples. The presence of cell binding domains in the 6mer+BSP protein within the BSP sequence [11, 12], may be responsible for the cell response when compared with control samples. For the 6mer films, osteoblast-like morphology was not as evident and a reduction in viability/proliferation was observed after 3, 7 and 14 days in osteogenic medium. The expression of bone-related genes by hMSCs cultured on 6mer+BSP indicated significant ($p<0.05$) up-regulation of ALP, IBSP and COL1A1 during 14 days of cell culture. For the 6mer samples a significant decrease ($p<0.05$) in expression level was observed specially for ALP and COL1A1 from days 3 to day 14, and the expression of IBSP gene was low at days 3 and 7, and increased at day 14.

ALP transcript levels for both 6mer+BSP and 6mer films were similar for days 3 and 7, while at 14 days transcript levels were significantly higher on the 6mer+BSP samples. ALP is considered an osteoblast marker [37] and an increase in the level of ALP transcript suggests ordered deposition of mineral phase within the extracellular matrix [38]. The genesis of biological apatite is considered a biochemical process controlled by different enzymes such as carbonic anhydrase [39] and alkaline phosphatase [40]. Alkaline phosphatase is responsible for the release of orthophosphates through the cleavage of polyphosphates or pyrophosphates [41, 42]. *In vitro* studies indicate that the polyphosphates function as inhibitors of apatite formation [43] and also responsible for inactivation of polyphosphate, an inhibitor of

calcium phosphate nucleation [44]. Humans and mice lacking ALP exhibit a decrease in bone biomineralization [42]. These functions for ALP suggest possible reasons why ALP is important in the mineralization process. In the present study, the difference in ALP responses may suggest one reason for the differences in mineralization that was observed with the SEM and EDS data.

With the onset of mineralization other genes are expressed [38]. This is the case for IBSP expression, usually confined to later stages of osteoblast differentiation and early stages of mineral deposition [36]. The IBSP gene codes for BSP, a protein synthesized mostly in bone tissue and involved in mineralization, constituting approximately 15% of the noncollagen matrix in young bone [45]. Furthermore, BSP is capable of binding to calcium ions and hydroxyapatite and inducing cell and collagen attachment through its cell binding and collagen binding domains, respectively. For the 6mer+BSP samples, a significant up-regulation of IBSP transcript from day 3 to day 14 of cell culture (Figure III.8) was observed. This result is in good agreement with the results for ALP gene expression, suggesting active mineralization in 6mer+BSP films. IBSP up-regulation also reflects the induction of synthesis of other extracellular proteins[41], such as collagen type I. Type I collagen is the most abundant extracellular matrix protein in bone tissue and is involved in early stages of the mineralization, as described earlier [46, 47]. Type I collagen also functions as a scaffold where non-collagenous proteins bind to act as mineral nucleators. In this way, collagen I fibers play an important role in bone formation as both a primary building block and for higher organized architectures related to this process [36]. The transcript data indicate significant up-regulation of COL1A1 for the 6mer+BSP samples, indicating a progressive increase of type I collagen. In the 6mer+BSP samples, the up-regulation of COL1A1 transcripts accompanied the increase in ALP and IBSP expression levels after 3, 7 and 14 days in culture. For the 6mer samples, COL1A1 transcripts were significantly ($p<0.05$) down-regulated between days 3 and day 14, although transcript levels were higher when compared with the 6mer+BSP samples at 3 and 7 days of cell culture. After 14 days down-regulation for COL1A1 was lower than those for the 6mer+BSP samples. The absence COL2A1 transcript, a chondrogenic gene, confirmed that no chondrogenic differentiation was taking place in the 6mer+BSP or in the control 6mer samples.

Real-time RT-PCR for ALP, IBSP and COL1A1 suggest that controlled mineralization is occurring on the 6mer+BSP films during culture in osteogenic medium when compared with the control 6mer films. These findings concur with the Ca/P ratios determined by EDS characterization, which increased from day 3 to 14 of culture, with an increase from 0 to 1.53-1.72, values similar to tricalcium phosphate (1.50) and hydroxyapatite (1.67), respectively [36]. The *in vitro* results suggest that these films are actively involved in the mineralization process. Osteoblasts are the main cells responsible for the osteogenic process, involved in the deposition of bone organic matrix and in mineralization. This extracellular matrix is formed by collagen, non-collagen proteins (BSP, osteopontin, osteocalcin) and polysaccharides [36]. Osteoblasts also secrete alkaline phosphatase, an enzyme responsible for the hydrolysis of pyrophosphate, a known inhibitor of mineralization, into orthophosphate for incorporation along with calcium ions into the growing mineral lattice [41, 42, 48]. The osteogenic potential of the hMSCs used in the present study was confirmed by the deposition of a calcified matrix, based on both SEM and EDS analyses, as well as the real-time RT-PCR data. These results indicate early up-regulation of IBSP, a marker usually confined to the later stages of osteoblast differentiation [36], and ALP, a frequently used marker for osteoblast activity, as well as the absence of transcripts for COL2A1 gene, a marker for chondrogenic differentiation.

5. Conclusions

In summary, the successful design of a new chimeric protein conjugating spider silk with human bone sialoprotein (BSP) is described. The combination of both silk and BSP domains in a single protein chain did not interfere with the functions of each of these domains. This includes the ability of the spider silk to self-organize into a β-sheet conformation, an important feature related with its mechanical properties, and the aptitude of BSP to induce the nucleation of calcium phosphates. During the 14 days of culture this new chimeric protein sustained hMSC proliferation and differentiation into the osteogenic lineage. These data are evident for cells seeded onto the 6mer+BSP, indicating that the conjugation with the amino acid sequence of human BSP improve cellular function towards the osteoblastic phenotype. These promising results suggest the potential for this new chimeric protein as a new biomaterial for tissue engineering

applications, especially for the construction of grafts for bone regeneration. Additionally, these results also highlight the potential of chimeric proteins as multifunctional biomaterial systems allowing the control over different types of cellular response such as cell differentiation, cell migration and cell adhesion, protein adsorption, etc. The importance of this approach relies in its ability to engineer nanoscale composite systems that can be used in the fabrication of new families of smart biomaterials capable of self-modification either before, *in vitro*, or after implantation, *in vivo*.

Acknowledgements

The authors acknowledge Olena Rabotyagova for advice in protein sequence design. Sílvia Gomes thanks the Portuguese Foundation for Science and Technology (FCT) for providing her a PhD grant (SFRH/BD/28603/2006). This work was carried out under the scope of the European NoE EXPERTISSUES (NMP3-CT-2004-500283), the FIND & BIND project funded by the agency EU-EC (FP7 program), the FCT R&D project ProteoLight (PTDC/FIS/68517/2006) funded by the FCT agency, the Chimera project (PTDC/EBB-EBI/109093/2008) funded by the FCT agency, the NIH (P41 EB002520) Tissue Engineering Resource Center and the NIH (EB003210 and DE017207).

References

1. Kruyt MC, Delawi D, Habibovic P, Oner FC, Blitterswijk CAv, Dhert WJA. Relevance of bone graft viability in a goat transverse process model. J Orthop Res 2009;27:1055-1059.

2. Dawson JI, Oreffo ROC. Bridging the regeneration gap: Stem cells, biomaterials and clinical translation in bone tissue engineering. Arch Biochem Biophys 2008;473:124-131.

3. Xu M, Lewis RV. Structure of a protein superfiber: Spider dragline silk. Proc Natl Acad Sci USA 1990;87:7120-7124.

4. Scheibel T. Spider silks: recombinant synthesis, assembly, spinning, and engineering of synthetic proteins. Microb Cell Fact 2004;3(1):14-24.

5. Hayashi CY, Shipley NH, Lewis RV. Hypotheses that correlate the sequence, structure, and mechanical properties of spider silk proteins. Int J Biol Macromol 1999;24(271–275).

6. Beek JDv, Hess S, Vollrath F, Meier BH. The molecular structure of spider dragline silk: folding and orientation of the protein backbone. Proc Natl Acad Sci USA 2002;99:10266-10271.

7. Bini E, Foo CWP, Huang J, Karageorgiou V, Kitchel B, Kaplan DL. RGD-functionalized bioengineered spider dragline silk biomaterial. Biomacromolecules 2006;7:3139-3145.

8. Rabotyagova O, Cebe P, Kaplan DL. Self-assembly of genetically engineered spider silk block copolymers. Biomacromolecules 2009;10:229–236.

9. Foo CWP, Patwardhan SV, Belton DJ, Kitchel B, Anastasiades D, Huang J, et al. Novel nanocomposites from spider silk–silica fusion (chimeric) proteins. Proc Natl Acad Sci USA 2006;103(25):9428–9433.

10. Huang J, Wong C, George A, Kaplan DL. The effect of genetically engineered spider silk-dentin matrix protein 1 chimeric protein on hydroxyapatite nucleation. Biomaterials 2007;28:2358–2367.

11. Bellahcène A, Bonjean K, Fohr B, Fedarko NS, Robey FA, Young MF, et al. Bone sialoprotein mediates human endothelial cell attachment and migration and promotes angiogenesis. Circ Res 2000;86:885-891.

12. Mizuno M, Imai T, Fujisawa R, Tani H, Kuboki Y. Bone sialoprotein (BSP) is a crucial factor for the expression of osteoblastic phenotypes of bone marrow cells cultured on type I collagen matrix. Calcif Tissue Int 2000;66:388-396.

13. Valverde P, Zhang J, Fix A, Zhu J, Ma W, Tu Q, et al. Overexpression of bone sialoprotein leads to an uncoupling of bone formation and bone resorption in mice. J Bone Miner Res 2008;23(11):1775-1778.

14. Bernards MT, Chunlin Qin SJ. MC3T3-E1 cell adhesion to hydroxyapatite with adsorbed bone sialoprotein, bone osteopontin, and bovine serum albumin. Colloids Surf B Biointerfaces 2007;64(2):236-247.

15. Bernards MT, Qin C, Ratner BD, Jiang S. Adhesion of MC3T3-E1 cells to bone sialoprotein and bone osteopontin specifically bound to collagen I. J Biomed Mater Res A 2007;86(3):779-787.

16. Karadag A, Fisher LW. Bone sialoprotein enhances migration of bone marrow stromal cells through matrices by bridging MMP-2 to αvβ3-integrin. J Bone Miner Res 2006;21(10):1627-1636.

17. Karadag A, Ogbureke KUE, Fedarko NS, Fisher LW. Bone sialoprotein, matrix metalloproteinase 2, and αvβ3 integrin in osteotropic cancer cell invasion. J Natl Cancer Inst 2004;96(12):956-965.

18. Rapuano BE, Wu C, MacDonald DE. Osteoblast-like cell adhesion to bone sialoprotein peptides. J Orthop Res 2004;22:353–361.

19. Wang J, Zhou H-Y, Salih E, Xu L, Wunderlich L, Gu X, et al. Site-specific in vivo calcification and osteogenesis stimulated by bone sialoprotein. Calcif Tissue Int 2006;79:179-189.

20. Xu L, Anderson AL, Lu Q, Wang J. Role of fibrillar structure of collagenous carrier in bone sialoprotein-mediated matrix mineralization and osteoblast differentiation. Biomaterials 2007;28(4):750–761.

21. Graf H-L, Stoeva S, Armbruster FP, Neuhaus J, Hilbig H. Effect of bone sialoprotein and collagen coating on cell attachment to TICER and pure titanium implant surfaces. Int J Oral Maxillofac Surg 2008;37:634-640.

22. Baht G, Hunter G, Goldberg H. Bone sialoprotein–collagen interaction promotes hydroxyapatite nucleation. Matrix Biol 2008;27:600–608.

23. Traub W, Arad T, Weiner S. Three-dimensional ordered distribution of crystals in turkey tendon collagen fibers. Proc Natl Acad Sci USA 1989;86:9822-9826.

24. Weiner S, Traub W. Bone structure: from angstroms to microns. FASEB J 1992;6(3):879-885.

25. Fujisawa R, Nodasaka Y, Kuboki Y. Further characterization of interaction between bone sialoprotein (BSP) and collagen. Calcif Tissue Int 1995;56(2):140-144.

26. Fisher LW, Torchia DA, Fohr B, Young MF, Fedarko NS. Flexible structures of SIBLING proteins, bone sialoprotein, and osteopontin. Biochem Biophys Res Commun 2001;280:460–465.

27. Goldberg H, Warner K, Li M, Hunter G. Binding of bone sialoprotein, osteoprotein and synthetic polypeptides to hydroxyapatite. Connect Tissue Res 2001;42(1):25-37.

28. Fedarko NS, Fohr B, Robey PG, Young MF, Fisher LW. Factor H binding to bone sialoprotein and osteopontin enables tumor cell evasion of complement-mediated attack. J Biol Chem 2000;275(22):16666–16672.

29. Huang J, Valluzzi R, Bini E, Vernaglia B, Kaplan DL. Cloning, expression, and assembly of sericin-like protein. J Biol Chem 2003;278(46):46117-46123.

30. Yan S-Z, Beeler JA, Chen Y, Shelton RK, Tang W-J. The regulation of type 7 adenylyl cyclase by its C1b region and Escherichia coli peptidylprolyl isomerase, SlyD. J Biol Chem 2001;276(11):8500-8506.

31. Liu Q, Weng J, Wijn JGCd, Blitterswijk TRv. A novel in vitro model to study the calcification ability of biomaterials. Fifht World Biomaterials Congress; 1996 May 2nd; Toronto, Canada; 1996. p. 29.

32. Lancaster MV, Fields RD, inventors. Antibiotic and cytotoxic drug susceptibility assays using resazurin and poising agents. Patent United States, 1996.

33. Foo CWP, E.Bini, Huang J, Lee SY, Kaplan DL. Solution behavior of synthetic silk peptides and modified recombinant silk proteins. Appl Phys Mater Sci Process 2006;82:193–203.

34. Rabotyagova OS, Cebe P, Kaplan DL. Role of polyalanine domains in β-sheet formation in spider silk block copolymers. Macromol Biosci 2010;10:49-59.

35. Schmidt C, Kaspar D, Sarkar MR, Claes LE, Ignatius AA. Scanning electron microscopy study of human osteoblast morphology on five orthopedic metals. J Biomed Mater Res 2002;63(3):252 - 261.

36. Palmer LC, Newcomb CJ, Kaltz SR, Spoerke ED, Stupp SI. Biomimetic systems for hydroxyapatite mineralization inspired by bone and enamel. Chem Rev 2008;108:4754–4783.

37. Choong PFM, Martin TJ, Ng KW. Effects of ascorbic acid, calcitriol, and retinoic acid on the differentiation of preosteoblasts. J Orthop Res 1993;11(638-647).

38. Lian JB, Stein GS. Development of the osteoblast phenotype: molecular mechanisms mediating osteoblast growth and differentiation. Iowa Orthop J 1995;15:118-140.

39. Krishnamurthy VM, Kaufman GK, Urbach AR, Gitlin I, Gudiksen KL, Weibel DB, et al. Carbonic anhydrase as a model for biophysical and physical-organic studies of proteins and protein−ligand binding. Chem Rev 2008;108(3):946-1051.

40. Coleman JE. Structure and mechanism of alkaline phosphatase. Annu Rev Biophys Biophys Chem 1992;21: 441-483.

41. Hirschler A, Lucas J, Hubert J-C. Bacterial involvement in apatite genesis. FEMS Microbiol Lett 1990;73(3):211-220.

42. Murshed M, Harmey D, Millán JL, McKee MD, Karsenty G. Unique coexpression in osteoblasts of broadly expressed genes accounts for the spatial restriction of ECM mineralization to bone. Genes Dev 2005;19:1093-1104.

43. Fleish H, Neuman WF. Mechanisms of calcification: role of collagen, polyphosphates, and phosphatase Am J Physiol 1961;200:1296-1300.

44. Fleish H, Bisaz S. Mechanism of calcification: inhibitory role of pyrophosphate. Nature 1962;195:911.

45. Meinel L, Karageorgiou V, Hofmann S, Fajardo R, Snyder B, Li C, et al. Engineering bone-like tissue in vitro using human bone marrow stem cells and silk scaffolds. J Biomed Mater Res A 2004;71A(1):25-34.

46. Jackson SF. The fine structure of developing bone in the embryonic fowl. Proc Biol Sci 1956;146(923):270-280.

47. Weiner S, Wagner HD. The material bone: structure-mechanical function relations. Annu Rev Mater Res 1998;28:271-298.

48. Balcerzak M, Hamade E, Zhang L, Pikula S, Azzar G, Radisson J, et al. The roles of annexins and alkaline phosphatase in mineralization process. Acta Biochim Pol 2003;50(4):1019-1038.

Abstract

Atomic force microscopy (AFM) was used to assess a new chimeric protein consisting of a fusion protein of the consensus repeat for *Nephila clavipes* spider dragline protein and bone sialoprotein (6mer+BSP). The elastic modulus of this protein in film form was assessed through force curves, and the calculation of film surface roughness was also determined. The results showed a significant difference between the elastic modulus of the chimeric silk protein, 6mer+BSP, and control films consisting of only the silk component (6mer). The behaviour of the 6mer+BSP and 6mer proteins in aqueous solution in the presence of calcium ions (Ca^{2+}) was also assessed to determine interactions between the inorganic and organic components related to bone interactions, anchoring and biomaterial network formation. The results demonstrated the formation of protein networks in the presence of Ca^{2+} ions, characteristics that may be important in the context of controlling materials assembly and properties related to bone-formation with this new chimeric silk-BSP protein.

1. Introduction

With the potential importance of tissue engineering in healthcare the design of new biopolymers with improved mechanical and biocompatibility characteristics has become a major goal in the field of biomaterials research. Spider dragline silk fibers exhibit remarkable viscoelastic properties, combining a tensile strength similar to steel and Kevlar with a high elasticity that is comparable to rubber [1]. In part these mechanical properties are a consequence of the amino acid chemistry where the hydrophilic GGX motif (G stands for glycine, X is mostly glutamine) alternates with poly-alanine (poly-A) motifs [2]. The GGX motif adopts a helical conformation forming an amorphous region that connects the poly-A motifs, providing elasticity to the silk fiber. The hydrophobic poly-A motifs are responsible for the formation of rigid and highly packed anti-parallel β-sheets [3] resulting from hydrogen bonding and hydrophobic interactions [4]. The remarkable mechanical properties together with the inherent biocompatibility suggest spider silk as a promising biopolymer for bone repairs and bone growth [5].

Recombinant spider silk offers advantages over natural spider silk. With recombinant DNA technology the protein amino acid sequence and length can be controlled to tailor the sequence chemistry and polymer features to the target needs in terms of structure and functional features [6, 7]. Our previous work [8] described the synthesis of a new chimeric protein through the fusion of a spider silk (6mer) with six repeats of the consensus amino acid block from the native sequence of the major ampullate dragline silk I protein, MaSpI, from the spider specie *Nephila clavipes*, with bone sialoprotein sequence (BSP) designated by 6mer+BSP (Figure IV.1). BSP is a noncollageneous protein present in bone tissue that can induce the deposition of calcium phosphate in the form of hydroxyapatite to bind to collagen fibers [9]. At the cellular level BSP induces the attachment and differentiation of osteoblasts [10] and stimulates osteoclast activity [11], thereby playing an important part in the remodelling process of bone. In previous work we have demonstrated that the fusion protein 6mer+BSP maintains the ability to induce the deposition of calcium phosphate, due to the presence of the BSP domain [8].

SGRGGLGGQGAGAAAAAGGAGQGGYGGLGSQGTSGRG
GLGGQGAGAAAAAGGAGQGGYGGLGSQGTSGRGGLGG
QGAGAAAAAGGAGQGGYGGLGSQGTSGRGGLGGQGAG
AAAAAGGAGQGGYGGLGSQGTSGRGGLGGQGAGAAAA
AGGAGQGGYGGLGSQGTSGRGGLGGQGAGAAAAAGGA
GQGGYGGLGSQGTSWPSRPTMKTALILLSILGMACAFSM
KNLHRRVKIEDSEENGVFKYRPRYYLYKHAYFYPHLKRFP
VQGSSDSSEENGDDSSEEEEEEEETSNEGENNEESNED
EDSEAENTTLSATTLGYGEDATPGTGYTGLAAIQLPKKAG
DITNKATKEKESDEEEEEEEEGNENEESEAEVDENEQGIN
GTSTNSTEAENGNGSSGGDNGEEGEEESVTGANAEGTT
ETGGQGKGTSKTTTSPNGGFEPTTPPQVYRTTSPPFGKT
TTVEYEGEYEYTGVNEYDNGYEIYESENGEPRGDNYRAY
EDEYSYFKGQGYDGYDGQNYYHHQGLMGH Stop

Figure IV.1. Amino acid sequence for the 6mer+BSP protein. The linkers for the BSP sequence are underlined. The 6mer is represented in black and the BSP sequence is represented in gray.

In the present study atomic force microscopy (AFM) was used to collect topographic images of 6mer and 6mer+BSP films, to measure surface roughness of these films and to assess the elasticity of the films AFM can also be used to determine local mechanical properties of soft samples. The AFM tip is used to indent the sample resulting in a force curve that can be analyzed for elastic response of the sample to the small loading force applied by the tip [12]. The Hertz model for elastic indentations can be used to calculate Young's modulus (*E*) [13]. Previous studies have used AFM to measure the elastic properties of spider silk either by stretching a spider silk fiber

attached to the AFM tip [6] or by indentation into the fiber [13]. In the present work, AFM was used to assess the elasticity of 6mer+BSP films vs the controls.

Since 6mer+BSP was synthesized for bone-related biomaterial needs, the behaviour of 6mer+BSP in the presence of divalent Ca^{2+} ions was also assessed with AFM imaging. The deposition of calcium phosphate induced by BSP is related to the negatively charged polyglutamic sequences that interact with positively charge calcium ions [14, 15]. The binding with Ca^{2+} ions was important in the formation of calcium mediated networks of osteopontin proteins, increasing the ability of these networks to dissipate energy in response to applied forces, contributing to bone plasticity [16]. The study of 6mer+BSP in the presence of Ca^{2+} ions is important to gain insight into how these types of molecules form calcium mediated networks related to bone regeneration. The presence of these types of networks between calcium-BSP mediated binding fully integrated with a robust silk biomaterial could be useful both in osteointegration as well as for structural support.

2. Materials and Methods

2.1. Cloning and protein expression

The clone carrying the DNA sequence coding for BSP was purchased from the Harvard clone collection (Clone Identification: HsCD00082642, "The ORFeome Collaboration" Dana-Farber/Harvard Cancer Center, Boston, MA, USA) and inserted in the vector pET30L (Novagen, San Diego, CA, USA) carrying the silk block copolymer[7], as we have described previously [8]. The 6mer+BSP protein was expressed in *E. coli* RY-3041 strain grown in Hyper Broth™ (0107-S, Athens Enzyme Systems, Baltimore, MD, USA) to an OD_{600} of 1 in the presence of kanamycin 25 μg/ml. Expression was induced with isopropyl β-D-thiogalactoside (IPTG, 15529019, Invitrogen, Carlsbad, CA, USA) 0.5 mM. The cells were harvested by centrifugation and cell pellet was lysed under denaturating conditions using the buffer 100 mM NaH_2PO_4, 10 mM Tris HCl, 8 M urea (pH 8.0). Insoluble cell debris was excluded from the mixture by centrifugation and the supernatant was collected. After incubating the supernatant with Ni-NTA resin (30250, Qiagen, Valencia, CA, USA) for two hours, the mixture was loaded in a column and washed several times with denaturating buffer at pH 8 and at pH 6.0.

Protein was eluted using denaturating buffer at pH 4.5. Protein solution was loaded into snake skin membranes (131054, Spectra/por Biotech, Rancho Dominguez, CA, USA) and dialysed against 20 mM sodium acetate buffer (pH 4.75) followed by dialysis in MQ water. Finally protein solution was lyophilized in a LabConco (Kansas city, MO, USA) lyophilizer.

2.2. Sample preparation

The 6mer+BSP and 6mer protein (silk control) were dissolved in MQ water to a final concentration of 2% (m/v). Then 20 µl of protein solution was cast onto freshly cleaved mica surfaces and left to dry at room temperature. After drying the protein films were treated with 70% methanol solution for two hours to induce the transition of secondary structure from random coil to β-sheet, providing stability in aqueous solutions. These protein films were used to collect force curves. To study the formation of protein networks, the 6mer+BSP and 6mer proteins were dissolved in three different solutions: 4-(2-hydroxyethyl)-1-piperazineethanesulfonic acid (HEPES, pH 7.4) 0.1 mM buffer, HEPES 0.1 mM buffer containing magnesium (Mg^{+2}) ions in a molar ratio of 1:1000 (protein:Mg) and HEPES 0.1 mM buffer containing calcium (Ca^{+2}) ions in a molar ratio of 1:1000 (protein:Ca) [17]. The final protein concentration was 0.01 mg/ml. Protein solution was deposited onto a freshly cleaved mica surfaces and left to dry at room temperature.

2.3. AFM imaging and force spectroscopy

An AFM (Veeco Dimension V 3100 Scanning Probe Microscope, NY, USA) with a scanning range of 90 μm^2 and a z range of 7-8 µm was used for imaging and force-curve measurements. AFM cantilevers (Veeco, FESP) made of silicon with a spring constant of 3.152 N/m were used and AFM imaging and force-curve measurements were performed in the dry mode. A total of 100 force curves were recorded for both 6mer+BSP and 6mer films, respectively, using the software NanoScope V (Veeco). Mica was used as a control. Force curves were collected using contact mode AFM. Samples were imaged with tapping mode AFM. The tapping mode operation allowed the visualization of weakly adsorbed samples by eliminating the lateral forces between the

probe tip and the sample [18]. The heights of the structures imaged on mica were determined by section analysis using Nanoscope image analysis software. Roughness measurements were performed with the NanoScope V (Veeco). Two values were measured: the root mean square (RMS) and the arithmetic average height (R_a). RMS represents the standard deviation of the height values within a given area and allows the surface roughness to be determined by statistical methods [19, 20]. R_a is the most frequently used roughness parameter and is defined as the average deviation of the roughness irregularities from the mean line over one sampling length [19, 20]. Because roughness values change with the scan size the measurements were performed using three different scan windows: 20 x 20 μm^2, 10 x 10 μm^2 and 2 x 2 μm^2.

2.4. Analysis of the data from the force curve measurements

In a force curve, the cantilever deflection (d) is registered as a function of its vertical position (*z*) [equation 1 (Eq. 1)]. The slope of the force curve gives a qualitative idea of the sample elastic properties. For a stiff sample the force curve is characterized by a flat area when the tip is approaching the sample and by a slope region where the cantilever deflection is identical to the *z* movement, $d = z$ [12, 13]. However, in the case of a soft sample this slope region becomes shallower as a result of the decrease in the deflection value due to elastic indentation (δ),

$$d = z - \delta \quad \text{(Eq. 1)}$$

Hooke's law relates the deflection with the applied force through the force constant of the cantilever (k)

$$F = kd = k(z - \delta) \quad \text{(Eq. 2)}$$

The Hertz model relates the indentation δ with the loading force *F* and by using the Sneddon modification [21, 22] we have

$$F = \frac{2}{\pi} \cdot \frac{E}{1 - \nu^2} \cdot \delta^2 \cdot \tan(\alpha) \quad \text{(Eq. 3)}$$

where *E* is the elastic or Young's modulus, v is the Poisson ration of the sample, assumed to be 0.5 for incompressible materials [23], and α is the opening angle of the AFM tip. By combining equations 2 and 3 we have

$$kd = \frac{2}{\pi} \cdot \frac{E}{1 - v^2} \cdot \delta^2 \cdot \tan(\alpha) \quad \text{(Eq. 4)}$$

Whit the rearrangement of equation 3 we have an expression for indentation *δ*

$$\delta = \sqrt{\frac{kd}{(2/\pi)\,[E/(1-v^2)]\,\tan(\alpha)}} \quad \text{(Eq. 5)}$$

Since *δ* can not be detected directly by AFM it can be replaced by combining equations 1 and 5 [24]

$$z = d + \sqrt{\frac{kd}{(2/\pi)\,[E/(1-v^2)]\,\tan(\alpha)}} \quad \text{(Eq. 6)}$$

For data treatment we will use the more general form

$$|z - z_0| = d - d_0 + \sqrt{\frac{k\,(d - d_0)}{(2/\pi)\,[E/(1-v^2)]\,\tan(\alpha)}} \quad \text{(Eq. 7)}$$

d_0 and z_0 are the initial values of deflection and height, respectively [25].

Equation 7 was used to fit the date from the recorded force curves and to calculate the value of the elastic modulus, *E*, for the 6mer+BSP and 6mer films.

2.5. Secondary structure analysis

Since β-sheet and random coli/helix content are considered major factors related to the mechanical properties of spider silk materials, Attenuated-Total Reflectance Fourier Transform Infrared Spectroscopy (ATR-FTIR) was performed to assess the secondary conformation of both the 6mer and 6mer+BSP proteins. These data provide structural details to support the interpretation of mechanical properties from the AFM studies, including the differences between the calculated Young's modulus for the 6mer and 6mer+BSP films. ATR-FTIR measurements were performed

with the 6mer and 6mer+BSP films, prepared as mentioned in section 2.2, using a Jasco model FT/IR-6200 type A equipment (Jasco Inc. MD, USA). Spectra were collected in absorption mode at 8 cm^{-1} resolution using 64 scans in the spectral range 4000 to 400 cm^{-1}. The quantification of secondary structure was based on the analysis of the amide I region (1700 to 1600 cm^{-1}) and was determined through the deconvolution of the spectra followed by the normalization of the obtained values to the total area of the amide I region [26].

2.6. Circular dichroism

Circular dichroism (CD) spectroscopy was performed with an Aviv, Model 410 (Biomedical, Inc. NJ USA) equipment. The spectra were collected between 260 and 180 nm with a step size of 1 nm, an averaging time of 1s. A total of five scans were collected. A baseline spectrum was subtracted from the samples. Cells of 0.1 cm path length were used and measurements were performed with 1 mg/ml protein solutions in 0.1 mM HEPES buffer (pH 7.4) and in 0.1 mM HEPES containing Ca ions in a molar ratio of 1:1000 (protein:Ca), as mentioned in section 2.2. The procedure was repeated in the presence of Mg^{2+} ions, 0.1 mM HEPES containing Mg^{2+} ions in a molar ratio of 1:1000 (protein:Mg). CD provided a check to determine if there were any differences in secondary conformation of the 6mer+BSP and 6mer when in a buffer solution with pH of 7.4 in the presence of Ca^{2+} or Mg^{2+} ions.

2.7. Statistical analysis

Statistical analysis was performed with SPSS 17.0. Shapiro-Wilk test was use to test for the normality of the data. Because the data had no normal distribution, the nonparametric Mann-Whitney test was used to test for significant differences. In the case of data with normal distribution the parametric test t was used. Statistical significance was defined as $p<0.05$.

3. Results

3.1. Force curves and Young's modulus (*E*) calculations

Figure IV.2 shows the force curves for the 6mer and 6mer+BSP films and on a hard sample control, mica. By comparing the slope regions the elastic modulus (*E*) was calculated using the d and *z* values extracted from the force curves collected using equation 7 (2.4. Materials and Methods section). The *E* values for both the 6mer and 6mer+BSP films were 1.1 GPa and 1.5 GPa, respectively. Statistical analysis indicated that the Young's modulus value calculated for the 6mer film was significantly lower than the value obtained for the 6mer+BSP film ($p<0.05$). *E* values were calculated by averaging over all points where the force curves were collected.

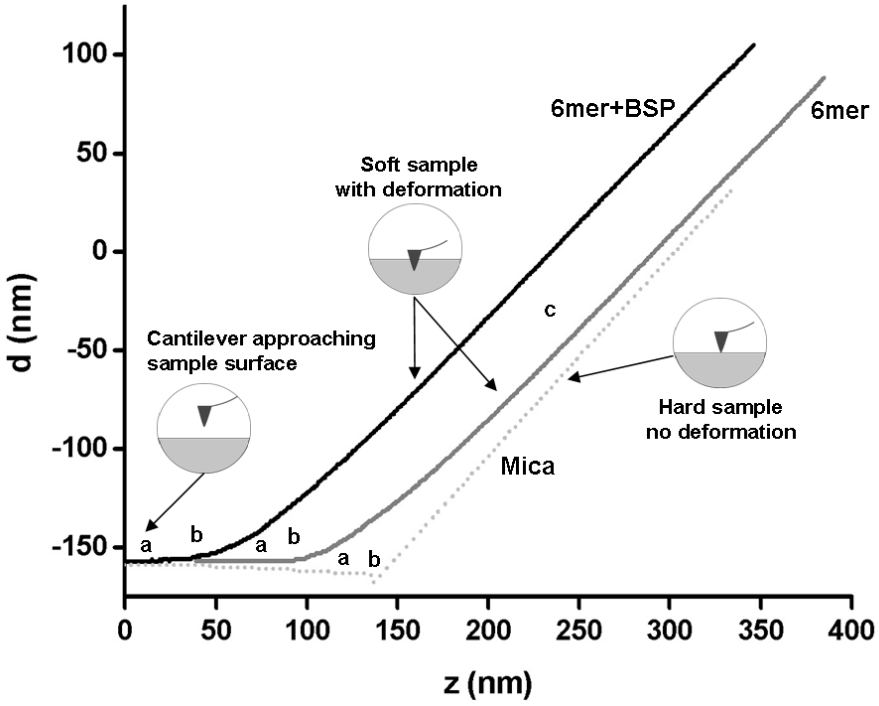

Figure IV.2. Force curves on 6mer and 6mer+BSP films, and on mica: a) cantilever approaching the surface; b) contact point; c) cantilever in contact with the surface.

3.2. Secondary structure analysis

For both the protein films, 6mer control and 6mer+BSP, ATR-FTIR spectra revealed no major differences between secondary structures. For both proteins two peaks were observed, at 1624 and 1520 cm^{-1}, indicative of an antiparallel β-sheet conformation, and a third peak was found at 1650 cm^{-1} corresponding to a helix/random coil conformation [2, 7, 27] (Figure IV.3). Spectral deconvolution

indicated that both proteins had similar percentages of β-sheet and helix/random coil (Table IV.1) and statistical analysis indicated no significant difference ($p>0.05$).

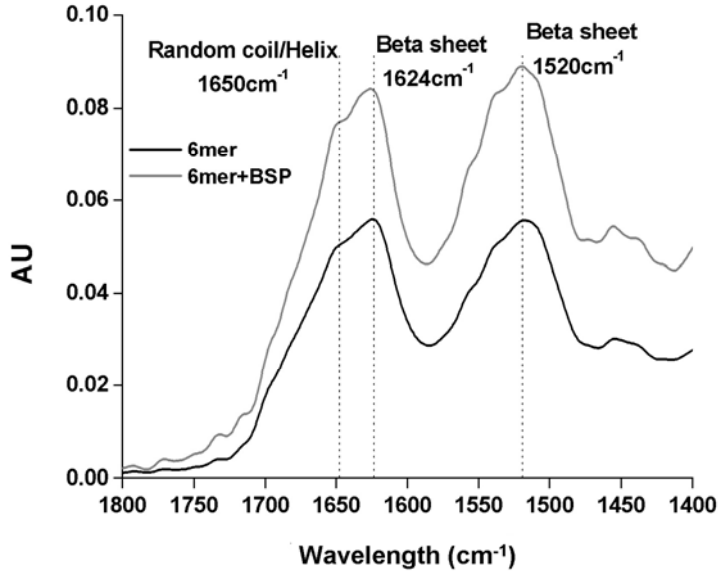

Figure IV.3. ATR-FTIR spectra of the 6mer and 6mer+BSP films after 2 hours of treatment with 70% methanol.

Table IV.1. Percentage of β-sheet and helix/random coil for 6mer control and 6mer+BSP films.

Sample	β-sheet	helix/random coil
6mer	34.5±6	31.3±7
6mer+BSP	34.3±3	33.4±9

3.3. Roughness measurements

Figure IV.4 shows representative surface topographies from AFM images of the 6mer and 6mer+BSP films, used for the calculation of the roughness values RMS and R_a. RMS and R_a values were similar for the 6mer and 6mer+BSP films (Table IV.2) and statistical comparison indicated no significant difference ($p>0.05$). The RMS value for blank mica using the scan sizes of 20 x 20 μm^2, 10 x 10 μm^2, 2 x 2 μm^2 were 0.881, 0.455 and 0.085 nm, respectively. For R_a these values were 0.712, 0.377 and 0.067 nm for 20 x 20 μm^2, 10 x 10 μm^2 and 2 x 2 μm^2 scan sizes, respectively.

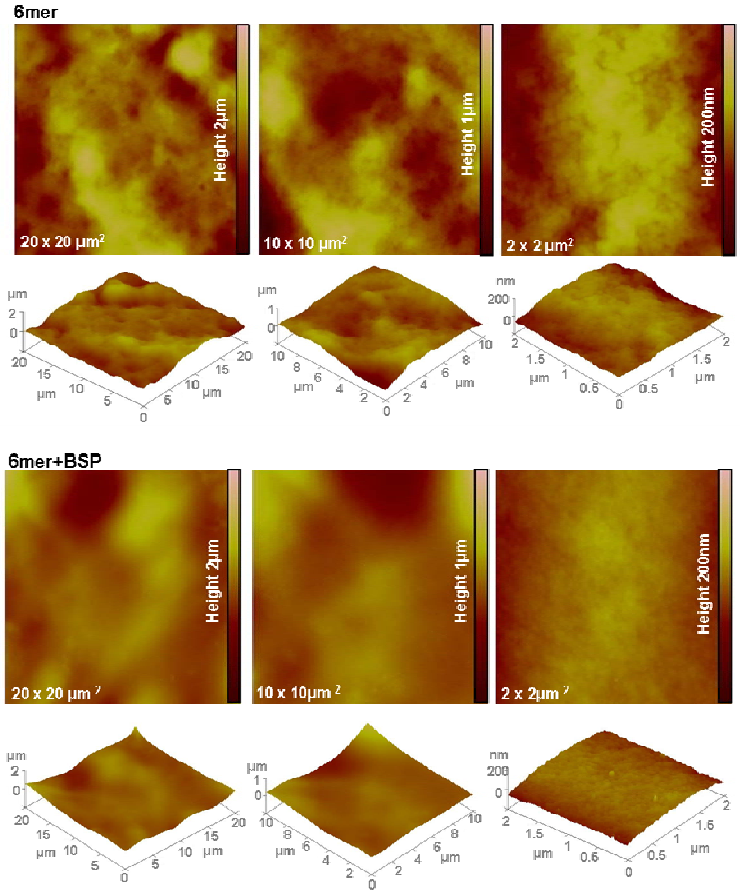

Figure IV.4. Topographies of AFM images (tapping mode) for 2% 6mer and 6mer+BSP films using 20 x 20 μm^2, 10 x 10 μm^2 and 2 x 2 μm^2 scan sizes.

Table IV.2. Surface roughness, RMS and R_a for the 6mer and 6mer+BSP films using different scan sizes.

	6mer		6mer+BSP		Mica	
	RMS(nm)	R_a(nm)	RMS(nm)	R_a(nm)	RMS(nm)	R_a(nm)
20 x 20μm^2 scan size	252.8±43.2	194.2±32.0	249.4±70.4	201.8±61.4	0.881	0.712
10 x 10μm^2 scan size	124.4±11	99.6±8.8	144.8±79.1	115.1±63.0	0.455	0.377
2 x 2μm^2 scan size	23±5.1	18.3±4.8	14.6±6.0	12.2±5.5	0.084	0.066

3.4. AFM imaging

Tapping mode AFM imaging showed that when dissolved in HEPES 0.1 mM (pH 7.4) most of the 6mer appeared as large globular, amorphous protein aggregates (Figure IV.5A). The aggregates had different sizes, with diameters ranging from 0.489 to 0.736 µm and heights varying from 122.7 to 134.7 nm. Aggregates with similar morphology and size were also observed when the 6mer protein was dissolved in

HEPES buffer containing Mg^{2+} ions in a molar ratio of 1:1000, protein:Mg (Figure IV.6A). However, after dissolving the 6mer protein in HEPES buffer containing Ca^{2+} ions in a molar ratio of 1:1000 (protein:Ca) the 6mer appeared more fibrous with a tendency to form fiber aggregates (Figure IV.7A). The cross-sections of these fibers or aggregates showed a width ranging from approximately 0.1 to 0.04 µm and a height between 2.6 and 5.8 nm.

In the case of the 6mer+BSP dissolved in HEPES, AFM imaging revealed two different forms of aggregates: elongated sheets forming large assemblies and spherical particles (Figure IV.5B). The sheets had heights between 1.4 and 1.8 nm. The second population of aggregates corresponding to spherical particles had heights between 6 and 7 nm (Figure IV.5B) and widths around 0.098 µm. Both types of aggregates had different shapes from those observed in the case of the 6mer protein dissolved in HEPES. Similarly to what happen with the 6mer protein, when the 6mer+BSP was dissolved in HEPES buffer containing Mg^{2+} ions the aggregates observed were similar to those obtained when dissolved in HEPES solution only. Once again large assemblies of elongated sheets were detected together with particles with an amorphous shape. These sheets had heights ranging between 1.89 and 1.35 nm, as observed for the HEPES solution (Figure IV.6B).

When the 6mer+BSP protein was dissolved in HEPES with Ca two distinct structures were observed, one corresponding to protein networks with different widths and another corresponding to individualized particles (monomers and dimmers). The widths for the aggregate networks varied, the smaller ones in Figure IV.7B1 have widths of around 0.2 nm and the largest ones corresponding to number 3 had diameters of 1.1 nm as seen in cross-sectional images. The height values for these structures were between 1.9 and 2.3 nm. The second population of structures corresponded to particles with diameters of 0.02 to 0.04 µm and heights of around 0.8 nm (see section for Figure IV.7B3). Once again the forms observed were different from those imaged with the 6mer protein and also different from those detected for the 6mer+BSP dissolved in HEPES and HEPES with Mg added.

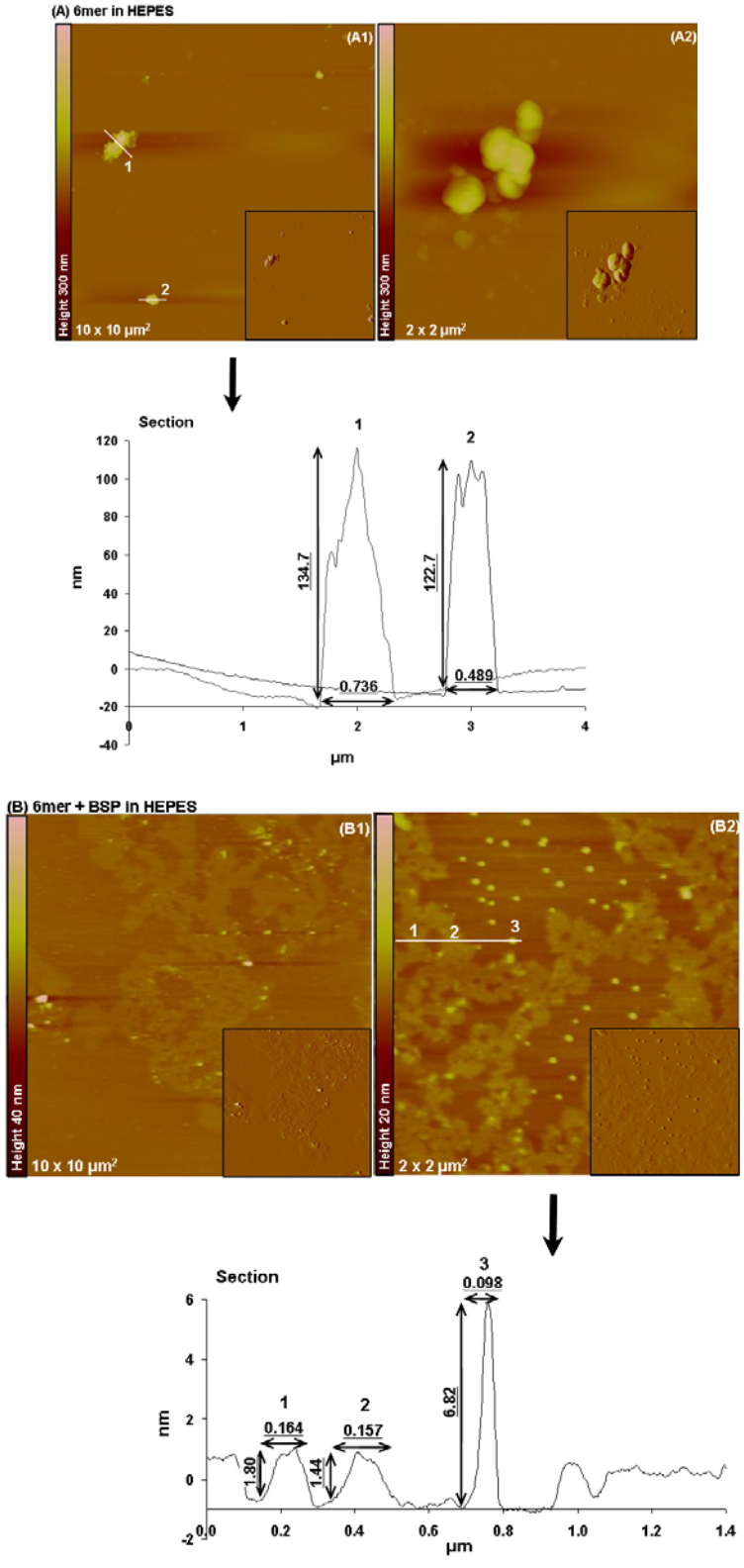

Figure IV.5. Topographies of AFM images (tapping mode) and corresponding section analysis of 6mer (A1-A2) and 6mer+BSP (B1-B2,) proteins in HEPES buffer 0.1 mM (pH 7.4).

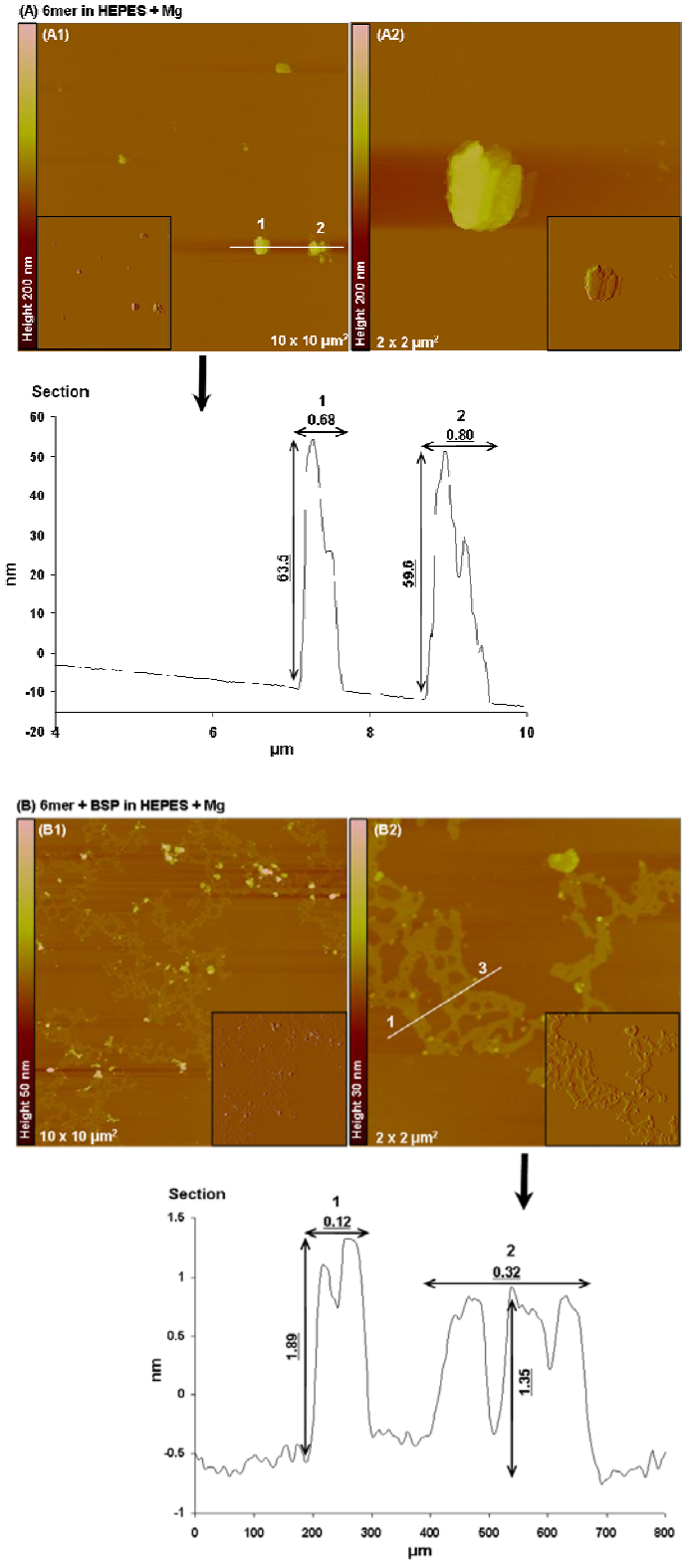

Figure IV.6. Topographies AFM images (tapping mode) and corresponding section analysis of 6mer (A1-A2) and 6mer+BSP (B1-B2) proteins in HEPES buffer 0.1 mM with Mg in a ratio of 1:1000 (protein:Mg).

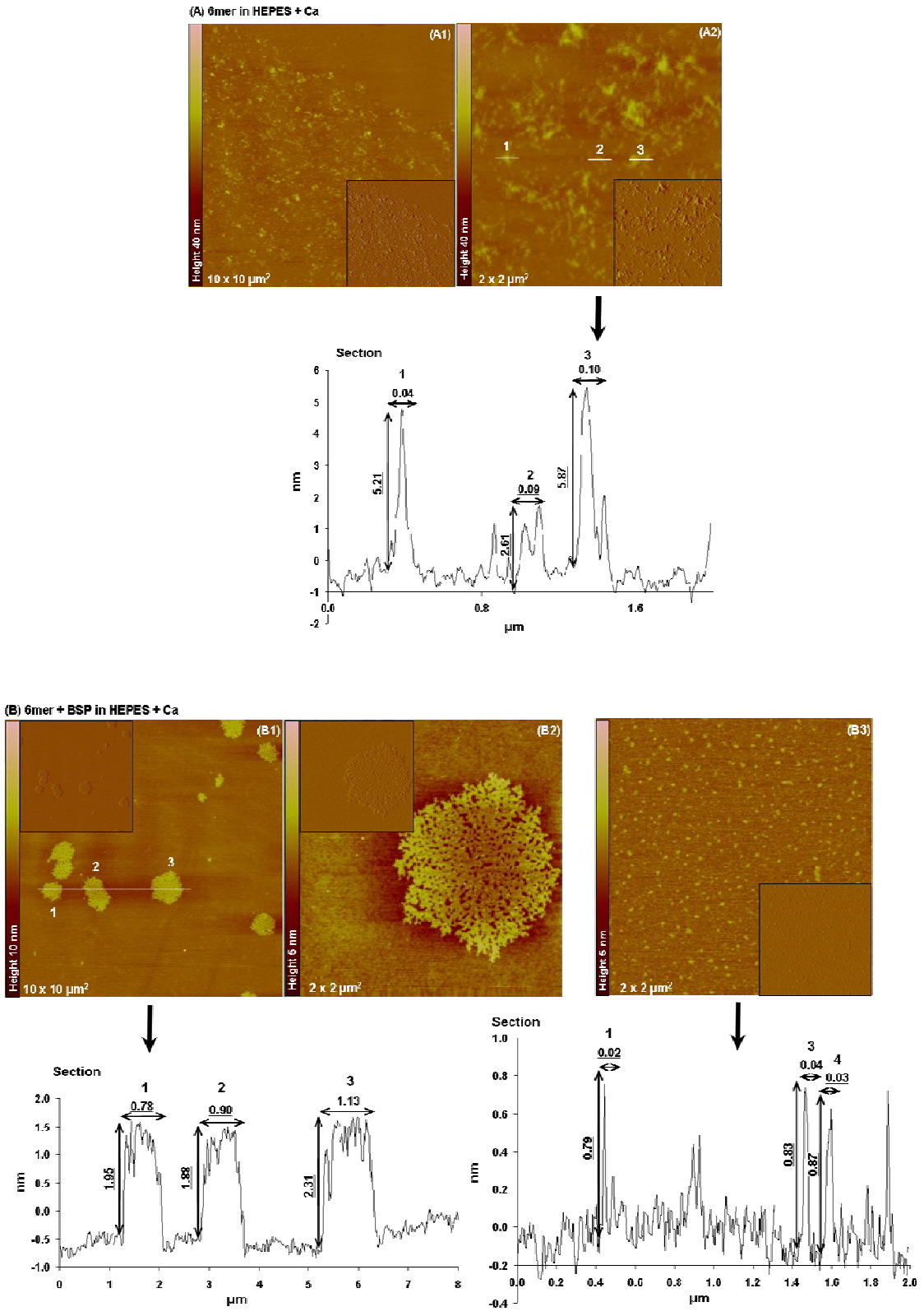

Figure IV.7. Topographies AFM images (tapping mode) and corresponding section analysis of 6mer (A1-A2) and 6mer+BSP (B1-B3) proteins in HEPES buffer 0.1 mM with Ca in a ratio of 1:1000 (protein:Ca).

3.5. CD analysis

CD spectroscopy for the 6mer protein showed no apparent difference between the spectra collected for the protein dissolved in HEPES and that dissolved in a HEPES with Ca or Mg added. For the three spectra a predominance of β-hairpin conformation (Figure IV.8) was found, characterized by a negative ellipticity with a minimum at approximately 202 nm [28, 29]. Also for the BSP+6mer protein no major differences were observed between the spectra collected in the presence of Ca or Mg and in HEPES. In the three spectra the presence of β-sheet and α-helix were observed, with two minima at 210 and 220 nm [28, 29] (Figure IV.8).

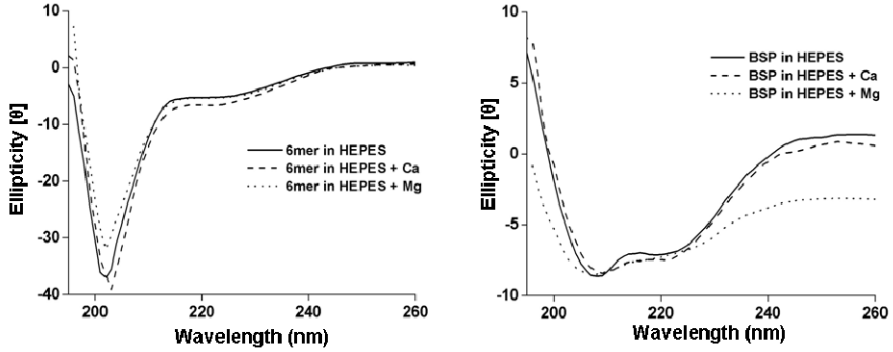

Figure IV.8. CD spectra for the 6mer and 6mer+BSP recombinant proteins dissolved in HEPES buffer 0.1 mM (pH 7.4), in HEPES buffer 0.1 mM with Ca in a ratio of 1:1000 (protein:Ca) and in HEPES buffer 0.1 mM with Mg in a ratio of 1:1000 (protein:Mg).

4. Discussion

In the present work the Young's modulus was calculated for the 6mer control and 6mer+BSP films based in the force curves. The values for the Young's modulus were 1.1 and 1.5 GPa for the 6mer and 6mer+BSP films, respectively, and statistical analysis showed a significant difference ($p<0.05$). This divergence may be due to the insertion of the BSP domain which could interfere with the ability of the silk to form β-strands, resulting in a change in assembly and thus in mechanical characteristics. However, ATR-FTIR analysis showed a similar presence of the β-sheet (1624 and 1520 cm^{-1}) for both the 6mer and 6mer+BSP films, after treatment with methanol. Furthermore, with the deconvolution of ATR-FTIR spectra the percentage of β-sheet and random coil (Table IV.1) showed no statistical differences ($p>0.05$) between the 6mer and 6mer+BSP films.

An alternative explanation for the differences in mechanical properties determined by AFM could be the high content of the amino acid glutamic acid in the BSP domain [14] of the 6mer+BSP protein. Mechanical studies performed on silkworm silk fibers treated with four different solvents (water, acetone, ethanol and isopropanol) showed that immersion in acetone, ethanol and isopropanol leads to an increase in stiffness when compared with water. In contrast, the immersion of fibers in water resulted in a decrease in tensile modulus of the fibers. These results were explained by the fact that water disrupts inter- and intra-molecular hydrogen bonding in the silk matrix. This disruption allows the molecules to move with greater freedom resulting in more flexible and elastic fibers [30] with a consequent decrease of stiffness, which was also observed for other biopolymers such as chitosan in the presence of water [31]. These hydrogen bonds occur between the amide hydrogen and carbonyl oxygen present in adjacent protein chains [32]. In the 6mer+BSP sequence the carboxyl groups present in the side chains of the glutamic acid residues constitutes an additional hydrogen donor increasing the number of hydrogen bonds occurring between protein chains. Different studies performed with poly-glutamic peptides demonstrate the ability of these molecules to form strong hydrogen bonds [33, 34]. The presence of several glutamic acid residues with carboxyl groups in their side chains in the BSP sequence may also contribute to an increase in the number hydrogen bonds in the 6mer+BSP proteins [14]. This gain in hydrogen bonding between 6mer+BSP proteins chains may be a reason for the higher stiffness observed for 6mer+BSP films when compared with 6mer films. As mentioned above, the increase in number of hydrogen bonds between silk chain segments, as a consequence of the treatment with organic solvents, resulted in an increase in elastic modulus values for silk [35].

Furthermore, the values of 1.1 and 1.5 GPa obtained for the 6mer and 6mer+BSP films are close to the values obtained for silk fibroin films, 2.7 GPa [36] but still far from the values of 20-22 GPa for stiffness attributed to the major ampullate dragline silk from the spider *Nephila clavipes* [37]. This difference indicates that there remains a lot to learn about processing and assembly of silk proteins related to functional properties.

AFM was also used to provide topographic images and roughness for the 6mer and 6mer+BSP films. The topographic images show that the 6mer+BSP films had a smoother surface that the 6mer films, however, a statistical comparison showed no significant difference between. Furthermore, the roughness values indicated a relationship between this parameter and the size of the scanned area; an increase in the size of the scanned area resulted in an increase in roughness values. This phenomenon was observed for both the 6mer and 6mer+BSP films (Table IV.2). Similar results were obtained in other studies when measuring the roughness properties of different materials using AFM [38-42]. A possible reason for this result is the effect of tip geometry on the measurements of surface roughness. At small scan sizes, if the tip is larger than the features causing the surface texture the surface will appear flatter as a consequence of poor access to lower points on the surface, and the roughness values will be lower [42]. With the increase of the scan size there is an increase of roughness values [40]. In this way, by changing the scan size it is possible to acquire different surface topographies, with different roughness values [38].

Finally, the behaviour of the 6mer+BSP protein in the presence of divalent ions, Ca and Mg, was investigated. During the past few years the role of Ca^{2+} ion in the formation of protein networks has been studied due to the importance of these networks in mechanical properties. For example, the abalone shell is a good example of a composite material formed by calcium carbonate plates arranged between organic matrix layers of β-chitin and proteins named lustrins [43]. The organic layers are responsible for the remarkable properties of these natural composites [43-45] acting as a organic adhesive holding the calcium carbonate plates together. Smoth and co-workers [44] used AFM to carry out pulling experiments on freshly cleaved nacre surfaces and obtained force-extension curves with a saw-tooth pattern probably resultant from the repeated unfolding of molecules, such as lustrin A. This unfolding is the outcome of successive opening of folded or looped domains of long molecular chains. When the pulling force rises to a value close to that needed to break the molecule backbone a domain unfolds or a loop opens and the molecule needs to be pulled again until another domain unfolds or a loop opens. Only when all the domains are unfolded and loops opened does the molecule finally break [44]. Furthermore,

when the applied force is relaxed the unfolded domains and open loops have the ability to reform acting as a self-healing mechanism [44]. These sacrificial bonds are believed to be the key for the outstanding mechanical properties of natural biocomposites [44] [46]. Divalent ions like Ca^{2+} and Mg^{2+} are crucial for the formation of these sacrificial bonds since this mechanism relies in the formation of intra and inter-chain ionic bond cross-links. Nacre organic matrix is rich in acidic macromolecules in which carboxylate groups are strong calcium binders [45] and are probably involved in the formation of sacrificial bonds. Other AFM studies performed with the cement tube of *Phragmatopoma californica* worms [47] and with the cell wall of *Cylindrotheca fusiformis* diatom give similar results [48].

Bone is also a good example of a natural biocomposite where the formation of calcium mediated sacrificial bonds and the presence of unfolded lengths are responsible for the stiffness and enhanced energy dissipation [46, 49-53]. The presence of many noncollagenous proteins in bone organic matrix such as bone sialoprotein and osteopontin, in the case of bone, and amelogenin [54] in the case of dental enamel, with a high number of negatively charged groups are capable of binding together through the formation of Ca ionic bonds [53]. This organic matrix acts as glue embedding the mineralized collagen fibrils and is capable of dissipating energy through the rupture of sacrificial bonds and stretching molecules, preventing the formation of cracks and increasing the total energy needed to fracture the material, thereby contributing to the improved toughness [50]. As in the case of nacre, when the applied force is removed the sacrificial bonds reform allowing the bone to repair itself [46].

Because it is still unclear which molecules are involved in the formation of these protein networks and what bonds are responsible for keeping them together some studies addressing the network forming behaviour of different proteins present in tooth and bone organic matrix have been published. Fincham and co-workers studied the self-assembly of a recombinant amelogenin protein and found that this protein was capable of forming supra-molecular aggregates which the authors suggest to be responsible for controlling the formation of enamel crystals [54]. More recently, a recombinant osteopontin protein was reported to form long aggregate networks and

to dissipate large amounts of energy when its molecules were pulled by an AFM cantilever tip [16]. In the presence of Ca^{2+} ions the resistance of these protein networks to the pulling force increased considerably [16]. The same authors performed similar experiments with other proteins, namely BSP [16] and dentin matrix protein [55], and the same network-forming tendency was observed. As in the case of osteopontin the presence of Ca potentiated the network-forming behaviour.

In the present work one of the objectives was to study the behaviour of 6mer+BSP protein in the presence of Ca^{2+} ions. In the same way as other negatively charged proteins, osteopontin, BSP, amelogenin and dentin matrix protein, our chimeric silk-BSP protein retained the ability to form supramolecular aggregates and in the presence of Ca^{2+} ions these aggregates generated networks which, as in the case of amelogenin [54], co-existed with protein monomers and multimers. These structures were not observed in the presence of Mg^{2+} ion which suggests affinity of the BSP domain to Ca^{2+} over other divalent ions as Mg^{2+}. The size of Ca^{2+} ion electron cloud may be the cause for this selectivity [56].

Furthermore, in the case of the 6mer+BSP protein the network-forming behaviour could be potentiated due to the presence of the spider silk domain (6mer). AFM mechanical and structural studies with a recombinant dragline silk protein showed that this protein spontaneously forms long nanofibers with high intersegment flexibility. When subjected to a pulling force the force *vs.* piezo extension curves displayed a saw-tooth rupture pattern most probably due to the presence of sacrificial bonds [6]. Similar patterns were obtained with the capture silk fibers from *Araneus*, a orb-weaving spider, where a pulling force revealed rupture peaks due to the break of sacrificial bonds, that reform after relaxation of the fibers [57]. These rupture peaks are also characteristic of the composite materials and proteins mentioned above, placing silk fibers in the category of the self-healing biomaterials [57]. Although we did not observe the formation of nanofibers when the 6mer was dissolved in HEPES alone, the formation of supra-molecular complexes resembling fibers was observed when Ca was added to the HEPES solution. These results are in accordance with the outcomes of other studies where AFM [58] and dynamic light scattering (DLS) [59] were used to assess the behaviour of fibroin, from *Bombix mori*, in the presence of Ca^{2+} ions. In

these studies, silk fibroin molecules gave rise to intermolecular networks through the formation of ionic bonds between divalent ions, mainly Ca, and the anionic carboxylic groups (COO^-) of fibroin amino acid groups [58, 59].

CD spectra indicated that no conformational change was induced by the presence of Ca^{2+} ions, suggesting that the interaction between 6mer+BSP and 6mer and Ca is probably induced by electrostatic attractions rather than by a conformational change in the protein structure [60].

As mentioned previously and based on the results obtained by different authors, Ca^{2+} ions seems to be a crucial element for the maintenance of mechanical integrity of many biological systems. The development of new biocomposite materials for biomedical applications is a desired goal. The design of novel organic-inorganic hybrid biomaterials [61], such as those described in the present work, may provide a new family of high performance structures for bone regeneration. The results discussed above re-enforce the potential of 6mer+BSP proteins in the development of these types of new hybrid biomaterials, where design principles can be employed in specialized designs for structural and functional outcomes.

5. Conclusions

The main goal of the present study was to assess the mechanical and structural characteristics of a new recombinant protein, 6mer+BSP, using AFM for imaging and force spectroscopy. In our previous work [8] this protein retained mineralization potential attributed to the BSP domain and sustained human mesenchymal stem cell proliferation and differentiation into the osteogenic lineage. However, if this protein is to be used for bone regeneration applications additional mechanical and structural studies were required. The force curves collected for the 6mer and 6mer+BSP films showed that the 6mer+BSP had a higher stiffness, likely due to the glutamic acid residues. Furthermore, the behaviour of the new recombinant protein in the presence of Ca, and as reported previously by others for osteopontin, amelogenin and dentin matrix protein, the present chimeric protein retained the ability to form supramolecular networks in the presence of Ca^{2+} ions through ionic crosslinking. This study shows the potential for new bioengineered polymers, such as 6mer+BSP, for the

design of new nanocomposite systems. The presence of the silk domain in 6mer+BSP protein allows this biopolymer to be processed into different three-dimensional scaffolds. In addition, the BSP domain with its calcium affinity provides functions as an organic glue for use in new synthetic nanoscale composites, cross-linking organic and inorganic components, such as hydroxyapatite crystals, and increasing the stiffness and toughness of these systems by dissipates energy through the break of sacrificial bonds.

Acknowledgements

Sílvia Gomes thanks the Portuguese Foundation for Science and Technology (FCT) for providing her a PhD grant (SFRH/BD/28603/2006). This work was carried out under the scope of the European NoE EXPERTISSUES (NMP3-CT-2004-500283), the Chimera project (PTDC/EBB-EBI/109093/2008) funded by the FCT agency, the NIH (P41 EB002520) Tissue Engineering Resource Center and the NIH (EB003210 and DE017207).

References

1. Scheibel T. Spider silks: recombinant synthesis, assembly, spinning, and engineering of synthetic proteins. Microb Cell Fact 2004;3(1):14-24.

2. Foo CWP, E.Bini, Huang J, Lee SY, Kaplan DL. Solution behavior of synthetic silk peptides and modified recombinant silk proteins. Appl Phys Mater Sci Process 2006;82:193–203.

3. Hayashi CY, Shipley NH, Lewis RV. Hypotheses that correlate the sequence, structure, and mechanical properties of spider silk proteins. Int J Biol Macromol 1999;24(2-3):271-275.

4. Beek JDv, Hess S, Vollrath F, Meier BH. The molecular structure of spider dragline silk: folding and orientation of the protein backbone. Proc Natl Acad Sci USA 2002;99:10266-10271.

5. Altman GH, Diaz F, Jakuba C, Calabro T, Horan RL, Chen J, et al. Silk-based biomaterials Biomaterials 2003;24(3):401-416.

6. Oroudjev E, Soares J, Arcidiacono S, Thompson JB, Fossey SA, Hansma HG. Segmented nanofibers of spider dragline silk: atomic force microscopy and single-molecule force spectroscopy. Proc Natl Acad Sci USA 2002;99(2):6460–6465.

7. Rabotyagova O, Cebe P, Kaplan DL. Self-assembly of genetically engineered spider silk block copolymers. Biomacromolecules 2009;10:229–236.

8. Gomes S, Leonor IB, Mano JF, Reis RL, Kaplan DL. Spider silk-bone sialoprotein as a novel fusion protein for bone tissue engineering. Soft Matter 2010;Submitted.

9. Baht GS, Hunter GK, Goldberg HA. Bone sialoprotein–collagen interaction promotes hydroxyapatite nucleation. Matrix Biology 2008;27:600–608.

10. Mizuno M, Imai T, Fujisawa R, Tani H, Kuboki Y. Bone sialoprotein (BSP) is a crucial factor for the expression of osteoblastic phenotypes of bone marrow cells cultured on type I collagen matrix. Calcif Tissue Int 2000;66:388-396.

11. Valverde P, Zhang J, Fix A, Zhu J, Ma W, Tu Q, et al. Overexpression of bone sialoprotein leads to an uncoupling of bone formation and bone resorption in mice. J Bone Miner Res 2008;23(11):1775-1778.

12. Domke J, Radmacher M. Measuring the elastic properties of thin polymer films with the atomic force microscope. Langmuir 1998;14:3320-3325.

13. Schäfer A, Vehoff T, Glisŏvić A, Salditt T. Spider silk softening by water uptake: an AFM study. Eur Biophys J 2008;37:197-204.

14. Ganss B, Kim RH, Sodek J. Bone sialoprotein. Crit Rev Oral Biol Med 1999;10(1):79-98.

15. Goldberg H, Warner K, Li M, Hunter G. Binding of bone sialoprotein, osteoprotein and synthetic polypeptides to hydroxyapatite. Connect Tissue Res 2001;42(1):25-37.

16. Fantner GE, Adams J, Turner P, Thurner PJ, Fisher LW, Hansma PK. Nanoscale ion mediated networks in bone: osteopontin can repeatedly dissipate large amounts of energy. Nano Lett 2007;7(8):2491-2498.

17. He G, Dahl T, Veis A, George A. Dentin matrix protein 1 initiates hydroxyapatite formation *in vitro*. Connect Tissue Res 2003;44(1):240-245.

18. Kowalewski T, Holtzman DM. In situ atomic force microscopy study of Alzheimer's β-amyloid peptide on different substrates: new insights into mechanism of β-sheet formation. Proc Natl Acad Sci USA 1999;96:3688–3693.

19. Cacciafesta P, Hallam KR, Watkinson AC, Allen GC, Miles MJ, Jandt KD. Visualisation of human plasma fibrinogen adsorbed on titanium implant surfaces with different roughness. Surf Sci 2001;491(3):405-420.

20. Gadelmawla ES, Koura MM, Maksoud TMA, Elewa IM, Soliman HH. Roughness parameters. J Mater Process Technol 2002;123:133-145.

21. Johnson KL. Contact mechanics. Cambridge: Cambridge University Press, 1994.

22. Sneddon IN. The relation between load and penetration in the axisymmetric boussinesq problem for a punch of arbitrary profile. Int J Eng Sci 1965;3(1):47-57.

23. Schäfer A, Vehoff T, Glišović A, Salditt T. Spider silk softening by water uptake: an AFM study. European Biophysics Journal 2008;37:197–204.

24. Radmacher M, Fritz M, Kacher CM, Cleveland JP, Hansma PK. Measuring the viscoelastic properties of human platelets with the atomic force microscope. Biophys J 1996;70:556-567.

25. Wagh AA, Roan E, Chapman KE, Desai LP, Rendon DA, Eckstein EC, et al. Localized elasticity measured in epithelial cells migrating at a wound edge using atomic force microscopy. Am J Physiol Lung Cell Mol Physiol 2008;295:L54-L60.

26. Hu X, Kaplan D, Cebe P. Determining beta-sheet crystallinity in fibrous proteins by thermal analysis and infrared spectroscopy. Macromolecules 2006;39(18):6161-6170.

27. Rabotyagova OS, Cebe P, Kaplan DL. Role of polyalanine domains in β-sheet formation in spider silk block copolymers. Macromol Biosci 2010;10:49-59.

28. Cerpa R, Cohen FE, Kuntz ID. Conformational switching in designed peptides: the helix/sheet transition. Fold Des 1996;1(2):91-101.

29. Kelly SM, Jess TJ, Price NC. How to study proteins by circular dichroism. Biochim Biophys Acta 2005;1751:119 – 139.

30. Pérez-Rigueiroa J, Viney C, Llorca J, Elices M. Mechanical properties of silkworm silk in liquid media. Polymer 2000;41:8433–8439.

31. Mano JF. Viscoelastic properties of chitosan with different hydration degrees as studied by dynamic mechanical analysis. Macromol Biosci 2008;8(1):69-76.

32. Marsha RE, Coreya RB, Pauling L. An investigation of the structure of silk fibroin. Biochim Biophys Acta 1955;16:1-34.

33. Fulara A, Dzwolak W. Bifurcated Hydrogen Bonds Stabilize Fibrils of Poly(L-glutamic) Acid. J Phys Chem B 2010;114(24):8278–8283.

34. Zanuy D, Alemán C, Muñoz-Guerra S. On the helical conformation of un-ionized poly(γ-Image -glutamic acid) Int J Biol Macromol 1998;23(3):175-184.

35. Pérez-Rigueiro J, Viney C, Llorca J, Elices M. Mechanical properties of silkworm silk in liquid media. Polymer 2000;41:8433–8439.

36. Yin J, Chen E, Porter D, Shao Z. Enhancing the toughness of regenerated silk fibroin film through uniaxial extension. Biomacromolecules 2010;10.1021/bm100643q.

37. Gosline JM, Guerette PA, Ortleepp CS, Savage KN. The mechanical design of spider silks: from fibroin sequence to mechanical function. J Exp Biol 1999;202:3295-3303.

38. Boussu K, Bruggen Vd, Volodin A, Snauwaert J, Haesendonck CV, Vandecasteele C. Roughness and hydrophobicity studies of nanofiltration membranes using different modes of AFM. J Colloid Interface Sci 2005;286:632-638.

39. Koinkar VN, Bhushan B. Effect of scan size and surface roughness on microscale friction measurements. J Appl Phys 1997;81(6):2472-2479.

40. Poon CY, Bhushan B. Comparison of surface roughness measurements by stylus profiler, AFM and non-contact optical profiler. Wear 1995;190:76-88.

41. Poon CY, Bhushan B. Surface roughness analysis of glass-ceramic substrates and finished magnetic disks, and Ni-P coated Al-Mg and glass substrates. Wear 1995;190:89-109.

42. Sedin DL, Rowlen KL. Influence of tip size on AFM roughness measurements. Appl Surf Sci 2001;182(1-2):40-48.

43. Jackson AP, Vincenta JFV, Turner RM. A physical model of nacre. Compos Sci Technol 1989;36(3):255-266.

44. Smith BL, Schäffer TE, Viani M, Thompson JB, Frederick NA, Kindt J, et al. Molecular mechanistic origin of the toughness of natural adhesives, fibres and composites. Nature 1999;399:761-763.

45. Weiner S. Organization of Extracellularly Mineralized Tissues: A Comparative Study of Biological Crystal Growth. Crit Rev Biochem Mol Biol 1986;20(4):365-408.

46. Thompson JB, Kindt JH, Drake B, Hansma HG, Morse DE, Hansma1 PK. Bone indentation recovery time correlates with bond reforming time. Nature 2001;414:Nature.

47. Sun C, Fantner GE, Adams J, Hansma PK, Waite JH. The role of calcium and magnesium in the concrete tubes of the sandcastle worm. J Exp Biol 2007;210:1481-1488.

48. Kroger N, Bergsdorf C, Sumper M. A new calcium binding glycoprotein family constitutes a major diatom cell wall component. EMBO 1994;13(19):4676-4683.

49. Currey J. Biomaterials: Sacrificial bonds heal bone. Nature 2001;414:699.

50. Fantner GE, Hassenkam T, Kindt JH, Weaver JC, Birkedal H, Pechenik L, et al. Sacrificial bonds and hidden length dissipate energy as mineralized fibrils separate during bone fracture. Nat Mater 2005;4:612-616.

51. Gupta HS, Fratzl P, Kerschnitzki M, Benecke G, Wagermaier W, Kirchner HOK. Evidence for an elementary process in bone plasticity with an activation enthalpy of 1 eV. J R Soc Interface 2007;4(13):277-282.

52. Gupta HS, Wagermaier W, Zickler GA, Aroush DR-B, Funari SS, Roschger P, et al. Nanoscale Deformation Mechanisms in Bone. Nano Lett 2005;5(10):2108–2111.

53. Hansma PK, Fantner GE, Kindt JH, Thurner PJ, Schitter G, Turner PJ, et al. Sacrificial bonds in the interfibrillar matrix of bone. J Musculoskelet Neuronal Interact 2005;5(4):313-315.

54. Fincham AG, Moradian-Oldak J, Simmer JP, Sarte P, Lau EC, Diekwisch T, et al. Self-Assembly of a Recombinant Amelogenin Protein Generates Supramolecular Structures. J Struct Biol 1994;112(2):103-109.

55. Adams J, Fantner GE, Fisher LW, Hansma PK. Molecular energy dissipation in nanoscale networks of dentin matrix protein 1 is strongly dependent on ion valence. Nanotechnology 2008;19(38):384008-384015.

56. Williams RJP. A general introduction to the special properties of the calcium ion and their deployment in biology. In: Siegel FL, Carafoli E, Kretsinger RH, MacLennan DH, Wasserman R, editors. Calcium Binding Proteins: Structure and Function. NY: Elsevier Noth Holland Inc., 1980.

57. Becker N, Oroudjev E, Mutz S, Cleveland JP, Hansma PK, Hayashi CY, et al. Molecular nanosprings in spider capture-silk threads. Nat Mater 2003;2:278-283.

58. Yamada K, Tsuboi Y, Itaya A. AFM observation of silk fibroin on mica substrates: morphologies reflecting the secondary structures. Thin Solid Films 2003;440:208-216.

59. Hossain KS, Nemoto N. Dynamic and Static Light Scattering of Dilute Aqueous Solutions of Silk Fibroin Collected from Bombyx Mori Silkworms. Langmuir 1999;15(12):4114-4119.

60. Yang Y, Cui Q, Sahai N. How does bone sialoprotein promote the nucleation of hydroxyapatite? A molecular dynamics study using model peptides of different conformations. Langmuir 2010;26(12):9848-9859.

61. Tang Z, Kotov NA, Magonov S, Ozturk B. Nanostructured artificial nacre. Nat Mater 2003;2:413-418.

Abstract

Genetically engineered fusion proteins offer potential as multifunctional biomaterials for utility in the medical field. In the present study, three new fusion proteins were designed, cloned and expressed and assessed for function, by combining the consensus sequence of dragline spider silk with three different antimicrobial peptides. The spider silk domain maintained its self-assembly features, a key aspect of these new polymeric protein biomaterials, allowing the formation of β-sheets to lock in structures via physical interactions without the need for chemical cross-linking. The human antimicrobial peptides human neutrophil defensin 2 (HNP-2), human neutrophil defensins 4 (HNP-4) and hepcidin were fused to the spider silk during the bioengineering process. These new functional silk proteins were assessed for antimicrobial activity against *Escherichia coli* and *Staphylococcus aureus*, a Gram negative and positive, respectively, and microbicidal activity was demonstrated. Dynamic light scattering was used to assess protein aggregation to clarify the antimicrobial patterns observed. *In vitro* cell studies with a human osteosarcoma cell line (SaOs-2) demonstrated the compatibility of these new proteins with mammalian cells with two of the three proteins studied.

1. Introduction

Around 350 billion dollars are spent worldwide on organ replacement therapies to prolong the lives of more than 20 million patients. Most organ replacement surgeries rely on the use of organometallic devices, most of which were developed in the 1960s [1]. Tissue engineering is an emerging interdisciplinary field focused on the development of tissues and organs that can be used to replace damaged and failing tissues and organs. One of the major goals of tissue engineering is to replace permanent implanted prostheses with temporary implants with reconstructive and regenerative characteristics capable of directing the full restoration of normal tissue structure and function in the body; thus they must be fully degradable over time [2]. Achieving this goal would revolutionize healthcare treatment as well as patient well being [3]. The biomaterials field contributes directly toward this goal through the development of polymers with diverse mechanical and biological characteristics [4-7] that can be used to facilitate the regeneration of damaged tissues. In the case of bone

repair, meeting mechanical and functional requirements at the implant site remains a challenge for most polymeric biomaterials [8, 9].

In the present work, spider silk was selected for the core polymer due to its potential as a biomaterial to meet the requirements for both mechanical stability and biocompatibility necessary for bone tissue engineering, as well as its accessibility to bioengineering [10-12]. Furthermore, recombinant DNA technologies allow the generation of spider silk proteins fused to other protein domains not normally found in spider silks, thereby expanding the function of these protein polymers. These new chimeric or multifunctional spider silk-like molecules combine the properties of silk (e.g., self-assembly, robust material properties, physical cross-linking to stabilize materials) with characteristics of the new domains added to the silk. These types of new multifunctional polymeric biomaterials provide a new route to control of biomaterial features related to both material features and biological interactions. The addition of antimicrobial peptides to reduce or control infections at the site of implantation was the direction sought in the present study.

There are more than 600 peptides known with antimicrobial activity, most with broad activity against different microorganisms, including Gram+ and Gram- bacteria, virus, protozoa and fungi [13]. These peptides play an important role in inflammation [14], and chemotaxis for monocytes and T cells to activate the acquired immune response system [15]. These peptides also intervene in the wound healing [16] by stimulating the proliferation of fibroblasts and epithelial cells [17, 18], induce neovasculogenesis [19] and mobilize cytokines [20]. Human α-defensins are cationic cysteine-rich peptides containing between 29 and 35 amino acids [21, 22]. Six α-defensins have been described, human neutrophil defensins 1 to 4 (HNP-1, HNP-2, HNP-3 and HNP-4) [23], which are expressed in neutrophils, and human defensins 5 to 6 (HD-5 and HD-6) expressed by Paneth cells of the small intestine and by the epithelial cells of the female urogenital track [24]. HNP-2 manifests bactericidal activity against both Gram+ and Gram- bacteria [25]. HNP-4 was considered more effective against Gram- *Escherichia coli* and *Enterobacter aerogene*s. Moreover, HNP-4 was more effective than HNP-1, HNP-2 and HNP-3 in protecting human peripheral blood mononuclear cells from infection by both X4 and R5 HIV-1 strains [26].

Resembling the human neutrophil defensins described above, hepcidin (also named LEAP-1 for liver expressed antimicrobial peptide), is also a cysteine rich peptide. Hepcidin mRNA was found primarily in the liver and was isolated initially from human blood [27] and later detected in urine [28]. Hepcidin exhibits bactericidal and fungicidal activity with activity against Gram+ and Gram- bacteria. Hepcidin was active against the Gram- *E. coli* ML35 strain and *Neisseria cinerea*, and against the Gram+ *Staphylococcus aureus*, *Staphylococcus epidermis*, *Staphylococcus carnosus*, *Bacillus cereus*, *Bacillus megaterium*, *Bacillus subtilis*, *Micrococcus luteus* and group B *Streptococcus* [27-31]. After incubation of K562 cells (American Type Culture Collection leukemic cell line CCL-243) for 15 hours with hepcidin at a concentration of 30 μM, viability of 74% was found [32]. Thus the cytotoxicity of hepcidin was much lower than after incubation of these cells with 30 μM α-defensin HNP-1, where only 9% of the cells were viable over the same time frame [28]. Based on the antimicrobial activities of HNP-2, HNP-4 and hepcidin, these peptides were selected for fusion with the silk protein major ampullate spidroin protein (MaSpI) in the present study. The silk was selected as the main protein component as it has been shown to self-assemble into impressively strong and tough protein-based biomaterials, is biodegradable due to the activity of proteases, and can be formed into a range of material formats using water [33-35].

Due to the relatively low cytotoxicity, resistance to microorganism adaptation and broad spectra of action some antimicrobial peptides are considered strong candidates to be used in coatings of polymeric surfaces to help preventing microbial contamination. However, few studies have addressed this topic. In the past few years different antimicrobial peptides were expressed together with a carbohydrate binding module from *Clostridium thermocellum*, to enable attachment to different cellulosic surfaces for antimicrobial properties [36, 37]. The chemical coupling of antimicrobial peptides to different types of surfaces, such as: polyamide resins [38], polystyrene-polyethylene glycol beads [39-41] and titanium [42], has also been reported. To our knowledge this is the first study describing fusion proteins combining both silk and antimicrobial domains.

The goal of the present study was to construct three new fusion proteins combining spider silk with antimicrobial features hepcidin, HNP-2 and HNP-4 (Figure

V.1A). Three different antimicrobial peptides were selected due to the possible decrease in activity when the peptides were coupled with the spider silk. In this way, the activities of the three different fusion proteins could be compared to identify the most useful sequence for biomaterials formation and characterization. The silk domain in the proteins carries six repeats of the consensus repeat for the native sequence of the protein major ampullate dragline silk I (MaSpI) from the spider *Nephila clavipes*. Each silk repeat is formed by a hydrophilic GGX motif and a hydrophobic poly-A motif (Figure V.1B).

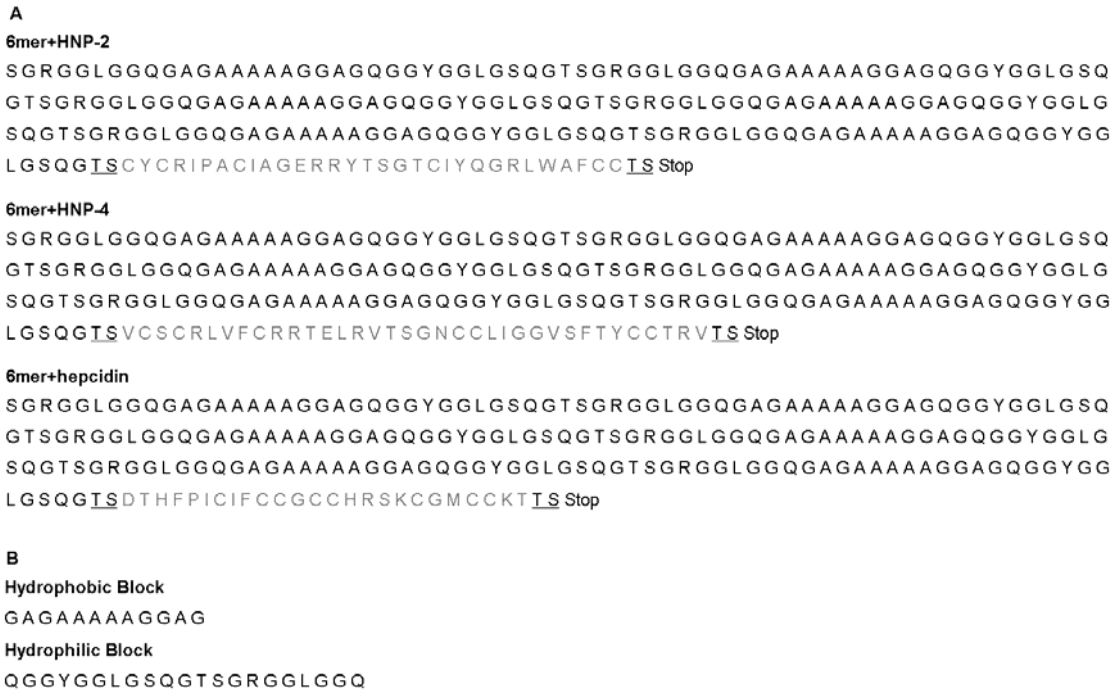

Figure V.1. (A) Amino acid sequences for the chimeric proteins carrying silk block copolymer (6mer) and the HNP-2 (a), HNP-4 (b) and the hepcidin (c) peptide sequences. The 6mer block is represented by black. The HNP-2 (a), HNP-4 (b) and hepcidin (c) sequences are represented by a gray. The restriction sites for the insertion of HNP-2, HNP-1 and hepcidin sequences are underlined. (B) Amino acid sequences for the hydrophobic and hydrophilic blocks present in each of the six units forming the silk block copolymer (6mer).

The three different silk-antimicrobial fusions were successfully expressed and characterized for structure and function. The antibacterial activity was studied by radial diffusion. Secondary structure of the recombinant proteins was assessed by attenuated-total reflectance Fourier transform infrared spectroscopy (ATR-FTIR) and Circular Dichroism (CD). Dynamic light scattering (DLS) was used to assess aggregation

related to antimicrobial activity in solution. Finally, cytotoxicity tests were performed to confirm the potential utility of these new multifunctional silk proteins in contact with mammalian cells.

2. Materials and Methods

2.1. Cloning HNP-2, HNP-4 and hepcidin into pET30L vector containing silk modules

Vector pET30a+ (Novagen, San Diego CA) was used for the construction of the vector pET30L carrying the silk block copolymer using procedures described in our previous work [43]. The silk block copolymer carries six repeats of the consensus repeat for the native sequence of the protein major ampullate dragline silk I from the specie *N. clavipes*. This spider silk block copolymer (6mer) was cloned with six histidine residues to facilitate protein purification, and with two restriction sites, one for *Spe*I and another *Nhe*I, flanking its edges to allow the addition of other DNA [43].

The HNP-2, HPN-4 and hepcidin cDNA sequences were prepared through the annealing of synthetic single strand oligonucleotide sequences (Invitrogen, CA, USA): HNP-2 top and HNP-2 bottom, HNP-4 top and HNP-4 bottom and hepcidin top and hepcidin bottom. The annealing reactions were carried out by decreasing the temperature of the oligonucleotide solution from 95ºC to 20ºC with a gradient of 0.1ºC/s. The presence of the annealed products was verified with 5% agarose gels. At the edges of each cDNA sequence restriction sites were present for *Spe*I and for *Nhe*I for the insertion of the cDNA sequences into the vector pET30L. This vector already carried the DNA encoding the silk block copolymer. For the insertion of the cDNA sequences into pET30L, the vector was digested with *Spe*I (New England Biolabs, MA, USA, R0133S), dephosphorylated with calf intestinal phosphatase (CIP) (New England Biolabs, M0290S) and run on 0.8% agarose gels. The linearized vector was purified using the QIAquick gel extraction kit (Qiagen, CA, USA, 28706). The cDNA sequences were double digested with *Spe*I and *Nhe*I and the digestion products run in a 0.8% gel and the bands for the cDNA sequences were purified using a QIAquick gel extraction kit. HNP-2, HPN-4 and hepcidin cDNA were ligated individually to the silk 6mer present in the expression vector pET30L using T4 DNA ligase enzyme (New England Biolabs, M0202S).

Escherichia coli DH5α cells (Invitrogen, 18258-012) were transformed with the ligation products and successful transformants were identified by plating on agar plates containing 25 μg/ml kanamycin. The presence of the HNP-2, HPN-4 and hepcidin inserts was confirmed by DNA sequencing (Tufts Core Facility, Boston, MA) using T7 primers and the new constructs were named: 6mer+HNP-2, 6mer+HNP-4 and 6mer+hepcidin.

2.2. Protein expression and purification

The 6mer, 6mer+HNP-2, 6mer+HNP-4 and 6mer+hepcidin were expressed in *E. coli* RY-3041 strain, a mutant strain of *E. coli* BLR(DE3) defective in the expression of SlyD protein[44, 45]. Cells were cultivated at 37ºC in LB medium, with 25 μg/ml kanamycin until an OD_{600} between 0.9 and 1 was reached. At this point expression was induced with isopropyl β-D-thiogalactoside (IPTG, Invitrogen, 15529019) to a final concentration of 0.5 mM. After 2 hours of expression the cells were harvested by centrifugation at 6,500 rpm. The cell pellet was resuspended in denaturating buffer (100 mM NaH_2PO_4, 10 mM Tris HCl, 8 M urea, pH 8.0) and left overnight with stirring for complete cell lysis. Insoluble cell fragments and soluble proteins present in the cell lysate were separated through centrifugation at 11,000 rpm. The supernatant was mixed with Ni-NTA resin (Qiagen, 30250) and left for 2 hours with stirring. The supernatant/Ni-NTA resin mixture was loaded onto a glass Econo-column (Biorad) and washed several times with denaturating buffer at pH 8 and then pH 6.0. The 6mer+HNP-2, 6mer+HNP-4 and 6mer+hepcidin proteins were eluted using denaturating buffer at pH 4.5. The purified proteins were dialysed first in a 20 mM sodium acetate buffer followed by extensive dialysis in MQ water using cellulose ester snake skin membranes with a 100-500 Da molecular weight cut off (Spectra/Por Biotech, 131054). The dialyzed proteins were lyophilized in a LabConco lyophilizer. Protein sequencing (Tufts Core Facility, Boston, MA), SDS-PAGE and western blot were used to confirm protein identity.

2.3. Protein identification by western blot

Proteins were mixed with NuPAGE LDS sample buffer (Invitrogen, NP0007) and heated to 80ºC for 10 minutes. The samples were separated using a Bis-tris 4-12% gel

(Invitrogen, NP0321BOX). For the western blot the His-Tag AP western kit provided by Novagen, EMD Biosciences, NJ, USA (70972) was used with the protocol provided. Briefly, bands were electro-transferred onto a nitrocellulose membrane at 30V for 16 hours. Membranes were blocked for one hour with 3% bovine serum albumin (BSA) in TBS buffer (blocking solution). After washing with TBS buffer the membrane was incubated for 1 hour with mouse anti-histidine monoclonal antibody (Novagen) diluted 1:1000 in blocking solution. Following proper washing with TBSTT buffer the membrane was incubated for 1 hour with goat anti-mouse IgG AP conjugated antibody diluted 1:5000 in blocking solution. Colorimetric detection was performed with developing solution of 5-bromo-4-chloro-3-indolylphosphate (BCIP) and nitrobluetetrazolium (NBT).

2.4. Film formation and ATR-FTIR secondary structure analysis

Recombinant 6mer+HNP-2, 6mer+HNP-4, 6mer+hepcidin and 6mer proteins were dissolved in MQ water to a final concentration of 2% (w/v). Then 60 µl of each protein solution was cast onto a non adherent polystyrene surface and left to dry at room temperature. The films obtained were treated with 70% methanol for 2 hours to induce the transition of secondary structure from random coil to β-sheet. This treatment produced films with improved mechanical properties and more resistant to dissolution in water or other aqueous environments such as culture media. For cell studies the films were treated with 70% (w/w) ethanol solution for sterilization purposes. ATR-FTIR (Jasco Inc., MD, USA, model FT/IR-6200) was performed before and after methanol treatment of the films to investigate secondary structure. Spectra were collected in absorption mode at 8 cm^{-1} resolution and a 4000 to 400 cm^{-1} region was scanned. The quantification of the secondary structure was based on the analysis of the amide I and amide II regions (1700 to 1450 cm^{-1}). The average percentage for the secondary structures, mainly β–sheet content for the 6mer (control situation), 6mer+HNP-2, 6mer+HNP-4 and 6mer+hepcidin proteins was calculated through the integration of the area of each deconvoluted curve followed by the normalization of the obtained value to the total area of the amide I and amide II regions [46].

2.5. Antibacterial assay

The purified recombinant proteins were tested for antimicrobial activity against *E. coli* (American-Type Culture Collection ATCC 25922, VA, USA,) and *S. aureus* (ATCC 25923), purchased from American-Type Culture Collection. The radial diffusion assay [47] was used to test three concentrations of the purified proteins dissolved in phosphate buffer (pH 7.4): 10, 50 and 100 μg/ml. The 6mer protein solutions were used as controls. *E. coli* and *S. aureus* lawns were plated on LB-agar plates, using liquid *E. coli* and *S. aureus* cultures grown overnight at 37ºC. A biopsy punch 8 mm in diameter was use to cut circles from filter paper (Whatman, 09-845B) that were used as blank susceptibility disks. For sterilization, the disks were immersed in a 70% (v/v) ethanol solution for 1 hour and left to dry for two hours in a hood. After drying, the discs were immersed in the different protein solutions, placed on the bacterial lawns and incubated overnight at 37ºC. The zones of growth inhibition formed around the susceptibility disks were measured using *Image J* software. The 6mer protein was used as a negative control in order to exclude the effect from silk itself and from possible contaminants derived from the expression and purification processes. Experiments were carried out in triplicate.

2.6. Aggregation

A Zetasizer NanoZS instrument (ZEN3600, MALVERN Instruments, Worcestershire, UK) was used for DLS measurements. DLS was performed on solutions at the same concentrations used for the antibacterial assay (section 2.5): 10, 50 and 100 μg/ml. Samples were prepared with phosphate buffer (pH 7.4). The scattering light was collected at a 173º scattering angle.

2.7. Circular dichroism spectroscopy

Circular Dichroism (CD) spectroscopy was performed on an Aviv, Model 410 (Biomedical, Inc. NJ USA) instrument. The spectra were collected between 260 and 180 nm with a step size of 1 nm, an averaging time of 1s and five scans were collected for each sample. A baseline spectrum was subtracted from the samples. Sample cells with a 0.1 cm path length were used and measurements were performed with 1 mg/ml protein solutions in phosphate buffer (pH 7.4).

2.8. Cytotoxicity assay

Human osteosarcoma cell line (SaOs-2) is an immortalized cell line with osteoblastic phenotype (HTB-85) and was purchased from the American-Type Culture Collection. Cells were cultured using basal medium consisting in Dulbecco's modified Eagle's medium (DMEM) supplemented with 10% (v/v) fetal bovine serum (FBS), 1% penicillin-streptomycin (v/v), at 37ºC with 5% CO_2 in a humidified environment. After reaching confluence, cells were harvested with trypsin/EDTA and after counting cells they were seeded at $3.0x10^3$ cells/cm^2 in a 96 well plate coated with the four different types of protein films (6mer+HNP-2, 6mer+HNP-4, 6mer+hepcidin, 6mer (control) films, prepared as in section 2.3. Tissue culture plate (TCP) was used as a positive control in this assay. The Alamar blue (Invitrogen) assay was used to determine cell viability/proliferation after 3 days of culture. Alamar Blue reagent was added to the growth media in a 1:10 dilution ratio and data was collected using fluorescence at 530-560 nm excitation and 590 nm emission [48].

2.9. Statistical analysis

SPSS 17.0 was used to perform statistical analysis. The Shapiro-Wilk test was use to test for the normality of the data. To test for significant differences between different experimental groups (6mer+HNP-2, 6mer+HNP-4, 6mer+hepcidin, 6mer) one-way ANOVA with a Dunet's T3 post hoc comparison was used. Statistical significance was defined as $p<0.05$.

3. Results

3.1. Cloning and expression of HNP-2, HNP-4 and Hepcidin

The presence of the HNP-2, HNP-4, hepcidin inserts in the cloning vector containing the silk modules was confirmed through DNA sequencing (Tufts Core Facility, Boston, MA). SDS-PAGE and Western blots (Figure V.2) indicated that both expression and purification of 6mer (control), 6mer+HNP-2, 6mer+HNP-4 and 6mer+hepcidin proteins was successful and protein sequencing at Tufts Core Facility, Boston, MA confirmed the N-terminal amino acid sequence for the all three proteins. For 6mer+HNP-2, 6mer+HNP-4, 6mer+hepcidin and 6mer proteins the theoretical molecular weights were approximately 24.6, 25, 24.1 and 21.8kDa, respectively, and

with SDS-PAGE and Western blot assays bands were observed at around 28kDa (Figure V.2). Furthermore, with SDS-PAGE and Western blot the presence of dimers and multimers corresponding to aggregation products of the monomer forms were also observed, together with pre-terminated sequences representing proteins whose expression was incomplete and therefore present a lower molecular weight than the monomeric complete proteins. After purification, dialysis and lyophilization the yield of 6mer+HNP-2, 6mer+HNP-4, 6mer+hepcidin were approximately 12 mg/L for each of the proteins, and for the 6mer control protein the yield was 25 mg/L.

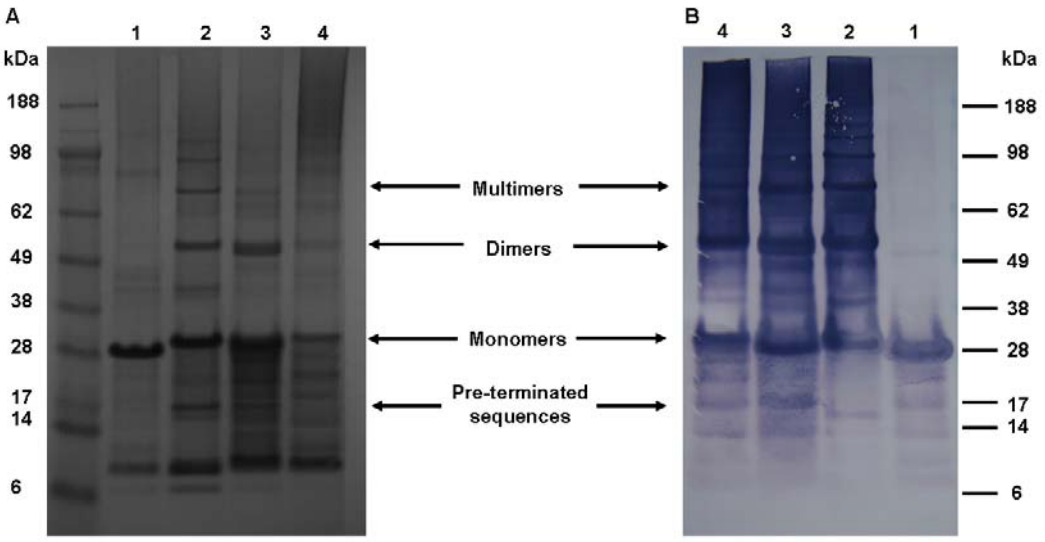

Figure V.2. SDS-PAGE gel stained with colloidal blue (A) and western-blot using anti-histidine antibody (B). 1 - 6mer, 2 - 6mer+hepcidin, 3 - 6mer+HNP-2 and 4 - 6mer+HNP-4.

3.2. Film formation and secondary structure analysis

The ATR-FTIR spectra for the 6mer (control), 6mer+HNP-2, 6mer+HNP-4 and 6mer+hepcidin films, before and after methanol treatment, exhibited strong amide I (1700-1600 cm^{1}) and amide II (1600-1500 cm^{-1}) regions (Figure V.3). Before methanol treatment the ATR-FTIR spectra for 6mer+HNP-2, 6mer+HNP-4, 6mer+hepcidin and 6mer protein films exhibited vibrational modes in the range of 1650-1647 cm^{-1}, amide I region, indicative of helix/random coil conformations. After methanol treatment two peaks appeared, one in the range of 1620-1630 cm^{-1}, amide I region, and another in the range of 1510-1530 cm^{-1}, amide II region. Both peaks were indicative of antiparallel β-sheet structures [43, 49, 50]. Spectra deconvolution revealed the percentage of helix/random coil conformations and of antiparallel β-sheet structures for the

6mer+HNP-2, 6mer+HNP-4, 6mer+hepcidin and for 6mer films before and after methanol treatment (Figure V.3). For all four films an increase of β-sheet content was observed with a corresponding decrease in the helix/random coil conformation after methanol treatment (Figure V.3). The β-sheet content after methanol treatment was similar for all four constructs ranging between 39.8% for 6mer+HNP-2 and 42.8% for 6mer+HNP-4. For the 6mer and the 6mer+hepcidin films the content was 40.8% and 41.9%, respectively.

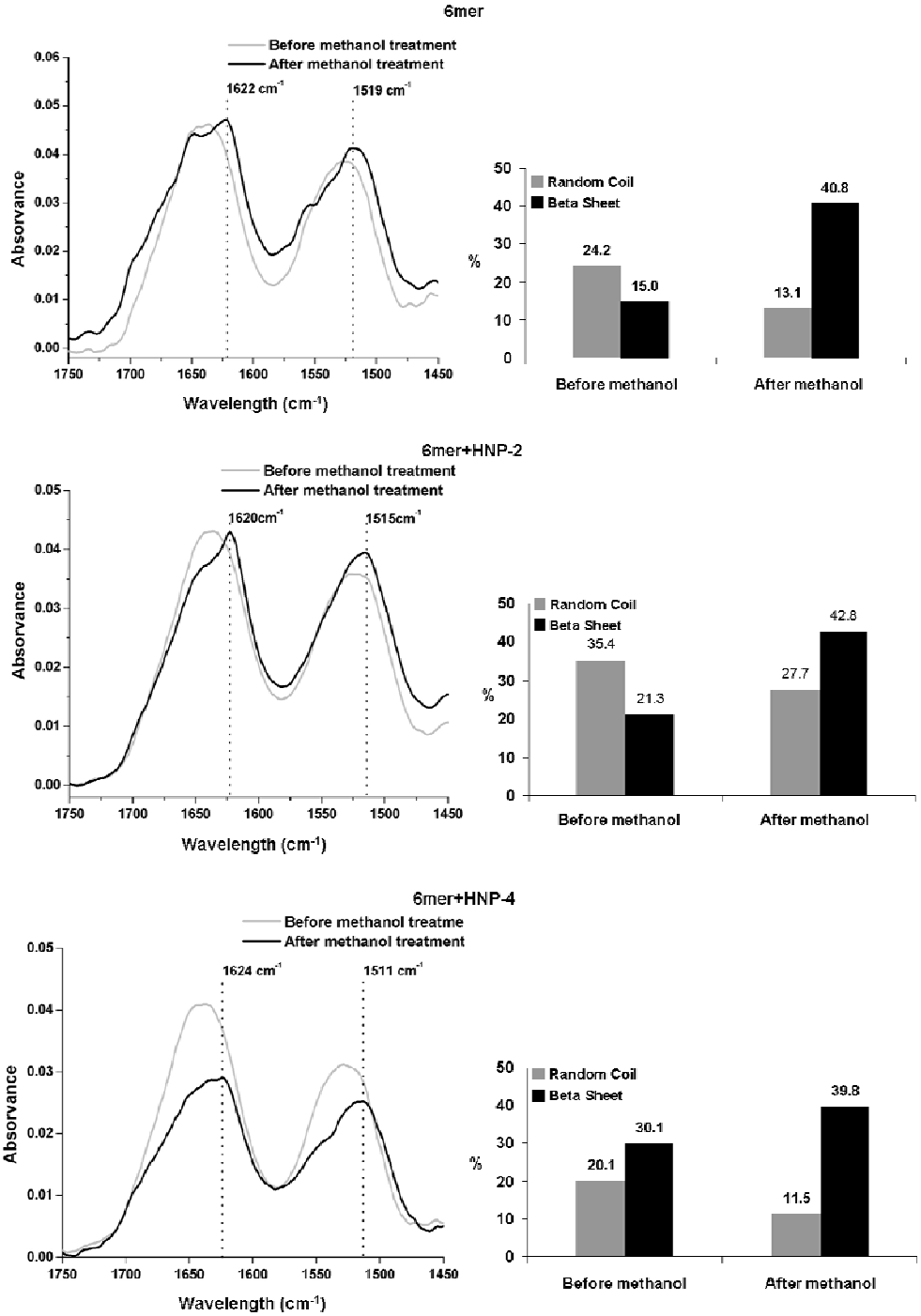

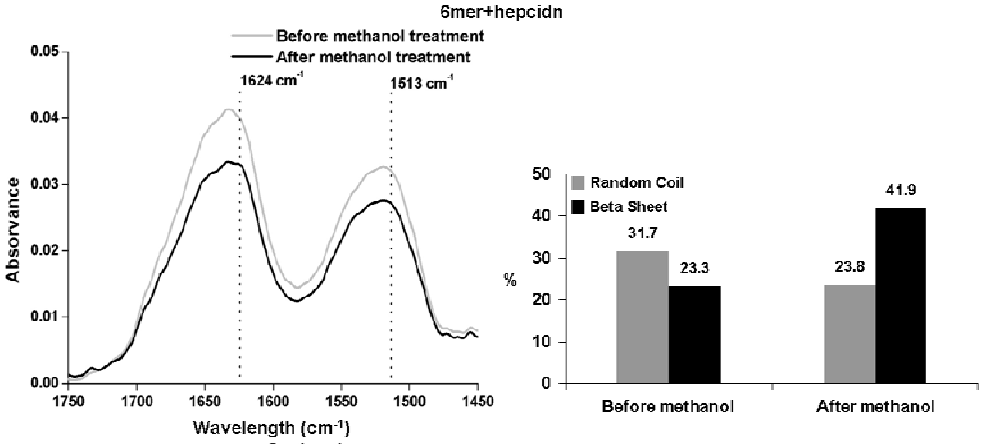

Figure V.3. ATR-FTIR spectra of 6mer, 6mer+HNP-2, 6mer+HNP-4, 6mer+hepcidin films before and after treatment with 70% methanol and respective percentage of β-sheet and random coil/helix conformations after ATR-FTIR spectra deconvolution.

3.3. Antimicrobial activity of 6mer+HNP-2, 6mer+HNP-4 and 6mer+hepcidin proteins

The antimicrobial activity of 6mer+HNP-2, 6mer+HNP-4 and 6mer+hepcidin against the Gram- *E. coli* and the Gram+ *S. aureus* was studied using the radial diffusion assay. The three proteins displayed antimicrobial activity against *E. coli* with the formation of inhibition zones at all three concentrations tested (Figures V.4, V.5). In the case of *E. coli*, 6mer+HNP-4 and 6mer+hepcidin registered higher bactericidal values when compared with the 6mer+HNP-2 peptide. For all three proteins the highest antimicrobial activity was at a concentration of 10 µg/ml ($p<0.05$). Against *S. aureus* there was a decrease in bactericidal activity for all the three peptides when compared to *E. coli*, based on the smaller diameter inhibition zone, especially in the case of the 6mer+hepcidin and 6mer+HNP-2 (Figure V.5). For the proteins tested there was a decrease in the bactericidal activity from 10 to 100 µg/ml ($p<0.05$). The 6mer protein was used as a negative control and no inhibition zones were detected for the three concentrations tested (Figure V.5).

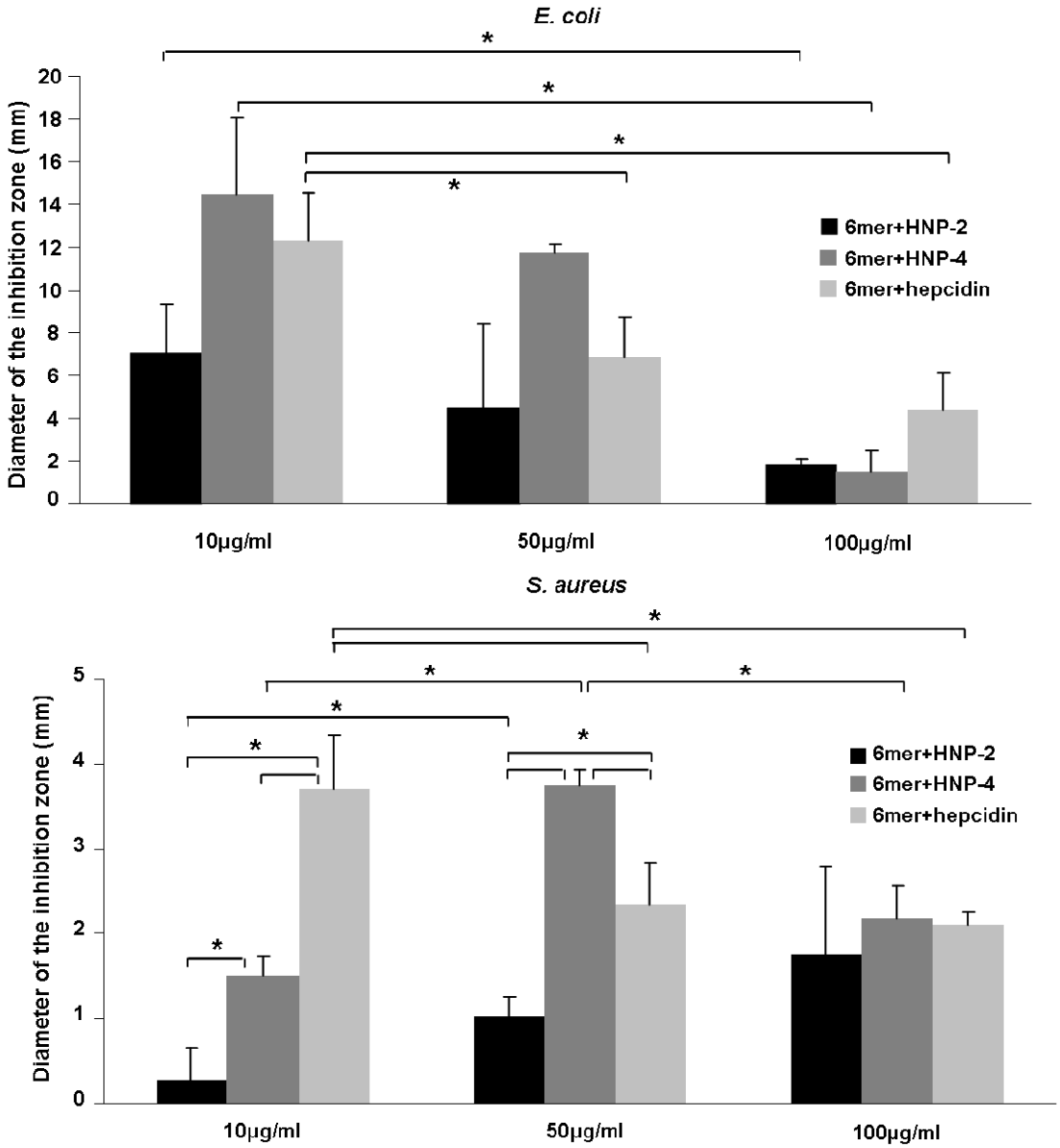

Figure V.4. Graphics representing the antimicrobial activity of 6mer+HNP-2, 6mer+HNP-4 and 6mer+hepcidin using a radial diffusion assay. Recombinant 6mer+HNP-2, 6mer+HNP-4, 6mer+hepcidin proteins were used in concentrations of 10 µg/ml, 50 µg/ml and 100 µg/ml against *E. coli* and *S. aureus*. 6mer was used as control. As mentioned in section 3.4. No inhibitory effect was detected for the 6mer protein and for that reason it was not included in the graphic representation.

6mer against *E. coli*

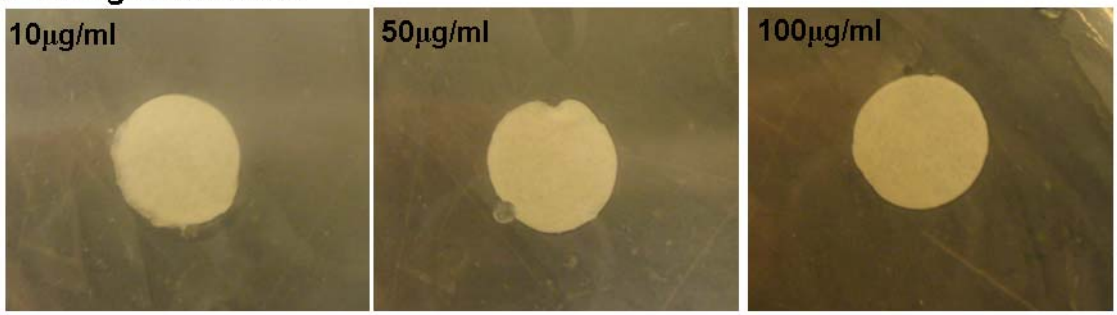

6mer+HNP-2 against *E. coli*

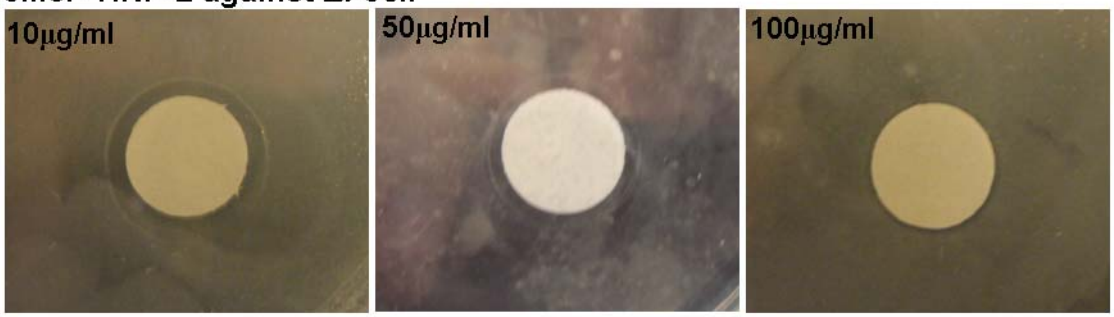

6mer+HNP-4 against *E. coli*

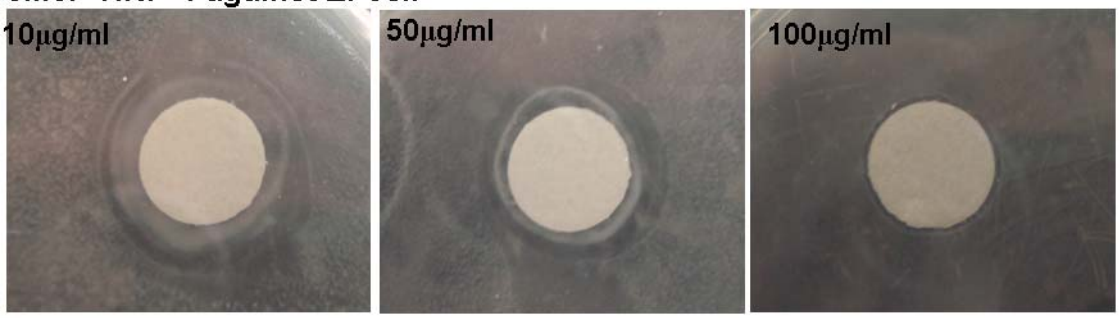

6mer+hepcidin against *E. coli*

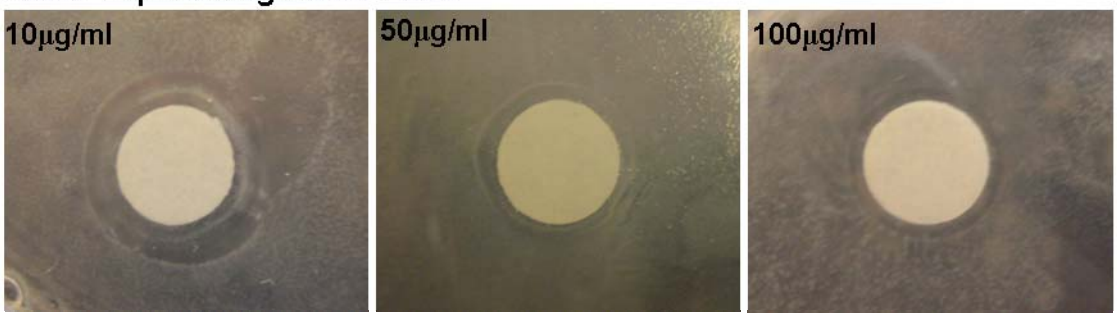

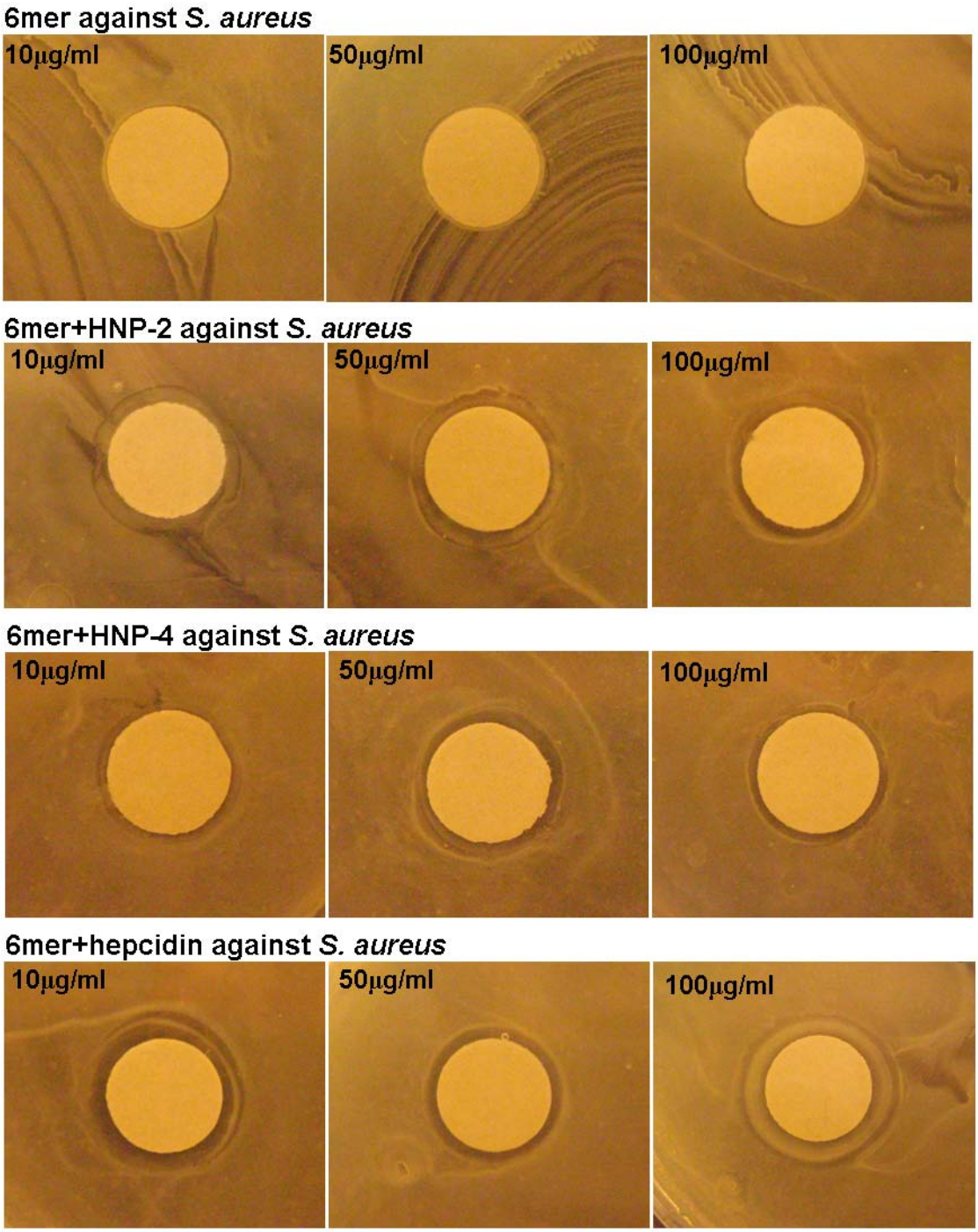

Figure V.5. Images showing the antimicrobial activity of 6mer+HNP-2, 6mer+HNP-4 and 6mer+hepcidin using radial diffusion assay. Recombinant 6mer+HNP-2, 6mer+HNP-4, 6mer+hepcidin proteins were used at concentrations of 10 µg/ml, 50 µg/ml and 100 µg/ml against *E. coli* and *S. aureus*. 6mer was used as control. Discs were 8 mm in diameter.

3.4. Aggregation

For the 6mer, 6mer+HNP-2, 6mer+HNP-4 and 6mer+hepcidin, DLS measurements detected an increase in particle diameter with increasing protein concentration, indicating that aggregation was dependent on protein concentration (Figure V.6). In the case of the 6mer, only one peak was detected for each of the three concentrations measured. In contrast, for 6mer+HNP-2, 6mer+HNP-4 and 6mer+hepcidin two peaks were always detected, except for 6mer+hepcidin at concentration of 100 μg/ml. These data indicated the coexistence of smaller (between 24 and 44 nm) and larger (between 110 and 238 nm) aggregates, the size of which decreased with decreasing protein concentration.

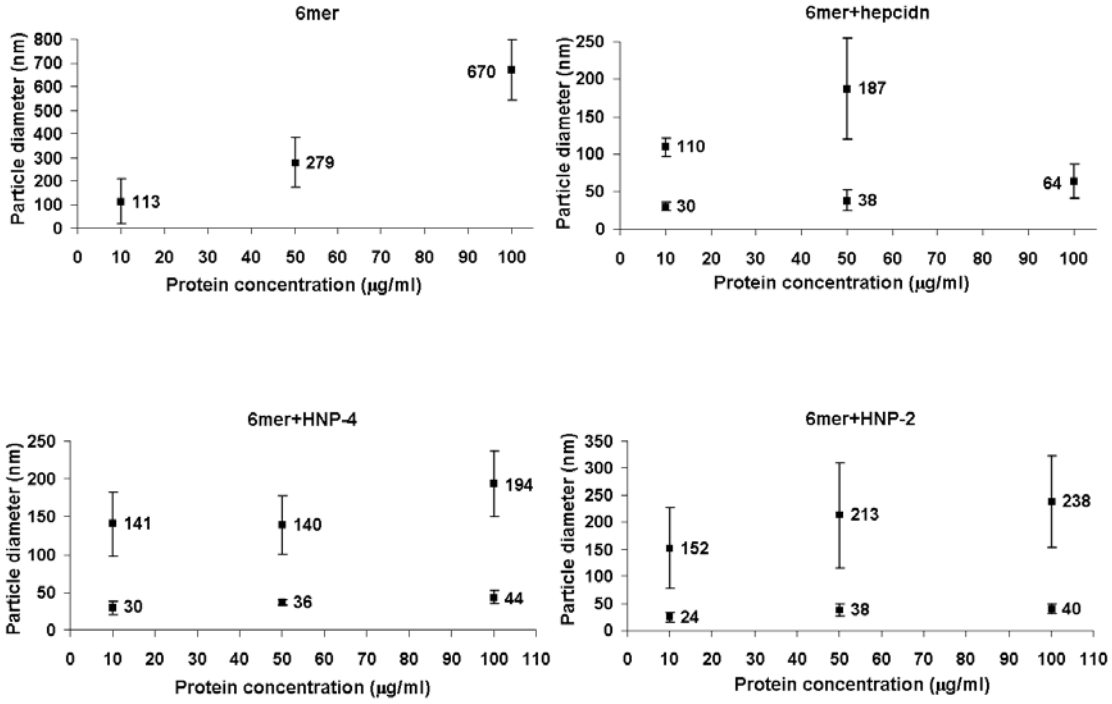

Figure V.6. DLS measures of particle diameter (nm) as a function of protein concentration.

3.5. Circular dichroism spectroscopy

CD spectroscopy was carried out for the four recombinant proteins, 6mer+HNP-2, 6mer+HNP-4, 6mer+hepcidin and 6mer, in phosphate buffer (pH 7.4). The spectra of the 6mer indicated a dominant β-hairpin conformation characterized by a negative ellipticity with a minimum at approximately 203 nm (Figure V.7). In the case of 6mer+HNP-2, 6mer+HNP-4 and 6mer+hepcidin the spectra suggested the presence of both β and α conformations with two minima at 204-208 and 220nm [51-54].

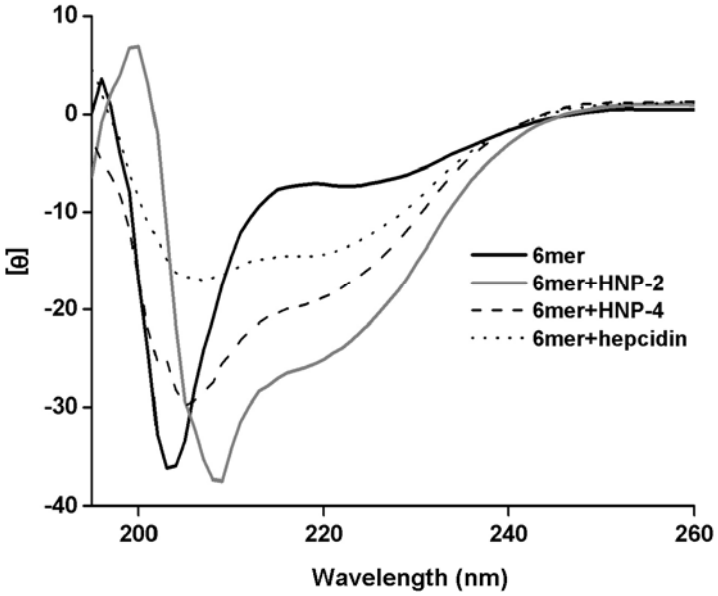

Figure V.7. CD spectra for the recombinant 6mer+HNP-2, 6mer+HNP-4, 6mer+hepcidin and 6mer.

3.6. Cytotoxicity

Cell viability/proliferation with the SaOs-2 cells was measured after 3 days of culture using the Alamar Blue assay. The results indicated that there were no significant differences ($p<0.05$) in cell viability/proliferation between cells cultured on 6mer+HNP-2, 6mer+HNP-4, 6mer+hepcidin and 6mer films. Furthermore, when cell viability/proliferation results (expressed in cell number) for 6mer+HNP-2, 6mer+HNP-4 and 6mer+hepcidin films were compared with the results for the positive control TCP, only the 6mer+HNP-4 films had a cell number significantly lower than TCP, $p<0.05$ (Figure V.8).

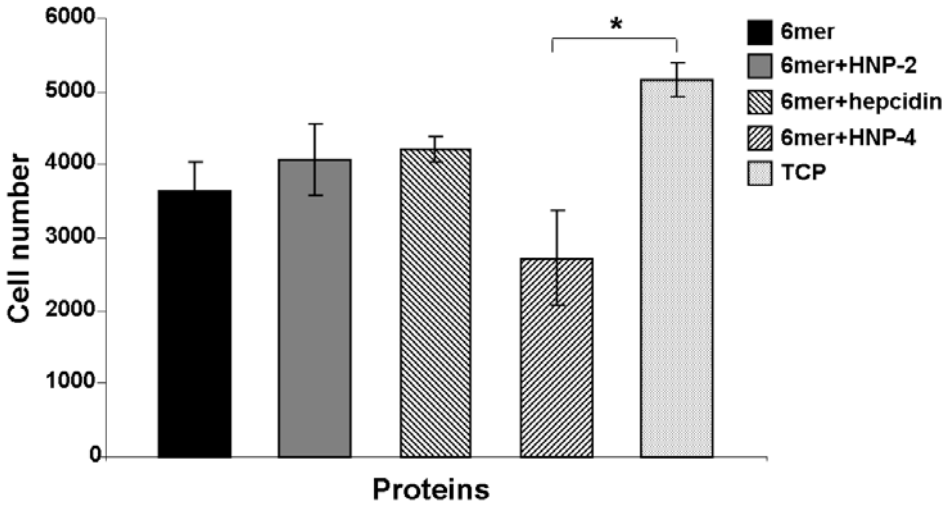

Figure V.8. Alamar blue for cells cultured on 6mer+HNP-2, 6mer+HNP-4, 6mer+hepcidin and 6mer films after 3 days. TCP stands for tissue culture plastic, used as a positive control, and * stands for $p<0.05$.

4. Discussion

The design and successful expression of three new chimeric proteins is presented through the fusion of the consensus repeat for spider silk protein MaSp1 (6mer) with hepcidin, HNP-2 and HNP-4 (Figure V.1). ATR-FTIR was used to confirm the integrity of the 6mer sequence in the three proteins (Figure V.3). The spectra collected for the three new proteins films, 6mer+HNP-2, 6mer+HNP-4 and 6mer+hepcidin, demonstrated the presence of β-sheet, with peaks in 1620-1630 cm^{-1} for amide I region and 1510-1530 cm^{-1} for amide II region [43, 49, 50], after methanol treatment. Furthermore, spectral deconvolution indicated an increase of β-sheet content for 6mer+HNP-2, 6mer+HNP-4 and 6mer+hepcidin, after methanol treatment, reaching values similar to those obtained for the 6mer control (Figure V.3); with 39.8% for 6mer+HNP-2, 40.8% for the 6mer, 42.8% for 6mer+HNP-4 and 41.9% in the case of 6mer+hepcidin. These data demonstrate that the core self-assembling spider silk domain retained function related to the generation of beta sheet crystals in these new fusion systems. This is important for the material performance of these new proteins to attain self-standing material formats, such as the films studied here.

The three new fusion proteins, 6mer+HNP-2, 6mer+HNP-4, 6mer+hepcidin, also retained antimicrobial activity attributed to the inserted motifs HNP-2, HNP-4 and

hepcidin, respectively (Figure V.4 and V.5). Previous studies have demonstrated the efficacy of HNP-2, HNP-4 and hepcidin against different strains of *E. coli* [32]. 6mer+HNP-4 presented the highest antibacterial activity, except for the concentration 100 μg/ml, whereas 6mer+HNP-2 manifested the lowest bactericidal activity. These data support the functional attributes of the antimicrobial component of the fusion proteins, the second critical component of the protein polymer designs, to add to the silk material properties above.

The three proteins had a decrease in their antimicrobial activity against *S. aureus* when compared to *E. coli*. This reduction in activity was also detected previously in the case of hepcidin. Park and co-workers isolated two different hepcidin peptides, hepcidin 20 and hepcidin 25, from human urine and tested their bactericidal activity against different bacterial strains, *E. coli* ML35p and *S. aureus*. Both peptides were antimicrobial against *E. coli* ML35p but showed a reduction in activity against *S. aureus* [32]. Ericksen and colleagues [55] studied the activity of different α-defensins (HNP-1, HNP-2, HNP-3, HNP-4, HD-5 and HD-6) against different bacterial strains and demonstrated that HNP-4 was the most effective against Gram- bacterial strains, one of which was *E. coli* ATCC 25922, the same strain as used in this present study.

Furthermore, in the present work for a concentration of 10 μg/ml the 6mer+hepcidin was more efficient against *S. aureus* than the other two proteins. However, with an increase in the protein concentration from 10 to 50 μg/ml the 6mer+HNP-4 became more effective. For both *E. coli* and *S. aureus* 6mer+HNP-2 proved to be the less bactericidal. Wilde and colleagues [56] compared the antimicrobial activities of HNP-4 and a mixture of HNP-1, HNP-2 and HNP-3 and concluded that HNP-4 was approximately 100-fold more potent against Gram- *E. coli* and about 4-fold more potent against Gram+ *Streptococcus faecalis*. This difference in efficacy may be one of the reasons why human neutrophils produce HNP-1, HNP-2 and HNP-3 at a 60-fold greater abundance when compared with the production of HNP-4 [55, 57]. These results are similar to those obtained in the present work where 6mer+HNP-4 had higher antimicrobial activity when compared with 6mer+HNP-2.

Additionally, in order to facilitate the comparison between the present study and previous studies, using the same antimicrobial domains, the peptide concentrations studied here were kept within the same range of concentrations as

those used previously [55, 56, 58, 59]. However, in the present study and in contrast to what was observed in previous reports, the antimicrobial activity of the new chimeric proteins was not always concentration dependent. The presence of the 6mer silk domain explains this behaviour, since silk proteins are known to aggregate in solution with increased concentration. The 6mer protein, similar to the silk fibroin collected from the silk worm *Bombyx mori*, is rich in hydrophobic amino acids having a high percentage of the hydrophobic amino acids alanine and glycine. The presence of these hydrophobic cores induce the assembly of 6mer+HNP-2, 6mer+HNP-4 and 6mer+hepcidin proteins toward the more thermodynamically stable assembly resulting in a structural reorganization with reduction of exposure of hydrophobic residues [60]. In the case of the silk domains, this stability is achieved by self-assembly or by aggregation. In the present study a relationship between protein concentration and size of the aggregates was found as measured by DLS (Figure V.6). The 6mer registered the highest values of aggregate size for the 50 and 100 μg/ml concentrations with an average of 279 and 670 nm, respectively. The other three proteins, 6mer+HNP-2, 6mer+HNP-4 and 6mer+hepcidin, presented bi-modal distributions of sizes, except for 6mer+hepcidin at a concentration of 100μg/ml. In most cases the aggregate size generated by these proteins was smaller than in the case of the 6mer alone. This fact can be explained by the presence of the antimicrobial domain which increases the number of charged amino acid residues resulting in a reduction of the tendency of these proteins to aggregate by enhancing interactions with the solvent. A previous study where DLS was applied to the dynamic behaviour and the conformational characteristics of *B. mori* silk fibroin demonstrated that this molecule forms large and stable aggregates even in very dilute solutions, supporting the tendency of silk molecules to form aggregates even in dilute conditions [61].

In the present work the decrease in antimicrobial activity of the new chimeric proteins as their concentration in solution increased can be explained by the occurrence of aggregation resulting in larger and more stable aggregates as protein concentration was increased. This interaction leads to a depletion of protein monomers in solution leaving fewer molecules free in solution to act against the bacteria.

CD analyses indicated that in aqueous medium 6mer+HNP-2, 6mer+HNP-4 and 6mer+hepcidin displayed both β-hairpin and α conformations. In the case of the 6mer β-hairpin or β-sheet are the predominant conformations (Figure V.7) [51-54].

For quantitative evaluation of the cytotoxic response to the chimeric proteins, the osteosarcoma cell line SaOs-2 was cultured on 6mer+HNP-2, 6mer+HNP-4 and 6mer+hepcidin films. The 6mer+HNP-2 and 6mer+hepcidin 2% films showed the same ability as TCP to support viable cells ($p>0.05$), while the 6mer+HNP-4 films showed a significant difference ($p<0.05$) from TCP (Figure V.8). No significant difference was observed between TCP and 6mer+HNP-2, 6mer+HNP-4, 6mer+hepcidin and 6mer films. These results indicated that these chimeric proteins, when processed into films, are capable of supporting cell proliferation, and the bactericidal activity does not impact mammalian cell function.

Many drug delivery systems for antibiotics have been described. Hydroxyapatite microspheres can be loaded with an antibiotic and used as a local drug delivery system for the treatment of periodontitis [62], chronic osteomyelitis [63], as just two examples. Nonetheless, hydroxyapatite-carrying systems tend to have a initial burst releasing the entire antibiotic in the first hours [62] and in many cases the antibiotics elute only for a short period of time [64, 65]. This can be problematic if the final purpose is to obtain a more controlled release of the drug through time. In recent studies, different biopolymers have also been tested for potential applications as drug delivery systems. Silk fibroin [66, 67], collagen [68, 69] and hyaluronic acid [70] are examples of natural polymers that have been used as a carrier systems for growth factors, such as bone morphogenetic proteins (BMPs), and antibiotics, in the form of micro-particles, membranes and scaffolds.

Antibiotic-doped biomaterials can be used to address growing concerns with the selection and spreading of multiresistant pathogens [71]. Antimicrobial peptides, as new chemotherapeutic molecules due to their activity against different types of microorganisms, are also important options, including antimicrobial functions as well as immune response [72] and wound repair [16] impacts. However, due to their peptidic nature these biomolecules are more susceptible to proteolytic digestion [73]. Therefore, their combination with a suitable delivery system, such as the one presented in this work, may represent an advantage by decreasing proteolitic digestion

[74] and by allowing for more controlled release of these peptides to prolong effectiveness over time. This more controlled release is important in maintaining regional or localized effects, more precisely at the interface between the implant/host tissues, where bacterial colonization and posterior inflammation development first take place [71].

5. Conclusions

The present study outlines the formation of new silk-based chimeric proteins with antimicrobial potential. Secondary structure analysis, performed by ATR-FTIR, indicated that silk maintains β-sheet formation capability even after adding the antimicrobial domains, HNP-2, HNP-4 and hepcidin. The maintenance of the capacity to form β-sheet is important, since these physical cross-links are responsible for the exceptional mechanical properties, stability and slow degradability of silk. Moreover, activity tests against Gram- and Gram+ organisms showed that the antimicrobial domains present in 6mer+HNP-2, 6mer+HNP-4 and 6mer+hepcidin proteins maintained bactericidal activity. Cytotoxicity/proliferation studies demonstrated that the new proteins were capable of sustaining the proliferation of mammalian cells. These new chimeric proteins suggest a new multifunctional approach to generate biomaterials with useful properties, in this case, control of infections due to the addition of the antimicrobial peptides.

Acknowledgements

The authors acknowledge Olena Rabotyagova for advice in protein sequence design. Sílvia Gomes thanks the Portuguese Foundation for Science and Technology (FCT) for providing her a PhD grant (SFRH/BD/28603/2006). This work was carried out under the scope of the European NoE EXPERTISSUES (NMP3-CT-2004-500283), the FIND & BIND project funded by the agency EU-EC (FP7 program), the FCT R&D project ProteoLight (PTDC/FIS/68517/2006) funded by the FCT agency, the Chimera project (PTDC/EBB-EBI/109093/2008) funded by the FCT agency, the NIH (P41 EB002520) Tissue Engineering Resource Center and the NIH (EB003210 and DE017207).

References

1. Lysaght MJ, Reyes J. The growth of tissue engineering. Tissue Eng 2001;7(5):485-493.

2. Kohna J, Welshb WJ, Knight D. A new approach to the rationale discovery of polymeric biomaterials. Biomaterials 2007;28:4171–4177.

3. Williams DJ, Sebastine IM. Tissue engineering and regenerative medicine: manufacturing challenges. IEE Proc Nanobiotechnol 2005;156(6):207-210.

4. Santos MI, Pashkuleva I, Alves CM, Gomes ME, Fuchs S, Unger RE, et al. Surface-modified 3D starch-based scaffold for improved endothelialization for bone tissue engineering. J Mater Chem 2009;19(24):4091–4101.

5. Santo VE, Frias AM, Carida M, Cancedda R, Gomes ME, Mano JF, et al. Carrageenan-based hydrogels for the controlled delivery of PDGF-BB in bone tissue engineering applications. Biomacromolecules 2009;16(6):1392-1401.

6. Reis RL, Neves NM, Mano JF, Gomes ME, Marques AP, Azevedo HS. Natural-based polymers for biomedical applications: Woodhead Publishing, 2008.

7. Mano JF, Silva GA, Azevedo HS, Malafaya PB, Sousa RA, Silva SS, et al. Natural origin biodegradable systems in tissue engineering and regenerative medicine: present status and some moving trends. J R Soc Interface 2007;4(17):999-1030.

8. Harris LD, Kim B-S, Mooney DJ. Open pore biodegradable matrices formed with gas foaming. J Biomed Mater Res B Appl Biomater 1998;42(3):396 - 402.

9. Suh H. Recent advances in biomaterials. Yonsei Med J 1998;39:87-96.

10. Huang J, Wong C, George A, Kaplan DL. The effect of genetically engineered spider silk-dentin matrix protein 1 chimeric protein on hydroxyapatite nucleation. Biomaterials 2007;28:2358–2367.

11. Yang L, Hedhammar M, Blom T, Leifer K, Johansson J, Habibovic P, et al. Biomimetic calcium phosphate coatings on recombinant spider silk fibres. . Biomed Mater 2010;5(4):1-10.

12. Foo CWP, Patwardhan SV, Belton DJ, Kitchel B, Anastasiades D, Huang J, et al. Novel nanocomposites from spider silk–silica fusion (chimeric) proteins. Proc Natl Acad Sci USA 2006;103(25):9428–9433.

13. Marr AK, Gooderham WJ, Hancock REW. Antibacterial peptides for therapeutic use: obstacles and realistic outlook. Curr Opin Pharmacol 2006;6:468–472.

14. Befus AD, Mowat C, Gilchrist M, Hu J, Solomon S, Bateman A. Neutrophil defensins induce histamine secretion from mast cells: mechanisms of action. J Immunol 1999;163:947-953.

15. Grigat J, Soruri A, UForssmann, Riggert J, Zwirner J. Chemoattraction of macrophages, T lymphocytes, and mast cells is evolutionarily conserved within the human α-defensin family. J Immunol 2007;179(6):3958-3965.

16. Aarbiou J, Verhoosel RM, Wetering Sv, Boer WId, Krieken JHJMv, Litvinov SV, et al. Neutrophil defensins enhance lung epithelial wound closure and mucin gene expression In vitro. Am J Respir Cell Mol Biol 2004;30:193-201.

17. Aarbiou J, Ertmann M, Wetering S, Noort P, Rook D, Rabe KF, et al. Human neutrophil defensins induce lung epithelial cell proliferation in vitro. J Leukoc Biol 2002;72:167-174.

18. Murphy CJ, Foster BA, Mannis MJ, Selsted ME, Reid TW. Defensins are mitogenic for epithelial cells and fibroblasts. J Cell Physiol 1993;155(2):408-413.

19. Chavakis T, Cines DB, Rhee J-S, Liang OD, Schubert U, Hammes H-P, et al. Regulation of neovascularization by human neutrophil peptides (α-defensins): a link between inflammation and angiogenesis. FASEB J 2004;18(11):1306-1308.

20. Bals R. Epithelial antimicrobial peptides in host defense against infection. Respir Res 2000;1:141–150.

21. Schneider JJ, Unholzer A, Schaller M, Schäfer-Korting M, Korting HC. Human defensins. J Mol Med 2005;83:587–595.

22. Smet KD, Contreras R. Human antimicrobial peptides: defensins, cathelicidins and histatins. Biotechnol Lett 2005;27:1337-1347.

23. Selsted ME, Harwig SSL, Ganz T, Schilling JW, Lehrer RI. Primary Structures of Three Human Neutrophil Defensins. J Clin Invest 1985;76:1436-1439.

24. Jones DE, Bevins CL. Paneth cells of the human small intestine express an antimicrobial peptide gene. J Biol Chem 1992;267(15):23216-23225.

25. Pazgier M, Lubkowski J. Expression and purifcation of recombinant human α-defensins in *Escherichia coli*. Protein Expr Purif 2006;49:1–8.

26. Wu Z, Cocchia F, Gentlesa D, Ericksena B, Lubkowskib J, DeVicoa A, et al. Human neutrophil a-defensin 4 inhibits HIV-1 infection in vit. FEBS letters 2005;579:162–166.

27. Krause A, Neitz S, Mägert H, Schulz A, Forssmann W, Schulz-Knappe P, et al. LEAP-1, a novel highly disulfide-bonded human peptide, exhibits antimicrobial activity. FEBS Letters 2000;480:147-150.

28. Park CH, Valore EV, Waring AJ, Ganz T. Hepcidin, a urinary antimicrobial peptide synthesized in the liver. Journal of Biological Chemistry 2001;276(11):7806–7810.

29. Koliaraki V, Marinou M, Samiotaki M, Panayotou G, Pantopoulos K, Mamalaki A. Iron regulatory and bactericidal properties of human recombinant hepcidin expressed in *Pichia pastori*. Biochimie 2008:1-10.

30. Zhang H, Yuan Q, Zhu Y, Ma R. Expression and preparation of recombinant hepcidin in *Escherichia coli*. Protein Expression and Purifcation 2005;41:409–416.

31. F.Wallace D, Jones MD, Pedersen P, Rivas L, Sly LI, Subramaniam VN. Purification and partial characterisation of recombinant human hepcidin. Biochimie 2006;88:31–37.

32. Park CH, Valore EV, Waring AJ, Ganz T. Hepcidin, a urinary antimicrobial peptide synthesized in the liver. J Biol Chem 2001;276(11):7806–7810.

33. Xu M, Lewis RV. Structure of a protein superfiber: Spider dragline silk. Proc Natl Acad Sci USA 1990;87:7120-7124.

34. Scheibel T. Spider silks: recombinant synthesis, assembly, spinning, and engineering of synthetic proteins. Microb Cell Fact 2004;3(1):14-24.

35. Cao Y, Wang B. Biodegradation of silk biomaterials. Int J Mol Sci 2009;10:1514-1524.

36. Guerreiro CIPD, Fontes CMGA, Gama M, Domingues L. Escherichia coli expression and purification of four antimicrobial peptides fused to a family 3 carbohydrate-binding module (CBM) from *Clostridium thermocellum*. Protein Expr Purif 2008;59:161–168.

37. Ramos R, Domingues L, Gama M. *Escherichia coli* expression and purification of LL37 fused to a family III carbohydrate-binding module from *Clostridium thermocellum*. Protein Expr Purif 2010;71:1-7.

38. Haynie SL, Crum GA, Doele BA. Antimicrobial activities of amphiphilic peptides covalently bonded to a water-insoluble resin. Antimicrob Agents Chemother 1995;39(2):301–307.

39. Bagheri M, Beyermann M, Dathe M. Immobilization reduces the activity of surface-bound cationic antimicrobial peptides with no influence upon the activity spectrum. Antimicrob Agents Chemother 2009;53(3):1132–1141.

40. Appendini P, Hotchkiss JH. Surface modification of poly(styrene) by the attachment of an antimicrobial peptide. J Appl Polymer Sci 2001;81(3):609-616.

41. Choa W-M, Joshia BP, Choa H, Lee K-H. Design and synthesis of novel antibacterial peptide-resin conjugates. Bioorg Med Chem Lett 2007;17(21):5772-5776.

42. Gabriel M, Nazmi K, Veerman EC, Amerongen AVN, Zentner A. Preparation of LL-37-grafted titanium surfaces with bactericidal activity. Bioconjug Chem 2006;17(2):548-550.

43. Rabotyagova O, Cebe P, Kaplan DL. Self-assembly of genetically engineered spider silk block copolymers. Biomacromolecules 2009;10:229–236.

44. Huang J, Valluzzi R, Bini E, Vernaglia B, Kaplan DL. Cloning, expression, and assembly of sericin-like protein. J Biol Chem 2003;278(46):46117-46123.

45. Yan S-Z, Beeler JA, Chen Y, Shelton RK, Tang W-J. The regulation of type 7 adenylyl cyclase by Its C1b region and *Escherichia coli* peptidylprolyl isomerase, SlyD. J Biol Chem 2001;276(11):8500-8506.

46. Hu X, Kaplan D, Cebe P. Determining beta-sheet crystallinity in fibrous proteins by thermal analysis and infrared spectroscopy. Macromolecules 2006;39(18):6161-6170.

47. Lehrer RI, Rosenman M, Harwig SSSL, Jackson R, Eisenhauer P. Ultrasensitive assays for endogenous antimicrobial polypeptides. J Immunol Methods 1991;137(2):167-173

48. Lancaster MV, Fields RD, inventors. Antibiotic and cytotoxic drug susceptibility assays using resazurin and poising agents. USA Patent No. 5501959, 1996.

49. Foo CWP, E.Bini, Huang J, Lee SY, Kaplan DL. Solution behavior of synthetic silk peptides and modified recombinant silk proteins. Appl Phys A: Mater Sci Process 2006;82:193–203.

50. Rabotyagova OS, Cebe P, Kaplan DL. Role of polyalanine domains in β-sheet formation in spider silk block copolymers. Macromol Biosci 2010;10:49-59.

51. Varkey J, Nagaraj R. Antibacterial activity of human neutrophil defensin HNP-1 analogs without cysteines. Antimicrob Agents Chemother 2005;49(11):4561–4566.

52. Kelly SM, Jess TJ, Price NC. How to study proteins by circular dichroism. Biochim Biophys Acta 2005;1751:119 – 139.

53. Cerpa R, Cohen FE, Kuntz ID. Conformational switching in designed peptides: the helix/sheet transition. Fold Des 1996;1(2):91-101.

54. Mamdal M, Nagaraj R. Antibacterial activities and conformations of synthetic α-defensin HNP-1 and analogs with one, two and three disulfite bridges. J Pept Res 2002;59:95-104.

55. Ericksen B, Wu Z, Lu W, Lehrer RI. Antibacterial activity and specificity of the six human α-defensins. Antimicrob Agents Chemother 2005;49(1):269–275.

56. Wilde CG, Griffith JE, Marra MN, Snable JL, Scott RW. Purification and characterization of human neutrophil peptide 4, a novel member of the defensin family. J Biol Chem 1989;264(5):11200-11120.

57. Harwig SS, Park AS, Lehrer. RI. Characterization of defensin precursors in mature human neutrophils. Blood 1992;79:1532–1537.

58. Zhang H, Yuan Q, Zhu Y, Ma R. Expression and preparation of recombinant hepcidin in *Escherichia coli*. Protein Expr Purif 2005;41:409–416.

59. Wallace DF, Jones MD, Pedersen P, Rivas L, Sly LI, Subramaniam VN. Purification and partial characterisation of recombinant human hepcidin. Biochimie 2006;88:31–37.

60. Calamai M, Canale C, Relini A, Stefani M, Chiti F, Dobson CM. Reversal of protein aggregation provides evidence for multiple aggregated states. J Mol Biol 2005;346:603–616.

61. Hossain KS, Nemoto N. Dynamic and static light scattering of dilute aqueous solutions of silk fibroin collected from *Bombyx mori* silkworms. Langmuir 1999;15:4114-4119.

62. Ferraz MP, Mateus AY, Sousa JC, Monteiro FJ. Nanohydroxyapatite microspheres as delivery system for antibiotics: Release kinetics, antimicrobial activity, and interaction with osteoblasts. J Biomed Mater Res A 2007;81(4):994-1004.

63. Krisanapiboon A, Buranapanitkit B, Oungbho K. Biocompatability of hydroxyapatite composite as a local drug delivery system. J Orthop Surg 2006;14(3):315-318.

64. Kanellakopoulou K, Giamarellos-Bourboulis EJ. Carrier systems for the local delivery of antibiotics in bone infections. Drugs 2000;59(6):1223-1232.

65. Shinto Y, Uchida A, Korkusuz F, Araki N, Ono K. Calcium hydroxyapatite ceramic used as a delivery system for antibiotics. J Bone Joint Surg 1992;74:600–604.

66. Bessa PC, Balmayor ER, Azevedo HS, Nürnberger S, Casal M, Griensven Mv, et al. Silk fibroin microparticles as carriers for delivery of human recombinant BMPs. Physical characterization and drug release. J Tissue Eng Regen Med 2010;4:349–355.

67. Lia C, Veparia C, Jin H-J, Kim HJ, Kaplan DL. Electrospun silk-BMP-2 scaffolds for bone tissue engineering. Biomaterials 2006;27:3115–3124.

68. Ruszczak Z, Friess W. Collagen as a carrier for on-site delivery of antibacterial drugs. Adv Drug Deliv Rev 2003;55:1679-1698.

69. Schlapp M, Friess W. Collagen/PLGA microparticle composites for local controlled delivery of gentamicin. J Pharm Sci 2003;92(11): 2145-2151.

70. Luo Y, Kirker KR, Prestwich GD. Cross-linked hyaluronic acid hydrogel films: new biomaterials for drug delivery. J Control Release 2000;69:169-184.

71. Campoccia D, Montanaro L, Speziale P, Arciola CR. Antibiotic-loaded biomaterials and the risks for the spread of antibiotic resistance following their prophylactic and therapeutic clinical use. Biomaterials 2010;31:6363-6377.

72. Ganz T. Defensins: antimicrobial peptides of innate immunity. Nature 2003;3:710-720.

73. Bruschi M, Pirri G, Giuliani A, Nicoletto SF, Baster I, Scorciapino MA, et al. Synthesis, characterization, antimicrobial activity and LPS-interaction properties of SB041, a novel dendrimeric peptide with antimicrobial properties. Peptides 2010;31:1459-1467.

74. Numata K, Subramanian B, Currie HA, Kaplan DL. Bioengineered silk protein-based gene delivery systems. Biomaterials 2010;30(29):5775–5784.

Abstract

Auto- and allografts are widely used for the treatment of injured tissues or organs, accounting for 90% of the grafts used, despite significant drawbacks. Bone healing treatments would benefit from the development of biodegradable, osteoinductive, biocompatible and mechanically strong biomaterials. Recombinant 6mer+BSP protein, combining six repeats of the consensus sequence for *Nephila clavipes* dragline (6mer) and bone sialoprotein sequence (BSP), has shown good support for cell viability and induced the nucleation of hydroxyapatite and tricalcium phosphate during osteoblast *in vitro* culture. The present study was conducted to further characterize this bioengineered protein-based biomaterial for *in vivo* behaviour related to biocompatibility. Films formed from the recombinant protein were implanted in subcutaneous pouches in the back of mice and responses were evaluated at 2 and 6 weeks by flow cytometry analysis and histology. For flow cytometry analysis five different surface markers, CD14, CD3, CD25, CD8 and CD4, were selected to assess the number and type of immune cells present at the implant site, and later were compared with histology. The results obtained for the 6mer+BSP films were compared with controls of 6mer (silk films alone), poly-lactic-glycolic-acid (PLGA) films, and empty implant sites. The results showed no major differences between the inflammatory responses induced by 6mer+BSP films and the responses observed for the controls. Therefore, this new chimeric protein could represent an alternative for bone regeneration applications when considering the outcome from the inflammatory reaction and the prior *in vitro* cell studies.

1. Introduction

Advances in genetic and metabolic engineering have provided a route for the development of new custom-design biopolymers with potential for future fabrication of high-value medical devices [1]. Genetic engineering has proven to be a particularly useful tool for the design, cloning and expression of protein polymers and block copolymers with repetitive amino acid sequences [2, 3]. This is the case of silk, a natural biopolymer with a highly repetitive amino acid sequence [4]. Natural spider silk proteins have a molecular weight ranging from 70 to 700 kDa [4] and an amino acid

sequence characterized by repeats formed by hydrophobic poly-alanine (poly-A) motifs alternating with hydrophilic GGX (glycine-glycine-X) domains [5]. The alignment of the poly-A motifs, to form beta sheet physical cross-linked crystalline domains in the silk materials is responsible for strength. The GGX domains form amorphous regions and are responsible for the more flexible features of silk fibers [6]. The organization of these motifs leads to the formation of functionalized silk biomaterials with mechanical and biological characteristics which make silk one of the most remarkable fibers found in nature, combining durability, exceptional strength and toughness. These special mechanical features allied to its biocompatibility and biodegradability make of silk a biomaterial of interest for tissue engineering applications [4].

However, the large-scale production of spider silk is challenging due to the cannibalistic behaviour of spiders and the relatively low levels of silk production, when compared with *Bombyx mori* silkworm silk. The silkworm silk can be produced at a large scale through sericulture [4]. Therefore, genetic engineering has been explored in order to overcome the drawbacks with spider silks via cloning and expression of spider silk-like proteins [4]. Furthermore, genetic engineering also provides the opportunity to tailor biopolymer chemistry with biologically active motifs such as morphogens, cytokines and other extracellular matrix elements. For example, the RGD cell binding peptide sequence was fused with recombinant spider silk to improve cell responses of silk films [7]. Other chimeric proteins were also synthesized through the fusion of *Nephila clavipes* spider silk consensus sequences for major ampullate dragline silk I (MaSpI) with human dentin matrix protein 1 [8], and with silaffin-derived R5 peptide from *Cylindrotheca fusiformis* [9], to induce and control the deposition of calcium phosphates and silica particles, respectively. In this way, these new bioengineering strategies become powerful tools in the study of protein structure and function and also in the design of new biomaterials with tunable nanoscale features [4], providing a path forward for the fabrication of more complex and matrix-like scaffolds capable of controlling cell adhesion, migration and differentiation [7].

These bioengineered protein scaffolds mimic the extracellular matrix and have been suggested as future alternatives to decellularized extracellular matrix that has been used for different therapeutic applications but carries a risk of disease

transmission and immune response [10]. The extracellular matrix is a highly complex structure formed by different biopolymers such as collagens, fibrin and elastins which form part of the core architecture to direct cellular activities [11]. Besides its structural function, the extracellular matrix provides a reservoir of biologically active molecules. In the case of bone, elements responsible for the maintenance, remodelling and formation of new bone tissue are entrained in the matrix [12]. For instance, bone sialoprotein (BSP), a highly phosphorylated and glycosylated protein expressed by newly formed osteoblasts, is mostly found in mineralized connective tissues [13]. BSP is one of the main non-collagenous components of bone and is a member of the SIBLING (small integrin-binding ligand, N-linked glycoprotein) family together with osteopontin, dentin matrix protein 1, dentin sialophosphoprotein and matrix extracellular phosphoglycoprotein [14].

As the other members of the SIBLING family, BSP displays a tripeptide RGD motif that mediates cell adhesion [15] and is secreted into the extracellular matrix of mineralizing bone and dentin tissues [16]. During the first stages of mineralization the BSP acts as a nucleator for the deposition of apatite crystals on the collagen matrix. This nucleation ability is probably related to the presence of two poly-glutamic domains in the BSP amino acid sequence [17]. These findings are supported by the detection of labelled BSP in the hole zones between collagen fibers [18], a region where the deposition of hydroxyapatite crystals first occurs in growing bone [19, 20], highlighting the possible role of this protein in the mineralization process. Besides its interaction with hydroxyapatite, BSP also interacts with other binding partners such as collagen [21] and different cells types, inducing the attachment and migration of endothelial cells [22], adhesion and differentiation of osteoblasts [23] and stimulating osteoclast activity involved in bone remodelling [24]. Due to these features, previous studies described the incorporation of BSP into collagen [25, 26] and titanium [22] implants and the *in vivo* results showed an increase in osteoblast differentiation and proliferation and enhancement of osteoinductive effects.

More recently we expressed BSP together with six repeats of the consensus sequence for the spider dragline MaSpI [22]. This new chimeric protein was named 6mer+BSP (Figure VI.1). Infrared analysis showed that the presence of the BSP domain

did not interfere with the ability of the silk to self-assembly to form β-sheets. The incubation of 6mer+BSP films with a mineralizing solution showed the deposition of calcium phosphates (CaP) indicating that the BSP maintained its aptitude as a nucleator of CaP. Furthermore, human mesenchymal stem cells differentiated into osteoblasts with good expression of collagen I, BSP and alkaline phosphatase, and CaP deposits were formed on the films with a Ca/P ration of around 1.7 after 14 days of cell culture. These results prompted the present study in order to evaluate the *in vivo* behaviour of this new chimeric protein 6mer+BSP. Additionally, understanding the biological reactions taking place during foreign body reaction and accessing the extent and duration of this reaction is crucial for the development of high performance medical devices [27].

SGRGGLGGQGAGAAAAAGGAGQGGYGGLGSQGTSGRGGLGG
QGAGAAAAAGGAGQGGYGGLGSQGTSGRGGLGGQGAGAAAA
AGGAGQGGYGGLGSQGTSGRGGLGGQGAGAAAAAGGAGQGG
YGGLGSQGTSGRGGLGGQGAGAAAAAGGAGQGGYGGLGSQG
TSGRGGLGGQGAGAAAAAGGAGQGGYGGLGSQGTS WPSR
PT MKTALILLSILGMACAFSMKNLHRRVKIEDSEENGVFKYRP
RYYLYKHAYFYPHLKRFPVQGSSDSSEENGDDSSEEEEEEEET
SNEGENNEESNEDEDSEAENTTLSATTLGYGEDATPGTGYTGL
AAIQLPKKAGDITNKATKEKESDEEEEEEEEGNENEESEAEVDE
NEQGINGTSTNSTEAENGNGSSGGDNGEEGEEESVTGANAEG
TTETGGQGKGTSKTTTSPNGGFEPTTPPQVYRTTSPPFGKTTT
VEYEGEYEYTGVNEYDNGYEIYESENGEPRGDNYRAYEDEYSY
FKGQGYDGYDGQNYYHH QGLMGH

Figure VI.1. Amino acid sequence for the 6mer+BSP chimeric protein. The 6mer silk domain is highlighted in black and the BSP domain in gray. Linkers for the insertion of the BSP domain are underlined.

As mentioned above, BSP has a RGD cell binding domain capable of interacting with osteoblasts and osteoclasts and also with the integrin receptors of macrophages, and therefore increase the attachment of these and other cell types [28]. In a recent study, the attachment of macrophages (human promonocytic THP-1 cells) to an interpenetrating polymer network coating functionalized with a peptide sequence from rat bone sialoprotein containing the RGD motif [bsp-15(RGD)] and found that the presence of this peptide sequence promoted monocyte attachment when compared to the non-modified coating [28]. These findings underlie the importance of inflammation studies in the improvement of implant performance.

In the present study early inflammatory responses elicited by 6mer+BSP films after subcutaneous implantation in mice in comparison with controls, 6mer films, poly-

lactic-glycolic-acid - PLGA films, were assessed. PLGA is a synthetic polymer with good biocompatibility and biodegradability [29] and was approved by the Food and Drug Administration (FDA) for use in sutures, bone plates and drug delivery systems [30], reasons why it was selected as one of the controls in this study. The inflammatory responses were evaluated after 2 and 6 weeks of grafting by histology and flow cytometry analysis.

2. Materials and Methods

2.1. Design of synthetic coding sequence for 6mer and 6mer+BSP protein

Our prior studies described the cloning process for the 6mer [2, 7] and 6mer+BSP [31] coding sequences. Briefly, for the 6mer sequence the repeating unit is based on the consensus sequence (SGRGGLGGQGAGAAAAAGGAGQGGYGGLGSQGT) inspired by the back translation of the native sequence of MaSpI [2]. A cloning cassette linker was inserted in a pET30a+ vector (Novagen, San Diego, CA) and the resulting plasmid was designated pET30L. After, the pET30L vector was used for the insertion of the oligomers coding for spider silk block sequence repeats. In this study, a silk block copolymer with six repeating units was used, referred to as 6mer [2]. The 6mer block copolymer was cloned with six histidine residues for purification. The coding sequence for the BSP domain was extracted from a clone containing the bacterial plasmid pENTR223.1 carrying the human BSP cDNA sequence (Clone Identification: HsCD00082642). This clone was purchased from the Harvard clone collection "The ORFeome Collaboration" (Dana-Farber/Harvard Cancer Center, Boston MA). After growing in Luria Bertani (LB) medium pENTR223.1 plasmid was extracted with Qiagen miniprep kit (28704, Valencia, CA, USA). BSP cDNA sequence was extracted from the vector by digestion with *SfiI* (R0123S, New England Biolabs, Ipswich, MA, USA). The digestion product was later run in 0.8% agarose gels and a 951 bp band corresponding to BSP cDNA was purified with a QIAquick gel extraction kit (28706, Qiagen). For the ligation of BSP sequence to the silk block copolymer sequence, a linker carrying a restriction site for *Sfi*I and for *Spe*I (R0133S, New England Biolabs) and *Nhe*I (R0131S, New England Biolabs), related to the spider silk clone, was designed. After double digestion with *Spe*I and *Nhe*I restriction enzymes the linker was inserted into the

linearized vector pET30L, previously digested and dephosphorylated with *Spe*I and CPI (Alkaline Phosphatase, Calf Intestinal enzyme, New England Biolabs, M0290S), respectively. The BSP sequence was finally inserted by digesting the vector pET30L+linker with *Sfi*I enzyme followed by dephosphorylation with CPI. The ligation reaction was carried out with T4 DNA ligase (M0202S, New England Biolabs). The ligation product was used to transform *E. coli* DH5α cells (18258-012, Invitrogen, Carlsbad, CA, USA) and positive clones were identified by incubation on agar plates containing 25 μg/ml kanamycin (K1876, Sigma, St. Louis, MO, USA). The presence of the BSP insert was confirmed by DNA sequencing (Tufts Core Facility, Boston, MA) and the new constructs were named 6mer+BSP.

2.2. Protein expression and purification

Both spider silk block copolymer 6mer and 6mer+BSP encoding sequences were expressed as described previously [31] in a *E. coli* RY-3041 strain, a mutant strain of *E. coli* BLR (DE3) defective in the expression of SlyD protein [8, 32]. Cells were cultivated at 37ºC in Hyper Broth™ (Athens Enzyme Systems 0107-S), with 25 μg/ml kanamycin (Sigma, K1876) until an OD_{600} between 0.9 and 1 was reached. After, isopropyl β-D-thiogalactoside (IPTG, Invitrogen, 15529019) was added to the media at a concentration of 0.5mM to induce expression during 2 hours at 37ºC. Cells were harvested by centrifugation at 6500 rpm and cell pellet was lysed under denaturating conditions using a buffer solution of 100 mM NaH_2PO_4, 10mM Tris HCl, 8 M urea (pH 8.0). After overnight incubation insoluble cell debris were excluded from the mixture by centrifugation and the supernatant was collected, mixed with Ni-NTA resin (Qiagen, 30250) and left for 2 hours with stirring. The mixture was then loaded into a glass Econo-column (Biorad, Hercules, CA, USA) and washed several times with denaturating buffer at pH 8 and at pH 6.0. 6mer and 6mer+BSP proteins were eluted with denaturating buffer at pH 4.5. The purified proteins were then dialysed first against a 20 mM CH_3COONa buffer followed by dialysis against water using cellulose ester snake skin membranes with a 100-500 Da molecular weight cutting off (131054, Spectra/Por Biotech, Rancho Dominguez, CA, USA). After extensive dialysis, protein solutions were lyophilized. Protein size and purity were assessed through sodium dodecyl sulphate-

polyacrylamide gel electrophoresis (SDS-PAGE) and protein sequencing (Tufts Core Facility, Boston, MA) was used to confirm protein identity. For SDS-PAGE, gels (Invitrogen, NP0321BOX) were stained with a colloidal blue kit (Invitrogen, LC6025).

2.3. Film preparation

Recombinant 6mer+BSP and 6mer proteins were dissolved in Milli-Q water to a final concentration of 4% (w/v). Afterwards, 60 µl of each protein solution was cast onto a non adherent polystyrene surface and left to dry at room temperature. The films obtained were treated with 90% methanol (v/v) for 30 minutes to induce the transition of secondary structure from random coil to β-sheet. Films were left to dry for three days. This treatment produces films with improved mechanical properties and more resistant to dissolution in water or other aqueous environments such as culture media.

For sterilization, 6mer+BSP and 6mer films were immersed in 70% ethanol (v/v) solution for 2 hours and left to dry at room temperature. Before implantation each side of 6mer+BSP and 6mer films was treated for 15 minutes with ultraviolet (UV) light. ATR-FTIR (Jasco Inc., MD, USA, model FT/IR-6200) analysis was used to check if the UV treatment interfered wtih the secondary conformation of the proteins and the perecentage of β-sheet was assessed through spectral deconvolution.

PLGA with a molecular weight between 40-75kDa (P2191, Sigma) was dissolved in dichloromethane in a 1:15 ratio and 60 µl of this solution was cast onto a polystyrene surface and left to dry at least for 2 days to form films. Films were treated with 70% ethanol (v/v) solution and with UV for 15 minutes for sterilization.

Before in vivo studies, the films were hydrated with sterile PBS and after hydration their diameter was around 8 mm.

2.4. Animal procedures

All procedures were conducted under animal care protocols approved by Tufts Institutional Animal Care and Use Committee. All animals used in this study were five to seven weeks old balb/c female mice (Charles River breeding labs). A total of 40 mice were used in the experiment, distributed by four experimental groups each with two

time points, 2 and 6 weeks. The mice were randomly assign to the four experimental groups and only one sample was implanted in each mouse for a total of five mice per tested group: 6mer, 6mer+BSP, PLGA and a control group subjected to the same surgical procedures as the implanted groups but with no sample implanted.

Animals were maintained under general anesthesia with an isoflurane and oxygen delivery mask. Mice were positioned in ventral recumbency and their backs were aseptically prepared for surgery. Under anesthesia, a part of the dorsal back was shaved with an electric razor and disinfected with ethanol 70% (v/v). After, a longitudinal 1 cm length incision was performed with fine scissors and the hydrated sample was implanted into a void space created with the help of a scissors in the subcutaneous area between skin and muscle layer. After insertion the skin incision was closed with a surgical suture line and again disinfected with a Betadine solution.

The healing process at the incision region was coarse monitored during all study period and no deaths were registered during the experiment.

To check for inflammatory responses, mice were euthanized by cervical dislocation after 2 and 6 weeks post-implantation and samples explanted along with the overlying tissue for histological examination and flow cytometry analysis.

2.5. Cell Isolation and flow cytometry analysis

The protocol for cell isolation was adapted from Montanaro and co-workers [33]. The tissue surrounding the graft and overlying skin was used for cell extraction. When present, subcutaneous fat and muscle tissues were removed by scraping. The cleaned skin was minced with the help of fine scissors and digested for 2 hours, at 37ºC, in 5 ml mixture solution of 2 mg/ml collagenase IV (Invitrogen, 17104019) and 1.2 units/ml dispase (Invitrogen, 17105041) in PBS. After digestion the mixture was centrifuged at 1500 rpm for five minutes at 4ºC and the pellet was resuspended at a density of 10^6cells/ml in PBS supplemented with 0.5% bovine serum albumin (BSA), flow cytometry buffer. The suspension solution was filtered with a cell strainer with 100 µm pores to eliminate non-digested tissues and the cell suspension was collected in a 50 ml falcon flask and centrifuged at 1500 rpm for five minutes at 4ºC. To remove the red blood cells the pellet was resuspended in lysis buffer (NaCl 137 mM, Na_2HPO_4 8

mM, KH_2PO_4 1.46 mM, KCl 2.68 mM, in distilled water, pH 7.0) and incubated at room temperature for four to five minutes with occasional shaking. The lysis reaction was stopped by diluting the lysis buffer with 20 to 30 ml of PBS. Cells were spun down at 1500 rpm for five minutes at 4ºC followed by two washes with flow cytometry buffer. For antibody staining, cells pellets were resuspended in PBS, incubated for 15 minutes on ice in the presence of rat anti-mouse FcRII/III (clone 2.4G2, 553141, BD Pharmingen, San Jose, CA, USA) antibody, to block non-antigen-specific binding of immunoglobulins to Fc receptors. After washing and centrifugation the pellet was again resuspended on PBS. Finally, for cell surface marker antigen analysis approximately 50 µl of cell suspension were incubated for 30 minutes on ice with the secondary antibodies described in Table VI.1.

After incubation, samples were centrifuged at 1700 rpm for five minutes at 4ºC, washed twice with flow cytometry buffer and suspended in 200 to 300 µl of flow cytometry buffer with 5 mM ethylenediaminetetraacetic acid (EDTA, Sigma, 431788), to protect cells until further analysis. For live/dead discrimination 5 µl of 7-amino-actinomycin D (7-AAD, BD Pharmingen, 559925) was added to each sample. Cells were analyzed by a four-color FACSCalibur instrument (Becton Dickinson, NJ, USA) equipped with a 488 nm argon-ion laser and a 635 nm red diode laser and data was processed using FlowJo analysis software (Tree Star, Inc., OR, USA).

Table VI.1. Secondary antibodies used for cell labelling.

Secondary antibody	**Target cells**
Fluorescein isothiocyanate (FITC) conjugated rat anti-mouse monoclonal antibody CD3 (BD Pharmingen, 555274)	Thymocytes and mature T lymphocytes [34, 35]
Allophycocyanine (APC) rat anti-mouse polyclonal antibody CD25 (BD Pharmingen, 558643)	T and B lymphocytes [36, 37]
Alexa-conjugated rat anti-mouse monoclonal antibody CD4 (BD Pharmingen, 557667)	T helper (T_H) cells, immunosuppressive regulatory T cells and natural killer T (NK-T) cells [38, 39]
Alexa-conjugated rat anti-mouse monoclonal antibody CD8 (BD Pharmingen, 557668)	T suppressor/cytotoxfic cells [39, 40]
Phycoerythrin (PE) conjugated rat anti-mouse monoclonal antibody CD14 (BD Pharmingen, 557740)	Cells expressing CD14, a receptor for the complex formed by lipopolysaccharide (LPS) and a LPS binding protein present in plasma [41]

2.6. Histology

Histological sections were examined to assess the extent of film degradation and to look for local inflammatory responses at the implant-host interface, such as for neovascularisation, fibrosis and the presence of inflammatory cells. After collection, samples were immediately immersed in buffered 4% formalin solution in PBS and sent for processing at the Tufts Animal Pathology Core Lab (Boston, MA, USA) where samples were embedded in paraffin, cut into 10 µm sections and stained with hematoxylin and eosin (H&E). Additionally, sectioned samples were stained with Alizarin and Von Kossa dyes for detection of calcium deposits.

2.7. Statistical Analysis

SPSS 17.0 was used to perform statistical analysis. The Shapiro-Wilk test was use to test for the normality of the data. To test for significant differences between different experimental groups (6mer+BSP, 6mer, PLGA) one-way ANOVA with a Dunet's T3 post hoc comparison was used. Statistical significance was defined as $p<0.05$.

3. Results

3.1. SDS-PAGE and protein analysis

SDS-PAGE analysis showed the presence of two large broad bands, one at around 28 kDa for the 6mer (theoretical molecular weight of 21.8k Da) and another around 48 kDa for 6mer+BSP protein (theoretical molecular weight of 52 kDa). Lower molecular weight bands were observed for both proteins and correspond to pre-terminated products. Dimers are also present in the case of 6mer+BSP protein (Figure VI.2). Sequencing analysis of the bands of interest confirmed the N-terminal sequence for both 6mer and 6mer+BSP.

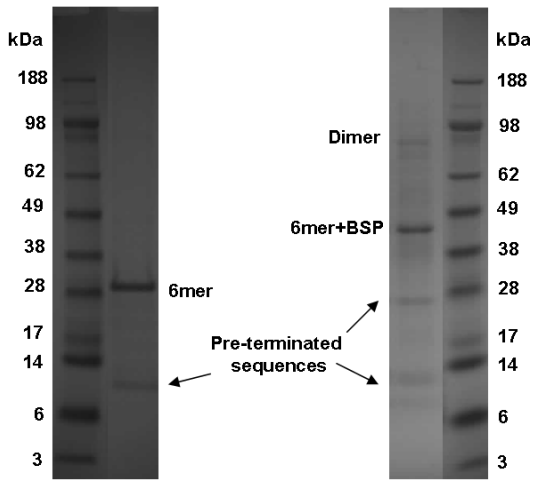

Figure VI.2. SDS-PAGE for the 6mer and 6mer+BSP proteins. Both gels were stained with colloidal blue.

3.2. Secondary structure analysis

According to the ATR-FTIR spectra, the UV treatment resulted in no apparent differences between treated and untreated protein films. As mentioned above, the β-sheet percentage was assessed through spectra deconvolution (Figure VI.3). In the case of the 6mer films the percentage of β-sheet conformation was 25% for the untreated films and 24% for the treated films. For 6mer+BSP films these percentages were around 26% for untreated films and 24% for irradiated films. Statistical comparison shows no significant difference ($p>0.05$) between treated and untreated films.

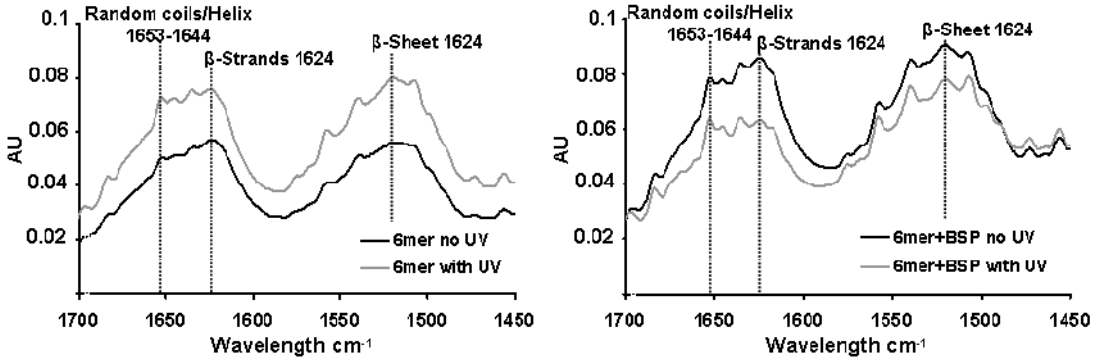

Figure VI.3. ATR-FTIR spectra for the 6mer and 6mer+BSP films before and after UV irradiation.

3.3. Comparison of surface markers on 6mer, 6mer+BSP, PLGA and control explants

No atypical animal or tissue responses were detected during coarse examination of the animals and grafts at the time of their retrieval.

The expression of CD14, CD25, CD8, CD3 and CD4 surface markers was analysed for the cells extracted from the tissue surrounding the 6mer, 6mer+BSP and PLGA films and the empty control (Figure VI.4 and VI.5). After 2 weeks flow cytometry analysis revealed two distinct cell populations for all samples: a population marked in gray, referring to a population of cells that do not express the markers listed above, and a second population of cells, marked in black, expressing the antigens of interest as it can be seen in Figure VI.4. The percentage of a side population of positive cells for each of the antigens studied was assessed by comparison to a control sample stained only with a primary antibody (Figure VI.5). The values obtained were used for statistical comparison. For the grafts explanted after 2 weeks the marker CD4 showed the highest fluorescence intensity with values of around 67.7%, 60.5%, 60.6% and 77.7% for 6mer, 6mer+BSP, PLGA and empty control, respectively (Figure VI.5). The lowest fluorescence intensity was observed for the CD3 antigen with values ranging between 12.4% and 6.8% for 6mer and empty control, respectively (Figure VI.5). Based in these results, after 2 weeks the expression patterns for the different surface markers was similar for the different implants and also for the empty control. Statistical analysis only found significant differences ($p<0.05$) for the CD25 marker, between the empty control and 6mer+BSP, and for the CD4 antigen, between the empty control and the PLGA.

After 6 weeks, flow cytometry analysis revealed an increase in the expression of most surface markers, and mainly in the case of CD25. At 6 weeks the CD4 marker registered the highest fluorescence intensity with average values of 51.5%, 70.6%, 69.9% and 71.7% for the 6mer, 6mer+BSP, PLGA and empty control, respectively, similarly to the results obtained at 2 weeks (Figure VI.5). For the CD25 the values were also high, ranging between 54.6 and 74.9% for the 6mer and 6mer+BSP, respectively. Also, as in the case of the 2 weeks explants, the CD3 showed the lowest marker intensity (Figure VI.5).

Statistical comparisons between time points at 2 and 6 weeks for the same samples showed a significant ($p<0.05$) increase in expression of CD3 and CD14 surface markers for PLGA samples. For CD25 this increment in expression from 2 to 6 weeks was also detected for the 6mer, 6mer+BSP and PLGA samples.

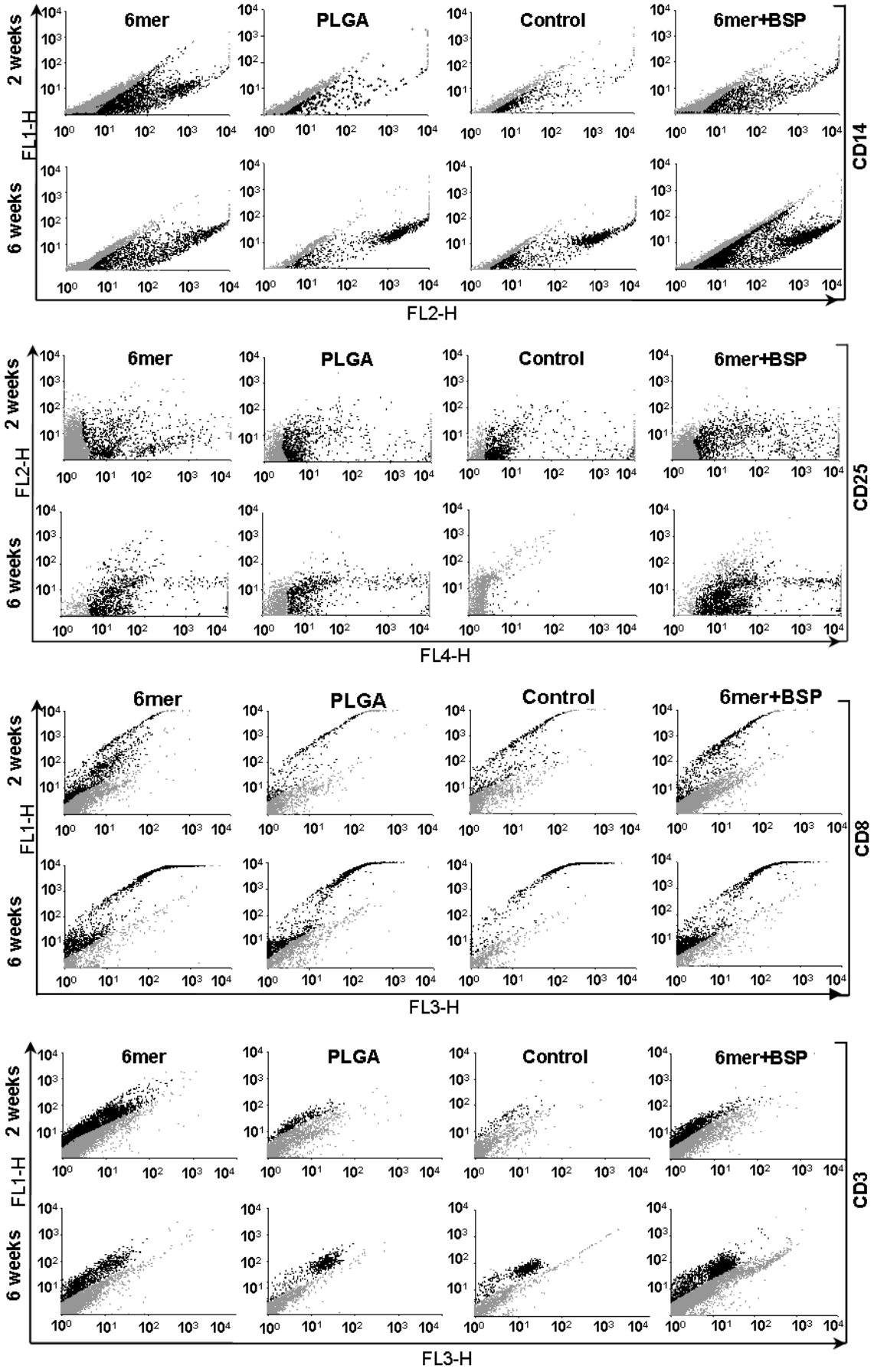
6mer
PLGA
Control
6mer+BSP
2 weeks
6 weeks
FL1-H
FL2-H
CD14
FL4-H
CD25
FL3-H
CD8
CD3

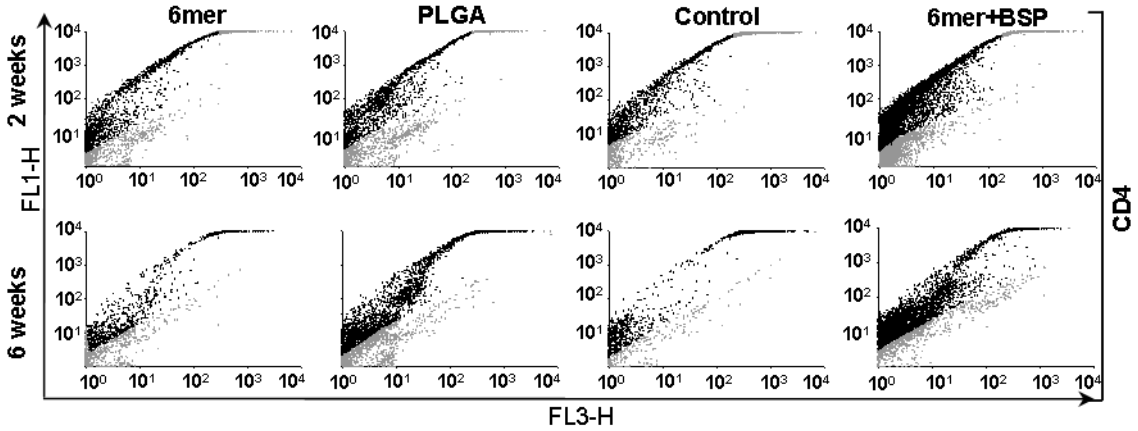

Figure VI.4. Flow cytometry profiles for CD14, CD25, CD8, CD3 and CD4 antigens after 2 and 6 weeks.

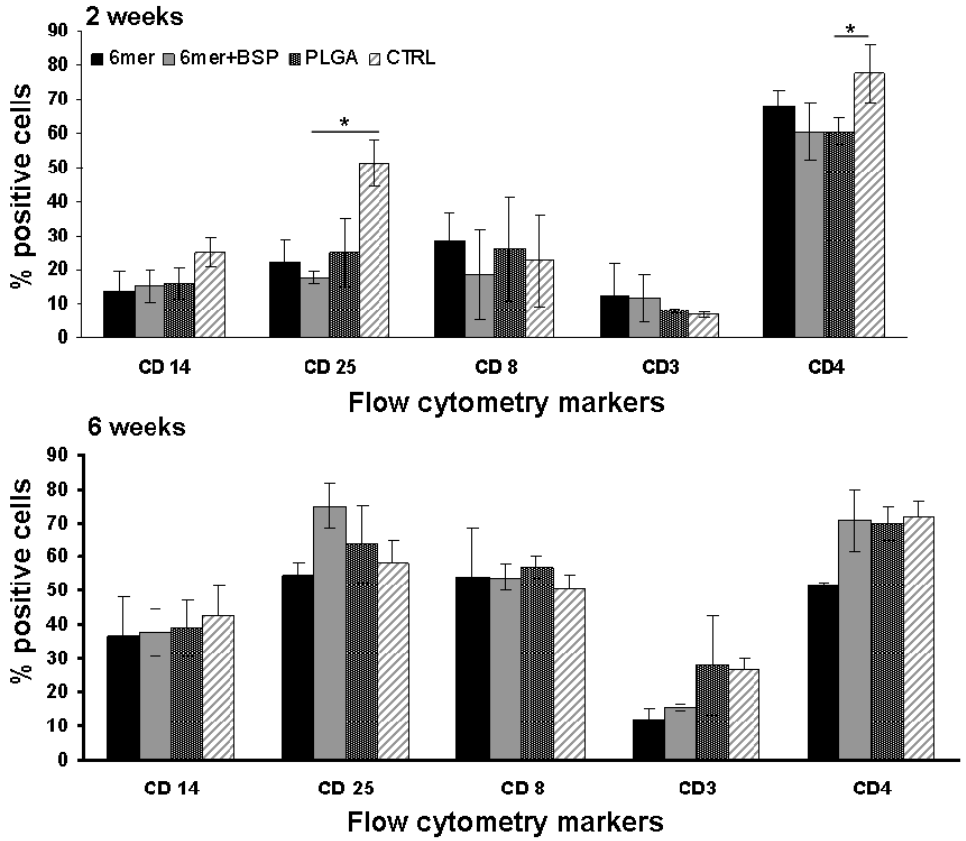

Figure VI.5. Graphic representation of the percentage of positive cells detected by flow cytometry based on the surface markers.

3.4. Histology

After 2 weeks of implantation H&E staining showed the presence of an acute inflammation response with inflammatory cells present in all of the implanted films and in the surrounding tissues, a process consistent with a mild inflammatory response

(Figure VI.6). After 6 weeks implantation, H&E staining showed a decrease in the inflammatory response for the 6mer and 6mer+BSP films, with less inflammatory cells being detected on the films and in the tissues adjacent to the implants. In the case of the PLGA films there were fewer inflammatory cells in the overlying tissue and a higher number of inflammatory cells infiltrated into the biomaterial. For all three types of films no encapsulation response was detected at the interface between the implant and the host tissue (Figure VI.6).

In the case of empty controls after 2 and 6 weeks fewer inflammatory cells were observed when compared with the implanted films. Vascularisation was observed in the three types of films and also in the empty controls, however few vessels were present and there were no major differences between the four experimental conditions.

Alizarin red and Von Kossa were used to detect calcium deposits in the tissue sections. Von Kossa detected calcium after 6 weeks in the 6mer+BSP films (Figure VI.7), while Alizarin red staining did not detect mineralization (data not shown). In the case of the empty controls and PLGA films, no deposits were detected after 2 and 6 weeks. For the 6mer films a few small deposits were present after 2 and 6 weeks however none of them had formed directly on the implanted silk (Figure VI.7).

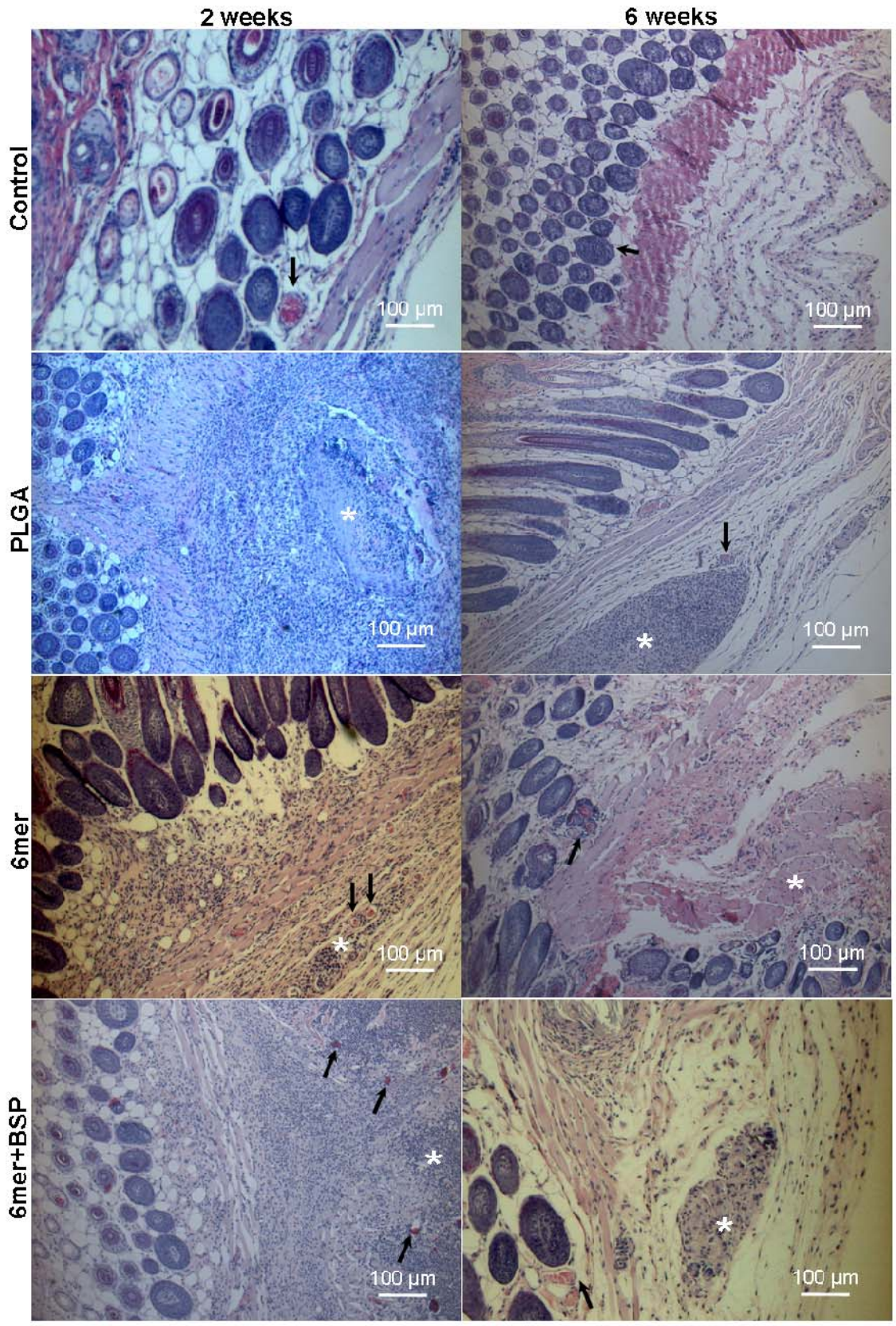

Figure VI.6. Host inflammatory response after 2 and 6 weeks after staining with hematoxylin and eosin (H&E). Images were obtained at 10x magnification. *marks the implant. Black arrow indicates blood vessel.

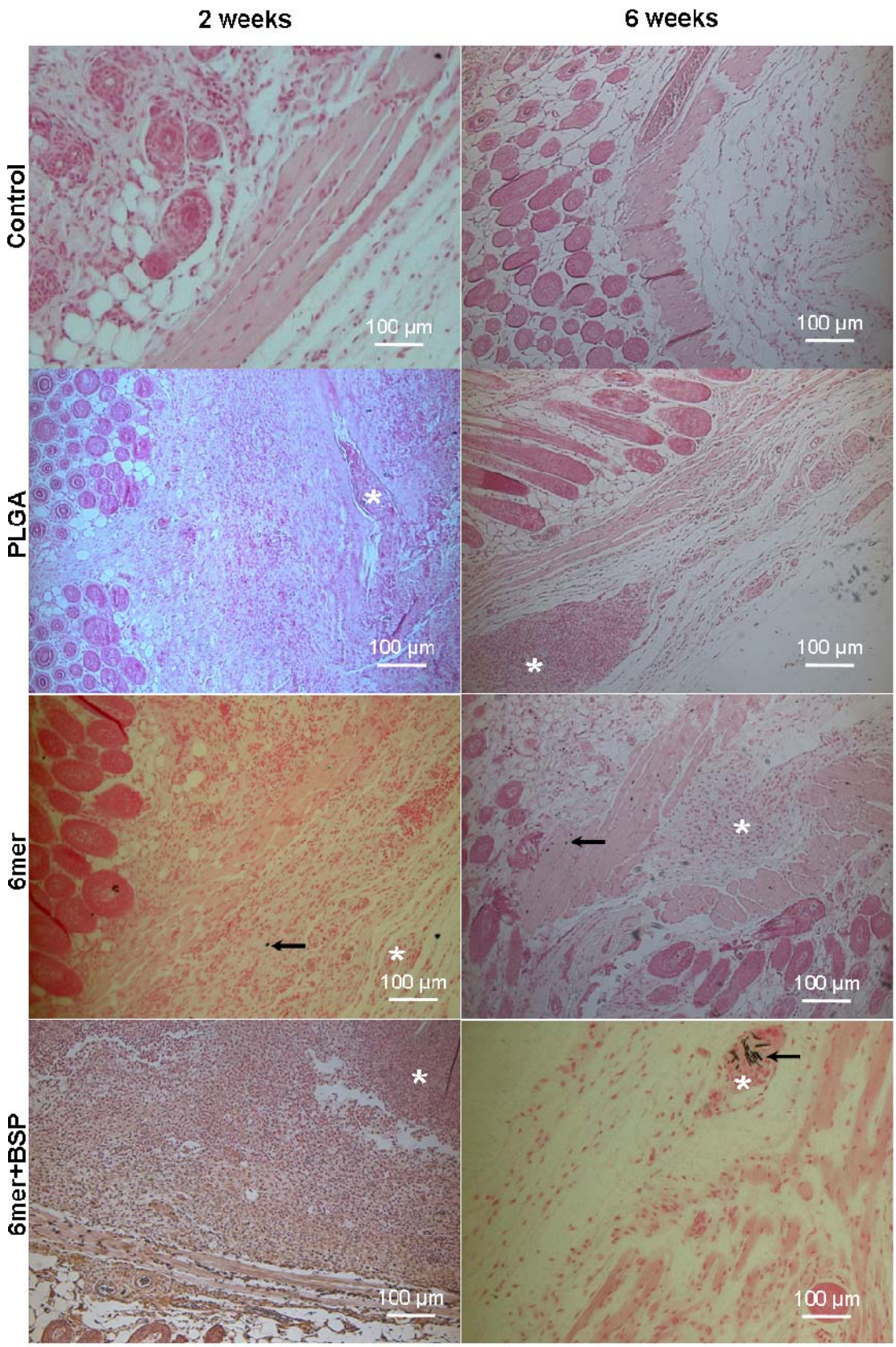

Figure VI.7. Histological analysis with von Kossa staining for the detection of calcium deposits. Images were obtained at 10x magnification. *marks the implant. Black arrow indicates calcium deposits.

4. Discussion

Since implantation initiates a wound-healing process through an inflammation response, the goal of the present study was to evaluate the *in vivo* response to a new chimeric protein, 6mer+BSP. This bioengineered protein was described in our previous study with promising results towards osteogenic outcomes in vitro [31]. The present report describes the subcutaneous implantation of the 6mer+BSP films and compares their inflammatory response with the reactions against control films, the genetically engineered spider-like silk alone (6mer) and PLGA films, as well as empty implant sites.

With implantation of a biomaterial the host engages a number of foreign body responses such as the adhesion of monocytes, macrophage differentiation and fusion to form foreign body giant cells [42]. In this study, flow cytometry and histology analysis were selected to follow these responses and the different aspects of tissue-material interactions, such as the number and type of immune cells at the implantation site as well the presence of a capsule surrounding the implant. For flow cytometry analysis CD14, CD4, CD3, CD25 and CD8 surface markers were selected. For 2 and 6 weeks time points CD4 was the marker showing the highest fluorescence intensity. CD4 marker is expressed by some groups of lymphocytes such as T helper and T immunosuppressive cells and natural killer cells. T helper cells activate and direct other immune cells through the secretion of cytokines and chemokines [42]. Additionally, CD8 and CD25 were also used to assess the presence for other types of lymphocytes mainly cytotoxic T cells and B lymphocytes, respectively. For both markers there was an increase in expression from 2 to 6 weeks of implantation. However this increment was only significant for CD25 marker for the 6mer, 6mer+BSP and PLGA films. Lymphocytes are important cells for the immune system response to foreign bodies. CD8 expressing cells are designated as cytotoxic T cells and are capable of directly killing target cells [43] and B lymphocytes contribute to the immune response through the production of antibodies [44]. Besides their broad spectra of functions during the immune process, lymphocytes also enhance macrophage adhesion to the biomaterial surface and induce the activation and fusion of these cells [45]. Additionally, lymphocytes adhere directly to the surface of biomaterials, affected by the surface chemistry of the materials [46, 47]. In this way, lymphocytes can be

considered important cells when addressing the inflammatory cell response to implanted materials. In the present study flow cytometry results for CD4 and CD25 markers after 2 weeks showed significant differences ($p<0.05$) between the 6mer+BSP and control with no implant, and between PLGA and the control with no implant. For 2 and 6 weeks no significant differences were detected between 6mer+BSP and PLGA films.

Furthermore, the presence of CD14 positive cells at the implantation site was also detected. CD14 marker is expressed by monocytes, macrophages and to a less extent by granulocytes. Since these cells constitute the first line of defence against foreign bodies they are the first to react after biomaterial implantation, either in soft or hard tissues. In the specific case of macrophages they are involved in both inflammation and foreign body responses as essential components in tissue regeneration through the recruitment and regulation of proliferation and differentiation of fibroblasts, osteoblasts and endothelial cells in the healing phase [48]. Additionally, macrophages mediate biomaterial degradation and resorption through phagocytosis or extracellular digestion [48]. In the case of the 6mer+BSP, flow cytometry analysis showed the presence of macrophages, however no significant differences were detected when comparing mice grafted with the 6mer+BSP films and mice implanted with the 6mer, PLGA or with no implant.

The flow cytometry results are in accordance with the observations from histology which showed the presence of immune cells in the implant region and in the surrounding host tissue with no major differences between the 6mer, PLGA and 6mer+BSP films. Finally, the expression of CD3 marker was also quantified by flow cytometry S analysis. This marker shows the lowest expression values when compared with the other markers, and as in the case of CD8 and CD14, there were no significant differences between experimental conditions.

The different types of immune cells described above are considered some of the key elements in directing and regulating host immune response to foreign bodies such as implanted biomaterials. The flow cytometry and histology results reveal no major differences between the immune responses observed in mice with no implants, where a post surgical healing process was taking place, and the mice implanted with

the different types of films, mainly the 6mer+BSP, 6mer and PLGA. Since there were no significant differences between the control with no implant and the implanted animals we can assume that the host immune response to the implanted materials is mild or low and restricted to a local reaction.

As mentioned above, after the implantation of a biomaterial the host body engages a foreign body reaction. The magnitude and duration of this reaction are two important features since they have a direct impact in the biomaterial stability and biocompatibility, dictating its efficacy as a future medical device [49]. So, understanding the biological reactions taking place during foreign body reaction is crucial for the development of high performance medical devices [27]. The early stages following biomaterial implantation are characterized by the formation of a thrombus/blood clot at the material-tissue interface. This thrombus/blood clot is a protein matrix formed by adsorbed proteins such as albumin, fibrinogen, fibronectin and vitronectin. These proteins form a cell recognition system due to the cell binding motifs present in their sequences which makes them able to interact with the adhesion receptors expressed by immune cells [50, 51]. The presence of an RGD triplet has been confirmed for many extracellular matrix proteins such as fibrinogen, fibronectin and vitronectin. Additionally, some cell membrane receptors expressed by different types of cells are capable of interacting with these RGD binding domains [49]. For instance, macrophages are cells capable of complexation with these RGD domains through their integrin $\alpha_1\beta_5$ and $\alpha_{IIb}\beta_3$ receptors [52]. RGD has been widely used to functionalize biomaterials with the purpose to improve their ability to induce cell biding. However, this approach can have drawbacks due to the redundancies existing between receptors and binding proteins [49]. As mentioned earlier, BSP has an RGD cell binding domain at the carboxy terminal region, which in the case of the 6mer+BSP protein films could induce and amplify the binding reaction of macrophages leading to a harsher inflammatory reaction. However, as mentioned above no major differences were observed between the inflammatory reactions to the 6mer+BSP and to the other implanted materials or even to the control with no implant. Further, the silk component of the bioengineered protein is void of such specific binding sites.

Few studies have used BSP for biomaterial functionalization. O'Toole and co-workers first described the use of BSP for enhancing bone-implant adherence [53]. BSP was used to coat titanium implants which were later implanted into rat femora. Results demonstrated that BSP coated implants had osteoinductive properties [53]. Later, Hilbig and colleagues tested and compared the efficiency of BSP-, collagen- and fibronectin-coated and noncoated implant materials for the development of adult human maxillar bone [54]. The authors observed higher cell survival in the case of the implants coated with BSP when compared with collagen-coated implants [54]. Recently to promote integration of implants into host tissue, BSP was used to coat the surface of titanium samples and its efficiency was compared with implants coated with collagen I or hydroxyapatite (TICER®) [22]. After three days in *in vitro* culture BSP-precoated implants showed uniformly distributed cells whereas the collagen pre-coated implants induced an irregular distribution of cells. Furthermore, when compared with collagen-coated implants, BSP-coated implants displayed superior osteoinductive performance as revealed by osteocalcin and osteonectin expression [22]. Besides metal implants, collagen was also used as a delivery matrix for BSP in rat calvarial defects and thoracic subcutaneous pouches. Results showed that in calvarial defects, BSP-collagen but not collagen alone induced mineral deposition after four to five days, followed by osteoblast differentiation and the formation of new bone [25].

These previous studies reporting the use of BSP for implant functionalization show promising results, both *in vivo* and *in vitro*. In the present *in vivo* study, good results were also obtained with the development of a mild to low inflammatory response to the 6mer+BSP implanted films with no apparent differences from the controls. Also, when compared with the implants described by these previous studies cited above, the 6mer+BSP has the advantage of being a chimeric protein combining the properties of BSP and silk. As mentioned before BSP has the ability to induce the deposition of calcium phosphate. In the present study Von kossa staining indicated the presence of calcium deposits for the 6mer+BSP films implanted after 6 weeks. The existence of these deposits are likely due to the BSP domain in the 6mer+BSP chimeric protein, since the deposits observed for 6mer control films were not formed directly on the implant surface but instead in the surrounding host tissue. However, these

findings and the potential for 6mer+BSP to be used in bone repair need to be confirmed with future *in vivo* studies to assess the ability of 6mer+BSP to induce osteoregeneration of critically sized bone defects. Finally, besides the BSP domain the presence of the spider silk domain can be advantageous due to its mechanical properties as well as its facility to be processed into fibers [55], films [56], porous matrices [57] and hydrogels [58].

5. Conclusions

In this study, we address the host inflammatory response to 6mer+BSP films implanted in mice. Flow cytometry and histology results show no differences between the inflammatory reaction to the 6mer+BSP samples and the responses observed for the controls including the silk film (6mer), PLGA films and the controls with no implant. The 6mer+BSP bioengineered proteins represents a promising protein-based biomaterial for future tissue engineering applications for bone regeneration. Furthermore, the results also highlight the potential of biotechnology approaches in the development of new multifunctional biomaterials as 6mer+BSP, an example of a multifunctional protein combining in one protein the mechanical properties and processability of silk and the function of BSP to interact with cells and collagen through its RGD and collagen binding regions, respectively, and to act as a calcium phosphate nucleator.

Acknowledgements

The authors thank Doctor Tírcia Santos for her advice in this paper. Sílvia Gomes thanks the Portuguese Foundation for Science and Technology (FCT) for providing her a PhD grant (SFRH/BD/28603/2006). This work was carried out under the scope of the European NoE EXPERTISSUES (NMP3-CT-2004-500283), the FIND & BIND project funded by the agency EU-EC (FP7 program), the FCT R&D project ProteoLight (PTDC/FIS/68517/2006) funded by the FCT agency, the Chimera project (PTDC/EBB-EBI/109093/2008) funded by the FCT agency, the NIH (P41 EB002520) Tissue Engineering Resource Center and the NIH (EB003210 and DE017207).

References

1. Yadav V, Paniliatis BJ, Shi H, Lee K, Cebe P, Kaplan DL. Novel *in vivo*-degradable cellulose-chitin copolymer from metabolically engineered *Gluconacetobacter xylinus*. Appl Environ Microbiol 2010;76(18):6257-6265.

2. Rabotyagova O, Cebe P, Kaplan DL. Self-assembly of genetically engineered spider silk block copolymers. Biomacromolecules 2009;10:229–236.

3. Sallach RE, Cui W, Wen J, Martinez A, Conticello VP, Chaikof EL. Elastin-mimetic protein polymers capable of physical and chemical crosslinking Biomaterials 2009;30(3):409-422

4. Altman GH, Diaz F, Jakuba C, Calabro T, Horan RL, Chen J, et al. Silk-based biomaterials. Biomaterials 2003;24(3):401-416

5. Vollrath F, Porter D. Spider silk as a model biomaterial Applied Physics A: Materials Science & Processing 2006;82(2):205-212.

6. Spiess K, Lammel A, Scheibel T. Recombinant spider silk proteins for applications in biomaterial. Macromol Biosci 2010;10(9):998-1007.

7. Bini E, Foo CWP, Huang J, Karageorgiou V, Kitchel B, Kaplan DL. RGD-functionalized bioengineered spider dragline silk biomaterial. Biomacromolecules 2006;7:3139-3145.

8. Huang J, Wong C, George A, Kaplan DL. The effect of genetically engineered spider silk-dentin matrix protein 1 chimeric protein on hydroxyapatite nucleation. Biomaterials 2007;28:2358–2367.

9. Mieszawska AJ, Nadkarni LD, Perry CC, Kaplan DL. Nanoscale control of silica particle formation via silk−silica fusion proteins for bone regeneration. Chem Mater 2010;22(20):5780-5785.

10. Wenk E, Murphy AR, Kaplan DL, Meinel L, Merkle HP, Uebersax L. The use of sulfonated silk fibroin derivatives to control binding, delivery and potency of FGF-2 in tissue regeneration Biomaterials 2010;31(6):1403-1413.

11. Rodgers UR, S.Weiss A. Integrin αvβ3 binds a unique non-RGD site near the C-terminus of human tropoelastin. Biochimie 2004;86:173-178.

12. Benesch J, Mano JF, Reis. RL. Proteins and their peptide motifs in acellular apatite mineralization of scaffolds for tissue engineering. Tissue Eng Part B 2008;14(4):433-445.

13. Ganss B, Kim RH, Sodek J. Bone sialoprotein. Crit Rev Oral Biol Med 1999;10(1):79-98.

14. Fisher LW, Torchia DA, Fohr B, Young MF, Fedarko NS. Flexible structures of SIBLING proteins, bone sialoprotein, and osteopontin. Biochem Biophys Res Commun 2001;280:460–465.

15. Qin C, Baba O, Butler WT. Post-translational modifications of sibling proteins and their roles in osteogenesis and dentinogenesis. Crit Rev Oral Biol med 2004;15(3):126-136.

16. Qin C, Brunn JC, Jones J, George A, Ramachandran A, Gorski JP, et al. A comparative study of sialic acid-rich proteins in rat bone and dentin. Eur J Oral Sci 2001;109(2):133-141.

17. Hunter GK, Goldberg HA. Modulation of crystal formation by bone phosphoproteins: role of glutamic acid-rich sequences in the nucleation of hydroxyapatite by bone sialoprotein. Biochem J 1994;15(302):175-179.

18. Fujisawa R, Nodasaka Y, Kuboki Y. Further characterization of interaction between bone sialoprotein (BSP) and collagen. Calcif Tissue Int 1995;56(2):140-144.

19. Traub W, Arad T, Weiner S. Three-dimensional ordered distribution of crystals in turkey tendon collagen fibers. PNAS 1989;86:9822-9826.

20. Weiner S, Traub W. Bone structure: from angstroms to microns. FASEB J 1992;6(3):879-885.

21. Tye CE, Hunter GK, Goldberg HA. Identification of the type I collagen-binding domain of bone sialoprotein and characterization of the mechanisms of interaction. J Biol Chem 2005;280(14):13487-13492.

22. Graf H-L, Stoeva S, Armbruster FP, Neuhaus J, Hilbig H. Effect of bone sialoprotein and collagen coating on cell attachment to TICER and pure titanium implant surfaces. Int J Oral Maxillofac Surg 2008;37(7):634-640.

23. Mizuno M, Imai T, Fujisawa R, Tani H, Kuboki Y. Bone sialoprotein (BSP) is a crucial factor for the expression of osteoblastic phenotypes of bone marrow cells cultured on type I collagen matrix. Calcif Tissue Int 2000;66:388-396.

24. Valverde P, Zhang J, Fix A, Zhu J, Ma W, Tu Q, et al. Overexpression of bone sialoprotein leads to an uncoupling of bone formation and bone resorption in mice. J Bone Miner Res 2008;23(11):1775-1778.

25. Wang J, Zhou H-Y, Salih E, Xu L, Wunderlich L, Gu X, et al. Site-specific in vivo calcification and osteogenesis stimulated by bone sialoprotein. Calcif Tissue Int 2006;79:179-189.

26. Xu L, Anderson AL, Lu Q, Wang J. Role of fibrillar structure of collagenous carrier in bone sialoprotein-mediated matrix mineralization and osteoblast differentiation. Biomaterials 2007;28(4):750–761.

27. Ward WK. A review of the foreign-body response to subcutaneously-implanted devices: the role of macrophages and cytokines in biofouling and fibrosis. J Diabetes Sci Technol 2008;2(5):768-777.

28. Irwin EF, Saha K, Rosenbluth M, Gamble LJ, Castner DG, Healy KE. Modulus-dependent macrophage adhesion and behavior. J Biomater Sci Polym Ed 2008;19(10):1363-1382.

29. Bala I, Hariharan S, Kumar MN. PLGA nanoparticles in drug delivery: the state of the art. Crit Rev Ther Drug Carrier Syst 2004;21(5):387-422.

30. Mishra N, Goyal AK, Khatri K, Vaidya B, Paliwal R, Rai S, et al. Biodegradable polymer based particulate carrier(s) for the delivery of proteins and peptides. Curr Med Chem Anti Inflamm Anti Allergy Agents 2008;7(4):240-251.

31. Gomes S, Leonor IB, Mano JF, Reis RL, Kaplan DL. Spider silk-bone sialoprotein as a novel fusion protein for bone tissue engineering. Soft Matter 2010;Submitted.

32. Yan S-Z, Beeler JA, Chen Y, Shelton RK, Tang W-J. The regulation of type 7 adenylyl cyclase by its C1b region and *Escherichia coli* peptidylprolyl isomerase, SlyD. J Biol Chem 2001;11(16):8500-8506.

33. Montanaro F, Liadaki K, Volinski J, Flint A, Kunkel LM. Skeletal muscle engraftment potential of adult mouse skin side population cells PNAS 2003;100(16):9336-9341.

34. Miescher GC, Schreyer M, MacDonald HR. Production and characterization of a rat monoclonal antibody against the murine CD3 molecular complex. Immunol Lett 1989;23(2):113-118.

35. Mysliwietz J, Thierfelder S. Antilymphocytic antibodies and marrow transplantation. XII. Suppression of graft-versus-host disease by T-cell-modulating and depleting antimouse CD3 antibody is most effective when preinjected in the marrow recipient. Blood 1992;80(10):2661-2667.

36. Chen J, Ma A, Young F, Alt FW. IL-2 receptor α chain expression during early B lymphocyte differentiation. Int Immunol 1994;6(8):1265-1268.

37. Malek TR, Schmidt JA, Shevach EM. The murine IL 2 receptor. III. Cellular requirements for the induction of IL 2 receptor expression on T cell subpopulations. Journal of Immunology 1985;134(4):2405-2413.

38. Bendelac A. Mouse NK1+ T cells. Curr Opin Immunol 1995;7(3):367-374.

39. Bierer BE, Sleckman BP, Ratnofsky SE, Burakoff SJ. The biologic roles of CD2, CD4, and CD8 in T-cell activation. Annu Rev Immunol 1989;7:579-599.

40. Janeway CAJ. The T cell receptor as a multicomponent signalling machine: CD4/CD8 coreceptors and CD45 in T cell activation. Annu Rev Immunol 1992;10:645-674.

41. Fearns C, Kravchenko VV, Ulevitch RJ, Loskutoff DJ. Murine CD14 gene expression in vivo: extramyeloid synthesis and regulation by lipopolysaccharide. . J Exp Med 1995;181(3):857-866.

42. Chang DT, Colton E, Matsuda T, Anderson JM. Lymphocyte adhesion and interactions with biomaterial adherent macrophages and foreign body giant cells. J Biomed Mater Res A 2009;91A(4):1210-1220.

43. Ruiz JH, Becker I. CD8 cytotoxic T cells in cutaneous leishmaniasis. Parasite Immunol 2007;29(12):671-678.

44. LeBien TW, Tedder TF. B lymphocytes: how they develop and function. Blood 2008;112(5):1570-1580.

45. Brodbeck WG, MacEwan M, Colton E, Meyerson H, Anderson JM. Lymphocytes and the foreign body response: lymphocyte enhancement of macrophage adhesion and fusion. J Biomed Mater Res A 2005;74A(2):222-229.

46. Bergman AJ, Zygourakis K. Migration of lymphocytes on fibronectin-coated surfaces: temporal evolution of migratory parameters Biomaterials 1999;20(23-24):2235-2244.

47. Groth T, Altankov G, Klosz K. Adhesion of human peripheral blood lymphocytes is dependent on surface wettability and protein preadsorption. Biomaterials 1994;15(6):423-428.

48. Xia Z, Triffitt JT. A review on macrophage responses to biomaterials Biomed Mater 2006;1(1):R1-9.

49. Kao WJ. Evaluation of protein-modulated macrophage behavior on biomaterials: designing biomimetic materials for cellular engineering. Biomaterials 2008;20(23-24):2213-2221.

50. Brodbeck WG, Colton E, Anderson JM. Effects of adsorbed heat labile serum proteins and fibrinogen on adhesion and apoptosis of monocytes/macrophages on biomaterials. . J Mater Sci Mater Med 2003;14(8):671-675.

51. Jenney CR, Anderson JM. Adsorbed serum proteins responsible for surface dependent human macrophage behavior. J Biomed Mater Res 2000;49(4):435-447.

52. Rudolph R, Cheresh D. Cell adhesion mechanisms and their potential impact on wound healing and tumor control. Clin Plast Surg 1990;17(3):457-462.

53. O'Toole GC, Salih E, Gallagher C, FitzPatrick D, O'Higgins N, O'Rourke SK. Bone sialoprotein-coated femoral implants are osteoinductive but mechanically compromised. J Orthop Res 2004;22(3):641-646.

54. Hilbig H, Kirsten M, Rupietta R, Graf HL, Thalhammer S, Strasser S, et al. Implant surface coatings with bone sialoprotein, collagen, and fibronectin and their effects on cells derived from human maxillar bone. Eur J Med Res 2007;12(1):6-12.

55. Jin H-J, Fridrikh SV, Rutledge GC, Kaplan DL. Electrospinning Bombyx mori Silk with Poly(ethylene oxide). Biomacromolecules 2002;3(6):1233-1239.

56. Jin H-J, Park J, Karageorgiou V, Kim U-J, Valluzzi R, Cebe P, et al. Water-stable silk films with reduced β-sheet content. Adv Funct Mater 2005;15(8):1241-1247.

57. Kim HJ, Kim U-J, Vunjak-Novakovic G, Min B-H, Kaplan DL. Influence of macroporous protein scaffolds on bone tissue engineering from bone marrow stem cells. Biomaterials 2005;26(21):4442-4452.

58. Kim U-J, Park J, Li C, Jin H-J, Valluzzi R, Kaplan DL. Structure and properties of silk hydrogels. Biomacromolecules 2004;5(3):786-792.

Abstract

The development of a new generation of multifunctional biomaterials is a continual goal for the field of materials science. The *in vivo* functional behaviour of a new fusion protein that combines the mechanical properties of spider silk with the antimicrobial properties of hepcidin was addressed in this study. This new chimeric protein, termed 6mer+hepcidin, fuses spider dragline consensus sequences (6mer) and the antimicrobial peptide hepcidin as we have recently described, with retention of bactericidal activity and low cytotoxicity. In the present study mice subcutaneous implants were studied to access the in vivo biological response to the 6mer+hepcidin, which were compared with controls of silk alone (6mer), poly-lactic-glycolic-acid (PLGA) films and empty defects. Along with visual observations, flow cytometry and histology analyses were used to determine the number and type of inflammatory cells at the implantation site. The results show a mild to low inflammatory reaction to the implanted materials and no apparent differences between the 6mer+hepcidin films and the other experimental controls, demonstrating that the new fusion protein has good *in vivo* biocompatibility, while maintaining antibiotic function.

1. Introduction

Over the past few decades natural polymers have been extensively studied and tailored for potential use in the design of new devices for medical applications, including vascular [1] and tendon [2] grafts and sealants [3, 4]. In the case of proteins such as collagen and fibrin, their main sources are animal tissues, namely skin, tendons [5, 6] and serum [4]. However, the use of materials from animal origins has disadvantages, including the risk of disease transmission and immune reactions [4] and batch-to-batch variations [7, 8]. Some proteins such as spider silks would be desirable due to their mechanical properties; however they are not easy to obtain from nature, unlike the case for gelatin and alginate. In the case of *Bombyx mori* silkworm silk, sericulture allows for a constant supply of silk from the textile industry that has been extensively utilized in the medical suture field [9]. In the case of spider silk the supply of natural protein is scarce since it is difficult to breed spiders [10]. In recent years genetically engineered spider silk has been prepared and studied for a range of fundamental and applied biomaterials needs [10] including cell culture

surfaces [11], nerve regeneration [12, 13] and wound dressings [14]. The outstanding mechanical properties of silks [15] together with biocompatibility and slow biodegradation *in vivo* [16], and Food and Drug Adminstration approval for silkworm silk biomaterials, drive the interest in a broader range of silk-based biomaterials for medical needs [17].

Spider dragline silk is one of the many different types of silks produced by some spiders and the core filament is formed by two spidroin protein molecules, the major ampullate spidroin protein 1 (MaSp1) and protein 2 (MaSp2) [18]. MaSp has two chemically distinct blocks or peptide regions: hydrophilic GGX motifs (G stands for glycine and X is mostly glutamine) and hydrophobic poly-alanine (poly-A) motifs [19]. GGX motifs assume a helical conformation forming less crystalline and amorphous regions with elastic properties [20] which alternate with the poly-A motif crystalline regions characterized by tightly packed anti-parallel β-sheets responsible for the stiffness of silk fibers [21]. Additionally, MaSp1 protein produced by the spider species *Nephila clavipes*, is one of the most studied silks via recombinant DNA technology [22-24]. MaSp1 production in heterologous expression systems, such as *Escherichia coli*, has advantages over natural sources, since these expression systems represent a constant source of spider silk providing sufficient amounts of protein for study. Further, this genetic engineering approachs provides a path for precise control over the amino acid sequence in the protein, including the chain length and the sequence chemistry. This approach also offers the possibility of enriching the native sequence with other protein motifs with specific bioactivities or functions, thereby generating new chimeric proteins with selective biological activity. Silk-based block copolymers have been fused with different protein motifs such as RGD, a cell binding domain known to improve cell adhesion, for the design of tailored silk systems for gene delivery [25]. Also, dentin matrix protein and bone sialoprotein motifs have also been combined with spider silk block copolymers to improve osseointegration, highlighting the potential of these bioengineered silk protein-based biomaterials for tissue engineering [26, 27].

In the present study the *in vivo* biological responses to a new chimeric protein with antimicrobial features, designated 6mer+hepcidin (Figure VII.1), were assessed. The 6mer stands for a spider silk block copolymer formed by six repeats of the MaSp1

consensus sequence. We previously described the design of this fusion protein and activity studies demonstrated that antimicrobial activity of the chimeric protein was preserved when evaluated against *E. coli* and *Staphylococcus aureus*. Cell viability and proliferation studies also supported that there were not obvious cytotoxic effects from the chimeric protein on mammalian cells [28]. These data set the stage for the current study, where in vivo responses to the protein were addressed to further determine feasibility of this type of protein for new biomaterial systems.

Hepcidin is a antimicrobial peptide expressed by the liver [29] and different studies have demonstrated its antibacterial activity against different stains of Gram+ and Gram- bacteria, such as: gram- *E. coli* ML35 strain and *Neisseria cinerea*, and gram+ *S. aureus*, *Staphylococcus epidermis*, *Staphylococcus carnosus*, *Bacillus cereus*, *Bacillus megaterium*, *Bacillus subtilis*, *Micrococcus luteus* and group B *Streptococcus* [30-32]. Besides being an antimicrobial peptide, hepcidin also emerged as an important regulator of iron homeostasis, acting as an iron regulatory hormone and behaving as a negative regulator of intestinal iron absorption, iron transport across the placenta and macrophage iron release [33]. Besides many other functions, iron is an important element in infections and many pathogens have developed the ability to sequester iron from host. Therefore, iron deficiency may limit bacteria growth and inhibit the formation of biofilms [34].

The role of hepcidin in iron metabolism was first demonstrated when overexpression of mRNA coding for hepcidin in the liver of iron overloaded mice was reported [35]. Hepcidin mRNA overexpression by hepatocytes was also observed after treatment of the mice with lipopolyssacharide (LPS) [33]. A 25-fold increase in hepcidin mRNA levels were found within 8 hours after treatment with interleukine-6 (IL-6), a cytokine produced by monocytes and macrophages exposed to LPS [36]. These studies showed that hepcidin expression is regulated by iron as well as by immune stimuli. Upon infection hepcidin acts in a dual way against bacteria, by reducing the amount of iron available for bacteria growth and also by attacking the bacteria directly [37]. Hepcidin's dual antimicrobial role in the infectious process makes it an attractive target in the design of biomaterials for biomedical applications. These biomaterials could be used in the design of a new generation of grafts to reduce infections after surgery and preventing the formation of bacterial biofilms, a significant cause of implant failure

[38, 39]. Promising results were obtained *in vitro* with the 6mer+hepcidin [28], where the potential of a highly tailored multifunctional protein system for biomaterials was described. The system combined the mechanical features of silk protein and the antimicrobial properties of hepcidin peptide. These *in vitro* results together with role of hepcidin in inflammation are the starting point for the present *in vivo* study. Early biological responses to 6mer+hepcidin films were assessed, along with controls including, poly-lactic-glycolic-acid (PLGA) films, and silk alone (6mer), as well as empty defects. PLGA is a synthetic polymer approved by the Food and Drug Administration (FDA) for drug delivery, diagnostic and other clinical and basic science applications such as cardiovascular disease, cancer, vaccines and tissue engineering [40]. Films were implanted subcutaneously in mice and responses were assessed visually, via histology and with flow cytometry analysis.

6mer+hepcidin

SGRGGLGGQGAGAAAAAGGAGQGGYGGLGSQGTSGRGGLGGQGAGAA
AAAGGAGQGGYGGLGSQGTSGRGGLGGQGAGAAAAAGGAGQGGYGGL
GSQGTSGRGGLGGQGAGAAAAAGGAGQGGYGGLGSQGTSGRGGLGGQ
GAGAAAAAGGAGQGGYGGLGSQGTSGRGGLGGQGAGAAAAAGGAGQG
GYGGLGSQG **TS** DTHFPICIFCCGCCHRSKCGMCCKT

Figure VII.1. Amino acid sequence for the new chimeric protein, 6mer+hepcidin. The 6mer sequence is depicted in black and gray stands for the hepcidin domain. The TS restriction site was used to insert hepcidin sequence.

2. Materials and Methods

2.1. Cloning

The design and cloning of the 6mer [22, 41] silk control, and the 6mer+hepcidin [28] sequences was described in our previous studies. Briefly, a pET30a(+)(Novagen, San Diego, CA) vector was used for the construction of pET30L carrying the 6mer silk bock co-polymer coding sequence with a *Spe*I restriction site next to it for further sequence insertions. The hepcidin cDNA sequence was prepared by annealing synthetic single stranded oligonucleotides (Invitrogen, Carlsbad, CA, USA) encoding for hepcidin. The resultant cDNA double strand sequence carried *Spe*I and *Nhe*I restriction sites for insertion into the vector pET30L+6mer. After digestion with *Spe*I (R0133S, New England Biolabs, Ipswich, MA, USA,) and *Nhe*I (R0131S, New England Biolabs), the

hepcidin cDNA sequence was inserted into pET30L+6mer vector using T4 DNA ligase (M0202S, New England Biolabs). The ligation product was transformed into *Escherichia coli* DH5α cells (18258-012, Invitrogen). Successful transformants were identified by plating on agar containing 25 μg/ml kanamycin. The presence of the hepcidin insert was confirmed by DNA sequencing (Tufts Core Facility, Boston, MA).

2.2. Protein expression, purification and characterization

2.2.1. Protein expression and purification

The constructs pET30L+6mer and pET30L+6mer+hepcidin were used to transform *E. coli* RY-3041, a mutant strain of *E. coli* BLR(DE3) defective in the expression of SlyD protein [42, 43]. Bacteria were cultivated at 37ºC in Hyper Broth™ (Athens Enzyme Systems 0107-S), with 25 μg/ml kanamycin (K1876, Sigma, St. Louis, MO, USA) until an OD_{600} between 0.9 and 1. Protein expression was induced with isopropyl β-D-thiogalactoside (IPTG, 15529019, Invitrogen) at a concentration of 0.5 mM. After 2 hours cells were harvested by centrifugation at 6,500 rpm and the bacterial pellet was lysed in denaturating buffer (100 mM NaH_2PO_4, 10 mM Tris HCl, 8 M urea, pH 8.0) and left overnight with stirring for complete cell lysis. For removal of cell debris the mixture was centrifuged at 11,000 rpm. The resultant protein solution was incubated for 2 hours with Ni-NTA resin (30250, Qiagen, Valencia, CA, USA) with stirring. The protein/Ni-NTA resin mixture was loaded onto a glass Econo-column (Biorad, Hercules, CA, USA). After washing several times with denaturating buffer at pH 8 and at pH 6.0, proteins were eluted with denaturating buffer with pH 4.5. Eluted protein solutions were dialysed first in a 20 mM sodium acetate buffer followed by extensive dialysis in Milli-Q (MQ) water using cellulose ester snake skin membranes with a 100-500 Da molecular weight cut off (131054, Spectra/Por Biotech, Rancho Dominguez, CA, USA) for salt removal. Finally, dialyzed proteins were lyophilized.

2.2.2. Sodium dodecyl sulfate polyacrylamide gel (SDS-PAGE)

The purity of the 6mer and 6mer+hepcidin proteins was verified by SDS-PAGE electrophoresis followed by colloidal blue staining. Briefly, proteins were mixed with NuPAGE LDS sample buffer (NP0007, Invitrogen) and heated at 80ºC for 10 minutes. The samples were loaded into a Bis-tris 4-12% gel (NP0321BOX, Invitrogen) for

electrophoresis separation. Afterwards, gels were stained with a colloidal blue kit (LC6025, Invitrogen) for protein band detection.

2.2.3. Amino acid composition analysis

Amino acid analysis was carried out at Yale University, W. M. Keck Foundation Biotechnology Resource Laboratory (New Haven, CT, USA) on a Hitachi L-8900 amino acid analyzer (Tokyo, Japan) following an overnight *in vacuo* acid hydrolysis at 115ºC. The analyzer uses an ion-exchange column with a pH and temperature gradient to separate the amino acids. EZChrome Elite for Hitachi software was used to run the analyzer, collect and finally to analyze the data.

2.2.4. Matrix assisted laser desorption time-of-flight (MALDI-TOF) and protein sequencing

MALDI-TOF (Voyager-DE Pro, Applied Biosystems, CA, USA) and protein sequencing (ABI 494, Applied Biosystems, CA, USA) were used to confirm protein identity and both analyses were performed at the Tufts University Core Protein Chemistry Facility (Boston, MA USA). For MALDI-TOF, samples were dissolved in water in a concentration of 2 mg/ml. Protein sequencing was carried out with samples extracted from the protein bands observed by SDS-PAGE after electrophoresis and colloidal blue staining.

2.3. Fabrication of protein films

Protein films were prepared by dissolving the lyophilized 6mer or 6mer+hepcidin proteins in MQ water to a final concentration of 2% (m/v). Then 60 µl of each protein solution was cast onto a non-adherent polystyrene surface and left to dry at room temperature. After complete drying the films were treated with 90% (v/v) methanol solution for 30 minutes to induce β-sheet conformation, thereby inducing insolubility of the proteins. With methanol treatment there was an improvement in the mechanical properties of the films as well as preventing immediate dissolution in culture media or *in vivo* in contact with body fluids. After methanol treatment films were left to dry for three days for methanol evaporation.

PLGA film controls were prepared by dissolving PLGA with a molecular weight between 40-75kDa (P2191, Sigma) in dichloromethane in a 1:15 ratio. After complete dissolution, 60 µl of PLGA solution was cast onto a polystyrene surface and left to dry at least for 2 days for complete dichloromethane evaporation. PLGA has been extensively studied because of its high biocompatibility and biodegradability [44] and is approved by the FDA for many clinical applications such as sutures, bone plates, abdominal meshes and drug delivery due to its [45]. These are the main reasons why PLGA was selected as one of the controls in this study.

For sterilization, the PLGA, 6mer and 6mer+BSP films were treated with 70% ethanol (v/v) solution for 30 minutes and immediately before implantation each film side was treated for 15 minutes with ultraviolet (UV) light.

Before implantation, films were hydrated with sterile PBS 15 minutes. Films had a final diameter around 8 mm.

2.4. Grafting

All procedures were conducted under animal care protocols approved by Tufts Institutional Animal Care and Use Committee. Subcutaneous grafting was performed in the back of balb/c female mice five to seven weeks old purchased from Charles River (Wilmington, MA, USA) breeding labs. A total of 40 animals were used in this study. The animals were divided into four groups of five animals. Three groups carrying the 6mer, 6mer+ hepcidin and PLGA films, respectively and a fourth control group, formed with animals subjected to the same surgical procedure but carrying no implant.

The animals were anesthetized with isoflurane and part of their back was shaved with an electric razor and disinfected with 70% (v/v) ethanol solution. Under anesthesia and after disinfection, a longitudinal dorsal incision approximately with 1 cm long was prepared with the help a fine scissors. Grafts were inserted in a subcutaneous pocket between skin and muscular layers. A single test sample was implanted in each animal. The incisions were closed with polyester/dacron suture line and surgical wounds were again disinfected with betadine. The incisions were monitored, as were the animals, for atypical signals. Animals were sacrificed by cervical dislocation after 2 and 6 weeks to retrieve the implanted materials and to check for inflammatory responses. The implants together with the overlying tissue

were removed and processed for flow cytometry and histology analysis as described in the next sections.

2.5. Flow cytometry analysis

2.5.1. Cell isolation

For cell isolation the tissue surrounding the implant was removed and minced with the help of scissors or scalpel. The minced tissue was digested in 2 mg/ml collagenase IV (Invitrogen, 17104019) and 1.2 units/ml dispase (Invitrogen, 17105041) solution, prepared in PBS, for 2 hours at 37ºC with occasional stirring. The digestion mixture was centrifuged at 1500 rpm for five minutes at 4ºC, the supernatant was removed and the pellet was resuspended at around 10^6 cells/ml in flow cytometry buffer (PBS supplemented with 0.5% (v/v) of bovine serum albumin, BSA). To eliminate undigested tissue the mixture was passed through a 100 µm pore cell strainer and collected in a 50 ml Falcon tubes and again centrifuged at 1500 rpm for five minutes at 4ºC. To remove the red blood cells, the cells pellet was resuspended in 5 ml of a lysis buffered solution containing NaCl 137 mM, Na_2HPO_4 8 mM, KH_2PO_4 1.46 mM, KCl 2.68 mM, in distilled water at pH 7.0. After 4 to 5 minutes of incubation 20 to 30 ml of PBS was added to stop the reaction. The cell suspension was centrifuged as before followed by two washes with flow cytometry buffer. Blocking was carried out by suspending the cell pellets in PBS followed by 15 minutes incubation on ice in the presence of rat anti-mouse FcRII/III antibody (clone 2.4G2, 553141, BD Pharmingen, Franklin Lakes, NJ, USA). The antibody reacts specifically with a common epitope on the extracellular domains of mouse FcγII/III receptors and blocks non-antigen-specific binding of immunoglobulins to the FcγII, FcγIII and possibly FcγI receptors, *in vitro* and *in vivo*. After spinning the cell pellet at 1500 rpm for five minutes at 4ºC, the cells were resuspended in 500 µl of flow cytometry buffer and used for cell immunostaining for flow cytometry analysis.

2.5.2. Cell labelling

For antibody staining, 50 µl of cell suspension prepared as above was aliquoted and gently mixed with second antibody solution and incubated on ice for around 30 minutes. Secondary antibodies were labelled with allophycocyanine (APC),

phycoerythrin (PE), alexa fluor® and fluorescein isothiocyanate (FITC) fluorescence dyes. After incubation with secondary antibody, the cells were washed twice with flow cytometry buffer and resuspended in 200 to 300 µl of the same buffer supplemented with ethylenediaminetetraacetic acid (EDTA, Sigma, 431788), to protect the cells until flow cytometry analysis. Brief descriptions of the secondary antibodies used in this study to assess biological responses to the implanted materials are given below:

PE conjugated CD14 (557740, BD Pharmingen, San Jose, CA, USA) antibody reacts with CD14 glycoprotein expressed by cells of monocyte and macrophage lineages and to a lesser extent by granulocytes. CD14 is a receptor for lipopolysaccharide (LPS) complex, a component of outer-membrane of Gram negative bacteria. After recognition of the LPS complex, cells from the immune system rapidly engage inflammatory defense mechanisms which in some cases can lead to septic shock [46].

Alexa fluor® conjugated CD4 (557667, BD Pharmingen) antibody recognizes CD4 surface marker, a transmembrane glycoprotein expressed by developing thymocytes, major histocompatibility class II restricted mature T lymphocytes, including T helper cells and immunosuppressive T cells [47], and a subset of natural killer T cells [48]. CD4 is critical in both thymocyte development and T-cell activation and the expression of CD4 surface marker by T-cells during development induces its differentiation into T-helper cells exclusively [47].

FITC conjugated CD3 (555274, BD Pharmingen) antibody reacts with the CD3 component of T-cell receptor (TCR), a multimeric surface complex resulting from the assembly of 7 different proteins. The T-cell receptor associated CD3 complex is expressed on many thymocytes and mature T lymphocytes and is essential for antigen recognition and the resulting specific immunity [49].

APC conjugated CD25 (558643, BD Pharmingen) antibody acts against the low affinity CD25 subunit (IL2 receptor α) forming the interleukin-2 receptor (IL-2R) a surface cell receptor expressed in activated T and B lymphocytes. IL-2R recognizes the interleukin-2 molecule which triggers cell proliferation and the emergence of effector T cells important for the full expression of immune responses [50].

Alexa fluor® conjugated CD8a (557668, BD Pharmingen) antibody recognizes the 38kDa α and 34kDa α' chains of the CD8 coreceptor, a T cell surface glycoprotein

expressed by the major histocompatibility class I restricted cytotoxic T cells and involved in antigen recognition by cytotoxic T lymphocytes. CD8, as CD4 coreceptor, are critical for the development and activation of T cells [51].

2.5.3. Instrumentation

Analyses were performed in a four-color FACSCalibur instrument (Becton Dickinson, NJ, USA) equipped with a 488 nm argon-ion laser and a 635 nm red diode laser and data were processed using FlowJo analysis software (Tree Star, Inc., OR, USA).

2.6. Histological procedure

Samples were retrieved after 2 and 6 weeks of implantation for histological examination. Immediately after collection, samples were immersed in a 4% formalin buffer solution and sent for processing and staining at the Tufts University Animal Pathology Core Laboratory. Samples were embedded in paraffin and 10 μm sections were prepared. Hematoxylin and eosin (H&E) were used for staining.

2.7. Statistics

All statistic analyses were performed with SPSS 17.0 software. The Shapiro-Wilk test was used to assess normality of the data. To test for significant differences between experimental groups (6mer+hepcidin, 6mer, PLGA and empty controls) one-way ANOVA was used in conjugation with Dunet's T3 post hoc for multiple comparison. $p<0.05$ was considered statistically significant.

3. Results

3.1. Protein Characterization

SDS-PAGE analysis of the proteins show an apparent molecular weight around 28 kDa for both the 6mer, with an expected molecular weight of 21.8 kDa, and the 6mer+hepcidin, with an expected molecular weight of 23 kDa (Figure VII.2). In the case of the 6mer+hepcidin higher molecular weight protein bands were also observed which correspond to dimers and multimers as preiviously observed [32]. Amino acid analysis confirmed the corrected composition of the chimeric protein (6mer+hepcidin)

and the control (6mer). As expected glycine and alanine are the most abundant amino acids in both 6mer and 6mer+hepcidin proteins (Table VII.1). MALDI-TOF analysis confirmed protein identity and showed a peak at 20.9 kDa for the 6mer protein, a value close to the expected molecular weight of 21.8 kDa. For the 6mer+hepcidin, MALDI-TOF analysis showed a peak at 22.9 kDa, a value very near to 23k Da predicted size. Finally, protein sequencing analysis confirmed the N-terminal sequence for both the 6mer and 6mer+hepcidin proteins.

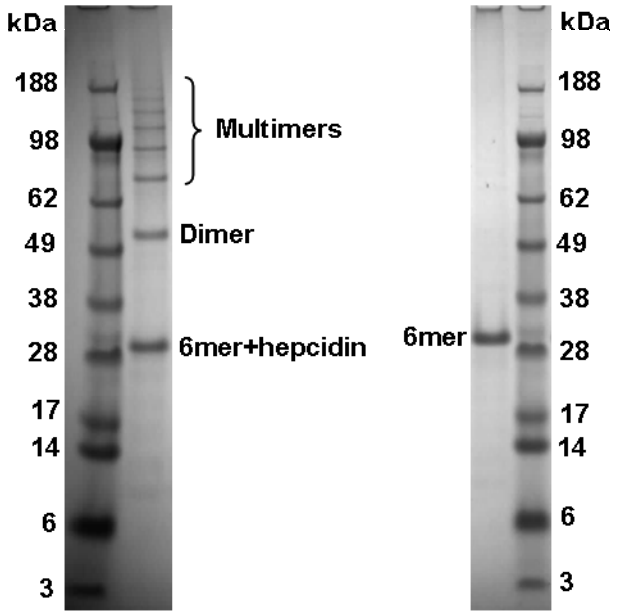

Figure VII.2. SDS-PAGE gel electrophoresis showing two bands of around 28 kDa for 6mer and 6mer+hepcidin. Dimers and multimers were also observed for the 6mer+hepcidin.

Table VII.1. Amino acid composition analysis of 6mer and 6mer+hepcidin recombinant proteins (only the major amino acids are represented).

Amino acid	6mer (20.7kDa)		6mer+hepcidin (23.0kDa)	
	Observed	Expected	Observed	Expected
	%		%	
Glutamine + Glutamic Acid	9.4	8.5	9.1	7.7
Serine	4.8	6.9	4.4	6.9
Glycine	36.4	40.6	24.4	37.3
Alanine	18.7	19.5	14.9	17.5
Leucine	6.1	5.7	7.3	5.1
Threonine	3.3	3.2	4.2	4

3.2. Cell characterization by flow cytometry analysis

All animals survived without visible signs of stress or inflammation. After cell isolations from the implant sites, five different surface markers were assessed for cell types present in the implantation region after 2 and 6 weeks: CD4, CD8, CD14, CD3 and CD25. In Figure VII.3 representative flow cytometry plots are shown for the labelling, and these data were used to determine the percentage of positive cells expressing the surface marker of interest (Figure VII.4). 2 weeks after grafting the CD3 marker had the lowest expression values ranging between 6.8% and 12.4% for the empty controls and the 6mer films, respectively. In Figure VII.4A no major differences betweens the plots for the samples and the empty control were found and statistical comparison shows no significant differences ($p<0.05$) between samples. CD4 showed the highest expression values with an average of 67.7, 60.6, 77.7 and 68.4% for the 6mer, PLGA, empty control and the 6mer+hepcidin, respectively (Figure VII.4A). For the CD4 marker the presence of a second population of positive cells with high fluorescent levels was evident from the flow cytometry plots in Figure VII.3. ANOVA analysis for CD4 showed significant differences, $p<0.05$, between samples and Dunet's T3 post hoc for multiple comparison showed significant differences between the PLGA and empty controls. For CD25 antigen ANOVA analysis showed a significant difference between PLGA, 6mer and 6mer+hepcidin and the controls with no implants.

After 6 weeks of implantation flow cytometry analysis showed an increase in the percentage of cells expressing surface markers CD14, CD8, CD25 and CD3. For CD4 marker expression increased only for the PLGA samples. Figure VII.4B shows the presence of a second population of positive cells that was not evident for the samples collected after 2 weeks. Also flow cytometry labelling (Figure VII.3) showed an increase in fluorescence intensity for most of the surface markers. As in the case of the samples collected after 2 weeks, after 6 weeks CD3 showed the lowest percentage of positive cells with 12, 38.5, 26.6 and 15.3% for the 6mer, PLGA, empty control and 6mer+hepcidin, respectively. Again CD4 antigen showed the highest expression for most samples with values ranging between 51.5 and 71.7% for the 6mer and empty control samples (Figure VII.4B). Statistical comparison showed no significant differences between the different samples for each marker. However, when comparing expression values obtained for the same samples after 2 and 6 weeks some significant

differences where observed. For CD4 a significant ($p<0.05$) increase in expression from 2 to 6 weeks for the 6mer and 6mer+hepcidin samples was found. A significant increase in expression was also observed for CD25 for the 6mer, PLGA and 6mer+hepcidin samples.

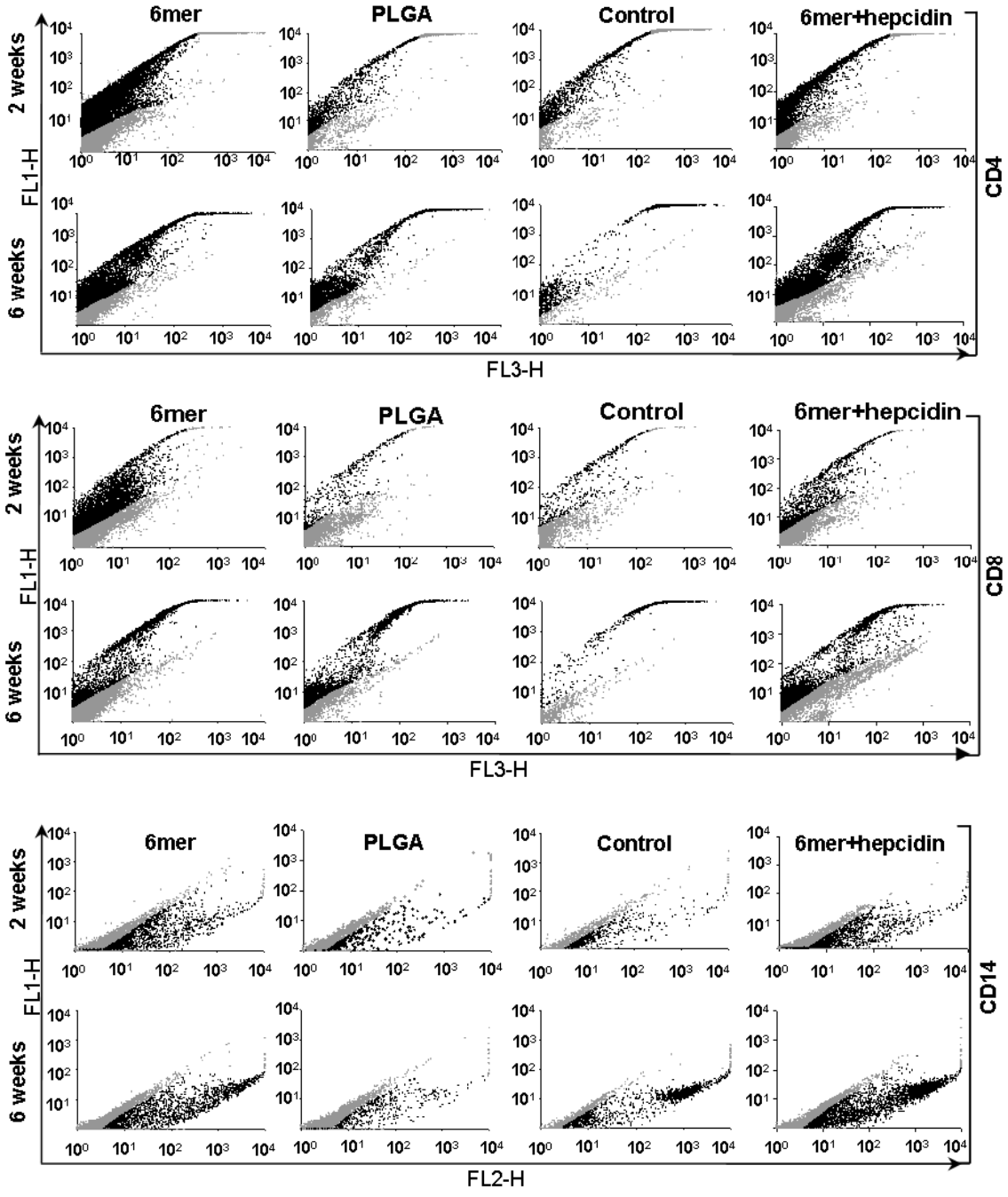

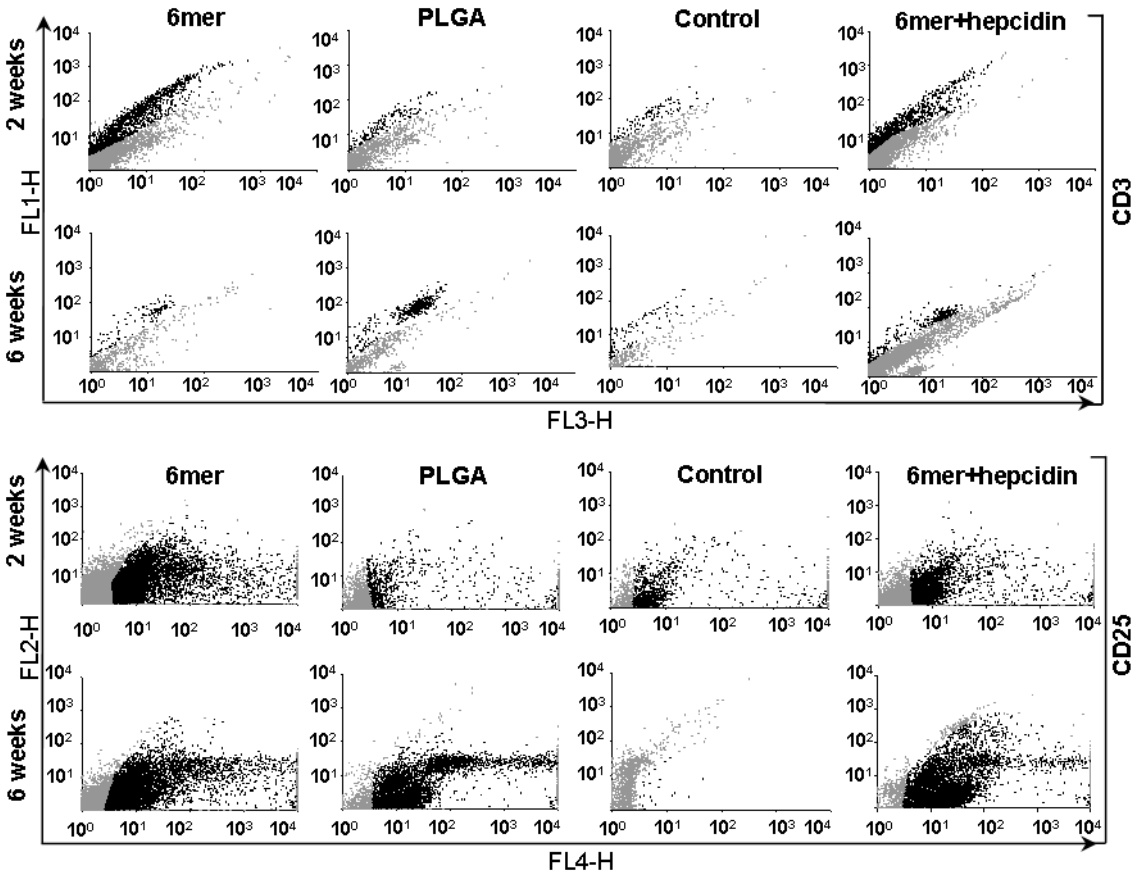

Figure VII.3. Representative flow cytometry plots for surface markers. Positive cells for the surface markers are depicted in black and gray stands for negative cell population.

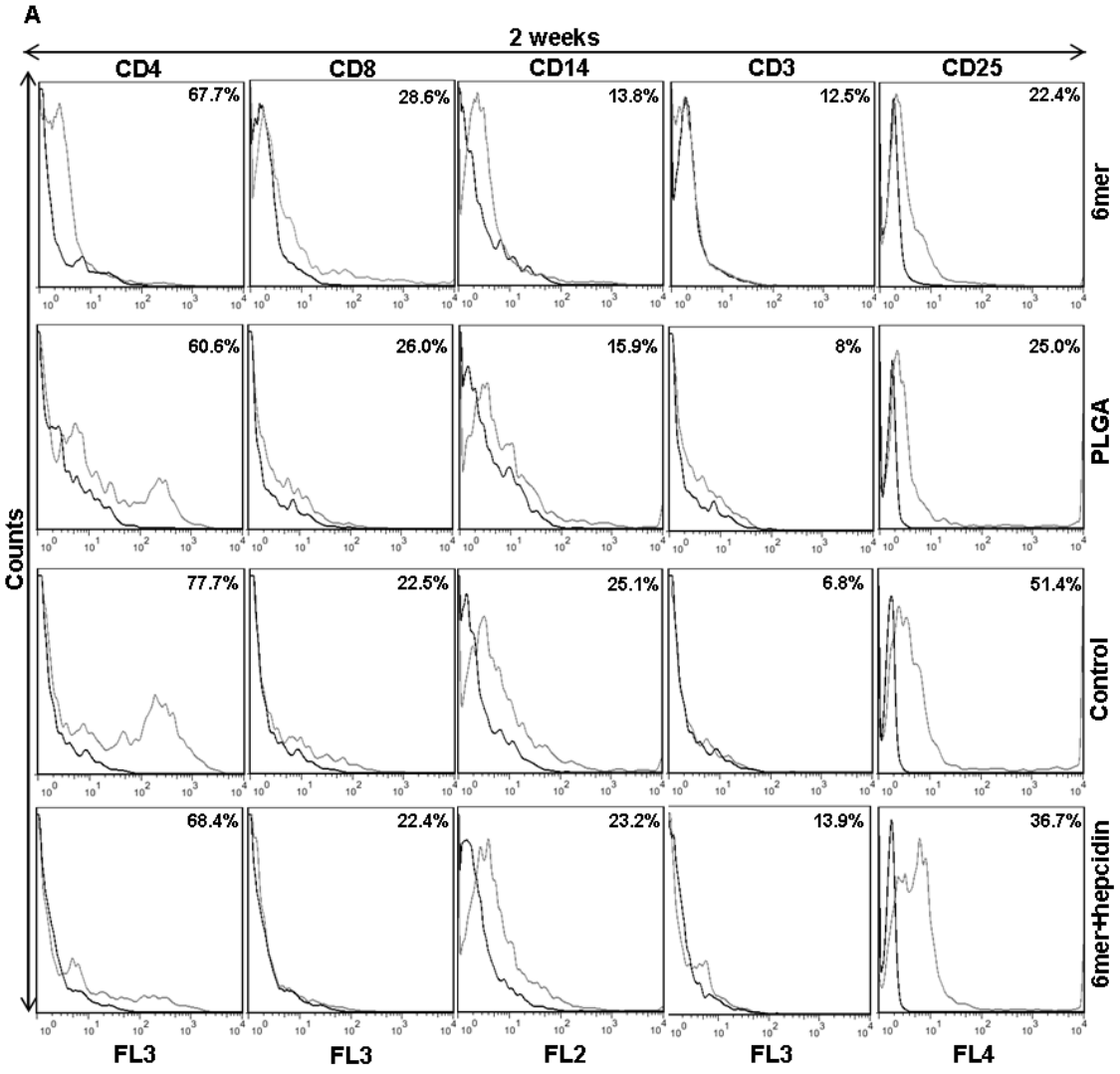
A
2 weeks
CD4
CD8
CD14
CD3
CD25
67.7%
28.6%
13.8%
12.5%
22.4%
6mer
60.6%
26.0%
15.9%
8%
25.0%
PLGA
77.7%
22.5%
25.1%
6.8%
51.4%
Control
68.4%
22.4%
23.2%
13.9%
36.7%
6mer+hepcidin
Counts
FL3
FL3
FL2
FL3
FL4

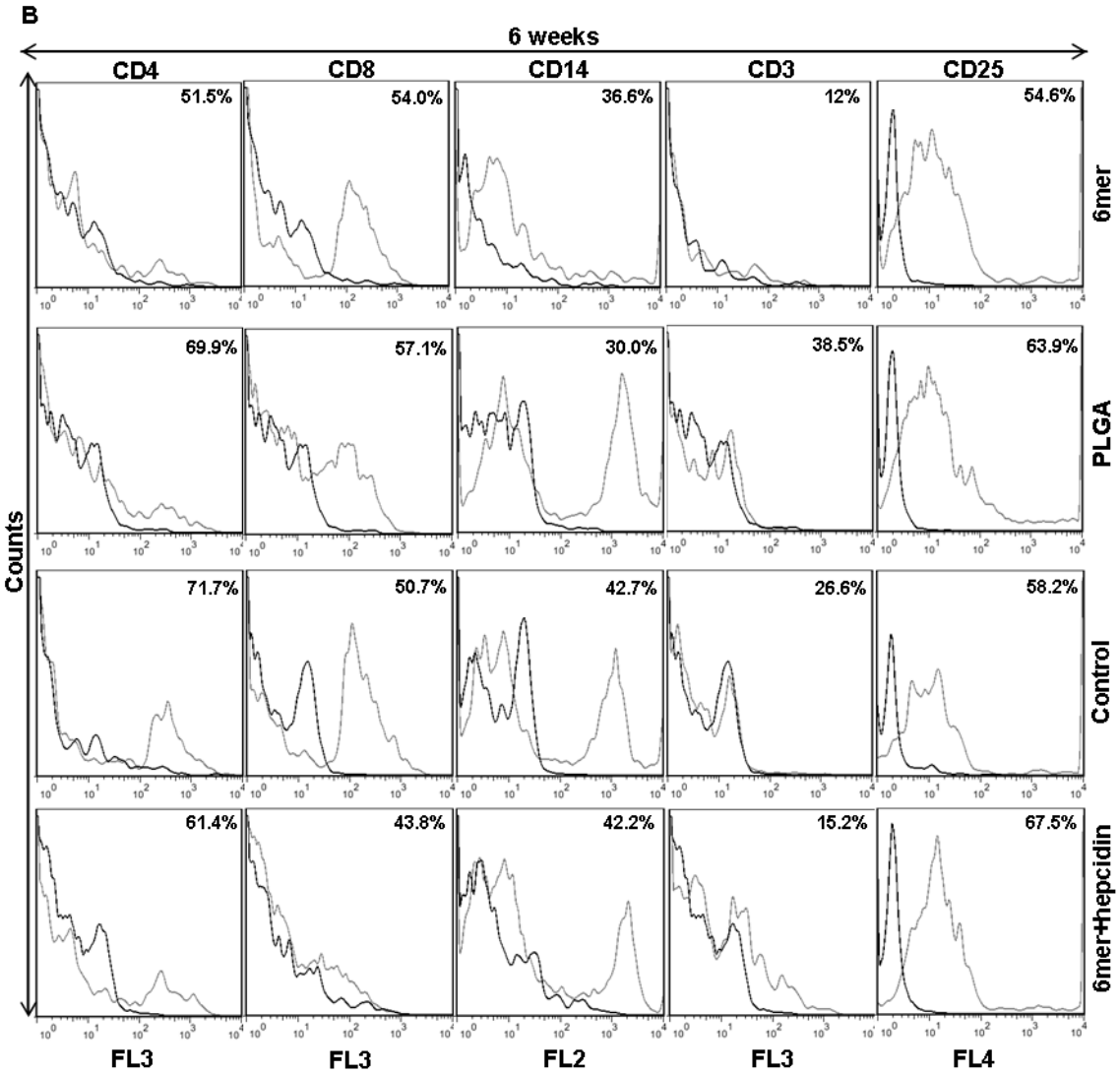

Figure VII.4. Representative plots of one experiment for the expression of CD4, CD8, CD14, CD3 and CD25 surface markers for the cells extracted from the region surrounding each implant sample at the end of 2 and 6 weeks. Numbers represent the average percentage of positive cells for each marker. Gray shows marker expression and black stands for the negative control, with no secondary antibody added.

3.3. Histological characterization

Histological characterization with H&E staining was also used to assess biological responses to the 6mer+hepcidin films and to compare this to the various controls (6mer, PLGA and empty implants). After 2 weeks a mild inflammatory reaction was detected around the 6mer, 6mer+hepcidin and PLGA implanted films, with fewer cells in the empty controls when compared to the implanted films (Figure VII.5).

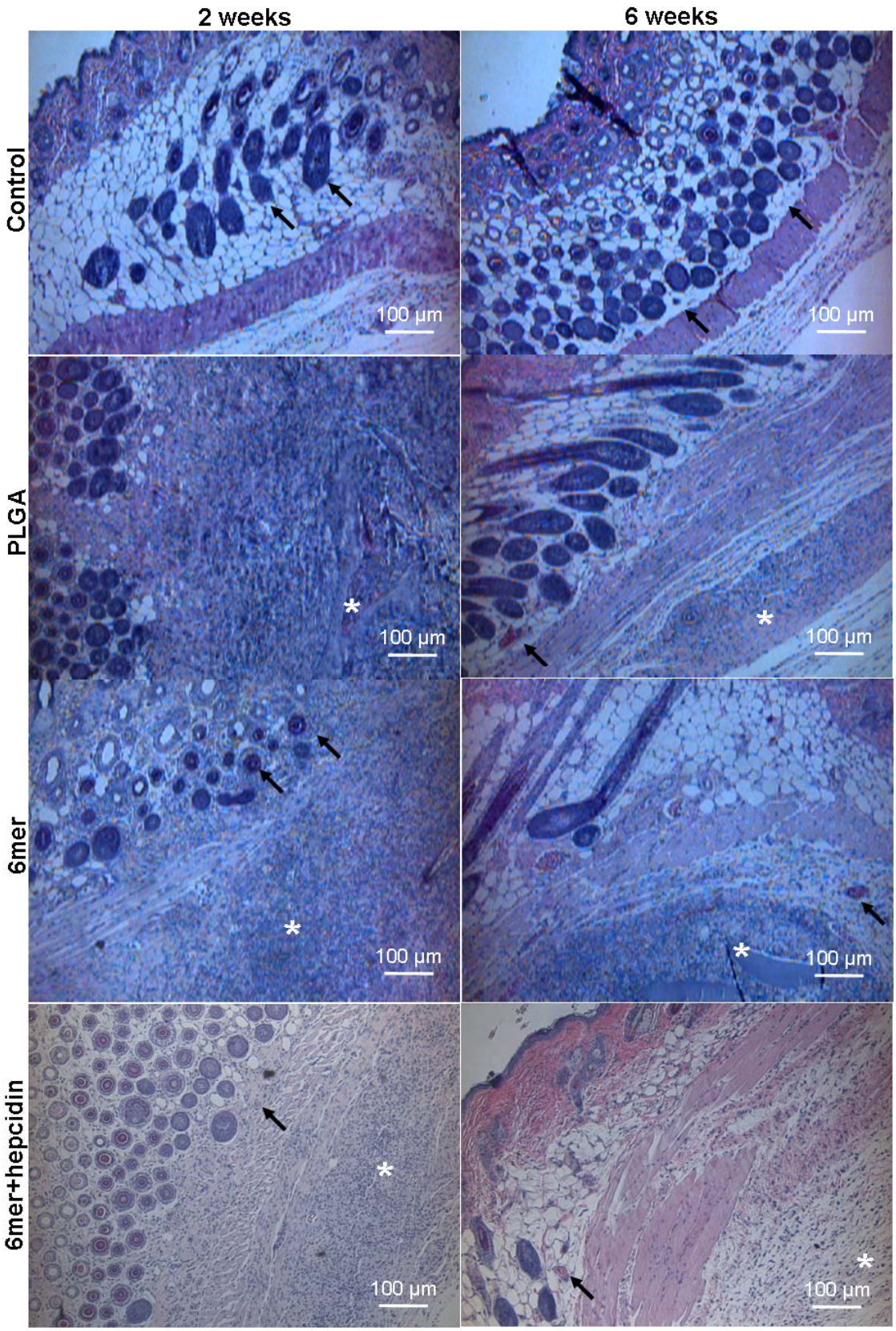

Figure VII.5. H&E staining of PLGA, 6mer and 6mer+hepcidin films and the empty control after 2 and 6 weeks of implantation. Magnification 10X. * marks the implant. Black arrows mark blood vessels.

After 6 weeks *in vivo* fewer cells could be observed in the tissues surrounding the implants and in the empty controls and a more localized cell response is observed. Moreover, the formation of a fibrous capsule was not detected for any of the implanted materials (Figure VII.5).

4. Discussion

The importance of antimicrobial peptides in the inflammation process has been previously discussed [32, 52, 53], functioning as chemotactic agent for monocytes and T cells or involved in activating the acquired immune response system [54]. These peptides are also important elements in wound healing [55], stimulating the proliferation of fibroblasts and epithelial cells [56, 57], inducing neo-vasculogenesis [58] and cytokine mobilization [59]. In the specific case of hepcidin, besides its direct antimicrobial activity against pathogens, it is also a key element in controlling plasma iron concentration. Due to its role in iron homeostasis, hepcidin is considered to be a crucial link between host defense and iron metabolism [60]. During the early stages of bacterial infections the exposure of monocytes and macrophage to LPS, a component of Gram negative bacteria outer-membrane, leads to the secretion of different types of cytokines [36]. The cytokine IL-6 is secreted by monocytes and macrophage [61] and induces hepcidin synthesis by hepatocytes during the acute phase of inflammation in mice and humans [62]. Hepcidin binds to ferroportin an iron transmembrane transporter, which blocks iron efflux from hepatocytes in liver, macrophages and absorptive enterocytes in the small intestine [63]. This binding leads to the degradation of ferroportin resulting in the trapping of iron inside hepatocytes, macrophages and enterocytes with a consequent decrease of available serum iron [63]. The decrease in blood iron diminishes the availability of iron for invading microorganisms. As mentioned previously, iron deprivation limits bacterial growth and inhibits biofilm formation, favouring the appearance of mobile individual forms, which are vulnerable to host attack [33]. Therefore, hepcidin has an important role in early stages of infection and inflammation, exerting dual antimicrobial activity by attacking bacteria directly and by reducing the amount of available iron necessary for microbial metabolism. These characteristics together with is low cytotoxicity [64] make hepcidin

a promising molecule for use in the design of biomaterials with antimicrobial properties to reduce the risk of infection after implantation.

However, this strong link between hepcidin and the immune system can also elicit an undesired inflammatory response to biomaterials carrying this molecule. For instance, the binding of hepcidin to the ferroportin receptor present in the cell membrane of macrophages [63] can promote macrophage adhesion to the implant surface, which could accelerate the degradation of the implanted biomaterial and also lead to an intensification of host immune response. For these reasons and since the evaluation of tissue-material responses are important in order to assess the suitability of a new biomaterial for biomedical applications, this study addresses the first stages of the inflammatory response to 6mer+hepcidin films implanted in mice. Flow cytometry analysis was used to access the expression of five different surface markers: CD4, CD8, CD3, CD25 and CD14. These five different markers are specific for different types of immune cells and were used to assess the cellular response to implanted films. Flow cytometry assay was complemented with histology studies and both analyses showed similar inflammatory responses between the three polymers tested (6mer+hepcidin, PLGA, an FDA approved polymer, and 6mer) and the empty controls.

Flow cytometry analysis provided a quantitative evaluation of the inflammatory response through different cell markers. CD4 marker had the highest expression levels at both 2 and 6 weeks. As mentioned previously this marker is expressed by sub-groups of T lymphocytes, such as mature T helper and immunosuppressive T cells, and also by natural killer cells. T helper cells activate and direct other immune cells such as cytotoxic T cells and maximize the bactericidal activity of macrophages [65]. Furthermore, the presence of positive cells for CD8, CD3, CD25 and CD14 was also observed, mainly after 6 weeks when these markers had stronger expression. Activated CD8 positive cytotoxic T cells are efficient and rapid killers of target cells [66]. These cells only become fully activated in the presence of CD4 T cells and they exert their effect either by releasing lytic granules, which carry molecules capable of forming pores in the membrane of target cells or by inducing cell apoptosis [67]. The detection of a CD25 positive cell population showed the presence of B and T lymphocytes, which are cells responsible for the production of antibodies and for cell-mediated immune responses, respectively [68]. Additionally, CD14 positive cells were

detected by flow cytometry which indicates monocytes, macrophages and granulocytes. Macrophage and granulocytes play a role in host inflammatory responses forming the first line of immune defence [69, 70].

In conclusion, the flow cytometry results are in concordance with the histology observations and both analyses showed a mild or low inflammatory host response to all of the implanted materials. Flow cytometry indicated the presence of different types of immune cells at the implant site and histological analysis showed these types of cells around the implant. Additionally, except for CD4 in the PLGA films and empty controls, flow cytometry analysis shows no significant differences in either the number or type of inflammatory cells for the 6mer+hepcidin films when compared with the 6mer, PLGA and empty controls. Since similar responses were observed for the implanted films and for the controls we conclude that the observed mild or low inflammatory response was not caused by the implanted films. Also, these results show that the host immune response is mild or low and restricted to a local reaction, mainly after 6 weeks.

The *in vivo* behaviour of different silk implants has been described. The inflammatory response induced after intramuscular implantation of silk and silk-RGD films in mice in comparison to polylactic acid (PLA) and collagen films has been reported [71]. The inflammatory response to the silk and silk-RGD films was equivalent to or less than that observed for collagen controls, and far less than to PLA film controls. Minimal inflammation responses were observed for silk, silk-RGD and collagen films after 6 weeks [71]. For PLA films the presence of granulomatous inflammation was found based on the presence of multinucleated giant cells and macrophages [71]. Degradation of silk films was not observed over the 6 week period, while for collagen there was considerable degradation and only remnants of these films detected [71]. Recently, recombinant spider silk films as a wound dressing biomaterials was evaluated in rats [14]. *In vivo* results showed that as a biomaterial, the recombinant spider silk films had good biocompatibility and were able to induce skin regeneration. For the silk films the wound healing extent was between 95 and 90% after 21 days [14]. Other studies also addressed the *in vivo* behaviour of silk-based scaffolds functionalized with bioactive molecules such as bone morphogenetic protein 2 (BMP-2) [72] and tissue growth factor (TGF-β) [73]. Although a considerable number

of studies addressed the *in vitro* and *in vivo* responses to silk-based materials, to our knowledge these are the first results reporting the *in vivo* inflammatory response to a protein graft, fabricated from a chimeric protein combining spider silk with an antimicrobial peptide.

In the literature, the use of biomaterials incorporating antimicrobial peptides is scarce. Recently, *Bombyx mori* silk fibroin films were modified with a cecropin B antimicrobial peptide, through the carbodiimide chemistry, showing satisfactory antimicrobial *in vitro* results [74]. Furthermore, cross-linked gelatin hydrogels for the delivery of lysozyme antimicrobial peptide prevented the adherence of bacteria to valves used in cardiac valve replacement [75]. Cross-linked gelatin showed sustained release of lysozyme during 30 hours after implantation, while the lysozyme content in the surrounding tissue was elevated for 50 hours. Later a chemically cross-linked gelatin-chondroitin sulphate hydrogel impregnated into Dracon grafts was used as a controlled release system for the delivery of two antimicrobial peptides: lysozyme and recombinant thrombocidin, a protein derived from human blood platelets [76]. The results showed that cross-linked gelatin-chondroitin sulphate hydrogels had a higher loading capacity for lysozyme and recombinant thrombocidin than cross-linked gelatin hydrogels. Also, *in vivo* assessments found that the hydrogels were biocompatible and degraded almost completely after 18 weeks of implantation [76].

Other studies have described the use of silk and other natural origin based scaffolds as delivery systems for antibiotic molecules [74, 77]. However, in most cases the scaffolds are soaked in the antibiotic solution and therefore uncontrolled desorption of the immobilized species is observed [78].

Microbial infections are major concerns to the medical community in cases of internal prostheses, cutaneous dressings and other medical devices such as contact lenses and catheters. To prevent these problems antibiotic pre-operative prophylaxis and antibiotic local delivery are used. However, even with the extensive use of antibiotics the frequency of implant related infections continues to be a major health care concern. Currently used methods of pre-operative prophylaxis and antibiotic local delivery have the major disadvantages of not assuring homogeneous delivery of the drug throughout the host body and of favouring the appearance of antibiotic-resistant strains [79]. Also, the generalized use of antibiotics can lead to the development of

resistant bacterial strains. Therefore, there remains an urgent need to develop new biocompatible biomaterials with antimicrobial properties, both to reduce the use of antibiotic drugs as well as to maintain localized release at the defect site, both issues that can be addressed with the functionalized antimicrobial biomaterial system addressed in the present study.

5. Conclusions

In the present study the biological responses are reported to a new chimeric protein, 6mer+hepcidin, with antimicrobial activity [28]. Flow cytometry and histology results showed no significant differences in the inflammatory responses between mice carrying the 6mer+hepcidin films and mice implanted with various controls; PLGA, 6mer or empty defects. These results are promising and give further support to the developing new bioengineered biomaterials with antimicrobial properties that offer a path forward in reduction in the use of antibiotics to prevent infection in implants. The 6mer+hepcidin and other future fusion proteins with antimicrobial properties may represent a new and promising approach to the design of a new generation of multifunctional biomaterials bioengineered to prevent the onset of infections, to be biocompatible and to elicit tissue integration during the tissue regeneration process.

Acknowledgements

The authors thank Doctor Tírcia Santos for her advice in this paper. Sílvia Gomes thanks the Portuguese Foundation for Science and Technology (FCT) for providing her a PhD grant (SFRH/BD/28603/2006). This work was carried out under the scope of the European NoE EXPERTISSUES (NMP3-CT-2004-500283), the FIND & BIND project funded by the agency EU-EC (FP7 program), the FCT R&D project ProteoLight (PTDC/FIS/68517/2006) funded by the FCT agency, the Chimera project (PTDC/EBB-EBI/109093/2008) funded by the FCT agency, the NIH (P41 EB002520) Tissue Engineering Resource Center and the NIH (EB003210 and DE017207).

References

1. Park IS, Kim SH, Kim YH, Kim IH, Kim SH. A collagen/smooth muscle cell-incorporated elastic scaffold for tissue-engineered vascular grafts. J Biomater Sci Polym Ed 2009;20(11):1645-1660.

2. Pabbruwe MB, Kafienah W, Tarlton JF, Mistry S, Fox DJ, Hollander AP. Repair next term of meniscal previous termcartilagenext term white zone tears using a stem cell/previous termcollagennext term-scaffold implant Biomaterials 2010;31(9):2583-2591.

3. Bessa PC, Balmayor ER, Azevedo HS, Nürnberger S, Casal M, Griensven Mv, et al. Silk fibroin microparticles as carriers for delivery of human recombinant BMPs. Physical characterization and drug release. J Tissue Eng Regen Med 2010;4(5):349-345.

4. Janmey PA, Winer JP, Weisel JW. Fibrin gels and their clinical and bioengineering applications. J R Soc Interface 2008;6(30):1-10.

5. Chung HJ, Park TG. Surface engineered and drug releasing pre-fabricated scaffolds for tissue engineering. Adv Drug Deliv Rev 2007;59:249-262.

6. Hubbell JA. Materials as morphogenetic guides in tissue engineering. Curr Opin Biotechnol 2003;14:551-558.

7. Langer R, Tirrell DA. Designing materials for biology and medicine. Nature 2004;428:487-492.

8. Romano NH, Sengupta D, Chung C, Heilshorn SC. Protein-engineered biomaterials: nanoscale mimics of the extracellular matrix Biochimica et Biophysica Acta 2010;doi:10.1016/j.bbagen.2010.07.005.

9. Omenetto FG, Kaplan DL. New opportunities for an ancient material. Science 2010;329(5991):528-531.

10. Spiess K, Lammel A, Scheibel T. Recombinant spider silk proteins for applications in biomaterial. Macromol Biosci 2010;10(9):998-1007.

11. Widhe M, Bysell H, Nystedt S, Schenning I, Malmsten M, Johansson J, et al. Recombinant spider silk as matrices for cell culture. Biomaterials 2010;doi:10.1016/j.biomaterials.2010.08.061.

12. Allmeling C, Jokuszies A, K KR, Kall S, Vogt PM. Use of spider silk fibres as an innovative material in a biocompatible artificial nerve conduit. J Cell Mol Med 2006;10(3):770-777.

13. Allmeling C, Jokuszies A, Reimers K, Kall S, Choi CY, Brandes G, et al. Spider silk fibres in artificial nerve constructs promote peripheral nerve regeneration. Cell Prolif 2008;41(3):408-420.

14. Baoyong L, Jian Z, Denglong C, Min L. Evaluation of a new type of wound dressing made from recombinant spider silk protein using rat models Burns 2010;36(6):891-896.

15. Heim M, Römer L, Scheibel T. Hierarchical structures made of proteins. The complex architecture of spider webs and their constituent silk proteins. Chem Soc Rev 2010;39(1):156-164.

16. Xu M, Lewis RV. Structure of a protein superfiber: Spider dragline silk. Proc Natl Acad Sci USA 1990;87:7120-7124.

17. Hardy JG, Scheibel TR. Silk-inspired polymers and proteins. Biochem Soc Trans 2009;37:677-681.

18. Mahoney DV, Vezie DL, Eby RK, Adams WW, Kaplan D. Aspects of the morphology of dragline silk of *Nephila clavipes*. In: Kaplan D, Adams WW, Farmer B, Viney C, editors. Silk Polymers: American Chemical Society, 1997. p. 196-210.

19. Hayashi CY, Shipley NH, Lewis RV. Hypotheses that correlate the sequence, structure, and mechanical properties of spider silk proteins. Int J Biol Macromol 1999;24(271–275).

20. Beek JDv, Hess S, Vollrath F, Meier BH. The molecular structure of spider dragline silk: folding and orientation of the protein backbone. Proc Natl Acad Sci USA 2002;99:10266-10271.

21. Sponner A, Vater W, Monajembashi S, Unger E, Grosse F, Weisshart K. Composition and hierarchical organisation of a spider silk. PLoS ONE 2007;2(10):e998.

22. Rabotyagova O, Cebe P, Kaplan DL. Self-assembly of genetically engineered spider silk block copolymers. Biomacromolecules 2009;10:229–236.

23. Scheibel T. Spider silks: recombinant synthesis, assembly, spinning, and engineering of synthetic proteins. Microb Cell Fact 2004;3(1):14-24.

24. Xiaa X-X, Qiana Z-G, Ki CS, Park YH, Kaplan DL, Lee SY. Native-sized recombinant spider silk protein produced in metabolically engineered *Escherichia coli* results in a strong fiber. . Proc Natl Acad Sci USA 2010;107(32):14059-14063.

25. Numata K, J JH, Subramanian B, Kaplan DL. Gene delivery mediated by recombinant silk proteins containing cationic and cell binding motifs. J Control Release 2010;146(1):136-143.

26. Gomes S, Leonor IB, Mano JF, Reis RL, Kaplan DL. Spider silk-bone sialoprotein as a novel fusion protein for bone tissue engineering. Soft Matter 2010;Submitted.

27. Huang J, Wong C, George A, Kaplan DL. The effect of genetically engineered spider silk-dentin matrix protein 1 chimeric protein on hydroxyapatite nucleation. Biomaterials 2007;28:2358–2367.

28. Gomes S, Leonor sB, Mano JF, Reis RL, Kaplan DL. Antimicrobial functionalized genetically engineered spider silk. Submitted.

29. Krause A, Neitz S, Mägert H, Schulz A, Forssmann W, Schulz-Knappe P, et al. LEAP-1, a novel highly disulfide-bonded human peptide, exhibits antimicrobial activity. FEBS Lett 2000;480:147-150.

30. Koliaraki V, Marinou M, Samiotaki M, Panayotou G, Pantopoulos K, Mamalaki A. Iron regulatory and bactericidal properties of human recombinant hepcidin expressed in *Pichia pastori*. Biochimie 2008;90(5):726-735.

31. Wallace DF, Jones MD, Pedersen P, Rivas L, Sly LI, Subramaniam VN. Purification and partial characterisation of recombinant human hepcidin. Biochimie 2006;88:31–37.

32. Zhang H, Yuan Q, Zhu Y, Ma R. Expression and preparation of recombinant hepcidin in *Escherichia coli*. Protein Expr Purif 2005;41:409–416.

33. Ganz T. Hepcidin, a key regulator of iron metabolism and mediator of anemia of inflammation. Blood 2003;102(3):783-788.

34. Singh PK, Parsek MR, Greenberg EP, Welsh MJ. A component of innate immunity prevents bacterial biofilm development. Nature 2002;417:552-555.

35. Pigeon C, Ilyin G, Courselaud B, Leroyer P, Turlin B, Brissot P, et al. A new mouse liver-specific gene, encoding a protein homologous to human antimicrobial peptide hepcidin, is overexpressed during iron overload. J Biol Chem 2001;16(276):7811-7819.

36. Nemeth E, Valore EV, Territo M, Schiller G, Lichtenstein A, Ganz T. Hepcidin, a putative mediator of anemia of inflammation, is a type II acute-phase protein. Blood 2003;101(7):2461-2463.

37. Falzacappa MVV, Muckenthaler MU. Hepcidin: Iron-hormone and anti-microbial peptide Gene 2005;364:37-44.

38. Rohde H, Frankenberger S, Zähringer U, Mack D. Structure, function and contribution of polysaccharide intercellular adhesin (PIA) to *Staphylococcus epidermidis* biofilm formation and pathogenesis of biomaterial-associated infections Eur J Cell Biol 2010;89(1):103-111.

39. Schierholz JM, Beuth J. Implant infections: a haven for opportunistic bacteria. J Hosp Infect 2002;49(2):87-93.

40. Lü J-M, Wang X, Marin-Muller C, Wang H, Lin PH, Yao Q, et al. Current advances in research and clinical applications of PLGA-based nanotechnology. Expert Rev Mol Diagn 2009;9(4):325-341.

41. Bini E, Foo CWP, Huang J, Karageorgiou V, Kitchel B, Kaplan DL. RGD-functionalized bioengineered spider dragline silk biomaterial. Biomacromolecules 2006;7:3139-3145.

42. Huang J, Valluzzi R, Bini E, Vernaglia B, Kaplan DL. Cloning, expression, and assembly of sericin-like protein. J Biol Chem 2003;278(46):46117-46123.

43. Yan S-Z, Beeler JA, Chen Y, Shelton RK, Tang W-J. The regulation of type 7 adenylyl cyclase by Its C1b region and *Escherichia coli* peptidylprolyl isomerase, SlyD. J Biol Chem 2001;276(11):8500-8506.

44. Bala I, Hariharan S, Kumar MN. PLGA nanoparticles in drug delivery: the state of the art. Crit Rev Ther Drug Carrier Syst 2004;21(5):387-422.

45. Mishra N, Goyal AK, Khatri K, Vaidya B, Paliwal R, Rai S, et al. Biodegradable polymer based particulate carrier(s) for the delivery of proteins and peptides. Curr Med Chem Anti Inflamm Anti Allergy Agents 2008;7(4):240-251.

46. Schütt C. CD14. International Journal of Biochemistry & Cell Biology 1999;31(5):545-549.

47. Bowers K, Pitcher C, Marsh M. CD4: A co-receptor in the immune response and HIV infection. International Journal of Biochemistry & Cell Biology 1997;29(6):871-875.

48. Bendelac A. Mouse NK1+ T cells Curr Opin Immunol 1995;7(3):367-374.

49. Clevers H, Alarcon B, Wileman T, Terhorst C. The T cell receptor/CD3 complex: a dynamic protein ensemble. Annu Rev Immunol 1988;6:629-662.

50. Chao K-H, Wu M-Y, Yang J-H, Chen S-U, Yang Y-S, Ho H-N. Expression of the interleukin-2 receptor α (CD25) is selectively decreased on decidual CD4+ and CD8+ T lymphocytes in normal pregnancies Mol Hum Reprod 2002;8(7):667-673.

51. Janeway CA. The T cell receptor as a multicomponent signalling machine: CD4/CD8 coreceptors and CD45 in T cell activation. Annu Rev Immunol 1992;10:645-674.

52. Hiemstra PS. Defensins and cathelicidins in inflammatory lung disease: beyond antimicrobial activity. Biochem Soc Trans 2006;34(2):276-278.

53. Tecle T, Tripathi S, Hartshorn KL. Review: defensins and cathelicidins in lung immunity. Innate Immun 2010;16(3):151-159.

54. Grigat J, Soruri A, UForssmann, Riggert J, Zwirner J. Chemoattraction of macrophages, T lymphocytes, and mast cells is evolutionarily conserved within the human α-defensin family. J Immunol 2007;179(6):3958-3965.

55. Aarbiou J, Verhoosel RM, Wetering Sv, Boer WId, Krieken JHJMv, Litvinov SV, et al. Neutrophil defensins enhance lung epithelial wound closure and mucin gene expression In vitro. Am J Respir Cell Mol Biol 2004;30:193-201.

56. Aarbiou J, Ertmann M, Wetering S, Noort P, Rook D, Rabe KF, et al. Human neutrophil defensins induce lung epithelial cell proliferation in vitro. J Leukoc Biol 2002;72:167-174.

57. Murphy CJ, Foster BA, Mannis MJ, Selsted ME, Reid TW. Defensins are mitogenic for epithelial cells and fibroblasts. J Cell Physiol 1993;155(2):408-413.

58. Chavakis T, Cines DB, Rhee J-S, Liang OD, Schubert U, Hammes H-P, et al. Regulation of neovascularization by human neutrophil peptides (α-defensins): a link between inflammation and angiogenesis. FASEB J 2004;18(11):1306-1308.

59. Bals R. Epithelial antimicrobial peptides in host defense against infection. Respir Res 2000;1:141–150.

60. Ganz T. Hepcidin and Its Role in Regulating Systemic Iron Metabolism. Hematology Am Soc Hematol Educ Program 2006;507:29-35.

61. Amersfoort ESV, Berkel TJCV, Kuiper J. Receptors, mediators, and mechanisms involved in bacterial sepsis and septic shock Clin Microbiol Rev 2003;16(3):379-414.

62. Nemeth E, Rivera S, Gabayan V, Keller C, Taudorf S, Pedersen BK, et al. IL-6 mediates hypoferremia of inflammation by inducing the synthesis of the iron regulatory hormone hepcidin. J Clin Invest 2004;113(9):1271–1276.

63. Vyoral D, Petrák J. Hepcidin: A direct link between iron metabolism and immunity. Int J Biochem Cell Biol 2005;37(9):1768-1773

64. Park CH, Valore EV, Waring AJ, Ganz T. Hepcidin, a urinary antimicrobial peptide synthesized in the liver. J Biol Chem 2001;276(11):7806–7810.

65. Zhu J, Paul WE. Heterogeneity and plasticity of T helper cells. Cell Res 2010;20:4-12.

66. Jenkins MR, Griffiths GM. The synapse and cytolytic machinery of cytotoxic T cells. Curr Opin Immunol 2010;22(3):308-313.

67. Ruiz JH, Becker I. CD8 cytotoxic T cells in cutaneous leishmaniasis. Parasite Immunol 2007;29(12):671-678.

68. LeBien TW, Tedder TF. B lymphocytes: how they develop and function. Blood 2008;112(5):1570-1580.

69. Alba-Loureiro TC, Munhoz CD, Martins JO, Cerchiaro GA, Scavone C, Curi R, et al. Neutrophil function and metabolism in individuals with diabetes mellitus. Braz J Med Biol Res 2007;40(8):1037-1044.

70. Haskó G, Pacher P, Deitch EA, Vizi ES. Shaping of monocyte and macrophage function by adenosine receptors. Pharmacol Ther 2007;113(2):264-275.

71. Meinel L, Hofmann S, Karageorgiou V, Kirker-Head C, McCool J, Gronowicz G, et al. The inflammatory responses to silk films in vitro and in vivo Biomaterials 2005;26(2):147-155.

72. Kirker-Head C, Karageorgiou, Hofmann S, Fajardo R, Betz O, Merkle HP, et al. BMP-silk composite matrices heal critically sized femoral defects. Bone 2007;41(2):247-255.

73. Tang QO, Shakib K, Heliotis M, Tsiridis E, Mantalaris A, Ripamonti U, et al. TGF-β3: A potential biological therapy for enhancing chondrogenesis. Expert Opin Biol Ther 2009;9(6):689-701.

74. Bai L, Zhu L, Min S, Liu L, Cai Y, Yao J. Surface modification and properties of *Bombyx mori* silk fibroin films by antimicrobial peptide Appl Surf Sci 2008;254(10):2988-2995.

75. Kuijpers AJ, Wachem PBv, Luyn MJAv, Engbers GHM, Krijgsveld J, Zaat SAJ, et al. In vivo and in vitro release of lysozyme from cross-linked gelatin hydrogels: a model system for the delivery of antibacterial proteins from prosthetic heart valves. J Control Release 2000;67(2-3):323-336.

76. Kuijpers AJ, Wachem PBv, Luyn MJAv, Brouwer LA, Engbers GHM, Krijgsveld J, et al. In vitro and in vivo evaluation of gelatin–chondroitin sulphate hydrogels for controlled release of antibacterial proteins Biomaterials 2000;21(17):1763-1772

77. Kilian O, Hossain H, Flesch I, Sommer U, Nolting H, Chakraborty T, et al. Elution kinetics, antimicrobial efficacy, and degradation and microvasculature of a new gentamicin-loaded collagen fleece. J Biomed Mater Res Part B Appl Biomater 2008;90B(1):210-222.

78. Beutner R, Michael J, Schwenzer B, Scharnweber D. Biological nano-functionalization of titanium-based biomaterial surfaces: a flexible toolbox. Journal of the Royal Society Interface 2010;7(1):S93-S105.

79. Campoccia D, Montanaro L, Speziale P, Arciola CR. Antibiotic-loaded biomaterials and the risks for the spread of antibiotic resistance following their prophylactic and therapeutic clinical use. Biomaterials 2010;31(25):6363-6377.

Chapter VIII

General conclusions

For centuries nature has been a source of different types of polymers and bioactive compounds with major importance in human actions. Proteins are within the most complex and sophisticated biopolymers in nature and during the past few decades different proteins, namely collagen, silk and elastin, have been the target of intense research in tissue engineering and regenerative medicine fields. One of the reasons for this increment is the similarity between these proteins and the extracellular matrix, making them suitable for the fabrication of new scaffolds with improved features to be used in tissue and organ repair or replacement. Additionally, these biopolymers can also be combined with molecules with biological activity to enhance their properties. In this way numerous bioactive molecules such as growth factors, hormones and other biomolecules with known activity, have been used to functionalize proteins as collagen and silk in order to improve their biocompatibility by inducing better cellular response. In most of these cases, this functionalization was accomplished through simple adsorption, chemically cross-linked or encapsulation of bioactive molecules into the protein-based scaffold. More recently, genetic engineering has been used for the synthesis of numerous proteins using different expression systems, avoiding the main drawbacks of proteins extracted from natural sources, mainly batch-to-batch variation and the risk of disease transmission attributed. Also, genetic engineering enables the design and expression of new fusion proteins, which can combine structural proteins such as silk or collagen with other protein or peptide domains with biological activity. These new fusion proteins are easier to process into different structures and shapes, due to the structural protein domain, and at the same time are functionalized with one or more bioactive motifs. This approach allows the design and tailoring of new biomaterials according with the characteristics of the tissue to repair or replace. Furthermore, control over biomaterial assembly and functionalization is of major importance for the control of important features namely material degradation rate, cell adhesion, proliferation and differentiation, mineral deposition, immunological response, among others.

The present thesis describes the use of recombinant DNA methodology to design new silk-based chimeric proteins for future applications in the tissue engineering and regenerative medicine. Different methodologies and techniques were used to assess the structure and composition of these new proteins and to test their activity and biological behaviour. Additionally, mechanical features such as elasticity and roughness were also studied for some of the developed proteins.

The present chapter intents to give a general overview over the main accomplishments and results achieved within this thesis, which are summarized as follows:

1. A Genetic engineering approach for protein functionalization

Different research studies demonstrate the growing importance of novel design approaches, namely genetic engineering, in the fabrication of new nature-inspired biopolymers with improved mechanical and biological features. In this thesis, four new chimeric proteins were design, cloned, expressed and purified. These new proteins were named 6mer+BSP, 6mer+HNP-2, 6mer+HNP-4 and 6mer+hepcidin.

In chapter III is described the fusion of bone sialoprotein sequence (BSP) with a silk block copolymer 6mer. Since our major goal with this study was to produce a biofunctional material for bone regeneration applications, BSP was selected due to its ability to induce the attachment, migration and differentiation of osteoblasts, being involved in bone formation and remodelling. Furthermore, BSP is also responsible for the deposition of calcium phosphate in bone tissues. In this way, with the fusion of BSP features with the remarkable mechanical and self-assembly properties of spider silk we were able to produce a new chimeric protein with promising features for future applications in bone tissue engineering. However, the fusion of both protein domains could interfere with the activity of these domains. In this work, the results show that the fusion of the BSP domain with the spider silk did had no interference in the self assembly capacity of the silk sequence, manifested through the formation of β-sheet after treatment with methanol. Furthermore, *in vitro* mineralization tests show that this new protein retained the function of BSP to induce the nucleation of calcium phosphate (CaP). After one hour incubation in accelerating calcification solution (ACS), energy dispersive spectrometer (EDS) shows the deposition of CaP with a Ca/P ratio varying between 1.72 and 1.86, values close to those for hydroxyapatite (1.67). CaP deposits were not detected in 6mer films.

The *in vitro* biological activity of 6mer+BSP films was also addressed in chapter III through the use of human mesenchymal stem cells (hMSC) cultivated in osteogenic differentiation medium. Alamar Blue tests indicated a good cell viability/proliferation on the 6mer+BSP samples while in 6mer films a reduction in viability/proliferation was observed after 3, 7 and 14 days in osteogenic medium. Furthermore, real time quantitative reverse transcription polymerase chain reaction (real time qRT-PCR) shows an up-regulation of ALP, IBSP and COL1A1 during 14 days of cell culture. For the 6mer samples a significant decrease in expression level was observed specially for ALP and COL1A1 from days 3 to day 14, and the expression of IBSP gene was low at days 3 and 7, and increased at day 14. Additionally, field-

emission scanning electron microscopy (FE-SEM) shows the deposition of CaP during cell culture and the EDS analysis indicates an evolution in Ca/P ratio from day three to fourteen of culture, with an increase from 0 to 1.53-1.72, respectively. In this way, Alamar Blue, real time quantitative Reverse Transcription-Polymerase Chain Reaction, SEM and energy dispersive spectroscopy (EDS) results indicate that during the 14 days of culture, this new chimeric protein sustained hMSC proliferation and differentiation into the osteogenic lineage.

In chapter IV atomic force microscopy (AFM) was used to assess the elasticity of the 6mer and 6mer+BSP films, to collect topographic images of the films to measure their surface roughness, and to address the behaviour of these proteins in the presence of the divalent ions calcium and magnesium. The elastic modulus of 6mer and 6mer+BSP protein films was assessed through force curves and results showed that 6mer+BSP films had a higher stiffness when compared with 6mer films, likely due to the glutamic acid residues present in BSP sequence. For roughness characterization, the topographic images showed apparent differences between 6mer+BSP and 6mer films, however, a statistical comparison of the roughness values showed no significant difference between.

Finally, different research studies showed the importance of calcium ions in the formation of calcium mediated networks increasing the ability of these networks to dissipate energy in response to applied forces, contributing to bone plasticity. In this way, the behaviour of the 6mer+BSP protein in the presence of divalent ions, calcium and magnesium, was investigated. This study give an important insight into how these types of molecules form calcium mediated networks that are related to bone regeneration. AFM imaging shows that the chimeric 6mer+BSP protein retained the ability of BSP to form supramolecular aggregates and in the presence of calcium ions these aggregates generated networks, which were not observed in the presence of magnesium. Additionally, these results also suggest the affinity of the BSP domain to calcium over other divalent ions such as magnesium.

Chapter V highlights the importance of designing fusion proteins with antimicrobial domains. For that, it was performed the design, cloning, expression and the activity and biological tests of a different set of chimeric proteins. These proteins combine the consensus sequence of dragline spider silk with three different antimicrobial peptides, HNP-2, HNP-4 and Hepcdin and were designed as 6mer+HNP-2, 6mer+HNP-4 and 6mer+Hepcdin. The DNA sequencing, protein sequencing, sodium dodecyl sulphate polyacrylamide gel electrophoresis (SDS-PAGE) and western blot confirmed that the cloning process and protein expression were successfully achieved.

As mentioned above the fusion of different protein domains can alter the activity of these domains. In the case of 6mer+HNP-2, 6mer+HNP-4 and 6mer+Hepcdin proteins,

attenuated total reflection Fourier transform infrared (ATR-FTIR) analysis demonstrated that the core self-assembling spider silk domain retained function related to the generation of beta sheet crystals in these new fusion systems. Additionally, a radial diffusion assay also demonstrated that these three proteins retained the antimicrobial activity attributed to the inserted motifs, HNP-2, HNP-4 and hepcidin.

The new chimeric proteins were tested against *Escherichia coli* and *Staphylococcus aureus* bacteria in three concentrations: 10, 50 and 100 μg/ml. 6mer+HNP-4 presented the highest antibacterial activity against *E. coli*, except for the concentration 100 μg/ml, whereas 6mer+HNP-2 elicited the lowest bactericidal activity. All three proteins had a decrease in their antimicrobial activity against *S. aureus* when compared to *E. coli*. However, in the present study and in contrast to what was observed in previous reports, the antimicrobial activity of the new chimeric proteins was not always concentration dependent and a decrease in the bactericidal activity from 10 to 100 μg/ml was observed. Since silk proteins are known to aggregate in solution with increased concentration the presence of 6mer domain could be the cause for this reduction in the bactericidal activity. Dynamic Light Scattering (DLS) results confirmed this assumption by showing the relationship between protein concentration and the size of the aggregates.

The cytotoxic response to the chimeric proteins was also addressed in Chapter V with an osteosarcoma cell line SaOs-2 seeded on 6mer+HNP-2, 6mer+HNP-4 and 6mer+hepcidin films and kept in culture for three days. Alamar Blue results show that these chimeric proteins films are capable of supporting cell proliferation, and the bactericidal activity does not have impact in the mammalian cell function.

The results described in chapters III, IV and V are promising and clearly emphasize the potential of using genetic engineering for the generation of new protein-based multifunctional biomaterials with useful properties. In the present work, we were able to improve osteogenic mineralization functions due to the presence of BSP and control infections due to the addition of the antimicrobial peptides. Moreover, the presence of the silk domain allows these new biofunctional materials to be processed into different structures such as fibers, films, porous matrices and hydrogels.

2. New protein-based biomaterials for biomedical applications

The promising results described above suggest the potential of these new chimeric proteins as new protein-based biomaterials for tissue engineering applications and prompted the use of animal models in order to evaluate the *in vivo* behaviour of some of these new fusion proteins. Chapters VI and VII describe two *in vivo* studies used to address the

inflammatory responses to 6mer+BSP and 6mer+hepcidin films, respectively. The selection of these proteins for *in vivo* studies was based in the promising results obtained during the *in vitro* studies. 6mer+hepcidin protein showed antimicrobial activity and was able to sustain the proliferation of mammalian cells and 6mer+BSP was able to induce the deposition of calcium phosphates and to sustain cell proliferation and differentiation into the osteogenic lineage. The films were implanted subcutaneously in the back of mice and the early inflammatory response was assessed through histology and flow cytometry. Additionally, in both studies the results obtained for 6mer+BSP and 6mer+Hepcdin films were compared with controls of 6mer (silk films alone), poly-lactic-glycolic-acid (PLGA) films, and empty implant sites.

In Chapter VI *in vivo* studies results show only a mild inflammatory reaction to the implanted materials and no apparent differences between 6mer+BSP films and the other experimental conditions demonstrating good *in vivo* biocompatibility and suggesting that this new chimeric protein represents an alternative for bone regeneration applications when considering the biological responses obtained here and the prior studies on osteogenic outcomes. Moreover, von Kossa staining indicated the occurrence of calcium deposits after six weeks for the 6mer+BSP films. The reason for this occurrence is most likely due to the presence of BSP domain in this chimeric protein. These findings and the potential for 6mer+BSP to be used in bone repair need to be confirmed with future *in vivo* studies to assess the ability of 6mer+BSP to induce osteoregeneration of critically sized bone defects.

Chapter VII describes the inflammatory response to 6mer+hepcidin. Flow cytometry and histology results show no relevant differences in the inflammatory response between the mice carrying 6mer+hepcidin films and the mice implanted with PLGA samples or without implant. These results are promising and give further support to the possibility of developing new biomaterials with antimicrobial properties that in the future can lead to a reduction in the use of antibiotics to prevent infection in prosthetic implantation.

The work developed in this thesis emphasized the importance of using genetic engineering approaches namely the recombinant DNA technology in the synthesis of new fusion proteins that can be used as a new generation of multifunctional materials for biomedical applications, creating a new paradigm in biomaterials design. Using this recombinant technology has significant advantages over the conventional production systems namely the development of new genetic variants carrying different functional domains, excluding the need for extensive chemical modifications or changing control conditions during preparation, and decrease the risk of disease transmission attributed to proteins extracted from natural sources.

Another important outcome from this thesis was the design and expression of four new chimeric proteins: 6mer+BSP, 6mer+HNP-2, 6mer+HNP-4 and 6mer+Hepcidin. The 6mer+BSP protein was develop for bone regeneration applications while the other three proteins with antimicrobial properties have a more broad range of applications and can be used in the fabrication of devices with antimicrobial properties for different tissue engineering purposes such as bone repair or wound dressing. In all four proteins, the presence of the spider silk domain is advantageous due to its self-assembly features and outstanding mechanical performance. Also, the presence of spider silk domain facilitates the processing of these proteins into different three-dimensional shapes such as porous scaffolds or hydrogels.

Finally, it is worth to say, even if this concept was not addressed during the experimental work of this thesis, that these four new chimeric proteins can be combined all together as an integrated structure with multifunctional properties, gathering together a better biocompatibility and cellular function of 6mer+BSP with the antimicrobial properties of 6mer+Hepcidin, or other antimicrobial proteins. However, since the combination of different proteins could interfere with their activity, this new and challenging approach needs a deeper and detailed study before being considered as a valid approach. For sure this demanding topic will be the subject of future studies and can open the doors to a new range of applications.